UNIVERSITY
OF TASMANIA

Frontotemporal dementia and amyotrophic lateral sclerosis proteins in neurite health and dysfunction

by

Rachel Alice Kathryn Atkinson

(neé Bain)

BMed Res BBiotech (Hons)

Submitted in fulfillment of the requirement for the
Degree of Doctor of Philosophy

Wicking Dementia Research and Education Centre
University of Tasmania

December, 2017

DECLARATION OF ORIGINALITY

This thesis contains no material which has been accepted for a degree or diploma by the Institute or any other University or institution, except by way of background information duly acknowledged in the thesis, and to the best of my knowledge and belief no material previously published or written by another person except where due acknowledgement is made in the text of the thesis, nor does the thesis contain any material that infringes copyright.

Rachel Atkinson

13.12.17

STATEMENT OF AUTHORITY OF ACCESS

Rachel Atkinson

13.12.17

STATEMENT OF CO-AUTHORSHIP

The following people and institutions contributed to the publication of work undertaken as part of this thesis:

Candidate: Rachel A.K. Atkinson, Wicking Dementia Research and Education Centre, University of Tasmania
Author 2: Anna E. King, Wicking Dementia Research and Education Centre, University of Tasmania, Australia
Author 3: Carmen M. Fernandez-Martos Wicking Dementia Research and Education Centre, University of Tasmania, Australia
Author 4: Julie D. Atkin, Australian School of Advanced Medicine, Macquarie University, Australia
Author 5: James C. Vickers, Wicking Dementia Research and Education Centre, University of Tasmania, Australia

Author details and their roles:

Publication entitled C9ORF72 expression and cellular localisation over mouse development. Located in Chapter 5 of this thesis, and PDF included in Appendix 8.4.

The candidate (70%) was the primary author and contributed to laboratory work, data analysis and manuscript preparation. Author 2 (corresponding author) (10%), author 3 (10%) assisted with data collection, analysis and conception and development of the project. Author 4 (5%) and author 5 (5%) contributed to the conception and development of the project, and data interpretation. All authors contributed to manuscript refinement and presentation.

We the undersigned agree with the above stated "proportion of work undertaken" for each of the above published (or submitted) peer-reviewed manuscripts contributing to this thesis:

Signed: _____ _____

Associate Professor Anna King
Supervisor
Wicking Dementia Research and Education Centre
School of Medicine
University of Tasmania

Professor Ben Canny
Head of School School of Medicine University of Tasmania

Date: 13.12.17 19.06.18

STATEMENT OF ETHICAL CONDUCT

The research associated with this thesis abides by the international and Australian codes on human and animal experimentation, the guidelines by the Australian Government's Office of the Gene Technology Regulator and the rulings of the Safety, Ethics and Institutional Biosafety Committees of the University.

Rachel Atkinson

13.12.17

PUBLICATION CONTRIBUTIONS DURING CANDIDATURE

Fernandez-Martos CM, **Atkinson RAK,** Chuah MI, Vickers JC, King, AE (2017) Combination treatment with leptin and pioglitazone in a mouse model of Alzheimer's disease. *Alzheimer's & Dementia: Translational Research & Clinical Inventions.* 3 pp 92-106.

Atkinson RAK, Fernandez-Martos CM, Atkin JD et al. (2015) C9ORF72 expression and cellular localisation over mouse development. *Acta Neuropathologica Communications* 3:51

Fernandez-Martos, CM, King, AE, **Atkinson, RAK**, et al. (2015) Neurofilament light gene deletion exacerbates amyloid, dystrophic neurite and synaptic pathology in the APP/PS1 transgenic model of Alzheimer's disease. *Neurobiology of Aging* 36:10 pp 2757-2767.

Soo KY, Sultana J, King AE, et al. (2015) ALS-associated mutant FUS inhibits macroautophagy which is restored by overexpression of Rab1. *Cell Death Discovery* 1, 15030.

Liu, Y, **Atkinson, RAK**, Fernandez-Martos, CM, et al. (2015) Changes in TDP-43 expression in development, aging, and in the neurofilament light protein knockout mouse. *Neurobiology of Aging* 36:2 pp 1151 – 1159.

Farg, MA, Sundaramoorthy, V, Sultana, JM, et al. (2014) C9ORF72, implicated in amyotrophic lateral sclerosis and frontotemporal dementia, regulates endosomal trafficking. *Human Molecular Genetics* 23:13 pp. 3579-3595.

CONFERENCE PRESENTATIONS DURING CANDIDATURE

2017

Scientific poster presentation at 13th MDN Australia Research Conference, Sydney, Australia, November 2017. Entitled: *Effects of altered TDP-43 on the neuronal cytoskeleton*.

2016

Scientific poster presentation at 10th International Conference on Frontotemporal Dementias, Munich, Germany, August 2016. Entitled: *The role of FTD/ALS proteins in neurite and synapse function.*

Scientific poster presentation at 7th Australian Neurotrauma Symposium, Hobart, Australia, December 2016. Entitled: *The role of FTD/ALS proteins in neurite and synapse function.*

Scientific poster presentation at Australasian Neuroscience Society, Hobart, Australia, December 2016. Entitled: *The role of FTD/ALS proteins in neurite and synapse function.*

2015

Scientific poster presentation at 25th Meeting of the International Society for Neurochemistry, Cairns, Australia, August 2015. Entitled: *The role of FTD/ALS proteins in neurite and synapse function.*

Scientific poster presentation at Asia Pacific FTD/MND Meeting, Sydney, Australia, September 2015. Entitled: *The role of FTD/ALS proteins in neurite and synapse function.*

Scientific poster at Tasmanian Health Students Research Conference, Hobart, Australia, June 2015. Entitled: *Developmental expression of frontotemporal dementia protein, C9ORF72 in vitro and in vivo.* This presentation won the poster competition ($500).

Scientific poster presentation at Wicking Dementia Research and Education Centre Dementia Intervention Symposium, Hobart, Australia, November 2015. Entitled: *The role of FTD/ALS proteins in neurite and synapse function.*

2014

Scientific poster at 9th International Conference on Frontotemporal Dementias, Vancouver, Canada, October 2014. Entitled: *Developmental expression of FTLD protein, C9ORF72 in vitro and in vivo.*

Selected oral presentation for Tasmanian Health Students Research Conference, Hobart, Australia, June 2014. Entitled: *Developmental expression of frontotemporal dementia protein, C9ORF72 in vitro and in vivo.* Highly commended oral presentation.

ACKNOWLEDGEMENTS

I would first like to thank my supervisory team, A/Prof Anna King, Prof James Vickers and Dr Matthew Kirkcaldie for the support and guidance they have provided me during my PhD. Their insight, patience and advice has made this project possible and I have learned a great deal from them.

Thank you to the members of the Wicking lab group, who have become like family. Without them, this experience wouldn't nearly have been as enjoyable. I would particularly like to thank Dr Carmen Fernandez-Martos for her expertise and friendship, and Kelsey Hanson, Kimberly Stuart, Jessica Collins, Andrew Phipps, Barbora Fulopova, James Bender and Sam Dwyer for doing this journey alongside me. I have learnt so much from these wonderful people. Thank you to the wider Wicking lab group and the Wicking Center for their support and encouragement. I would also like to extend a special thank you to Amanda, Megan, and Macarena for their friendship over the past eight years of university.

An additional thank you to Dr Jackie Leung, Graeme McCormack, Justin Dittmann, Olivier Bibari, Richard Wilson and Aidan Bindoff for their technical assistance, and to the animal care staff at CFF for their assistance also.

I would like to thank to Alzheimer's Australia Dementia Research Foundation for providing me with a scholarship to undertake my PhD studies and also to the Wicking Centre for providing additional support for scholarship and conference travel through out my PhD. Thank you to the Motor Neuron Disease Research Institute of Australia for funding of parts of this work.

Finally, I would like to thank my amazing network of friends and family outside of work. I am so grateful for their love and patience. In particular thank you to my husband, Tyson, who provided so much support and encouragement. Thank you.

SUMMARY

A number of proteins have been identified which are pathologically and/or genetically associated with both frontotemporal dementia (FTD) and amyotrophic lateral sclerosis (ALS). A hexanucleotide repeat expansion in the non-coding region of the *C9ORF72* gene is the largest genetic factor associated with FTD and ALS. Additionally, pathological inclusions of the TDP-43 protein are found in brains of approximately 50% of FTD cases and 90% of ALS cases. However, the normal function of these two proteins and how this relates to the degeneration of neurons in disease are not yet well understood. Accumulating evidence suggests that both proteins may have involvement with the neuronal cytoskeleton. The cytoskeleton is of particular interest in FTD/ALS due to significant axon pathology and loss observed in post mortem cases. It is known that the cytoskeleton is often a key effector to changes in axon integrity in many neurodegenerative diseases. This thesis examined the normal functions of TDP-43 and C9ORF72, and their links with the cytoskeleton through use of mouse primary cell culture, histological analysis of intact mouse brain, and viral-mediated expression of proteins of interest in a retina model in the mouse.

TDP-43 is a predominantly nuclear protein, with much known about its nuclear roles in DNA and RNA binding, and regulation of transcription and translation. Evidence suggests that TDP-43 is also important for neurite outgrowth, remodelling and can regulate many components of the neuronal cytoskeleton. The effects of overexpression of TDP-43 in primary cortical neurons were examined and demonstrated distinct alterations to actin-associated cellular processes including neurite branching and growth cone morphology, as well as down-regulation of actin-binding proteins in the proteome of these cells. To examine the effect of pathogenic alterations to TDP-43 *in vivo* AAV2 virus was used to mediate the expression of wildtype human TDP-43 and human TDP-43 with a mutation to the nuclear localisation signal (NLS) in mouse retinal ganglion cells, through intraocular injection of the virus. These changes induced axon pathology in the optic nerve, with indications of perturbed axonal transport due to presence of organelle accumulation.

Several mechanisms for how the non-coding repeat expansion in C9ORF72 may lead to disease have been described, however little is known about the normal function and the expression pattern of the C9ORF72 protein. This thesis characterized the expression pattern and cellular localisation of the three reported mouse isoforms of C9ORF72 in cell culture and *in vivo*, and demonstrated that C9ORF72 was present in synaptosomes and within actin-rich structures of neurons.

In summary, these results indicate that both C9ORF72 and TDP-43 may have links to the neuronal cytoskeleton, and in particular the actin cytoskeleton. Modulation of the neuronal cytoskeleton is a compelling target for providing therapeutic protection to vulnerable cellular components, such as the axon. Studies such as those described in this thesis may provide insight for whether TDP-43- and C9ORF72-related FTD/ALS are candidates for these types of interventions.

COMMON ABBREVIATIONS

AD	Alzheimer's disease
ALS	Amyotrophic lateral sclerosis
ANOVA	Analysis of variance
BSA	Bovine serum albumin
bvFTD	Behavioural variant frontotemporal dementia
°C	Degrees Celsius
C9ORF72	Chromosome 9 open reading frame 72
CBS	Corticobasal syndrome
CHMP2B	Charged multivesicular body protein 2B
CNS	Central nervous system
DAPI	4', 6-diamidino-2-phenylindole
DIV	Days in vitro
DNA	Deoxyribonucleic acid
E	Embryonic day
FTD	Frontotemporal dementia
FTLD	Frontotemporal lobar degeneration
FUS	Fused in sarcoma
g	Gram
GAPDH	Glyceraldehyde 3-phosphate dehydrogenase
GDP	Guanosine diphosphate
GFAP	Glial fibrillary acidic protein
GRN	Granulin
GTP	Guanosine triphosphate
HDAC	Histone deacetylase
hnRNP	Heterogeneous nuclear ribonucleoprotein
IgG	Immunoglobulin
kDa	Kilo Dalton
KO	Knockout
L	Litre
µl	Micro litre (10^{-6}l)
µm	Micrometre (10^{-6}m)

μM	Micro molar (10^{-6}M)
M	Molar
ml	millilitre
mm	millimetre
MAP	Microtubule associated protein
MAPT	Microtubule associated protein tau
mRNA	Messenger ribonucleic acid
NES	Nuclear export sequence
NFH	neurofilament heavy subunit
NFM	neurofilament medium subunit
NFL	neurofilament light subunit
NIFID	Neuronal intermediate filament inclusion disease
NLS	Nuclear localisation sequence
nm	Nanometer
PBS	Phosphate buffered saline
PFA	Paraformaldehyde
PNFA	Progessive nonfluent aphasia
PRGN	Progranulin
PSP	Progressive supranuclear palsy
PVDF	Polyvinylidene fluoride
RAN	Repeat-associated non-ATG
RNA	Ribonucleic acid
RRM	RNA recognition motif

SDS-PAGE	Sulfate-polyacrylamide gel electrophoresis
SEM	Standard error of the mean
SG	Stress granules
TBS	Tris-buffered saline
TDP-43	Transactive response-DNA-binding protein 43
UPS	Ubiquitin proteasome system
VCP	Valosin-containing protein
WT	Wild type

Table of Contents

1 Literature Review 2

1.1 Frontotemporal Dementia 2

1.2 Clinical subtypes of FTD 2

1.3 FTD and ALS as a continuum 3

1.4 Pathological subtypes of FTLD 3

1.5 Cellular changes in FTD 3

1.6 Does the pathology of ALS/FTD link to primary changes in the cytoskeleton? 5

1.7 The role of TDP-43 in cytoskeletal pathology and function 10

1.8 The role of C9ORF72 in cytoskeletal pathology and function 14

1.9 Summary and Project aims 16

2 Materials & Methods 2

2.1 Animal conditions and care 2

2.2 Primary Cell Culture 2

2.3 Immunocytochemistry 3

2.4 Animal Perfusion and Tissue Processing 4

2.5 Immunohistochemistry 4

2.6 Western Blotting 5

2.7 Statistical Analysis 7

3 Effects of overexpression of TDP-43 on the neuron proteome and morphology 2

3.1 Introduction 2

3.2 Methods 4

3.3 Results 13

3.4 Discussion 22

4 Effects of altered TDP-43 in a novel CNS disease model 2

4.1 Introduction 2

4.2 Methods 5

4.3 Results 13

4.4 Discussion 14

5 C9ORF72 expression and cellular localisation over mouse development 2

5.1 Introduction 2

5.2 Methods 5

5.3 Results 11

5.4 Discussion 21

6 Final Discussion 2
6.1 Alterations to neuron morphology 2
6.2 Actin cytoskeleton 4
6.3 Axon degeneration 5
6.4 Limitations and future directions 6
6.5 Therapeutic implications 8
6.6 Conclusions 9
7 References 10
8 Appendices 32
8.1 Common Laboratory Reagents 32
8.2 Chapter 3 appendix 33
8.3 Chapter 4 Appendix 37
8.4 Chapter 5 PDF version of C9ORF72 Expression and Localisation over mouse development 46

Chapter 1: Literature Review

1 LITERATURE REVIEW

1.1 FRONTOTEMPORAL DEMENTIA

1.1.1 Background

The frontotemporal dementias (FTD) are a group of early-onset diseases that cause dementia characterised by progressive changes to behaviour and/or language. Frontotemporal lobar dementia (FTLD) is the term routinely used to describe the pathological conditions that clinically present as FTD. FTD has a mean age of onset of 52.8 years and, after Alzheimer's disease (AD), is the second most common form of early-onset dementia with a prevalence of 15-22/100,00 (Onyike & Diehl-Schmid, 2013). FTD is fatal, with death generally occurring within 6 to 11 years after symptom onset (De Conti, Borroni, & Baralle, 2017). There are currently no effective treatments (Onyike & Diehl-Schmid, 2013). Gross examination of post mortem cases of FTD shows atrophy of the frontal and temporal lobes, as well as other brain areas depending on the subtype of disease. At the microscopic level, there is neuronal loss, protein aggregation, as well as an increase in the number of astrocytes (astrocytosis) within atrophied areas of the brain (Sieben et al., 2012). In individual cases, the observed pattern of atrophy in FTLD is variable, and clinical symptoms of disease correlate with these patterns (Sieben et al., 2012).

1.2 CLINICAL SUBTYPES OF FTD

Several different subtypes of FTD have now been described in terms of their key clinical features. These include behaviour (behavioural variant FTD, bvFTD), language (semantic variant primary progressive aphasia, svPPA; progressive non-fluent aphasia, PNFA), movement disorders (progressive supranuclear palsy, PSP; corticobasal syndrome, CBS), neuronal intermediate filament inclusion disease (NIFID) and FTD with amyotrophic lateral sclerosis (FTD-ALS, (Roberson, 2012; Sieben et al., 2012).

1.3 FTD AND ALS AS A CONTINUUM

Amyotrophic lateral sclerosis (ALS) is the most common form of motor neuron disease (MND) and involves impairment of both upper and lower motor neurons. It usually results in death within three to five years of diagnosis, in most cases due to respiratory failure. FTD and ALS are now considered to be at opposite ends of a disease spectrum (Burrell et al., 2016). Although physical symptoms of the two disorders may differ, many clinical, genetic and pathological characteristics overlap. ALS and FTD frequently occur in the same family, with many people living with ALS having impairments in frontotemporal functions such as cognition and behaviour, and conversely a large proportion of FTD patients with motor neuron dysfunction (Lomen-Hoerth, Anderson, & Miller, 2002; Phukan, Pender, & Hardiman, 2007). The close relationship between the disorders was first strengthened when the transactive response DNA-binding protein 43 (TDP-43), was determined to be the main protein component of the pathology of both ALS and FTD (Neumann et al., 2006). In 2011, the association between these two diseases was again confirmed when the repeat expansion of the hexanucleotide sequence, GGGGCC, in the *C9orf72* gene, was found to be the most common cause of familial ALS (37%) and FTD (21%), as well as being associated with sporadic ALS (6%) and FTD (6%; DeJesus-Hernandez et al., 2011; Rademakers, Neumann, & Mackenzie, 2012; Renton et al., 2011). The identified similarities between ALS and FTD have contributed greatly to understanding the pathological and genetic mechanisms by which the two disorders operate.

1.4 PATHOLOGICAL SUBTYPES OF FTLD

Frontotemporal lobar degeneration is similar to many other neurodegenerative diseases in that it is characterised by the presence of abnormal intracellular protein aggregates in surviving cells. These may consist of genetically mutated protein, but in many disease subtypes, the main aggregated species is not the mutant gene product. The pathological inclusions associated with specific gene mutations

are illustrated in Figure. 1.1. The accumulations of protein within these aggregates have been used to further subcategorise FTLD (Figure 1.1 B). The two major pathological subtypes of FTLD, FTLD-tau and FTLD-TDP-43, will be reviewed here.

1.4.1 FTLD-Tau

Tau (encoded by the *MAPT gene*) is a member of the microtubule associated protein (MAP) family and stabilises microtubules through tubulin binding (Hirokawa, 1994). FTLD-tau is characterised by both neuronal and glial inclusions comprised of hyperphosphorylated tau protein that are immuno-negative for ubiquitin. Tau-positive inclusions are observed in a range of neurodegenerative diseases, collectively described as tauopathies, of which several present as FTD. These include Pick's disease, PSP, CBS, globular glial tauopathy (GGT), and FTD caused by *MAPT* mutations which accounts for approximately 5 to 20% of familial FTD (Rademakers, Cruts, van Broeckhoven, 2004). In these conditions, tau has varying degrees of phosphorylation, and different isoforms of tau are present, which likely explains the variations in inclusion morphology and cell types affected.

1.4.2 FTLD-TDP

TDP-43 protein is encoded by the *TARDBP* gene and is an RNA binding protein involved in a range of RNA processing such as transcription, pre-mRNA splicing, stability, transport and translation (Buratti, 2001; 2008). Originally, cases of FTD which were immuno-negative for tau, but had ubiquitin-positive inclusions, were termed FTLD-U (Lipton, White, & Bigio, 2004). However, TDP-43 was later identified as the main protein present in inclusions of most FTLD-U cases (Neumann et al., 2006) and this subset was renamed 'FTLD-TDP'. In FTD, TDP-43 pathology is present in 40 to 50% of cases (Chare et al., 2014), but in cortical neurons of FTLD-TDP cases, nuclear staining of TDP-43 is frequently reduced.

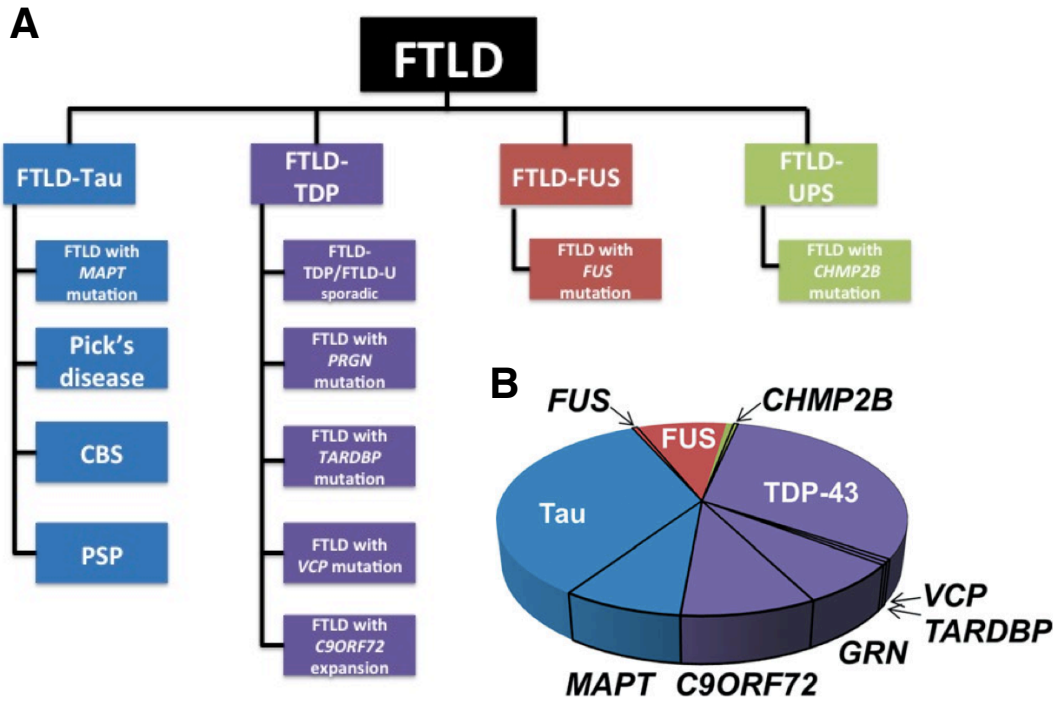
A
FTLD
FTLD-Tau
FTLD-TDP
FTLD-FUS
FTLD-UPS
FTLD with MAPT mutation
Pick's disease
CBS
PSP
FTLD-TDP/FTLD-U sporadic
FTLD with PRGN mutation
FTLD with TARDBP mutation
FTLD with VCP mutation
FTLD with C9ORF72 expansion
FTLD with FUS mutation
FTLD with CHMP2B mutation
B
FUS
CHMP2B
FUS
TDP-43
Tau
VCP
TARDBP
GRN
MAPT
C9ORF72

Figure 1.1 Classifications of FTLD (A) FTLD can be classified into disctinct neuropathologic subtypes based on proteins found within inclusions: FTLD-Tau, FTLD-TDP, FTLD-FUS, and FTLD-UPS. (B) The neuropathological subtypes based on proteins within cellular inclusions (colour) and known genetic causes (black outlines) of behavioural variant frontotemporal dementia (bvFTD), in proportion to frequency. Figure adapted from Halliday et al. (2012) and Roberson (2012)

TDP-43 and other RNA binding proteins, such as fused in sarcoma (FUS), which is also implicated in FTD/ALS, contain a nuclear localisation sequence (NLS) which binds to a transportin receptor to regulate transport in and out of the nucleus (Mihevc, Baralle, Buratti, & Rogelj, 2016). In disease, a common feature of TDP-43 pathology is mislocalisation of the protein from the nucleus to the cytoplasm. In the cytoplasm it becomes abnormally phosphorylated, ubiquitinated and insoluble, and can be cleaved to form C-terminal fragments (CTF) (Arai et al., 2006; Neumann et al., 2009; Neumann et al., 2006). It is currently unclear if these cytoplasmic protein aggregates are intrinsically toxic or whether they have a protective role in the cell by sequestering potential toxic protein species.

In FTLD-TDP, inclusions are most commonly observed in neurons of the frontotemporal neocortex and dentate granule cells of hippocampus, although pathology can also be found more subcortically. FTLD-TDP is characterised by neuronal cytoplasmic and intranuclear inclusions, as well as dystrophic neurites, which are immunopositive for TDP-43, ubiquitin and p62 (Irwin et al., 2015). Other TDP-43 pathology includes cytoplasmic inclusions in oligodendrocytes, diffuse neuronal cytoplasmic staining inclusions (or pre-inclusions), and wispy neurites (Cairns et al., 2007; Hatanpaa et al., 2008; Neumann et al., 2007). FTLD-TDP can be further subcategorised (types A to D, reviewed in (Burrell et al., 2016)) depending on the location and morphology of inclusions.

1.4.2.1 Familial FTLD-TDP

In comparison to FTLD-tau, which involves mutations to a single gene (*MAPT*), TDP-43 pathology in FTLD-TDP can be driven by mutations in a range of genes. The hexanucleotide repeat expansion of the *C9ORF72* gene is associated with brain TDP-43 pathology (FTLD-TDP), most commonly type B, although other TDP-43 pathology patterns have emerged (Mackenzie & Neumann, 2016). Mutations of *GRN,* the gene encoding progranulin, are associated with 5 to 20% of familial FTD, and 1 to 5% of sporadic FTD (I. Gijselinck et al., 2008) but are not associated with ALS. Progranulin mutations cause TDP-43 pathology (Cairns et al., 2007), most commonly presenting as neuronal cytoplasmic and

intranuclear inclusions (FTLD-TDP type A). Finally, a small number of cases of FTD are caused by mutations to valosin containing protein (VCP; Watts et al., 2004) and *TARDBP* (Sreedharan et al., 2008) which both result in TDP-43 pathology.

1.5 CELLULAR CHANGES IN FTD

Pathological examination of human FTD cases demonstrates that this disease is characterised by neurite and synaptic degeneration. Cytoskeletal alterations are a key driver of neuritic abnormalities, and are associated with several neurodegenerative diseases involving such alterations (Cairns, Lee, & Trojanowski, 2004; Eira, Silva, Sousa, & Liz, 2016; Hur, Saijilafu, & Zhou, 2012; McMurray, 2000; Vickers et al., 2009).

1.5.1 Histopathologic studies of neuritic and synaptic changes

Previous histopathological studies of FTD brains found swollen presynaptic terminals which were immunopositive for tau, high molecular weight neurofilament protein (NFH) and beta tubulin (Zhou et al., 1998). A case study of a patient with both FTD and MND revealed reduced dendritic arbours, proximal dendritic varicosities, shortened dendrites and a reduction in the number of dendritic spines (Ferrer, Roig, Espino, Peiro, & Matias Guiu, 1991).

Severe loss of axons and white matter is a common feature of FTD, and has been found in both tau- and TDP-43-associated FTD (Dickson et al., 1986). Diffusion tensor magnetic resonance imaging (DT MRI) of people living with FTD shows alterations to white matter tracts within the brain (Agosta et al., 2012; Schofield, 2003) from which cell body death and axon degeneration have been inferred, depending on whether correlated grey matter changes are observed. Such axonal alterations followed by degeneration are an early feature of FTD (Agosta et al., 2012; Schofield, 2003). Histological examination suggests that axon and white matter loss in FTD-tau is distinct from FTD-TDP pathology (D. W. Dickson et al., 1986; van Eersel et al., 2015). FTD-tau is associated with large swollen axons

(spheroids) filled with neurofilament proteins, whereas these structures are absent from FTD-TDP cases (van Eersel et al., 2015). FTD-tau is also associated with "ballooned neurons", which have swollen perikarya filled with neurofilament proteins, and it has been suggested that this results from failed transport of neurofilament proteins along the axon (Dickson et al., 1986). Fewer detailed studies have examined TDP-43 neurite pathology, although dystrophic neurites are observed in both cortex and hippocampus in FTLD-TDP (Hatanpaa et al., 2008).

1.5.2 Cellular changes in ALS

Neurite pathology in ALS is well-characterised and axonal alterations within motor neurons are a likely cause of the clinical symptoms of disease. Pathological changes in ALS include large swellings of axons in the ventral horn of the spinal cord containing accumulations of phosphorylated neurofilament proteins, mitochondria and lysosomes (Corbo & Hays, 1992; Hirano, Donnenfeld, Sasaki, & Nakano, 1984; Hirano, Nakano, et al., 1984) as well as accumulations of kinesin, a key protein involved in transport of cargoes in the axon (Toyoshima et al., 1998). In addition, neurofilament proteins including NFL and alpha-internexin, and peripherin mRNA are decreased in motor neurons of sporadic ALS cases (Wong, 2000).

Further clues to the involvement of TDP-43 pathology and neurite abnormalities come from ALS cases. Alterations to tau proteins are not observed, but TDP-43 pathology is found in most cases of ALS (Arai et al., 2006). In addition to cytoplasmic mislocalisation of TDP-43 in ALS, phosphorylated TDP-43 accumulates in axons and dendrites of somatomotor neurons as skein-like and dash-like aggregates (Braak, Ludolph, Thal, & Del Tredici, 2010).

These data demonstrate that neurite changes are a common feature of diseases induced by both tau and TDP-43 pathology. While tau is an important driver of neurite abnormalities in many FTLD cases, and it is likely that tau alterations disrupt the neuronal cytoskeleton, the cause of neurite abnormalities in

FTLD-TDP and ALS-TDP-43 are less clear. In these cases, it is possible that TDP-43 may also drive neurite abnormalities via alterations to the neuronal cytoskeleton.

1.6 DOES THE PATHOLOGY OF ALS/FTD LINK TO PRIMARY CHANGES IN THE CYTOSKELETON?

1.6.1 Overview of cytoskeleton

The cytoskeleton plays a vital role in the maintenance of cellular shape, structural organisation, transport, cell division and movement. In highly polarised cells such as neurons, which have complex shapes, and sometimes extend processes over a distance of up to one meter, the tight regulation of cytoskeletal components is critical. The cytoskeleton is composed of three key elements: microtubules, intermediate filaments and microfilaments. Neuronal intermediate filaments include neurofilaments, comprised of the subunits NFL, neurofilament medium (NFM), NFH, alpha-internexin (in the CNS) and peripherin (in the PNS) (Ge, Volkening, Leystra-Lantz, Jaffe, & Strong, 2007). A substantial number of cytoskeleton-associated proteins are also required for linking, regulation and movement.

1.6.2 ALS/FTD genes associated with the cytoskeleton

A growing list of cytoskeletal gene mutations is associated with FTLD/ALS, outlined in Table 1.1. As mentioned previously, mutations in the microtubule associated protein tau (*MAPT)* are responsible for 5 to 20% of familial FTD cases (Hutton et al., 1998; Poorkaj et al., 1998; Rademakers, Cruts, van Broeckhoven 2004; Spillantini et al., 1998). In sporadic FTD, tau protein levels are reduced (Zhukareva, 2001) due to hyperphosphorylation or protein aggregation. Hyperphosphorylation of tau within its repeat domain causes a reduction in microtubule binding, leading to microtubule disassembly and hence possible axon transport deficits (reviewed in (Y. Wang & Mandelkow, 2016). Aggregation of tau leads to a reduction in available soluble tau, again leading to microtubule disassembly. In mouse models of tau loss of function, knockout mice are viable and fertile (Harada et al., 1994; Takei, Teng, Harada, & Hirokawa, 2000), likely due in part to compensation by other proteins such as microtubule

associated protein 1A (MAP1A). However, motor deficits are present in 12-month-old tau knockout mice (Lei et al., 2014), indicating that tau is necessary for normal neuronal functioning; delayed developmental maturation of neurons (Dawson et al., 2001) and changes to protein trafficking (Lei et al., 2012) are also observed. Therefore, it is likely that tau loss of function is sufficient to cause dysfunction and disease through processes involving the cytoskeleton.

Table 1.1 Cytoskeletal genes associated with ALS and FTD.

Mutation, Gene (protein)	Disease association	References
MAPT (tau)	FTLD	(Hutton et al., 1998; Poorkaj et al., 1998; Spillantini et al., 1998)
NEFH (neurofilament heavy chain)	ALS	(Al-Chalabi et al., 1999)
DCTN1 (dynactin)	ALS, ALS-FTLD	(Puls et al., 2003)
PFN1 (profilin)	ALS	(Wu et al., 2012)
TUBA4a (tubulin alpha, 4A)	ALS, atypical FTLD	(Smith et al., 2014) (Perrone et al., 2017)

ALS/FTD linked mutations within other genes are very rare, with some only described in one to a few cases. For example, mutations in the tail region of neurofilament heavy chain (*NEFH*), important for filament stability, were first reported in both sporadic and familial ALS cases in 1999 (Al-Chalabi et al., 1999). Additionally, disease-linked mutations within the microtubule-binding domain of *DCTN1*, thought to compromise microtubule-dependent retrograde transport of vesicles and organelles, have been identified (Puls et al., 2003) – initially in a patient with slow progressing, autosomal dominant ALS, and subsequently in a family with both ALS and FTD (Münch et al., 2005).

Profilin 1, which converts monomeric to filamentous actin, has also been linked to familial ALS (van Blitterswijk et al., 2013; Wu et al., 2012). Cells expressing this mutation show reduced axonal outgrowth, smaller growth cones and decreases in bound actin (Wu et al., 2012). More recent studies have also identified profilin 1 mutations in sporadic forms of ALS, and although none have been linked to FTD, genetic screening of large cohorts would be needed to eliminate the possibility (Tiloca et al.,

2013).

Mutations of *TUBA4a*, one of the proteins making up microtubules, have been found in familial ALS cases, and cause destabilisation of the microtubule network (Smith et al., 2014). A recent study found a novel mutation in TUBA4a in a patient with atypical FTD, which caused loss of the *TUBA4a* transcript (Perrone et al., 2017).

These associations underscore the importance of cytoskeletal regulation in maintaining healthy neurons, as well as the vulnerability of cells involved in ALS/FTD to cytoskeletal alterations.

1.6.3 ALS/FTD pathology and the cytoskeleton

Despite the evidence that cytoskeletal gene mutations can lead to ALS/FTD, the majority of cases are not associated with these types of mutations. This raises the question as to whether cytoskeletal alterations are involved in the pathogenesis of these other cases. In this regard, there is increasing evidence that ALS/FTD pathology, including changes to localisation, post-translational modifications and accumulations of proteins associated with FTD, also leads to disruptions to the cytoskeleton.

NIFID, a type of FTD, is characterised by disruption to the cytoskeleton. This early onset disease involves atrophy of the frontal and temporal lobes and symptoms similar to FTD (Cairns et al., 2004). Microscopically it presents with intraneuronal cytoplasmic inclusions, axonal swellings and spheroids containing NFL, NFM, NFH and a-internexin, which may be ubiquitinated and phosphorylated (Cairns et al., 2010). Accumulations of these cytoskeletal proteins may be due to impaired axonal transport. Alterations to FUS and progranulin can also cause changes to neurites which could indicate changes in the cytoskeleton. In disease models, *FUS* mutations cause defects including altered axon length and branching (Groen et al., 2013; Kabashi et al., 2011), and mutant *FUS* aggregates, which sequesters other proteins important for cytoskeletal maintenance (Groen et al., 2013). Progranulin mutations decrease levels of progranulin protein. Under normal conditions, progranulin and its cleaved fragments (granulins) promotes neurite outgrowth (Gao et al., 2010). Cell culture and zebrafish models have

demonstrated that a decrease in expression of progranulin leads to truncation and aberrant branching of neurons (Chitramuthu, Baranowski, Kay, Bateman, & Bennett, 2010; Gao et al., 2010; Gass et al., 2012) and that adding exogenous progranulin can rescue this phenotype (Chitramuthu et al., 2010; Gass et al., 2012) and increase neurite outgrowth (Gao et al., 2010; Van Damme et al., 2008). One of these studies also showed that knockdown of progranulin lead to a reduction of GSK-3b phosphorylation (Gao et al., 2010), a kinase shown to have a role in axon-dendrite polarity in development (Jiang, Guo, Liang, & Rao, 2005). In aged mice with constitutive knockout of progranulin (Petkau et al., 2012), similar abnormalities were observed, with altered morphology of apical dendrites of hippocampal CA1 pyramidal cells, decreased spine density and altered synaptic activity. Gao et al. (2010) suggested that the loss of progranulin expression in FTLD may be responsible for abnormalities in axonal repair and neuron loss in these diseases.

While the link between several key pathological proteins in FTD and neurite abnormalities has been well investigated, the role of TDP-43 is less clear. Additionally, the way in which *C9ORF72* mutations, the most common genetic cause of FTD and ALS, lead to neurodegeneration is also not well understood.

1.6.4 Pathological inks between TDP-43 and the cytoskeleton

Although studies to date are currently limited, there is evidence for cytoskeletal changes in human tissue with TDP-43 pathology. A study examining cases of FTLD-U and dementia lacking distinctive histopathology demonstrated that dystrophic neurites immuno-positive for TDP-43 are a common feature of these two diseases (Hatanpaa et al., 2008). Dystrophic neurites generally consist of swollen axons and dendrites, as well as accumulations of the internal cytoskeletal elements such as neurofilament proteins and tau (Dickson, King, McCormack & Vickers, 1999). In ALS, TDP-43 pathology is associated with abnormal neurite accumulations in vulnerable neurons, including somatomotor neurons of the lower brainstem and spinal cord (Braak et al., 2010). Additionally, white

matter tracts of FTLD-TDP cases undergo degeneration, characterised by vacuolation within the fibre tracts (Armstrong, 2017). These studies show that TDP-43 pathology occurs concurrently with alterations to neurites.

1.6.4.1 Cytoskeletal changes in TDP-43 experimental models

Further evidence from experimental models links cytoskeletal alterations to TDP-43 alterations. In a mouse model with cytoplasmic mislocalisation of TDP-43 from the nucleus to the cytoplasm, a reduction in the expression of NFL proteins within axons of the corticospinal tract was reported as well as axon degeneration and dieback of motor neurons from the neuromuscular junction (Igaz et al., 2009; Walker et al., 2015). Abnormal neurite morphology can be caused by both knockdown of TDP-43 and expression of missense mutations (including A315T, Q331K and M337V) in differentiated cortical neurons (Han et al., 2013), and by expressing either WT TDP-43 with mutated nuclear localisation signal (NLS) or mutant TDP-43 with mutated NLS (Han et al., 2013). Neurite outgrowth, branching and maintenance require coordinated structural changes to the cytoskeleton including microtubules, neurofilament and actin filaments. In particular, the Rho GTPases are key factors which regulate actin cytoskeleton elements (Woo & Gomez, 2006). In line with this, depletion of TDP-43 in neuronal cell lines alters neurite outgrowth through deregulation of the Rho family of GTPases (Iguchi et al., 2009).

A recent study by Tripathi and colleagues (2014) demonstrated that expression of mutant forms of TDP-43, including the M337V familial ALS mutation and Q331K sporadic mutation, induce cellular toxicity and mislocalisation of TDP-43 to the cytoplasm and axons in chick embryo spinal cords and primary cultured motor neurons. They also observed defasciculation of motor axons, impairing path-finding and synaptic targeting (Van Vactor, 1998), leading to truncation and a reduction in neurite outgrowth both *in vivo* and *in vitro* (Tripathi et al., 2014). Although mechanisms are still unclear, these

data provide evidence that changes to TDP-43 lead to dysregulation of the cytoskeleton and altered neuron integrity.

In mouse models with A415T and G348C TDP-43 mutations, the L5 ventral root of 10-month-old mice contained more small caliber and fewer larger caliber axons compared to wildtype (Swarup et al., 2011), suggestive of neurofilament disruption since these intermediate filaments, NFM in particular, are known to regulate axon caliber (Barry et al., 2012; Kirkcaldie & Dwyer, 2017).

The association of TDP-43 with cytoskeletal function is not limited to mammals. *Drosophila* lacking the TDP-43 homolog, *TBPH*, have motor dysfunctions, reduced lifespan and structural changes to neuromuscular junctions, which can be rescued by expression of human TDP-43 (Feiguin et al., 2009). Expression of mutant TDP-43 has been shown to cause altered localisation and aggregation in motor neurons, swimming deficits and shorter, excessively branched motor axons in zebrafish (Kabashi et al., 2010), rescued by co-expressing WT TDP-43.

Modulation of TDP-43 expression via the formation of pathological aggregates, mislocalisation from the nucleus to the cytoplasm and reduction in expression lead to neurite abnormalities consistent with alterations to the neuronal cytoskeleton. In order to understand how TDP-43 may affect neurites and the cytoskeleton, it is important to understand the normal function of the protein.

1.7 THE ROLE OF TDP-43 IN CYTOSKELETAL PATHOLOGY AND FUNCTION

1.7.1 Normal function of TDP-43

TDP-43 is a highly conserved and ubiquitously expressed protein, located on chromosome 1p36.2 (Buratti, 2001). Full length TDP-43 protein contains a number of functional domains including two RNA recognition motifs (RRM1 and RRM2); an NLS and nuclear export sequence (NES) which allow it to shuttle between the nucleus and cytoplasm; and a glycine-rich domain thought to be important for

protein-protein interactions (Figure 1.2). TDP-43 is part of the heterogeneous nuclear ribonucleoprotein (hnRNP) family of nuclear factors, which are highly regulated proteins which undergo autoregulation. By binding to its own 3' untranslated region (UTR) of mRNA, TDP-43 initiates nonsense-mediated decay and is able to degrade mRNAs with premature translation-termination codons (Ayala et al., 2011). Tight regulation of TDP-43 expression is important for its normal functioning with both increases and decreases causing neurodegeneration. In the healthy brain, TDP- 43 is predominantly nuclear in neurons (Fiesel et al., 2010) and is also present at lower levels within the cytoplasm. Knockout studies provide information about the normal the role of the protein and show that knockout of the *Tardbp* gene in mice is embryonic lethal within 3.5–7.3 days post-fertilisation (Kraemer et al., 2010; Sephton et al., 2010; Wu, Cheng, & Shen, 2012), suggesting that TDP-43 is critical during early developmental processes such as transcription and/or mRNA splicing and processing (Sephton et al., 2010). The protein has distinct nuclear and cytoplasmic functions, enabled by its NLS and NES domains. Within the nucleus, TDP-43 plays a variety of roles in the splicing of mRNA and processing of microRNAs. Within the cytoplasm it localises to stress granules where it is thought to play roles in trafficking and stabilizing mRNA (Colombrita et al., 2009; Dewey et al., 2011; McDonald et al., 2011).

1.7.2 Role of TDP-43 in neurites

Emerging evidence shows that TDP-43 may also play an important role in the development of neurites. TDP-43 is expressed at high levels during development within the mouse cortex and hippocampus (embryonic day 18 to postnatal day 7) and then decreases into adulthood (Liu et al., 2015). This timing corresponds to the period of maximum neurite outgrowth and branching (Workman et al., 2013) providing evidence for a role in the development of neurites. Neurite outgrowth may be regulated by TDP-43 in the nucleus (where it is predominately found), or out in the axons and synapses/growth cones, where TDP-43 is also present. Fallini and colleagues (2012) demonstrated that TDP-43 particles found within neurites are motile and increase in number following treatment with brain-derived

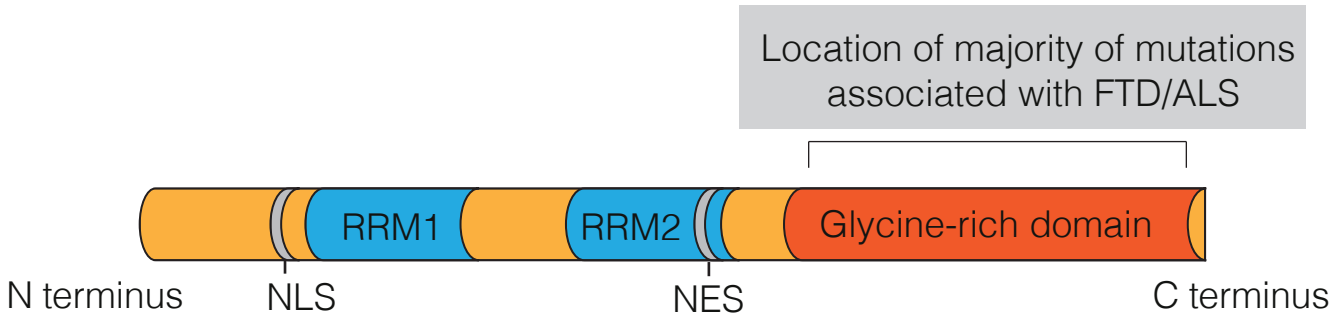
Location of majority of mutations associated with FTD/ALS
RRM1
RRM2
Glycine-rich domain
N terminus
NLS
NES
C terminus

Figure 1.2 TDP-43 protein structure. TDP-43 protein contains two RNA-cognition motifs (RRM1 and RRM2), a nuclear localisation signal (NLS), nuclear export signal (NES) and a carboxy-terminal glycine-rich domain. The majority of mutations associated with FTD/ALS occur in the glycine-rich domain. Figure adapted from Lee, Lee, and Trojanowski (2012).

neurotrophic factor (BDNF). In cultured motor neurons, these TDP-43 particles colocalise with other mRNA binding proteins (mRBPs) such as FMRP, IMP1 and HuD (Fallini et al., 2012). Subsequent studies located TDP-43 within messenger ribonuclear protein particles (mRNPs) which are bi-directionally transported and deliver mRNAs, such as both mouse and human *Nefh*/*NEFH*, down axons to their distal targets (Alami et al., 2014). This function may be particularly important for *in situ* protein translation, which TDP-43 may also regulate (Liu-Yesucevitz et al., 2011). Mutations to ALS-related genes may impair this TDP-43 function by reducing mRNP trafficking (Alami et al., 2014). Together, these studies demonstrate that TDP-43 is expressed in different neuronal compartments, and that it plays important roles wherever it is expressed.

1.7.3 Regulation of the neuronal cytoskeleton by TDP-43

Aside from its presence in distal neuronal compartments, implying transport-related interactions with the cytoskeleton, TDP-43 has also been shown to directly bind to and regulate several cytoskeletal elements. For example, it binds to the 3'UTR of *Nefl* mRNA, stabilising it within the nucleus and regulating its translocation to the cytosol, where it may also regulate its translation (Strong et al., 2007; Volkening, Leystra-Lantz, Yang, Jaffee, & Strong, 2009). In ALS, affected motor neurons within the spinal cord contain neurofilament aggregates with a proportionally lower amount of NFL than usual (Strong, Kesavapany, & Pant, 2005). In a NFL knockout mouse model, TDP-43 was abnormally increased, without abnormal localisation or aggregate formation (Liu et al., 2015), and age-related changes in the phosphorylation state of TDP-43 were also observed. This aberrant TDP-43 phosphorylation in disease might plausibly alter its binding to *NEFL* mRNA, which could contribute to aggregates by affecting NFL stability and transport.

TDP-43 may also be involved in microtubule stability. Silencing TDP-43 expression resulted in downregulation of histone deacetylase 6 (HDAC6), through a specific interaction between HDAC6 and the C-terminal and RNA binding domains of TDP-43 (Fiesel, Schurr, Weber, & Kahle, 2011;

Fiesel et al., 2010). HDAC6 deacetylates and thus destabilises microtubules (Hubbert et al., 2002) and is important in intracellular trafficking and branch formation (Valenzuela-Fernández, Cabrero, Serrador, & Sánchez-Madrid, 2008). Several lines of evidence using *Drosophila* show an interaction of the TDP-43 homolog, *TBPH,* and MAP1b homolog, *futsch*. Deletion of *TBPH* altered neuromuscular junctions and synaptic boutons which were attributed to cytoskeletal defects caused by down-regulating *futsch* (Godena et al., 2011). Further studies showed that TBPH binds to the 5'UTR of *futsch* mRNA and increases its translation (Romano et al., 2014). TBPH is also important for localisation and translation of futsch protein in motor neurons (Coyne et al., 2014).

These data provide further evidence that TDP-43 is a key regulator of cytoskeletal elements important for the health and maintenance of neurites, and that altering its expression (in models and human disease) can cause neurite pathology, and impact the integrity of neurons. Alterations to TDP-43 in ALS and FTLD cases may lead directly to changes to the neuronal cytoskeleton, ultimately damaging neurites and killing neurons. However, it is still not well understood how TDP-43 maintains cytoskeletal health, and how that becomes disrupted in disease, particularly in cases of FTLD and ALS where TDP-43 itself is not mutated.

A major genetic cause of TDP-43 pathology in both FTLD and ALS is mutations to *C9ORF72.* Little is known about the normal function of the C9ORF72 protein and it is currently unclear how *C9ORF72* mutations lead to abnormal accumulation and mislocalisation of TDP-43.

1.8 THE ROLE OF C9ORF72 IN CYTOSKELETAL PATHOLOGY AND FUNCTION

1.8.1 C9ORF72 and disease

In 2011, a repeat expansion in a non-coding region of *C9orf72* was identified as the most common genetic cause of FTD and ALS (DeJesus-Hernandez et al., 2011; Renton et al., 2011). The mechanisms by which this mutation causes disease are currently unknown, perhaps including RNA toxicity or unconventional translation of the nucleotides within the repeat expansion. Alternatively, disease could

be due to loss of function of the encoded protein. There are several reports of reduction in *C9ORF72* mRNA from FTD and ALS patient tissue and patient-derived cell lines (Belzil et al., 2013; Ciura et al., 2013; Cooper-Knock et al., 2012; DeJesus-Hernandez et al., 2011; Gijselinck et al., 2012; Xi et al., 2013) and also reduction of C9ORF72 protein within the affected frontal regions of FTD/ALS brains (Waite et al., 2014; Xiao et al., 2015).

1.8.2 Normal role of C9ORF72

Currently, little is known about the normal function of the C9ORF72 protein. In humans, the *C9ORF72* gene codes three alternatively spliced transcripts that are expressed widely, including the brain. Alternative splicing of these transcripts produces short and long isoforms (C9-S and C9-L) (Renton et al., 2011). Antibodies specific to these two isoforms have demonstrated that within Purkinje neurons and spinal motor neurons, C9-L has diffuse cytoplasmic labeling, whereas C9-S localises to the nuclear membrane (Xiao et al., 2015). Further descriptions of the expression and localisation of C9ORF72 are currently lacking.

The function of C9ORF72 has been inferred by homology with other proteins containing the Differentially Expressed in Normal Neoplasia (DENN) domain, which function as guanosine diphosphate/guanosine triphosphate (GDP/GTP) exchange factors (GEFs) for Rab GTPases (Levine, Daniels, Gatta, Wong, & Hayes, 2013). Rab proteins mediate membrane trafficking (Marat, Dokainish, & McPherson, 2011), implying that C9ORF72 may indirectly regulate this function (Levine et al., 2013). Farg et al. (2014) confirmed this role by showing C9ORF72 co-localisation with Rabs involved in endolysosomal trafficking; furthermore, knockdown of C9ORF72 expression impaired endocytosis and autophagy (Farg et al., 2014b). Additional studies have strengthened this association, showing that reduced expression of C9ORF72 in culture (Webster et al., 2016) or knockout mice (O'Rourke et al., 2015; Sullivan et al., 2016) disrupts autophagy.

1.8.3 C9ORF72 and the neuronal cytoskeleton

In line with evidence that other FTD/ALS proteins regulate the cytoskeleton, C9ORF72 has also been linked with actin and actin dynamics. Actin is an interacting partner of C9ORF72 and the two proteins colocalise in immunocytochemical studies (Farg et al., 2014), as does the cytoskeletal protein cofilin (Sivadasan et al., 2016). Cofilin is an actin binding protein which modulates actin organisation and dynamics (Bravo-Cordero, Magalhaes, Eddy, Hodgson, & Condeelis, 2013). shRNA knockdown of C9ORF72 in cultured motor neurons reduced actin filament production, and truncated axons and growth cones, accompanied by enhanced cofilin phosphorylation which is also observed in human iPSC-derived motor neurons and post mortem tissue from patients with C9ORF72 expansion (Sivadasan et al., 2016). The opposite was observed when C9ORF72 was overexpressed. C9ORF72 depletion also changed the activity of guanine nucleotide exchange factor protein family members, Rac1 and Arf6 (Sivadasan et al., 2016), which the authors suggested indicates that C9ORF72 modulates small GTPases and thus actin dynamics.

While the normal functions of the C9ORF72 protein are not yet well described, evidence suggests that C9ORF72 may influence the neuronal cytoskeleton.

1.9 SUMMARY AND PROJECT AIMS

Accumulating evidence suggests that proteins that become dysregulated in FTD and ALS may affect the neuronal cytoskeleton, which is of particular interest in these diseases due to the neurite pathology and dysfunction observed in post-mortem brains and animal models. Modulation of the neuronal cytoskeleton is a compelling target for providing therapeutic protection to vulnerable cellular components, such as the axon. The purpose of this thesis was to examine the normal function of TDP-43 and C9ORF72, and their links to the cytoskeleton.

Aim 1: Determine the effect of TDP-43 overexpression on neurite development in culture

TDP-43 is transported into neurites in an activity-dependent manner, where it regulates neurite growth, and is also involved in the transport of mRNA into the neurites for *in situ* protein translation. The way in which TDP-43 controls these processes is still not well understood. The first aim sought to investigate global protein changes and alterations to cytoskeleton-dependent processes such as neuron morphology and growth cone morphology, using a primary cell culture model from mice overexpressing wildtype TDP-43.

Aim 2: Determine the effects of altered TDP-43 on axons within the central nervous system

Mislocalisation of TDP-43 from the nucleus to the cytoplasm is a key pathological feature of FTD and ALS. The consequences of increased cytoplasmic expression of TDP-43 on axons are not well understood. This is partly due to the lack of mouse models that allow detailed examination of axon structures. The second aim of this thesis was to investigate the cellular effects of overexpression of wildtype TDP-43 and mislocalised TDP-43 within the retina ganglion cells and their axons. Additionally, this aim was directed at creating and optimizing a novel model to investigate axonal alterations *in vivo*, by using adeno-associated virus to induce altered expression of TDP-43 in retinal ganglion cells.

Aim 3: Examine the distribution of C9ORF72 to determine potential roles within neurites

Several mechanisms for how the non-coding repeat expansion in C9ORF72 may lead to disease have been described, however little is known about the normal function and the expression pattern of the C9ORF72 protein. This aim sought to characterise the expression pattern and cellular localisation of the three reported mouse isoforms of C9orf72 in order to provide insight into the normal function of this protein.

Chapter 2:

Materials & Methods

2 MATERIALS & METHODS

2.1 ANIMAL CONDITIONS AND CARE

All experiments involving animals were approved by the University of Tasmania Animal Ethics Committee (approvals A12780, A15120, A15121, A14189, A16522), in accordance with the Australian Code of Practice for the Care and Use of Animals for Scientific Purposes (National Health and Medical Research Council, 2013). Animals were housed in standard conditions at 20°C, on a 12/12-hour light/dark cycle with *ad libitum* access to food and water.

2.2 PRIMARY CELL CULTURE

2.2.1 Preparation of culture surfaces

Primary culture cells were plated onto a variety of surfaces. For immunocytochemistry, cells were plated onto 13mm coverslips (Menzel-Glaser) etched in 70% nitric acid for four hours, rinsed in running water for 30 minutes, then 3 x 10 minutes in MilliQ water, dried, autoclaved and placed singly into 24 well trays. For studies involving protein extraction, 12 well culture trays were utilised. All surfaces were coated with 10% poly-L-lysine (Sigma-Aldrich) diluted in Hanks Balanced Salt Solution (HBSS, Gibco) overnight. Poly-L-lysine was removed and replaced with initial plating media consisting of Neurobasal medium (Gibco), 2% B27 supplement, 10% fetal calf serum (Gibco), 0.5mM glutamine, 25mM glutamate and 1% antibiotic/antimycotic (Gibco).

2.2.2 Primary cortical neuron culture

Primary dissociated cortical cell cultures were prepared from embryonic day (E) 15.5 C57Bl/6 mice (unless otherwise stated), which were harvested from pregnant mice euthanised by carbon dioxide exposure. Fetuses were removed from their sacs and placed on ice followed by rapid decapitation. Brains were exposed by removing skin, skull and meninges, and cortical tissue from both hemispheres was collected into 5ml of HBSS. Tissue was dissociated with 0.0125% trypsin for 4

minutes, followed by addition of initial plating media described in section 1.2.1 above. Cells then underwent gentle trituration with a 1ml pipette. Viable cell numbers were assayed using Trypan Blue (Sigma Aldrich) exclusion and cells were plated onto 12mm coverslips (Menzel-Gläser, Germany; prepared as in section 2.2.1) in 24 well plates (Corning Inc) at a density of 30,000 (for 24 well plates) or 200,000 (for 12 well plates) viable cells per coverslip. Each well contained initial plating medium, replaced on the following day with subsequent growth medium (initial medium without the fetal calf serum and glutamate), after which half the media was replenished weekly with fresh subsequent growth medium. Cultures were grown at 37°C and 5% CO_2.

2.3 IMMUNOCYTOCHEMISTRY

Following removal of media, cells were gently washed with phosphate buffered saline (PBS; 0.01M) and fixed in 4% paraformaldehyde (PFA) for 15 minutes at room temperature on an orbital shaker. Coverslips were washed (3 x PBS, 10 minute intervals) and then blocked with blocking solution containing 0.01 PBS, 1% BSA (Sigma Aldrich) and 0.3% Triton X-100 (Sigma Aldrich) for 30 minutes. Coverslips were then placed on wax sheets in a humidity chamber and 50µL of primary antibody combinations diluted in 0.6% Triton X-100 in PBS (PBS-T) applied overnight at 4°C. Coverslips were returned to 24 well plates and washed to remove unbound antibody (3 x 10 minutes PBS). Species-appropriate secondary antibodies (Goat anti-chicken IgY, Thermofisher Scientific, reference number A11039, 1:1000; Goat anti-mouse IgG, Thermofisher Scientific, reference number A11029, 1:1000; Goat anti-rabbit IgG, Thermofisher Scientific, reference number A11034, 1:1000) were diluted in PBS, and applied for 2 hours with agitation in the dark at room temperature. Secondary antibodies were removed and coverslips were incubated with DAPI (Molecular Probes, Invitrogen) at a concentration of 5µg/ml in dH_2O for 5 minutes with agitation in the dark at room temperature.

Coverslips underwent final washes (2 x 10 minutes PBS, then milliQ rinse) and then mounted, cell-side down, onto slides (Livingston International) using fluorescent mounting medium (Dako).

2.4 ANIMAL PERFUSION AND TISSUE PROCESSING

Animals were euthanised by injection of sodium pentobarbitone (110mg/kg i.p.) and transcardially perfused with 4% PFA in PBS for immunohistochemical studies and PBS for biochemical studies. Tissue was dissected immediately and post-fixed for 24 hours in 4% PFA in PBS for immunohistochemical studies or snap frozen in liquid nitrogen and stored at -80°C for biochemical studies.

2.5 IMMUNOHISTOCHEMISTRY

2.5.1 Cryoprotection and sectioning

Tissue for immunohistochemistry was cryoprotected in increasing concentrations of sucrose (18% then 30%) with 0.2% NaN_3 in PBS until equilibrated, then embedded in Optimal Cutting Temperature (OCT; Tissue-Tek) medium, frozen and sectioned at -25°C using a Leica CM 1850 UV Cryostat.

2.5.2 Antigen Retrieval

Paraformaldehyde fixation can mask antigens to the extent that antibodies are unable to bind to their epitopes (Leong & Leong 2007), requiring antigen retrieval such as formic acid and citrate buffer treatments. Citrate buffer antigen retrieval optimised TDP-43 and C9ORF72 labeling for most tissue, and was subsequently used when labeling with these antibodies. Free floating sections were loaded into cassettes between two sections of Tally-Ho paper (Imperial Tobacco), or mounted onto charged slides (Dako), and were placed in a plastic container containing 5000ml of 0.1M citrate buffer,

prepared from citric acid (Sigma Aldrich; pH 6.0). This container was placed in a pressure cooker (Russel Hobbs) containing 500ml distilled water, set to maximum temperature for 6 minutes and then to moderate-high temperature for 14 minutes. Sections were cooled to 25°C prior to placing in PBS.

2.5.3 Indirect Fluorescent Immunohistochemistry (IHC)

Free-floating sections or mounted slides were washed (3 x 10 minute PBS) before non-specific binding sites were blocked in serum-free Protein Block solution (Dako) for 20 minutes at room temperature. Primary antibodies diluted in PBS-T were added, and incubated with agitation at room temperature overnight. Optimum concentrations were determined for each antibody and no-primary controls were performed. Sections were washed (3 x 10 min PBS-T) and species-specific secondary antibodies diluted in PBS were applied for 2 hours in the dark at room temperature with agitation. Sections were incubated with DAPI (Molecular Probes, Invitrogen) at a concentration of 5µg/ml in PBS for 5 minutes with agitation in the dark at room temperature. Sections underwent further washes (3 x PBS, 10 minute intervals) and were then mounted onto glass slides (Livingston International) and coverslipped (Livingston International) using fluorescent mounting medium (Dako).

2.6 WESTERN BLOTTING

2.6.1 Protein extraction for Western blotting

For cell culture studies, protein was extracted in 100µL radioimmunoprecipitation assay (RIPA) lysis buffer (Sigma Aldrich) containing protease (Complete Mini Protease Inhibitor Cocktail tablets, Roche) and phosphatase inhibitors (A.G. Scientific Inc). For tissue studies, 3mg/ml of lysis buffer was added to tissue. Samples were homogenised with an Ultra-Turrax homogeniser (IKA TIO basic, IKA Works). Protein from both cell culture and tissue studies was then maintained with constant agitation for 30

minutes at 4°C and the centrifuged for 20 minutes at 13,000rpm at 4°C. Supernatant was collected and frozen at -80°C until needed.

2.6.2 Nuclear and cytoplasmic fractionation studies

Nuclear and cytoplasmic fractionation was carried out on cultured cortical neurons (Chapter 3) or neocortical tissue (Chapter 5) according to manufacturer's instructions with some minor adjustments (NE-PER Nuclear and Cytoplasmic Extraction Kit, Thermofisher Scientific). Briefly, cultured cells were harvested from 12 well culture plates with 100µL of CERI, with protease and phosphatase inhibitors, using a cell scraper. Alternatively, neocortical tissue was homogenised in 200µL of CERI, with protease and phosphatase inhibitors, with a Ultra-Turrax homogeniser (IKA® TIO basic, IKA Works). Subsequent reagent volumes were adjusted accordingly and the protocol was completed using manufacturer's instructions.

2.6.3 Protein quantification

Concentrations of extracted protein were determined by performing a Bradford assay (Bio-Rad Laboratories) following manufacturer's instructions. BSA protein standards from 0.125mg/mL to 4mg/ml were prepared to construct a standard curve. Absorbance was measured on to SpectraMax Plus 384 Absorbance Reader (Molecular Devices) and subsequent protein concentrations were calculated using this standard curve.

2.6.4 Gel electrophoresis and Western blot

Bolt 4×lithium dodecyl sulphate (LDS) sample buffer and 10×Bolt sample reducing buffer were added to 15µg of protein and denatured at 95°C for 5 minutes. Samples were loaded onto 4-12% Bolt Bis-TRIS Plus gels and electrophoresed for 20 minutes at 200V in Bolt MES running buffer (all Life Technologies). Gel electrophoresis was performed per manufacturer's protocol (Life Technologies). Resolved proteins were then transferred to 0.2µm polyvinylidene fluoride (PVDF) membranes (Bio-

Rad Laboratories) via electrophoresis in Bolt Transfer buffer for 1 hour at room temperature. Following transfer, the membrane was washed in 1x Tris buffered saline with 0.1% Tween-20 (Bio-Rad Laboratories; TBS-T) and then non-specific binding was blocked via incubation in 5% commercial skim powder in TBS-T (blocking solution) for 2 hours at room temperature. The membrane was incubated in primary antibody diluted in blocking solution for 2 hours at room temperature. Membrane was washed (3 x 10 minutes TBS-T), followed by incubation with species-appropriate HRP secondary antibody (Dako) diluted in blocking solution for 2 hours at room temperature with agitation. Membranes were washed (3 x 10 minutes TBS-T) and then immunoreactivity was detected by incubation in Immobilon chemiluminescent HRP substrate (Millipore) for 2 minutes, and quantified using the Amersham Imager 600 (GE). If additional antibody labelling was required, membranes were stripped with 0.1M glycine, pH 2.9 for 30 minutes at room temperature with agitation. Membranes were rinsed in TBS-T and blocked overnight in blocking solution at 4°C with agitation. The following day, immunolabeling was carried out as described.

2.7 STATISTICAL ANALYSIS

All counts and analyses were performed blinded to genotype. Numbers of repeats (n) are detailed in each chapter, with a minimum of n=3 biological replicates for quantitation (animals (Chapters 4 and 5), cultures (Chapters 3 and 5) or embryos (Chapter 3)). For Chapter 3, a minimum of 3 embryos were taken from a minimum of 2 mother mice. Western blot analyses also had 3 experimental repeats from each sample to account for variation in blotting. Unless otherwise stated, statistical analyses were carried out using one-way ANOVA with Tukey's post hoc test (GraphPad Prism, version 5). Data are presented ± standard error of the mean (SEM) and significance set at $p<0.05$.

Chapter 3:

Effects of overexpression of TDP-43 on neuron proteome and morphology

3 EFFECTS OF OVEREXPRESSION OF TDP-43 ON THE NEURON PROTEOME AND MORPHOLOGY

3.1 INTRODUCTION

A prominent feature of ALS/FTD tissue are extensive neurite abnormalities, including neuromuscular dieback, axonal and dendritic swellings, swollen presynaptic terminals, reduced dendritic arbourisation, spine loss and transport deficits, indicated by accumulation of abnormal organelles (Brettschneider et al., 2014; Brettschneider et al., 2013; Ferrer et al., 1991; King, Maekawa, Bodi, Troakes, & Al-Sarraj, 2011; Sasaki & Iwata, 1996; Zhou et al., 1998). Neurite abnormalities are linked to cytoskeletal disruption (Vickers et al., 2009).

TDP-43 pathology is present in 95% of ALS cases and 50% of FTD cases, usually due to mislocalisation from the nucleus to the cytoplasm where it forms aggregates. TDP-43 pathology is also found within dystrophic neurites in ALS and FTD (Braak et al., 2010; Hatanpaa et al., 2008) and white matter tract degeneration is associated with FTLD-TDP (Armstrong, 2017). The links between TDP-43 pathology and neurite abnormalities are unclear, however there is accumulating evidence that TDP-43 plays a normal role in regulating the cytoskeleton, and that disruption to TDP-43 in disease conditions is sufficient for neurite abmormalities.

TDP-43 is essential during neuronal development (Sephton, Cenik, Cenik, Herz, & Yu, 2012) and is upregulated during development when circuit formation is occurring (Liu et al., 2015). TDP-43 binds directly to *NEFL* mRNA to stabilize it, and regulates translocation of *NEFL* mRNA to the cytosol (Strong et al., 2007; Volkening et al., 2009). TDP-43 is a predominantly nuclear protein where it exerts the majority of its functions (reviewed in Lee et al., 2012)) but is also present in distal neuron compartments where it is important for transport of messenger ribonucleoprotein particles down axons to their distal targets (Alami et al., 2014). The localisation of TDP-43 expression in neurites and its ability to directly regulate cytoskeletal elements suggest that alterations to TDP-43 expression may be

a driver of neurite abnormalities in disease. In fact, mutations to TDP-43 can cause cellular toxicity and abnormal expression of TDP-43 to axons (Tripathi et al., 2014) as well as impair the transport of messenger ribonuclear proteins and reduce axonal outgrowth (Alami et al., 2014; Fallini et al., 2012). These data suggest that mutations in TDP-43 relevant to ALS could cause impairment to axonal function through a direct role of TDP-43 in the regulation of the integrity of the cytoskeleton.

This study sought to further investigate how TDP-43 may exert effects on the neuronal cytoskeleton. Primary neuronal cultures were prepared from transgenic mouse overexpressing wildtype human TDP-43 under the control of the prion promoter (hTDP-43_{Prp}). The heterozygous and homozygous hTDP-43_{Prp} mice express at 1.9 and 2.5 times the rates of endogenous TDP-43 protein, respectively (Xu et al., 2010). Postnatal heterozygous mice are viable and lack pathological changes, however homozygous mice develop a severe degenerative phenotype by 4 to 6 weeks of age, accompanied by TDP-43 aggregates and mislocalisation to the cytoplasm in the brain and spinal cord (Xu et al., 2010). Other abnormalities include mitochondrial changes, gliosis and – importantly – axonal and myelin degeneration within the spinal cord (Xu et al., 2010).

Primary neurons cultured from these mice are an ideal way to carry out detailed examination of the effect of TDP-43 overexpression, which occurs in disease (Geser, 2008; Mishra et al., 2007), on the expression of cytoskeletal proteins and the downstream effects of this on the neurite. Two main approaches were taken in this study. Firstly, proteomics, which have previously been used to identify interacting partners of TDP-43 (Freibaum, Chitta, High, & Taylor, 2010) allow analysis of global changes to proteins following alteration to TDP-43 expression. Secondly, neuron morphology was analysed to determine the effect of TDP-43 alterations to developmental processes such as neurite outgrowth and branching, which require specific expression and organisation of the cytoskeleton. The results from these studies will provide further insight into how alterations in the expression level of TDP-43 may cause changes to neurites.

3.2 METHODS

3.2.1 Animals

TDP-43$_{Prp}$ mice (Xu et al., 2010) (C57BL/6-Tg(Prnp-TARDBP)3cPtrc/J, Jackson Laboratories, stock number 016608) were utilised in this study. Due to the phenotype developed by homozygous mice, colonies were maintained as heterozygotes for breeding stock. For culture studies, heterozygote mice were mated to obtain homozygous, heterozygous and wildtype embryos. All experiments involving animals were approved by the University of Tasmania Animal Ethics Committee (A15121) and were in accordance with the Australian Guidelines for the Care and Use of Animals for Scientific Purposes (National Health and Medical Research Council, 2013).

3.2.2 Genotyping

For genotyping of mice from the maintenance colony (heterozygous and wildtype mice), genomic DNA from tail clippings was obtained from mice at weaning was extracted according to manufacturer's instructions (Quanta Biosciences). Genotypes (heterozygote and wildtype) were then determined by conventional PCR using the MyTaq™ Red Mix (Bioline) using primers specific to hTDP-43 and Tcrd internal control (Table 3.1). The PCR conditions are outlined in Table 3.2. Products were electrophoresed in a 2% agarose gel, containing 1% SYBR safe DNA gel stain (Invitrogen) at 125V for 35 minutes. Gels were visualised using the Amersham Imager 600 (GE) with a 400bp band for mutant and 200bp band for wildtype. To determine zygosity of embryos cultured from two heterozygous parents, quantitative real time PCR (qPCR) was utilised. Genomic DNA was extracted from embryonic liver using the Isolate II Genomic DNA Extraction Kit (Bioline), with precaution taken to avoid contamination from the mother's blood. qPCR was carried out using GoTaq® Probe qPCR Master Mix with a maximum of 150ng of liver DNA and the following primer sets outlined in Table 3.3. qPCR conditions are outlined in Table 3.4.

Table 3.1 Conventional PCR primer information

Primer	Sequence 5'-3'
hTDP-43 Forward(20µM)	GGATGAGCTGCGGGAGTTCT
hTDP-43 Reverse (20µM)	TGCCCATCATACCCCAACTG
Tcrd internal control forward (20µM)	CAAATGTTGCTTGTCTGGTG
Tcrd internal control reverse(20µM)	GTCAGTCGAGTGCACAGTTT

Table 3.2 Conditions for conventional PCR

Cycle step	Incubation times
Initial denaturation	94°C 2 min
10 cycles	Step 1: 94°C for 20 sec Step 2: 64°C (-0.5°C/cycle) for 15 sec Step 3: 68°C for 10 sec
Amplification (28 cycles)	Step 1: 94°C for 15 sec Step 2: 60°C for 15 sec Step 3: 72°C for 10 sec
Final extension	72°C for 2 min
Hold	11°C infinite

Table 3.3 qPCR primer information

Primer	5' label	Sequence 5'-3'	3' label
Tg Forward(40µM)		GTACGGGGATGTGATGGATG	
Tg Reverse (40µM)		CGCAATCTGATCATCTGCAA	
Tg probe (40µM)	6-FAM	CCAAGCCATTCAGGGCCTTTGC	Black Hole Quencher 1
Apob internal control forward (100µM)		CACGTGGGCTCCAGCATT	
Apob internal control reverse(40µM)		TCACCAGTCATTTCTGCCTTTG	
Internal control probe (5µM)	Cy5	CCAATGGTCGGGCACTGCTCAA	Black Hole Quencher 2

Table 3.4 Conditions for qPCR

Cycle step	Incubation times
Initial denaturation	94°C 2 min
Hot start (10 cycles)	Step 1: 94°C for 30 sec Step 2: 64°C (-1°C/2 cycles) for 45 sec Step 3: 68°C for 30 sec
Amplification (28 cycles)	Step 1: 94°C for 30 sec Step 2: 60°C for 45 sec Step 3: 72°C for 30 sec (aquisition)
Final extension	72°C for 2 min

3.2.3 Primary Cell Culture

Primary dissociated cortical cultures were prepared as described in Chapter 2.2.2 with slight modifications. Heterozygous mice were mated and resulting embryos were harvested at embryonic day (E) 15.5. Each embryo was cultured individually and liver tissue was collected for genotyping as outlined in section 3.2.2. Following decapitation heads were stored in Hibernate media (Gibco) at 4°C until time of culture (10 minutes to 1 hour). Cortical tissue (including both cortex and hippocampus) were collected into 1ml HBSS and enzymatically dissociated in 0.0125% trypsin for 4 minutes, prior to plating. Cells were plated onto a variety of surfaces, pre-coated with poly L-lysine (Sigma Aldrich; details in Chapter 2.2.1). For immunofluorescence and neurite outgrowth assays, cells were plated onto 12mm coverslips at a concentration of 30,000 viable cells per coverslip. For protein harvest, whole cells were plated into 12 well trays at a concentration of 200,000 viable cells per well. Cells were grown as described in Chapter 2.2.2.

3.2.4 Western blotting

Protein was harvested from whole cells plated in 12 well trays at 3 DIV in 100µL of RIPA buffer (Sigma) containing protease (Complete Mini Cocktail, Roche) and phosphatase inhibitors (AG Scientific). Protein quantification and Western blotting were carried out as described in Chapter 2.6. Following western blotting, membranes were incubated in human TDP-43 (Novus Biologicals, reference number H00023435, 1:1000; Zhang, 2008), total TDP-43 (binding to both mouse and human

TDP-43; Proteintec Group; reference number 1078-2-AP, 1:1000), GAPDH (Millipore, reference number MAB374, 1:5000), Lamin-AC (Santa Cruz, reference number SC-376248, 1:250).

3.2.5 Nuclear and cytoplasmic distribution

The distribution of total TDP-43 in the nucleus and cytoplasm was determined by immunocytochemistry and nuclear/cytoplasmic fractionation. For immunocytochemistry (outlined in Chapter 2.3, and Chapter 3.7.2), careful attention was paid to ensure that coverslips were consistently fixed, incubated with antibody, washed and imaged with identical exposures. MAP2 and DAPI were used to delineate cytoplasm and nuclei, regions of interest (ROIs) were constructed around these cellular compartments and the integrated density of TDP-43 labeling in these areas was measured as previously described (Herzog, Deshpande, Shapiro, Rodal, & Paradis, 2017) (Figure 3.1A). For cellular fractionation, nuclear and cytoplasmic proteins were extracted from cells at 3 DIV as described in Chapter 2.6.2, followed by Western blotting (Chapter 2.6).

3.2.6 Proteomic mass spectrometry

3.2.6.1 Protein harvest

Protein was harvested from wildtype and homozygous neurons which had been plated in 12 well plates and grown to 10 DIV. One hundred microliters of lysis buffer (7M urea, 2M thiourea and 30mM tris) containing protease (Complete Mini Cocktail, Roche) and phosphatase inhibitors (AG Scientific) was used to extract protein. Cells were sonicated (for 1 minute with 15 seconds in the sonicator, 5 second out in ice), kept at 4°C for 2 hours, centrifuged at 13,000 rpm for 15 minutes, and supernatant collected. Protein concentration was determined by performing a Bradford assay as per manufactures protocol (BioRad Protein Assay, BioRad, Chapter 2.6.1). SDS-PAGE followed by silverstaining (BioRad, according to manufacterers instructions) was carried out on a sample of each of the extractions to verify that approximately equal amounts of protein were digested.

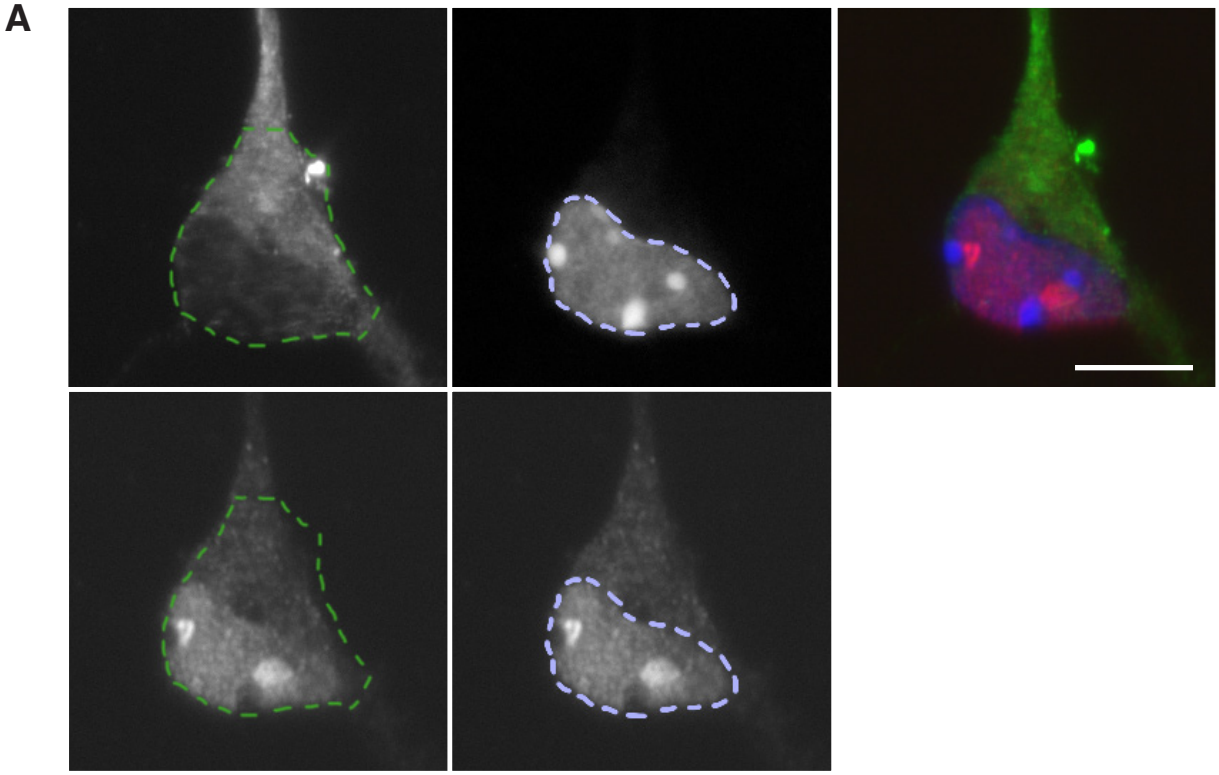
A

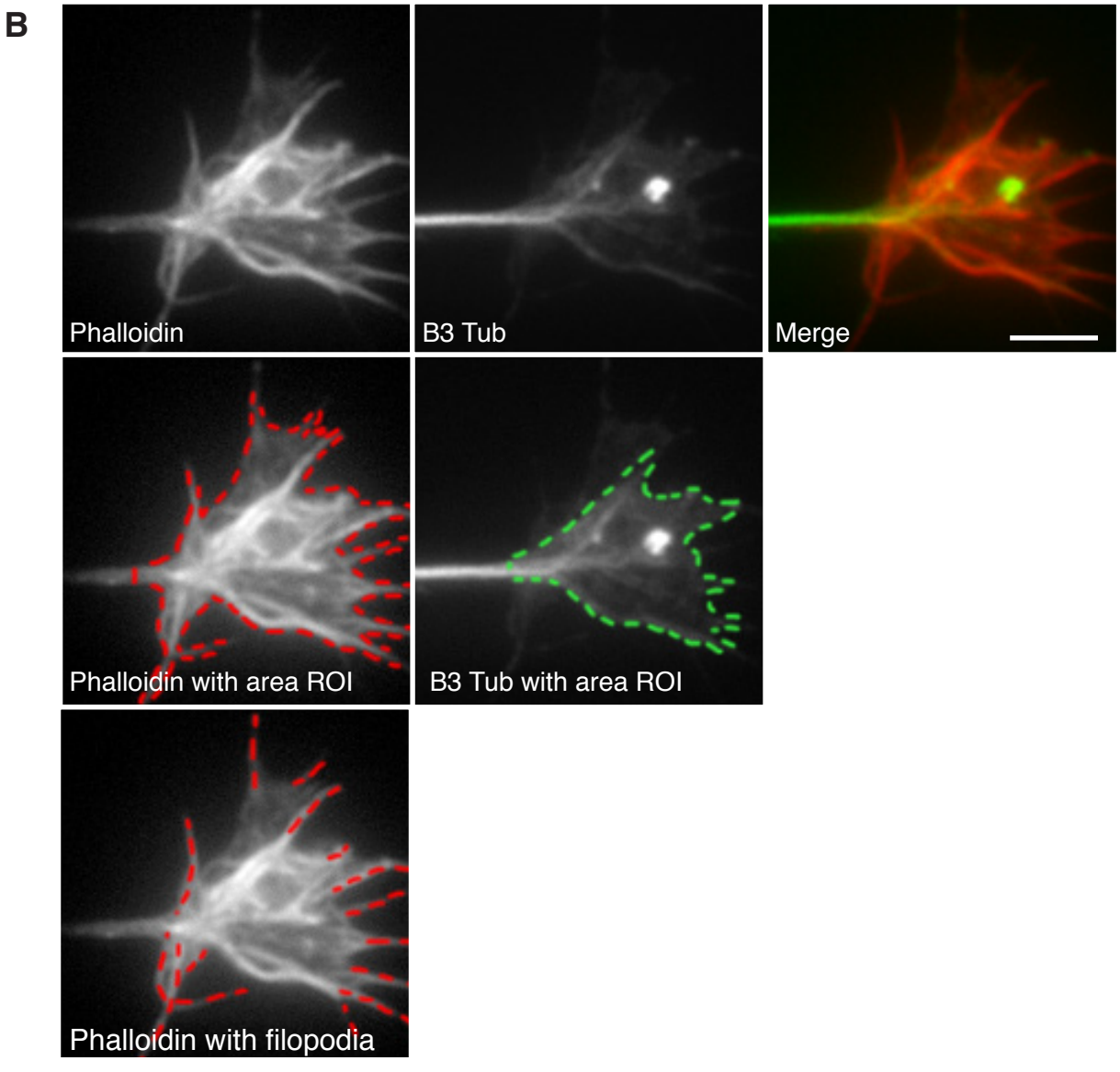
B
Phalloidin
B3 Tub
Merge
Phalloidin with area ROI
B3 Tub with area ROI
Phalloidin with filopodia

Figure 3.1 Quantitation of immunocytochemical images. (A) Representative images of cortical neurons immunolabelled with MAP2 (green), TDP-43 (red) and stained with DAPI (blue). Dotted lines show boundaries of MAP2 labelling (green) and DAPI staining (blue). (B) (I) Representative images of cortical neurons immunolabelled with B3 tubulin (green) and stained with phalloidin (red). (II) Dotted line (red) used to quantify F-actin area. (III) Dotted line (green) used to quantify tubulin area. (IV) Dotted line (red) used to quantify filopodia length. Scale bars: A 10μm, B 5μm.

3.2.6.2 Formation of tryptic peptides

Peptides were prepared from samples according to established methods (Wilson et al., 2010). Briefly, samples were reduced by adding 10µL of dithiothreitol (DTT; 100mM; BioRad) to 90µL of protein at a concentration of 1mg/ml and incubated overnight at 4°C. Samples were then alkylated by adding 11µL of iodoacetamide (500mM) and incubated for 2 hours in the dark at room temperature. Proteins were digested by adding 1µL of trypsin from porcine pancreas (Sigma-Aldrich, 1mg/ml) to the tube containing proteins and flushed into the sample with 1ml of chilled methanol. Samples were incubated overnight at -20°C. The resulting peptides were collected by centrifugation at 13,000rpm for 5 minutes. Pellets were air-dried and reconstituted in 100µl of ammonium bicarbonate (Sigma-Aldrich; 100 mM) for 5 hours at 37°C. After 3 hours of incubation, an additional 1µL of trypsin was added to samples.

3.2.6.3 Liquid chromatography separation and mass spectrometry

The resulting tryptic peptides, equivalent to ~ 1µg digested protein, were analysed using nano high performance liquid chromatography (HPLC) on an Ultimate 3000 RSLCnano system (Thermo Fisher Scientific, MA, USA). Firstly, peptides were concentrated on a 20mm x 75µm PepMap 100 trapping column (3µm C18) at a flowrate of 5µL/min, using 98% water, 2% acetonitrile and 0.05% trifluoroacetic acid (TFA). Peptides were then separated on a 250mm x 75µm PepMap 100 RSLC column (2µm C18) at a flowrate of 300nL/min, held at 40°C. Separation included a 240 minute gradient from 98% mobile phase A (0.1% formic acid in water) to 50% mobile phase B (0.08% formic acid in 80% acetonitrile and 20% water) and included the following steps: 3-10% B over 10 minutes, 10-40% B over 180 minutes, 40-50% B over 10 minutes, holding at 95% B for 10 minutes then re-equilibration in 2% B for 15 minutes. The HPLC system was coupled to an LTQ-Orbitrap mass spectrometer, controlled using Xcalibur 2.1 software in data-dependent mode. MS/MS spectra were acquired using a Top8 method and 30-second dynamic exclusion of fragmented peptides, as previously described (Wilson et al., 2016).

3.2.6.4 Protein identification and analysis

Data files were imported into MaxQuant version 1.5.1.2 (http://maxquant.org/) and MS/MS spectra were searched using the Andromeda engine against the complete *Mus musculus* reference proteome (ID 000000589) comprising 44,455 protein entries. Default settings for protein identification by LTQ-Orbitrap MS/MS and label-free quantitation (LFQ) included a maximum of two missed cleavages, mass error tolerances of 20 ppm then 4.5 ppm for initial and main peptide searches, respectively, 0.5 Da tolerance for fragment ions, variable methionine oxidation and fixed carbamidomethylation. A false discovery rate (FDR) of 0.01 was used for peptide-spectrum matches and protein identification. The full set of identified peptides and proteins (MaxQuant output files peptides.txt and proteinGroups.txt, respectively) are presented in Appendix 3.1.

The MaxQuant algorithm MaxLFQ was used for peptide intensity determination and normalisation (Cox et al., 2014), using pair-wise comparison of unique and razor peptide intensities and a minimum ratio count of 2. The MaxQuant proteinGroups output file was processed as follows: The normalised label-free quantification (LFQ) intensity values, MS/MS counts and the numbers of razor and unique peptides for each of the identified proteins were imported into Perseus software version 1.5.031 (http://perseus-framework.org/). Protein groups identified as potential contaminants and proteins only identified by site or by reverse database matching were removed and LFQ intensity values were $\log_2$–transformed. The proteins were filtered to include only those detected in all three replicates of at least one genotype. Missing values were replaced with random intensity values for low-abundance proteins based on a normal distribution of protein abundances using default MaxQuant parameters. To determine proteins that were significantly altered in abundance between genotypes a two-sided t-test was used with a permutation-based FDR of 0.05, using 250 randomisations, and a minimum fold-change cut-off of 1.3. The data was exported from Perseus into Excel (Appendix 3.2). To extract functional information from the proteomic data, proteins that were significantly up- or down-regulated in homozygote samples compared to wildtype samples were imported into the online bioinformatics

resource DAVID (version 6.8; https://david.ncifcrf.gov/; (Huang, Sherman, & Lempicki, 2009). Protein lists were analysed using the mouse genome database, and annotation clusters were ranked using the Functional Annotation Clustering tool based on default parameters, with p values < 0.05 after adjustment using the Benjamini-Hochberg correction for multiple testing considered significant. The complete set of Functional Annotation Clusters is reported in Appendix 3.2.

3.2.7 Immunocytochemistry

At 3 and 10DIV coverslips were rinsed, fixed and ICC was carried out as per Chapter 2.3. Primary antibodies were diluted in 0.6% Triton-X-100 (Sigma) and included: TDP-43 (mouse and human, Proteintec Group, reference number 10782-2-AP, 1:1000); MAP2 (Millipore, reference number MAB3418, 1:1000); beta 3 tubulin (Promega, reference number G712A, 1:5000), NFM (Millipore, reference number AB1987, 1:1000), SMI312 (Covance, reference number R500, 1:1000). Following overnight incubation at 4°C, coverslips were incubated in species-specific secondary antibodies for two hours. In some experiments, the f-actin stain phalloidin (1:200, Life Technologies) was applied to coverslips for 1 hour following secondary incubation. Nuclei were stained with DAPI (5µg/ml, Life Techologies) for 5 minutes. Coverslips were washed 3 x 10 minutes with PBS and mounted. Images were captured with a BX-50 Olympus microscope and a Photometrics Coolsnap HQ2 camera.

3.2.8 Growth cone analysis

Growth cones were analysed at 3DIV, and immunolabelled with beta 3 tubulin and f-actin. For each genotype, two coverslips from three different cultures (from different mothers) were examined. Growth cones were classified as filopodial, lamellipodial or blunt (Figure 3.6A), based on the paper by Khazaei et al. (2014). For classification, 100 growth cones from each genotype were systematically examined across two coverslips per culture (three cultures per genotype) by a researcher blinded to the genotype groups. Beta 3 tubulin labeling and f-actin staining were used to examine length and number of filopodia; size of growth cone; and ratio of actin to tubulin (Figure 3.1 B). Approximately 30 images

from the two coverslips for each culture were obtained, and ImageJ software was used for analysis as described previously (Khazaei et al., 2014).

3.2.9 Neuron morphology analysis

Phase contrast images of neurons at 3DIV were captured on a Nikon Live Cell microscope (Nikon Instruments Inc; NIS-Elements AR 4.00.12 Software, Nikon) by a researcher blinded to genotype groups. Approximately 60 individual neurons per genotype (two coverslips from three different cultures/mothers) were examined. Images were obtained systematically across each coverslip to capture neurons where the whole neurite tree could be visualised. Images were imported into Neurolucida (MBF Bioscience) and cell bodies and neurites were traced. Figure 3.7A demonstrates the decision-making process for branch points. The longest neurite, normally considered to be the axon, was also traced separately. Traced images were imported into Neurolucida Explorer (MBF Bioscience) to determine cell body size; length of longest neurite; number of neurite trees; total length of neurite tree; number of branches in each order; and total number of branch points.

3.2.9.1 Mitochondria staining and quantification

A mitochondrial tracking dye (MitoTracker Red CMXRos, Life Technologies) was added to 3 DIV live cortical cultures at a concentration of 100nM. Half the media from wells was removed and kept for washing after treatment. MitoTracker was added to culture wells for five minutes and then cells were washed using saved media. As MitoTracker was not well-retained after fixation, static counts of the number of mitochondria per 100µm of axon (from at least 50 axons from three different cultures per genotype) were carried out on two coverslips from three different cultures per genotype.

3.2.10 Statistical analysis

Unless otherwise stated, statistical analysis was carried out using a one-way ANOVA with Tukey's post hoc test. Neurolucida tracing data and growth cone morphology data were analysed using mixed models with random intercepts to account for clustering within culture batches. The assumptions of

normality of residuals and homogeneity of variance were checked using graphical methods (Q-Q and residual plots), and where the assumption of normality was violated, data were either log transformed or a generalised linear model with appropriate link function (*e.g.* Poisson link function for count data) was fitted to ensure that statistical conclusions were robust. Likelihood ratio tests were used to determine statistical significance. To test differences in the distribution of growth cone morphology between genotypes, Pearson's Chi-square test of homogeneity was calculated. *Post-hoc* comparisons were corrected using the Bonferroni method. All statistical analysis was conducted in the R statistical language (R Core Team, 2016). Mixed models were fitted using the 'lme4' package in R (Bates, 2015). Detailed analyses are documented in Appendix 3.3. Data are presented ± standard error of the mean (SEM) and significance set at $p<0.05$.

3.3 RESULTS

3.3.1 Expression of TDP-43 in development

Western blot analysis of protein harvested from cultured cortical neurons grown to 3DIV confirmed the presence of human TDP-43 in cells from both homozygous and heterozygous embryos, and the absence from wild type cells, using a human-specific TDP-43 antibody (Zhang, Tanji, Mori, & Wakabayashi, 2008) (Figure 3.2 A). Human TDP-43 was significantly increased in homozygote and heterozygote cells compared to wildtype ($p<0.05$) (Figure 3.2 B). Although there was no difference between heterozygote cells and wildtype cells, the blot (Figure 3.2 A) demonstrates the presence of the transgene. As TDP-43 is a self-regulating protein, the level of total TDP-43 expression was then determined using an antibody that recognizes both mouse and human (total) TDP-43. Total TDP-43 was significantly increased in both heterozygote and homozygote cells compared to wildtype cells ($p<0.05$) (Figure 3.1 C).

3.3.2 Cellular localisation of TDP-43

In ALS/FTD, there is evidence that mislocalisation of TDP-43 from the nucleus to the cytoplasm may cause both gain and loss protein function (Lee et al., 2012). To determine whether increased expression of human TDP-43 caused a change in localisation of protein expression, the distribution of TDP-43 (mouse and human) was analysed in the nucleus and cytoplasm at 3 DIV. Qualitative analysis of immunocytochemically labelled neurons suggested that TDP-43 was more abundant in the cytoplasm in homozygote cells (Figure 3.3 A). Integrated densitometry of TDP-43 fluorescence demonstrated higher levels in both the nucleus and cytoplasm in homozygote cells compared to wildtype cells ($p<0.05$) (Figure 3.3 B, C). These results qualitatively showed that both total TDP-43 and human TDP-43 were expressed at higher levels in the nuclear and cytoplasmic compartments in homozygote samples compared to heterozygote and wildtype samples.

3.3.3 Global alterations to protein expression following TDP-43 overexpression

TDP-43 interacts with over 30% of the genome (Sephton et al., 2011) and its effects are likely to be broad. A proteomics approach was used to determine global changes to protein expression in transgenic cells compared to wildtype. Protein was harvested from homozygous and wildtype neurons grown to 3 DIV and 10 DIV, however protein quantity and quality at 3 DIV was insufficient for downstream analysis. Principal component analysis of homozygote samples and wildtype samples demonstrated a relatively high degree of variability between the three homozygote replicates (Figure 3.4 A) and therefore statistical analyses were less stringent than would otherwise be used. In the 10 DIV samples, 85 proteins were downregulated and 94 proteins were upregulated in homozygote samples compared to wildtype samples (FDR < 0.05, FC ± 1.3) (Figure 3.4 B). The online bioinformatics database tool, DAVID, was used for functional annotation clustering to identify protein families that clustered together within up- or down-regulated protein groups (Figure 3.5 A). Functional terms associated with downregulated proteins included translation, rRNA binding, and mitochondria, whereas upregulated proteins were associated with the COP9 signalosome, proteasome complex and

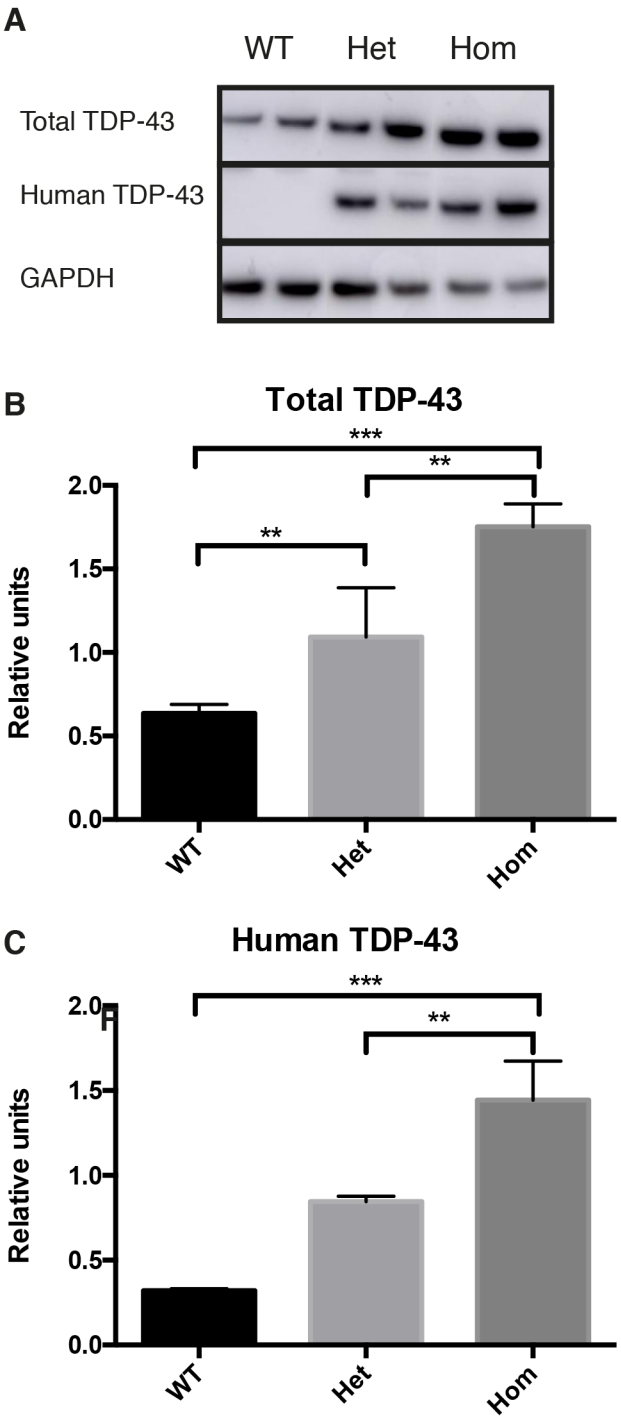
A
WT
Het
Hom
Total TDP-43
Human TDP-43
GAPDH
B
Total TDP-43
***
**
**
Relative units
2.0
1.5
1.0
0.5
0.0
WT
Het
Hom
C
Human TDP-43
***
**
Relative units
2.0
1.5
1.0
0.5
0.0
WT
Het
Hom

Figure 3.2. Characterisation of total and human TDP-43 expression. (A) Expression of total and human TDP-43 were analysed by Western blot from cortical neuron protein from the three genotypes at 3 DIV (n=3 cultures per genotype). Quantification was carried out relative to GAPDH for human TDP-43 (B) and total TDP-43 (C). Results are mean and standard error. Statistical significance is defined as *p<0.05, **p<0.01.

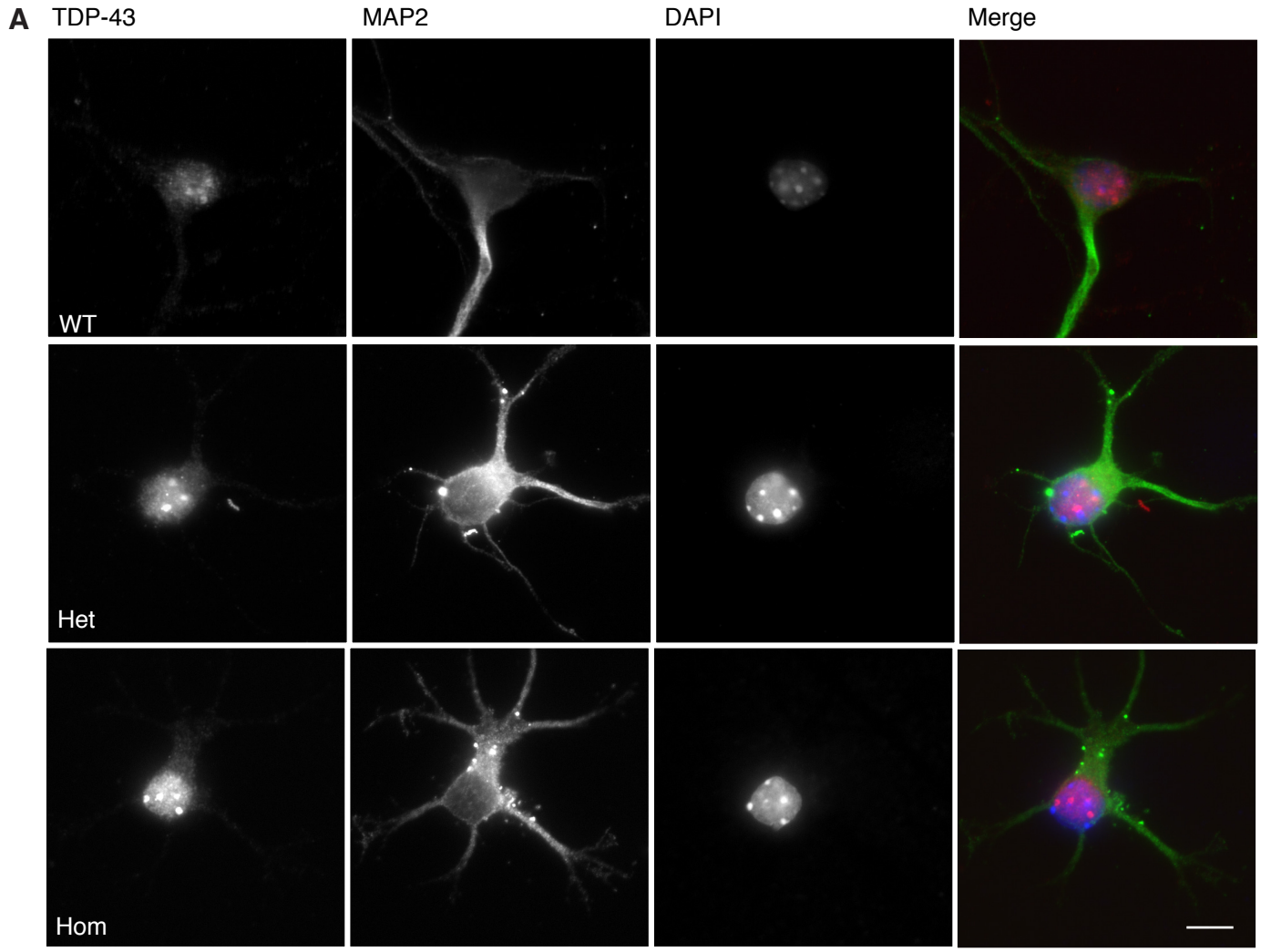
A
TDP-43
MAP2
DAPI
Merge
WT
Het
Hom

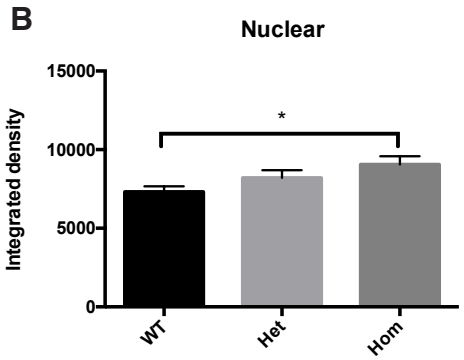
B
Nuclear
Integrated density
15000
10000
5000
0
*
WT
Het
Hom

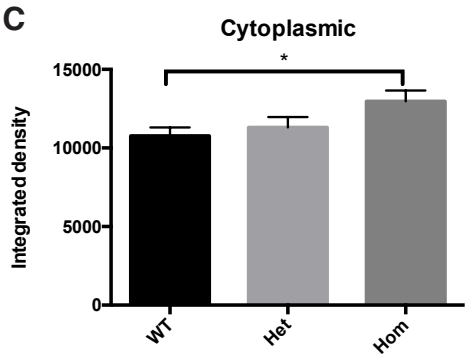
C
Cytoplasmic
Integrated density
15000
10000
5000
0
*
WT
Het
Hom

Figure 3.3 Cellular localisation of TDP-43. (A) Cortical neurons from the three genotypes at 3DIV (n= 3 cultures per genotype, n= >20 neurons per culture) immunolabelled for TDP-43 (red), MAP2 (green) and DAPI (blue). MAP2 and DAPI were used to delineate the nucleus (B) and cytoplasm (C) within which the integrated density of TDP-43 was determined. Results are mean and standard error. Statistical significance is defined as $*p<0.05$. Scale bar 10µm.

A

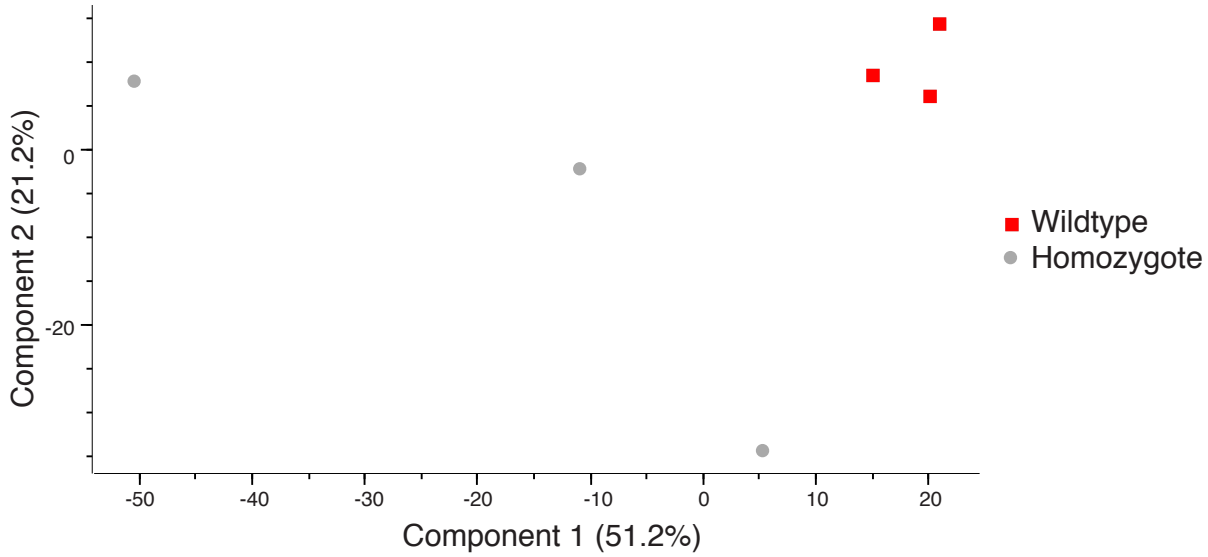
Component 2 (21.2%)
0
-20
-50
-40
-30
-20
-10
0
10
20
Component 1 (51.2%)
Wildtype
Homozygote

B

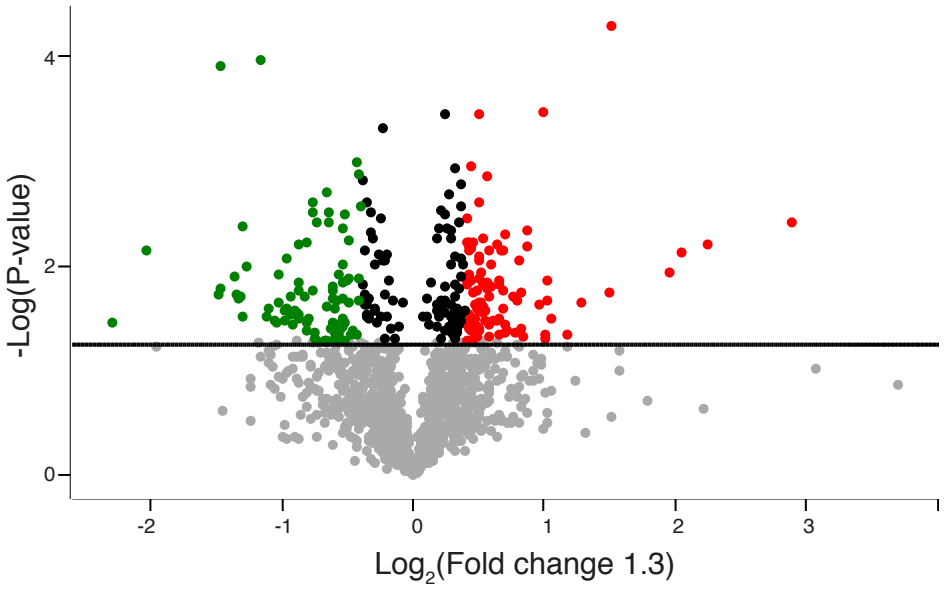
-Log(P-value)
4
2
0
-2
-1
0
1
2
3
Log2(Fold change 1.3)

Figure 3.4 Proteomic sample characterisation. Proteins extracted at 10 DIV from homozygote and wildtype cortical neurons (n= 3 cultures per genotype) were digested into peptides, separated via liquid chromatography and identified via mass spectrometry. (A) Principal component analysis was carried out. Homozygote samples were compared to wildtype samples. (B) Volcano plot showing $-\log_{10}$ transformed p-values compared to a $\log_2$ transformed fold change of 1.3. Proteins significantly above and below this value are demonstrated by red and green, respectively.

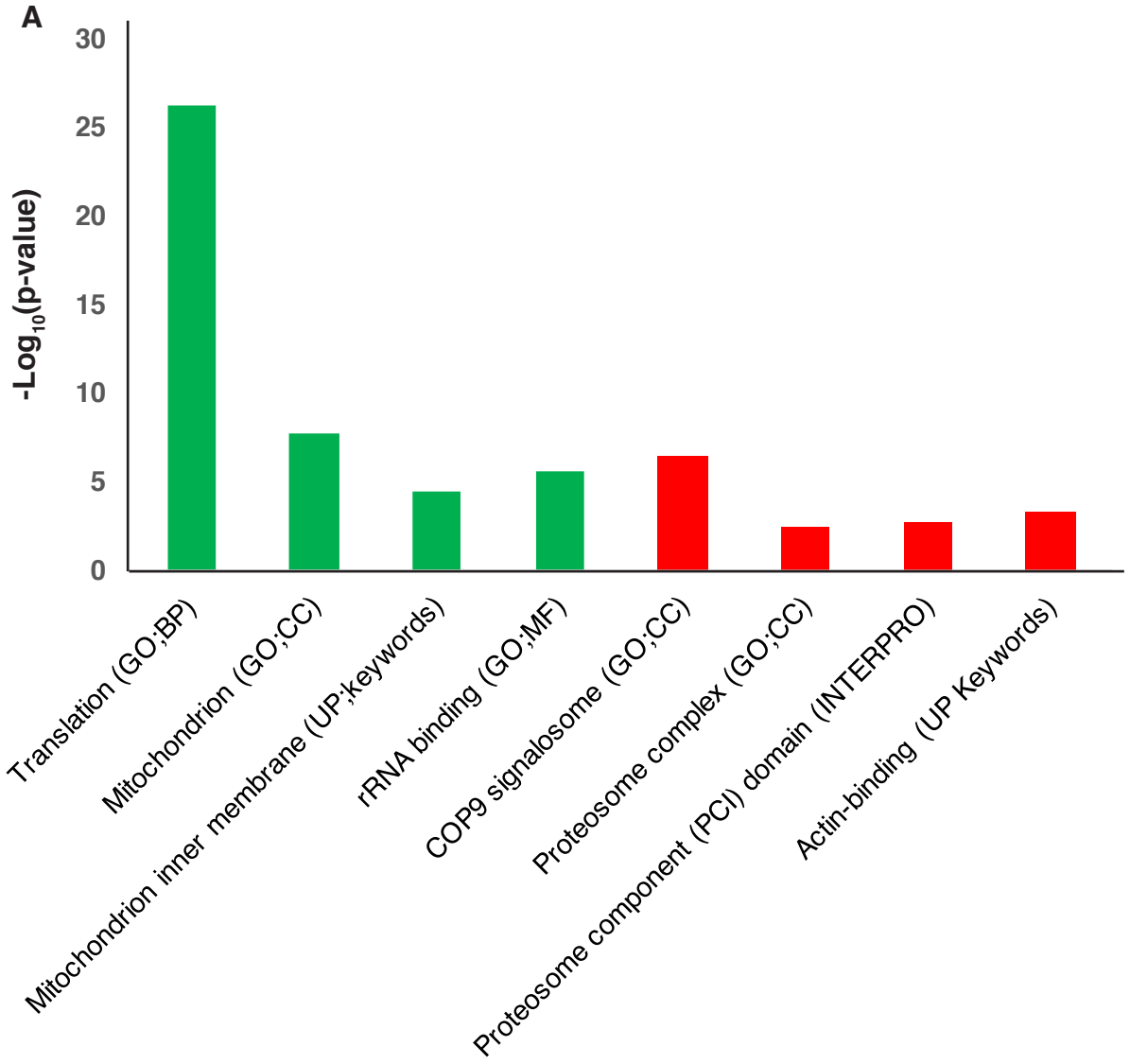
A
30
25
20
15
10
5
0
-Log10(p-value)
Translation (GO;BP)
Mitochondrion (GO;CC)
Mitochondrion inner membrane (UP;keywords)
rRNA binding (GO;MF)
COP9 signalosome (GO;CC)
Proteosome complex (GO;CC)
Proteosome component (PCI) domain (INTERPRO)
Actin-binding (UP Keywords)

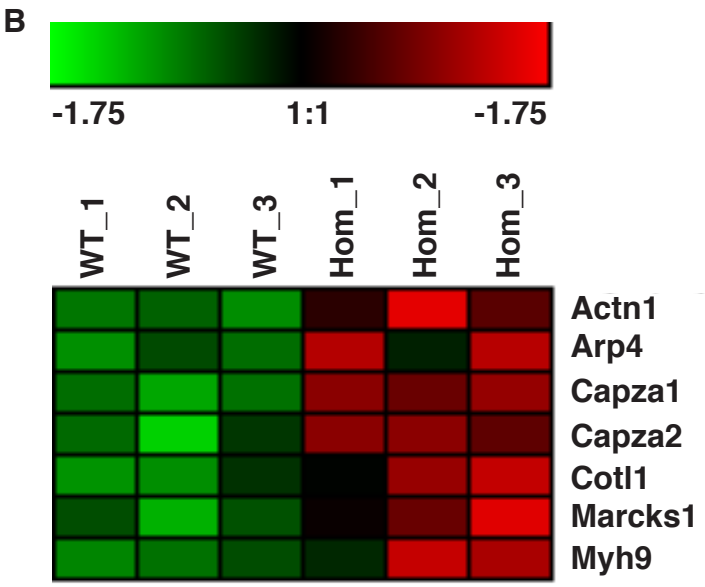
B
-1.75
1:1
-1.75
WT_1
WT_2
WT_3
Hom_1
Hom_2
Hom_3
Actn1
Arp4
Capza1
Capza2
Cotl1
Marcks1
Myh9

Figure 3.5 Protein families enriched in homozygote samples compared to wildtype samples. Significantly upregulated and downregulated proteins were analysed in functional terms. (A) Pathways with the enrichment scores higher than 2.0 (Fisher's exact test p-values for enriched terms were log transformed) are shown, with functional pathways implicated as upregulated (red) or downregulated (green). (B) Heat map of actin binding proteins showing the maximum z-score for each sample repeat, for each protein.

actin binding. These results demonstrated that proteins related to the normal function of TDP-43 were disrupted by increased expression, as well as proteins associated with functions known to be altered by abnormal TDP-43 (mitochondria and proteasome). Furthermore, increased expression of TDP-43 upregulated proteins related to actin binding, including Actn1, Arpc4, Capza1, Capza2, Cotl1, Marcksl1 and Myh9 (Figure 3.5 B). Many of these proteins are involved in the regulation of growth cone dynamics and axon outgrowth.

3.3.4 Effects of TDP-43 overexpression on growth cones

Previous studies have suggested that altered TDP-43 affects neurite outgrowth (Fallini et al., 2012; Tripathi et al., 2014). This is controlled by growth cones, found at the growing tip of neurites, in which attractive or repulsive extracellular guidance cues cause reorganisation of microtubules and actin filaments. Since altered TDP-43 expression affects actin-dependent processes, the morphology and cytoskeletal composition of growth cones in homozygous, heterozygous and WT TDP-43 cultured neurons were examined. Neuronal growth cones were examined at 3 DIV, when cortical neurons are actively pathfinding in culture before the majority of synapses form (Dotti, Sullivan, & Banker, 1988). Immunolabelling with beta 3 tubulin and staining with the f-actin stain, phalloidin, were used to visualize growth cones. Growth cones were classified as filopodial, lamellipodial or blunt (based on Khazaei et al. 2014) (Figure 3.6 A). A chi-squared test for homogeneity demonstrated a significant difference ($\chi^2_4 = 11$, $p<0.05$) in the distribution of growth cone morphologies between genotypes; specifically, heterozygote cultures had fewer lamellipodial growth cones, and more filopodial growth cones (Figure 3.6 B). Filopodial growth cones across the genotypes were further analysed for changes to the number (Figure 3.6 C) or length (Figure 3.6 D) of growth cone filopodia, however no differences were found. The area of phalloidin-stained f-actin (Figure 3.6 E) and beta 3 tubulin (Figure 3.6 F) within filopodial growth cones was similar between genotypes, as was the ratio of these areas (Figure 3.6 G).

3.3.5 Effects of overexpression of TDP-43 on neurite morphology

Initiation of neurites and branching is controlled by expression and reorganisation of cytoskeletal proteins. To investigate whether changes to TDP-43 expression cause cytoskeletal alterations, neuron morphology across the three different genotypes was examined. Neurons at 3 DIV were traced using Neurolucida and several morphological measures were assessed. Axonal outgrowth, quantitated by measuring the longest neurite in each cell, and the total length of all neurites showed no significant differences between genotypes (Figure 3.7 B, C). Neuritogenesis was examined by looking at the number of neurite trees coming from the cell body, the number of branches in each order (primary to quaternary) and the length of these branches (branching schematic demonstrated in Figure 3.7 A). From these analyses, the only parameter altered was the total number of branches in neurite trees, which was increased in heterozygous compared to wildtype cells ($p<0.05$) (Figure 3.7 E, F).

3.3.6 Axonal alterations following overexpression of TDP-43

Next, potential effects of TDP-43 overexpression on axons were characterised. Immunocytochemical labelling of neurofilament medium subunit (NFM) and phosphorylated neurofilament triplet protein, SMI312 was qualitatively examined. Wildtype cultures demonstrated intact axons with few examples of fragmentation or beading. Both homozygote and heterozygote cells at 10DIV demonstrated some features of axonal degeneration (Figure 3.8 A). Heterozygote cultures showed examples of ring structures that were positive for both NFM and SMI312 were present. These structures have previously been described in unhealthy axons in mSOD1 models of ALS (Anna E King, Blizzard, Southam, Vickers, & Dickson, 2012) and around beta amyloid plaques in Alzheimer's disease (Dickson et al., 2005; Dickson et al., 1999). Additionally, homozygote cultures showed examples of neurons with fragmentation of SMI312 labelling along axons, and frequent examples of axonal beading with accumulations of NFM in chains along the axons. Previous studies in this mouse model have

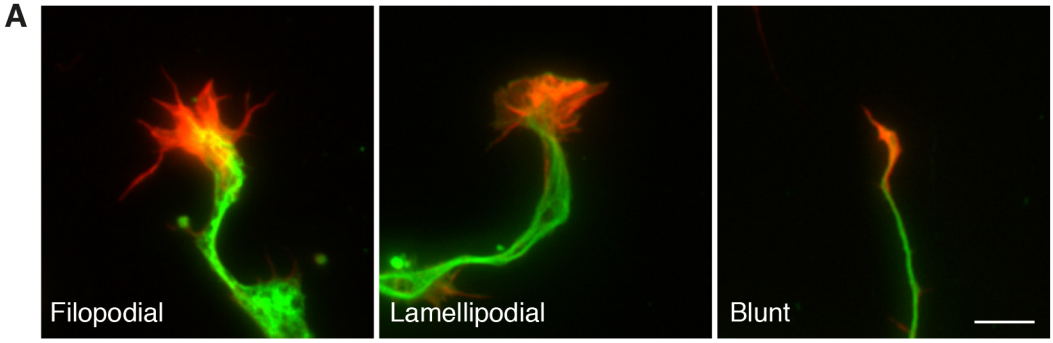
A
Filopodial
Lamellipodial
Blunt

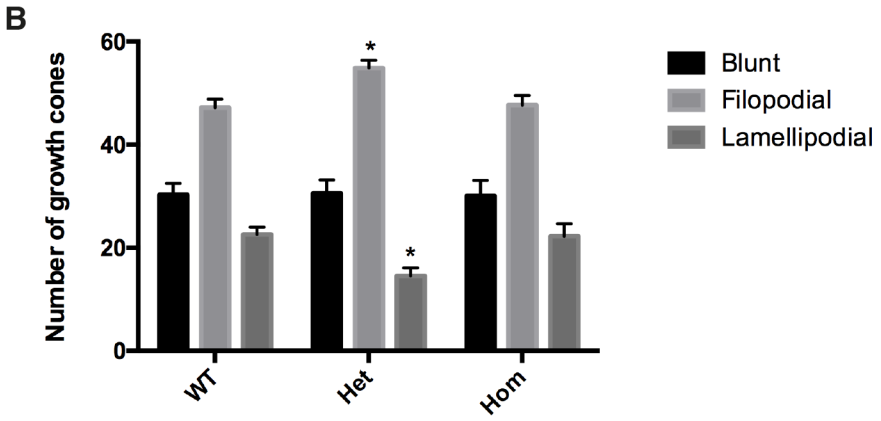
B
Number of growth cones
60
40
20
0
*
*
WT
Het
Hom
Blunt
Filopodial
Lamellipodial

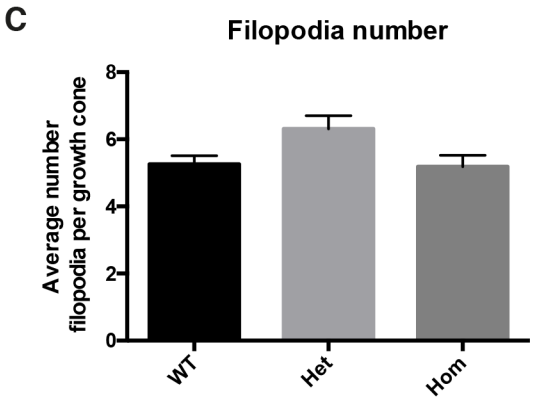
C
Filopodia number
Average number filopodia per growth cone
8
6
4
2
0
WT
Het
Hom

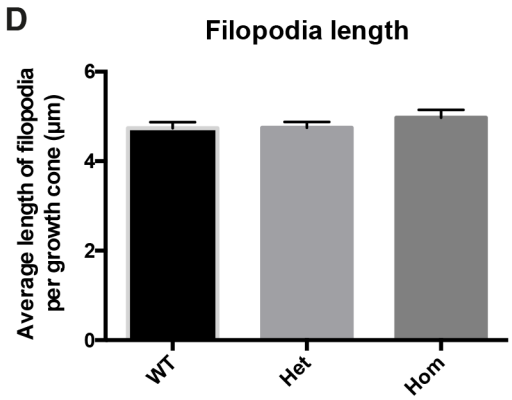
D
Filopodia length
Average length of filopodia per growth cone (µm)
6
4
2
0
WT
Het
Hom

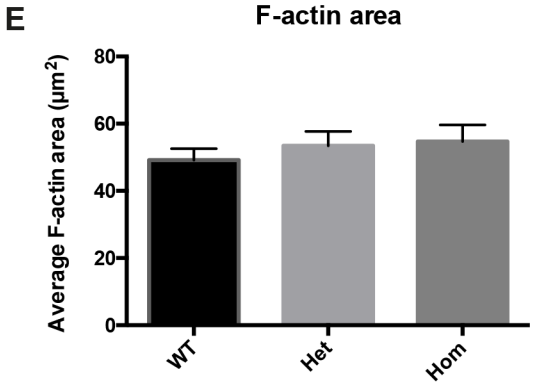
E
F-actin area
Average F-actin area (µm²)
80
60
40
20
0
WT
Het
Hom

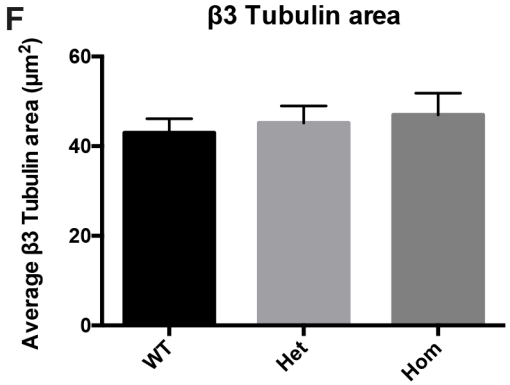
F
β3 Tubulin area
Average β3 Tubulin area (µm²)
60
40
20
0
WT
Het
Hom

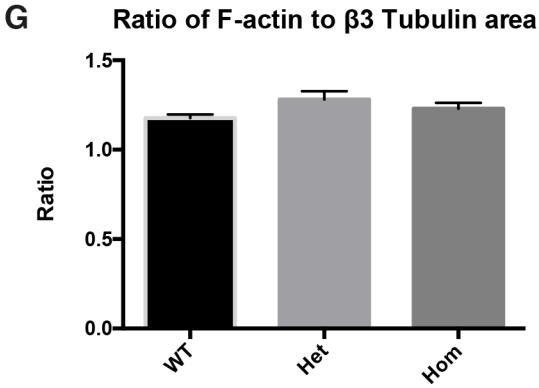
G
Ratio of F-actin to β3 Tubulin area
Ratio
1.5
1.0
0.5
0.0
WT
Het
Hom

Figure 3.6 Alterations to growth cones. Cortical neurons from the three genotypes at 3DIV (n= 3 cultures per genotype) were immunolabelled for B3 tubulin (green) and stained with phalloidin (red). Growth cones were classified as filopodial, lamellipodial or blunt (A) and counted for each genotype (n= 100 growth cones per culture) (B). Filopodial growth cones were analysed further (C-G) (n= >15 filopodial growth cones per culture). Values are mean and standard error. Statistical significance is defined as $*p<0.05$, scale bar 5μm.

demonstrated abnormal clustering of mitochondria and altered expression of proteins which control mitochondrial dynamics (Xu et al., 2010). To determine whether there were axonal mitochondrial alterations attributable to TDP-43 changes static observations of mitochondria distribution and numbers were carried out. There were no significant differences in the number of mitochondria per 100μm of axon, although there was a trend toward an increase in heterozygote cells compared to wildtype cells (Figure 3.8 B, C).

3.4 DISCUSSION

Following on from reports that TDP-43 plays a role in neurite development, this study focused on gaining a better insight into the relationship between TDP-43 and the neuronal cytoskeleton. Due to the large number of cytoskeletal proteins, and the known interactions between TDP-43 and a large number of proteins, a proteomic approach was taken. This demonstrated a range of proteins that were differentially regulated, of which actin-binding proteins were of particular interest. Additionally, non-pathological TDP-43 overexpression resulted in increased branching and altered growth cone morphology (Figure 3.9).

In the present study, overexpression of wildtype human TDP-43 resulted in increased expression of total and human TDP-43 in developing neurons. These results are in line with those from Xu et al. (2010) who demonstrated increases in both human and total TDP-43. These authors observed a larger increase in human TDP-43 than total TDP-43 when comparing transgenic mice to controls, which they attributed to downregulation of endogenous mouse TDP-43. Although TDP-43 is a highly regulated protein, capable of autoregulation, the results of the present study suggest that overexpressing two copies of human TDP-43 may exceed this regulatory capacity, resulting in higher overall levels.

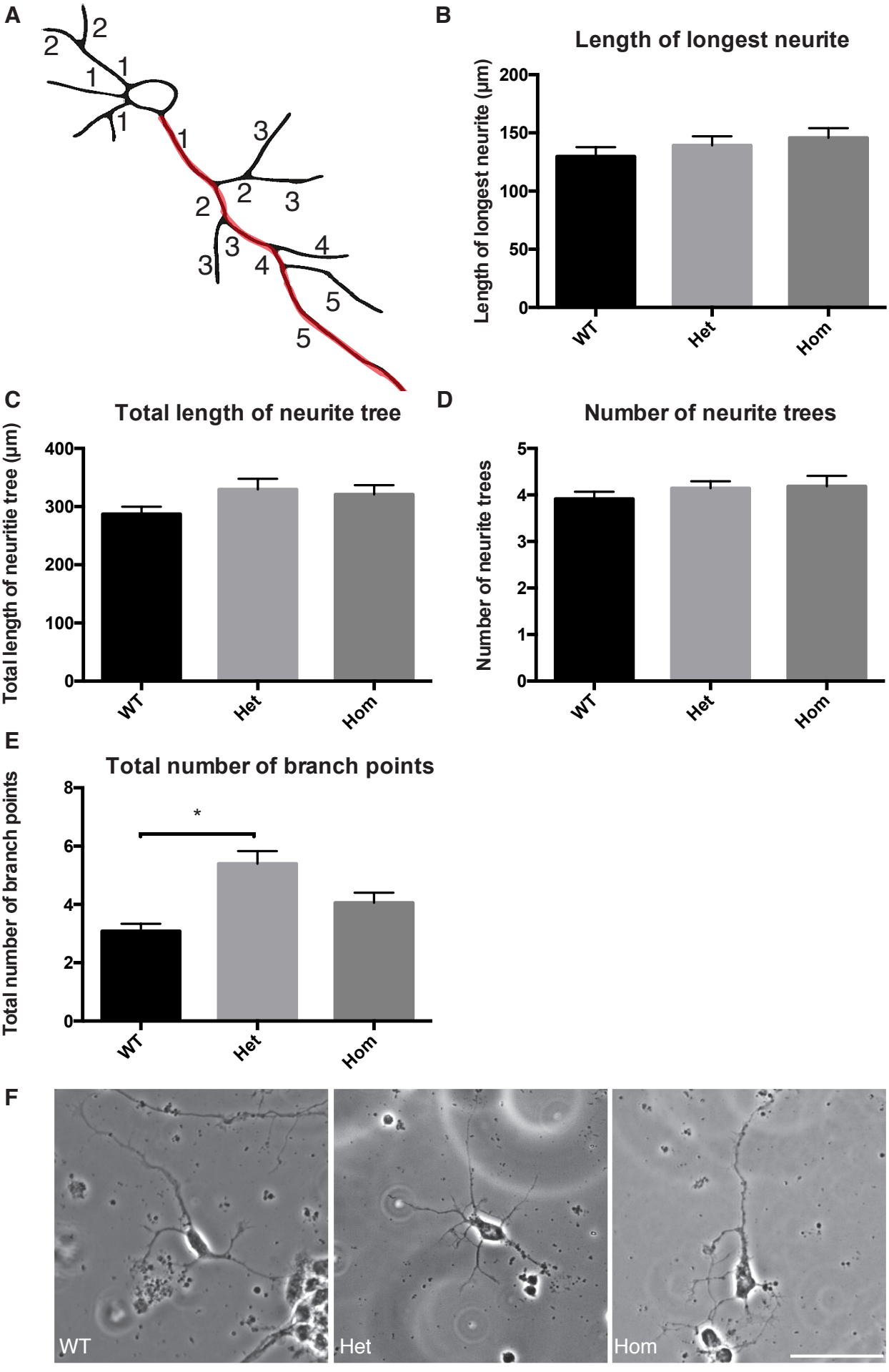
A
B
Length of longest neurite
Length of longest neurite (µm)
200
150
100
50
0
WT
Het
Hom
C
Total length of neurite tree
Total length of neuritie tree (µm)
400
300
200
100
0
WT
Het
Hom
D
Number of neurite trees
Number of neurite trees
5
4
3
2
1
0
WT
Het
Hom
E
Total number of branch points
Total number of branch points
*
8
6
4
2
0
WT
Het
Hom
F
WT
Het
Hom

Figure 3.7 Alterations of neuron morphology. Cortical neurons were imaged at 3DIV from the 3 genotypes (n=5 cultures per genotype, n= >20 neurons per culture). Cell bodies, neurites, and the longest neurites were traced using Neurolucida and branch points defined (A), yielding measures of morphological features (B-E). (F) Example phase contrast images of neurons showing branch morphology. Values are mean and standard error. Statistical significance is defined as $*p<0.05$. Scale bar 50μm.

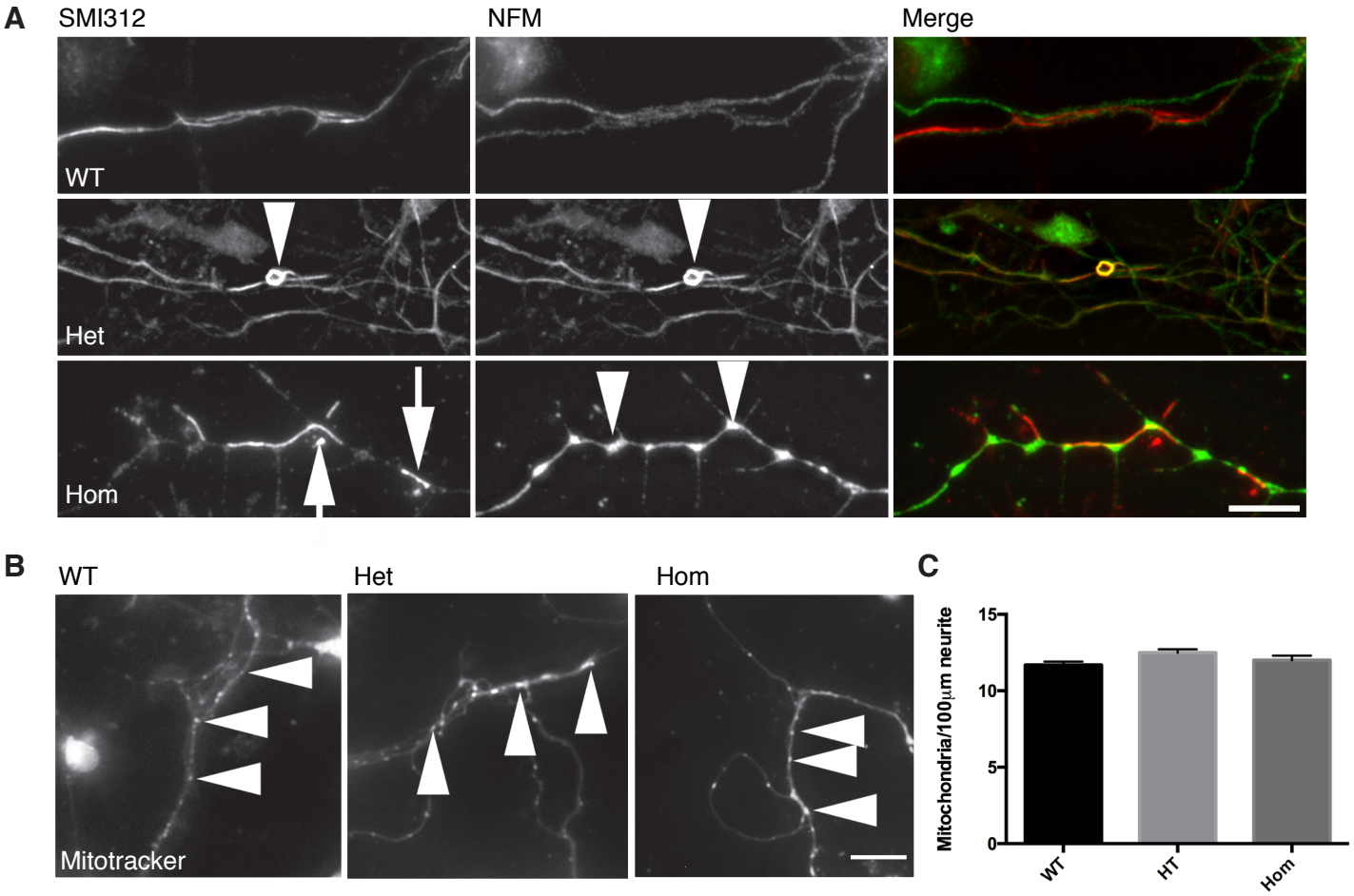
A
SMI312
NFM
Merge
WT
Het
Hom
B
WT
Het
Hom
Mitotracker
C
Mitochondria/100μm neurite
15
10
5
0
WT
HT
Hom

Figure 3.8 Alterations to axon structure and function. (A) Cortical neurons from the three genotypes at 10DIV (n= 3 cultures per genotype) were immunolabelled with SMI-312 (red) and NFM (green) antibodies. In heterozygous cultures, arrowheads show ring-like structures. In homozygous cultures, arrows indicate fragmented SMI312 and arrow heads indicate swellings along the axon. (B) Cortical neurons from the three genotypes at 4DIV stained with the mitochondrial marker, Mitotracker (mitochondria puncta indicated by arrowheads). (C) Static counts of mitochondria per 100µm axon were obtained. Results are mean and standard error. Scale bar 10µm.

A key pathological feature of FTD/ALS associated with TDP-43 is the mislocalisation of TDP-43 from the nucleus to the cytoplasm. The current data shows that homozygous neurons have a modest increase in TDP-43 within both cytoplasm and nuclei, which may explain the differences in morphology phenotypes between the homozygous and heterozygous neurons. Increased expression of TDP-43 could alter its role in both compartments, including interactions with DNA and RNA targets, as well as transport in mRNA granules (Alami et al., 2014). It was not surprising that a more robust change in TDP-43 levels within the nuclear and cytoplasmic compartments was not found between the genotypes. Xu et al., (2010) examined brain tissue from postnatal homozygote TDP-43$_{Prp}$ mice and also found that mislocalisation of human TDP-43 was only detected occasionally. It is has been demonstrated in other models of TDP-43 pathology, such as those expressing TDP-43 mutations, that cytoplasmic mislocalisation of TDP-43 is more prominent and that this is toxic to cells (Barmada et al., 2010). Results from the current study may indicate that there is a differential effect of increased TDP-43 in heterozygotes and TDP-43 with pathologic changes in homozygotes, demonstrated by changes to branching and growth cone morphology observed only in heterozygote mice. It is possible that the increased cytoplasmic expression of TDP-43 in homozygous neurons may have been undergoing early protein oligomerisation or aggregation, which produced toxic effects, negating the results observed in heterozygous neurons.

Global changes to protein expression

This study examined whether altered TDP-43 levels could result in changes to cytoskeletal proteins. Due to the vast number of interaction pathways affecting cytoskeletal and associated proteins, a proteomic approach was taken to give a global view. Bioinformatic analysis of the proteomes of wildtype and homozygous mice demonstrated changes across a range of functional domains, including several linked to established TDP-43 roles. For example, proteins related to RNA binding and translation were highly down-regulated. TDP-43 is a known RNA binding protein, interacting with

over 30% of the genome (Sephton & Yu, 2015), and is likely to regulate the translation of a number of mRNAs (Strong et al., 2007). Previous proteomic studies examining interacting partners of TDP-43 demonstrate strong associations with translation machinery (Freibaum, Chitta, High, & Taylor, 2010). Alterations to the localisation and therefore function of TDP-43 in homozygote cells would be consistent with alterations to these protein families. Other observed changes included the ubiquitin-proteosome system (UPS), which is highly associated with ALS/FTD. TDP-43 is ubiquitinated in aggregates of diseased tissue (Neumann et al., 2006). Mutations in ubiquilin-2, seqestosome-1 and valosin-containing protein (VCP) are associated with ALS/FTD with characteristic TDP-43 pathology. Levels of TDP-43 protein are regulated by the UPS through degradation of monomeric TDP-43, preventing accumulation and aggregation (Scotter et al., 2014), emphasizing the importance of regulation to this system. Overexpression of a protein is also consistent with an upregulation of the protein degradation system to try and normalise protein levels within the cell, and may be consistent with pathological TDP-43 aggregation.

Down regulation of mitochondrial proteins was also observed, in accordance with previous research, which demonstrated clustering of mitochondria within axons and dendrites in the same mouse model (Xu et al., 2010). In the current study, proteins related to mitochondrial function were downregulated in homozygote cells at 10DIV, although there were no alterations to the distribution or number of axonal mitochondria in cultures at 3DIV. Mitochondrial dysfunction is a common theme in TDP-43 mouse models of ALS and FTD, causing aggregation, fragmentation or vacuolation of mitochondria (Magrane, Cortez, Gan, & Manfredi, 2014; Wang et al., 2013). Abnormal mitochondria are also a feature of human disease with swollen and vacuolated mitochondria observed in neurofilamentous axon swellings (Sasako et al., 2007).

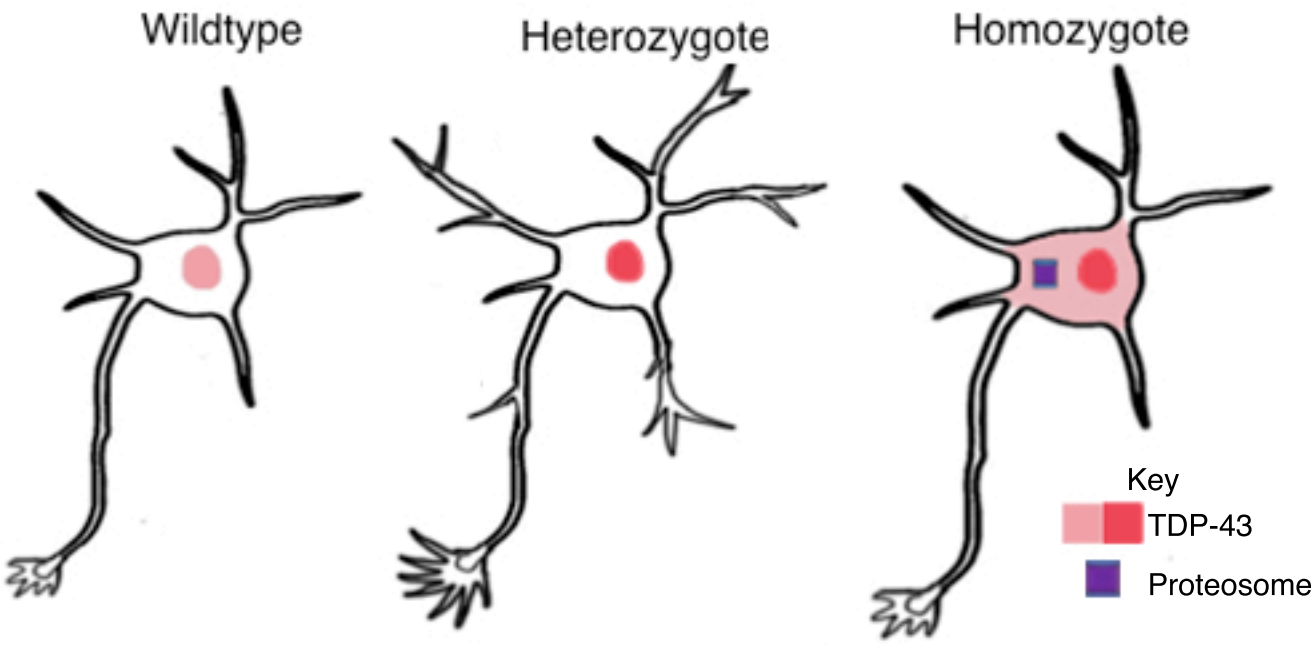

Heterozygote	Homozygote
Increased human TDP-43 expression	Increased human TDP-43 expression
No mislocalisation	Mislocalisation to cytoplasm
Increased branch number	Increased expression of proteosome proteins
Increased filopodial growth cones	Decreased translation proteins
Decreased lamellipodial growth cones	Increased actin-binding proteins

Enhanced normal TDP-43 function?

Altered TDP-43 expression - loss of function?

Figure 3.9 Summary of findings. Schematic summarising differences in TDP-43 localisation, branching, growth cone morphology and activation of the proteasome system from neurons cultured from the three genotypes. Pink/red colour demonstrates the localisation and level of TDP-43 expression.

The effect of TDP-43 alterations on the cytoskeleton

Of particular interest to the current study was the finding that actin-binding proteins were among the most up-regulated proteins in the proteomic analysis. Actin binding proteins are important for controlling the cytoskeletal network through actions such as filament nucleation, severing, crosslinking, end capping and monomer sequestering. For cortical neurons during development, these processes affect pathfinding, neurite outgrowth and branching. A number of actin binding proteins were altered, including non-muscular myosin heavy chain 11B (NMHC11-B), also known as myosin-9 (MYH9), which was upregulated in homozygote cells. This protein has previously been implicated in TDP-43 pathology; SH-SY5Y cells with a TDP-43 knockdown resulted in a cytoplasmic increase and a nuclear decrease of MYH9 levels compared to controls (Stalekar et al., 2015), and immunoprecipitation of HEK293T cells transfected with FLAG-TDP-43 demonstrated that MYH9 interacts with TDP-43 (Freibaum, Chitta, High, & Taylor, 2010). In neurons, MYH9 is important for driving neurite outgrowth, is involved in growth cone motility (Wylie, 1998) and for NMDA receptor trafficking (Amparan et al., 2005). Alterations to NMHC11-B protein expression have been found in both ALS patient brains containing TDP-43 aggregates and in transgenic pigs overexpressing the TDP-43 M337V mutation (Wang et al., 2015). This was hypothesised to be due to the co-mislocalsation of TDP-43 and the splicing factor proline-glutamine rich (PSF) and NeuN, which are both responsible for regulation of NMHC-11B alternative splicing (Kim, Kim, Adelstein, & Kawamoto, 2011). Mouse neurons expressing the M337V mutation had decreased neurite length, which was rescued by overexpression of the 'dominant' spliced exon (Wang et al., 2015). Although morphological differences were not detected in homozygous cells, they were found in heterozygous cells, suggesting that actin alterations could have downstream consequences on the neurons that could develop over time.

In more developed neurons, the actin cytoskeleton and actin binding proteins become important for supporting synaptic transmission and synaptic plasticity, as the main structural component of synapses

(Dillon, 2005). Arp2/3, highlighted by the proteomic data, aids the formation of F-actin networks (Dos Remedios, 2003). Its putative interaction with TDP-43 and the identified actin-binding proteins is yet to be determined. It will be important in future studies to follow up proteomic data with Western blots to confirm alterations to proteins identified.

Effects of altered cytoskeleton on neuronal phenotype

In the current study, morphology was examined at 3DIV because at this developmental stage cortical neurons have become polarised and are undergoing dynamic branching and pathfinding (Dotti et al., 1988). Filopodial growth cones, important for sampling the extracellular environment (Omotade, Pollitt, & Zheng, 2017), were also increased. The formation of filopodia and lamellipodia is thought to be controlled by rapid polymerisation of the actin cytoskeleton at the leading edge of the growth cone, followed by depolymerisation within the growth cone. TDP-43 interacts with members of the guanosine triphosphate hydrolase enzyme family (GTPase) involved in these processes. Rac1 is important for the formation of lamellipodia while Cdc42 is important for forming filopodia (Nobes, 2017). Knockdown of TDP-43 inactivated both Rac1 and Cdc42 (Iguchi et al., 2009), plausibly explaining alterations to growth cone morphology following TDP-43 overexpression.

In the current study, total branch number was also increased in heterozygous neurons, although the length of the neurite trees was similar across genotypes, implying that neurons became more ramified without a change in neurite length. It is known that overexpression of both wildtype and mutant cause a decrease in neurite outgrowth (Fallini, Bassell, & Rossoll, 2010; Tripathi et al., 2014) which is accompanied with redistribution of TDP-43 to the cytoplasm (Tripathi et al., 2014). Branch formation requires coordinated changes in actin and microtubules, and differs in axons and dendrites. Due to the early age of the cultures it was difficult to identify the axon, and for this reason branch data was pooled from all neurites. A general feature of neurite branching appears to be the protrusion of actin filaments from filopodia and/or lamellipodia on the neurite, followed by invasion of microtubules as the branch

matures and continues extending (Armijo-Weingart & Gallo, 2017). In line with these findings, Lu and colleagues (Lu, Ferris, & Gao, 2009) found that overexpression of *Drosophila* TDP-43, or human TDP-43 in *Drosophila*, increased dendritic branching of sensory neurons. Conversely, Schwenk and colleagues (2016) found that knockdown of TDP-43 in cultured hippocampal neurons reduced the complexity of dendrites at both 10 and 19DIV. These alterations were attributed to reduction of expression of cell surface receptors important for cell survival and neurite outgrowth (Schwenk et al., 2016).

TDP-43 interacts with a myriad of different proteins and mRNAs, and these cytoskeletal changes could occur through a range of pathways, such as that involving glycogen synthase kinase 3b (GSK-3b) and microtubule associated protein 1b (MAP1b). TDP-43 is known to activate GSK-3b (Stoica et al., 2014) and in fact loss of GSK-3b suppresses TDP-43 pathology in drosophila (Sreedharan, Neukomm, Brown, & Freeman, 2015). GSK-3b is known to directly phosphorylate MAP1b (Trivedi et al., 2005) and the GSK-3b- MAP1b pathway controls neurite branching (Barnat et al., 2016). The slight increase in TDP-43 in heterozygote cultures may have increased GSK-3b levels, and thereby MAP1b phosphorylation and neurite branching. In contrast, in homozygote cultures, higher levels of TDP-43 within both the nucleus and the cytoplasm may become toxic and impact on the normal function of TDP-43.

Axon pathology and degeneration are a feature of TDP-43-mediated disease. The TDP-43$_{Prp}$ model shows both axon and myelin degeneration in spinal cords. The mechanism of TDP-43-induced axon degeneration is thought to be distinct from Wallerian degeneration with evidence that axon degeneration is not altered by blocking genes associated with Wallerian degeneration in a Drosophila model with mutant TDP-43 (Sreedharan et al., 2015). In this study, a small increase in TDP-43 caused neurofilament ring-like structures to form, and a large increase caused fragmentation of SMI312 and blebbing of NFM. These observations are consistent with features of early axon degeneration.

During FTD/ALS cells are known to undergo loss of connectivity, and alterations to dendritic arbourisation and dendrite length have been observed in cases of FTD/ALS (Ferrer et al., 1991). During disease states, cells may increase their amount of TDP-43 to try and reestablish connectivity. However, concomitant stresses on the UPS system may alter the ability to degrade excess TDP-43, leading to aggregation and mislocalisation. Synaptic disruption with swollen pre-synaptic terminals is a feature of both ALS and FTD (Zhou et al., 1998) and is consistent with alterations to the actin cytoskeleton. The results of this study highlight the importance of tight regulation of TDP-43 levels, and suggest future studies examining TDP-43's role in regulation of the cytoskeleton.

Chapter 4:

Effects of altered TDP-43 in a novel CNS disease model

4 EFFECTS OF ALTERED TDP-43 IN A NOVEL CNS DISEASE MODEL

4.1 INTRODUCTION

There is now substantial evidence that TDP-43 plays important roles in regulating the outgrowth of neurites and synaptic morphology (Handley et al., 2016; Majumder et al., 2012). However, detailed understanding of the effect of TDP-43 alterations on neuronal morphology is still currently lacking. While the mSOD1 G93A mouse is a relatively good model of the axon pathology associated with ALS (King et al., 2012), axon pathology in models of TDP-43-mediated disease is less prominent, potentially due to the complex nature of premature death in many of these models. Select models do show features of neurite pathology. For example, overexpressing wildtype human TDP-43 under the prion promoter (described in Chapter 3) induces axon degeneration in the spinal cord (Xu et al., 2010), and mice expressing the A315T TDP-43 mutation and YFPH under the Thy1 promoter, exhibit altered synaptic function and dendritic spine morphology (Handley et al., 2016). Another model, expressing TDP-43 with a mutant nuclear localisation sequence (NLS) under the neurofilament heavy (*Nefh*) promoter, shows cytoplasmic accumulation of phosphorylated and ubiquitinated TDP-43 across the CNS, accompanied by axonal dieback from neuromuscular junctions then motor neuron loss (Walker et al., 2015).

Examining the cellular changes and mechanisms that induce axon pathology in animal models is challenging, due to the fine diameters and anatomical complexity of axon pathways in the CNS. The visual system is often used as a model to examine ultrastructural changes in axon degeneration following insults such as injury (Knoferle et al., 2010).

The visual system offers a unique opportunity to examine axonal defects *in vivo* by providing access to the central nervous system (CNS) without invasive surgery. Adeno-associated viruses (AAVs) can be used to efficiently transduce retinal ganglion cells (RGCs) with foreign genes (Grant, Ponnazhagan, Wang, Srivastava, & Li, 1997) via injection into the eye (Figure 4.1A). The RGCs are

A

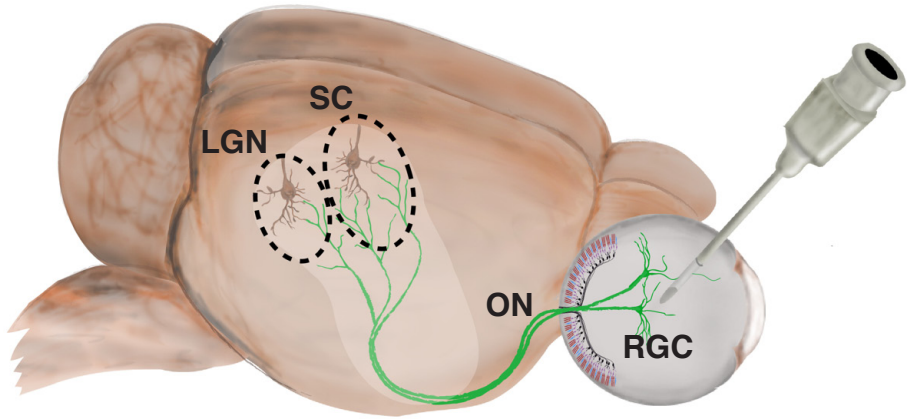

B

Intraocular injection:

CAG TDP-NLS⁻ GFP

CAG TDP-WT GFP

PBS vehicle

C

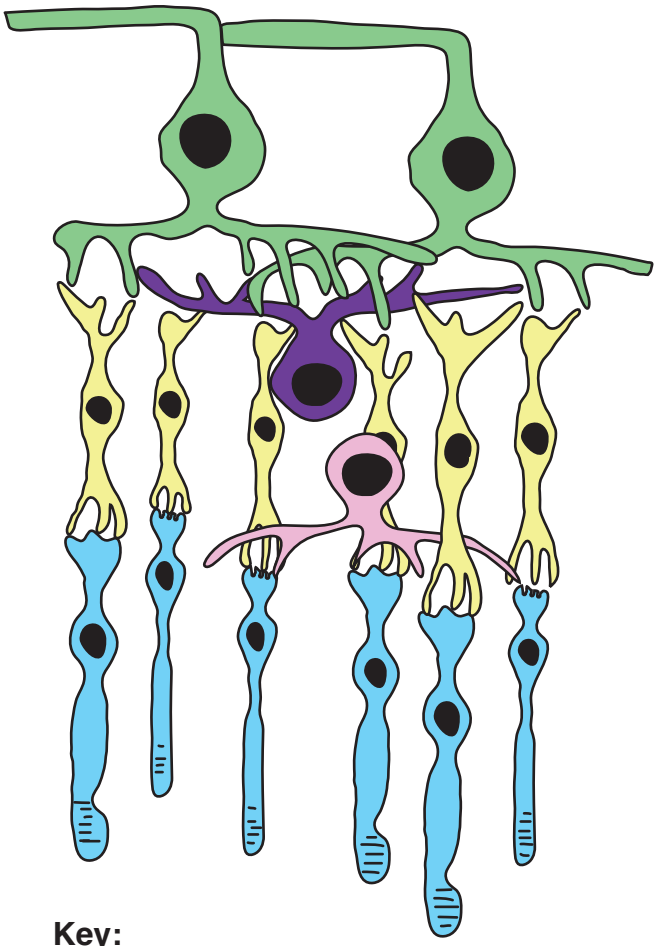

Ganglion cell layer (GCL)

Inner plexiform layer (IPL)

Inner nuclear layer (INL)

Outer plexiform layer (OPL)

Outer nuclear layer (ONL)

Photoreceptor layer (PL)

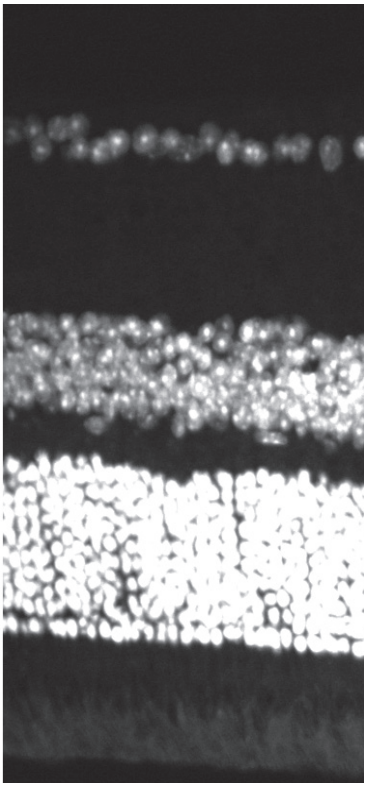

Key:
Retinal ganglion cells
Amacrine cell
Bipolar cell
Horizontal cell
Photoreceptors

Figure 4.1 Eye model and retina layers. (A) Drawing of the eye showing injection into the vitreous humour. Green neurons indicate retinal ganglion cells (RGC), passing through the optic nerve (ON) to the lateral geniculate nucleus (LGN). (B) Schematic indicating the three substances injected into the eye: AAV2 constructs containing TDP-NLS^{-}-GFP or TDP-WT-GFP, and PBS vehicle. (C) Drawing of layers and cell types within the retina (adapted from Swaroop, 2010) and DAPI stained cross-section of mouse retina.

a well-characterised population of neurons and their unique location in the retina (as demonstrated in Figure 4.1B) allows easy access for transduction of their soma as well as an opportunity for detailed analysis of dendrites within the retina, axons within the optic nerve and axon terminals within the visual target areas of the brain (including the lateral geniculate nucleus and superior colliculus) (Figure 4.1A). The functional consequences of foreign gene transduction of RGCs can be assessed by measuring the animals' visual acuity.

In order to investigate what might lead to the neurite abnormalities observed in FTD-TDP and ALS-TDP disease, an appropriate model of TDP-43 pathology is needed. Mislocalisation of TDP-43 from the nucleus to the cytoplasm is a key pathological feature of TDP-43-mediated disease (Neumann et al., 2006) and in cell culture models has been shown to be the most important driver of cellular toxicity (Barmada et al., 2010). In disease, TDP-43 is depleted from the nucleus, and this mislocalisation is proposed to impair its normal nuclear functions. In the cytoplasm, TDP-43 forms insoluble aggregates, positive for ubiquitin and phosphorylated TDP-43 epitopes, which may harm the cell by sequestering other RNA binding proteins (Lee et al., 2012). Several groups have manipulated the nuclear export sequence (NES) and NLS regions of TDP-43 which has resulted in alterations to neurites. In cultured neurons, mutation to the NLS caused cytoplasmic retention of TDP-43, altered neuron morphology and decreased length of axons and dendrites (Han et al., 2013); similar expression *in vivo* leads to axon degeneration (Walker et al., 2015). In the current study, TDP-43 with a defective NLS was expressed in the visual system to create a new TDP-43 disease model. RGCs of C57Bl/6, wildtype (WT), mice were transduced with AAV2 constructs containing the human TDP-43 sequence with a defective NLS, fused to GFP (TDP-NLS^{-}-GFP), and human wildtype TDP-43, fused to GFP (TDP-WT-GFP) (Figure 4.1). Detailed analysis of the cellular changes within the retina and optic nerve were carried out to assess the effects of overexpression of WT TDP-43 and mislocalisation of TDP-43 to the cytoplasm.

4.2 METHODS

4.2.1 Animals:

All experiments involving animals were approved by the University of Tasmania Animal Ethics Committee (A14189 and 16522) in accordance with the Australian Guidelines for the Care and Use of Animals for Scientific Purposes (National Health and Medical Research Council, 2013).

4.2.2 Generation of AAV2 viruses:

Constructs contained human wildtype TDP-43 (TDP-WT, refseq NM_007375) or human TDP-43 with a mutated nuclear localisation signal (TDP-NLS^{-}), fused at the C-terminus to mGFP. A commercial lentiviral TDP-43 plasmid (RC210639 TARDBP insert, cloned into pLenti-C-mGFP PS100071, Origene Technologies) was purchased, and site-directed mutagenesis of the human TDP-43 protein sequence was used to create a defective NLS through a missense mutation (ΔNLS1, K82A/R83A/K84A, as described in Winton et al. (2008). GFP-tagged TDP-43 inserts (TDP-WT-GFP and TDP-NLS^{-}-GFP) were cloned into AAV constructs by Vector Biolabs and AAV with serotype 2 (AAV2) virus produced. Both TDP-WT-GFP and TDP-NLS^{-}-GFP were under the control of the CAG hybrid promoter, consisting of the cytomegalovirus and chicken β-actin promoter (Martin, Klein & Quigley 2002). The TDP-WT-GFP virus had a titre of 2.7×10^{13} GC/ml and TDP-NLS^{-}-GFP virus had a titre of 1.2×10^{13} GC/ml.

4.2.3 Eye injections

Mice were anaesthetised with 5% isoflurane (Isothesia, Henry Schein) in oxygen (600 ml/min). Once mice were anaesthetised, isoflurane and oxygen were reduced to 2% and 300ml/min respectively. For intravitreal injection, a hole was created in the temporal quadrant of the sclera of the left eye with a 31-gauge needle and 1μL treatment solution was slowly injected into the vitreous humour using a 33-gauge needle connected to a Hamilton syringe (Intraocular injection kit, World Precision Instruments, (Massoll, Mando, & Chintala, 2013). The needle tip was inserted into the superior hemisphere of the

eye at the level of the pars plana, at a 45° angle through the sclera and into the vitreous body. This route of administration was used to avoid retinal detachment or injury to the eye structures, including the lens and iris. The injection was performed over a timecourse of 10 seconds and then the needle was held in place for an additional 30 seconds to prevent leakage of the virus/vehicle. Following this, the mouse was allowed to recover on a heating pad.

To determine the optimal injection titre of virus, twelve C57Bl/6 mice (aged 10 to 16 weeks of age) were injected with serially diluted TDP-WT-GFP in PBS (virus concentration and animal numbers in Table 4.1) and left for 1 month for the virus to be expressed. An additional pilot study was carried out to confirm whether similar results were obtained with the TDP-NLS^{-}-GFP AAV2. These mice were perfused over a timecourse of 7 (n=2), 14 (n=2) and 28 (n=2) days to determine when induction of virus expression could be observed.

In mice, synaptogenesis occurs within the first to third week of postnatal development (Pfrieger, 2009), with synapses subsequently pruned before reaching adult levels at approximately four months of age (De Felipe, 1997). Thus, to ensure synaptic maturity six-month-old C57Bl/6 mice were used. Using optimal levels determined previously, mice (n=21) were injected with either TDP-WT-GFP (n=7), TDP-NLS^{-}-GFP (n=7) or PBS vehicle (n=7). Mice were left for 3 months to allow expression of the constructs and development of pathology, based on evidence that an inducible TDP-43 mouse model overexpressing the same NLS defect developed axonal changes four weeks post transgene induction, and had severe denervation of neuromuscular junctions by 6 weeks post induction (Walker et al., 2015).

Table 4.1 Pilot study animal numbers and virus concentrations

Virus concentration (GC/ml)	Number of mice
1.35×10^{13}	2
6.75×10^{13}	1
3.375×10^{12}	2
1.69×10^{12}	1
8.44×10^{11}	2
4.22×10^{11}	1
2.11×10^{11}	1
1.05×10^{11}	1
5.27×10^{10}	1

4.2.4 Optomotor response

The optomotor response was used to measure alterations to visual acuity in mice injected with TDP-43 constructs or controls and was measured as previously described (Heitz et al., 2012) based on principles described by Abdeljalil et al. (2005). The testing rig (Figure 4.5 A) consisted of a 10cm platform, surrounded by a motorised drum (29 cm in diameter), which rotated clockwise or anti-clockwise at two rpm, lined with 5mm black and white vertical stripes. Mice were placed on the platform and habituated to the experimental setup for 5 minutes every day for 7 days prior to injection. The optomotor response (defined as head turning to match the speed of drum rotation) was tested by rotating the drum clockwise or anticlockwise. In mice, the left (treated) eye controls the clockwise optomotor response, and the right (untreated) eye controls the anticlockwise response (Heitz et al., 2012). Testing was carried out 1 week pre-injection, 1 week post-injection and then fortnightly for 3 months.

4.2.5 Perfusions

At 9 months of age, 3 months post-treatment, animals were euthanised for immunohistochemistry (IHC; n=4 animals/treatment) or transmission electron microscopy (TEM, n=3 animals/treatment). For

IHC, perfusions were carried out as per Chapter 2.4. For TEM, mice were anaesthetised as per Chapter 2.4, and then perfused with 0.9% saline until the paws and liver blanched. Perfusion with 60ml of 2% PFA 2.5% glutaraldehyde in phosphate buffer was then carried out. Brains were immediately dissected, severing the optic tract caudally to the optic chiasm. All tissue was post-fixed in perfusion solution at 4°C overnight. The following day, the left (injected) and right (uninjected controls) eyes were dissected under microscopic guidance to obtain retinas, and optic nerves as depicted in Figure 4.2.

4.2.6 Immunohistochemistry

Transduction efficiency and retina IHC was carried out using an antibody against RNA-binding protein with multiple splicing (RBPMS, a retinal ganglion cell marker), on free floating wholemount retina with a 48 hour primary antibody incubation as described in Chapter 2.5. Other IHC studies were carried out on 16μm cross-sectioned retina mounted on slides (cryopreservation and sectioning as described in Chapter 2.5.1), using the primary antibodies in Table 4.2.

Table 4.2 Primary antibody information

Name	Antigen	Species	Dilution	Supplier	Reference number
RBPMS	RNA-binding protein with multiple splicing (marker of RGCs)	Rabbit	1:1000	Genetex	GTX118619
GFP	Green fluorescent protein	Chicken	1:1000	Invitrogen	A10262
GFP	Green fluorescent protein – used in combination with NFH	Mouse	1:1000	NeuroMab	75-131
GFAP	Glial fibrillary acidic protein (marker of astrocytes)	Mouse	1:1000	NeuroMab	G3893
Iba1	Ionised calcium binding adaptor molecule 1 (marker of microglia)	Rabbit	1:1000	Wako	019-19741
NFH	Neurofilament heavy chain	Chicken	1:1000	Millipore	AB5539
Synaptophysin	Pre-synaptic vesicle marker	Rabbit	1:500	Millipore	AB9272

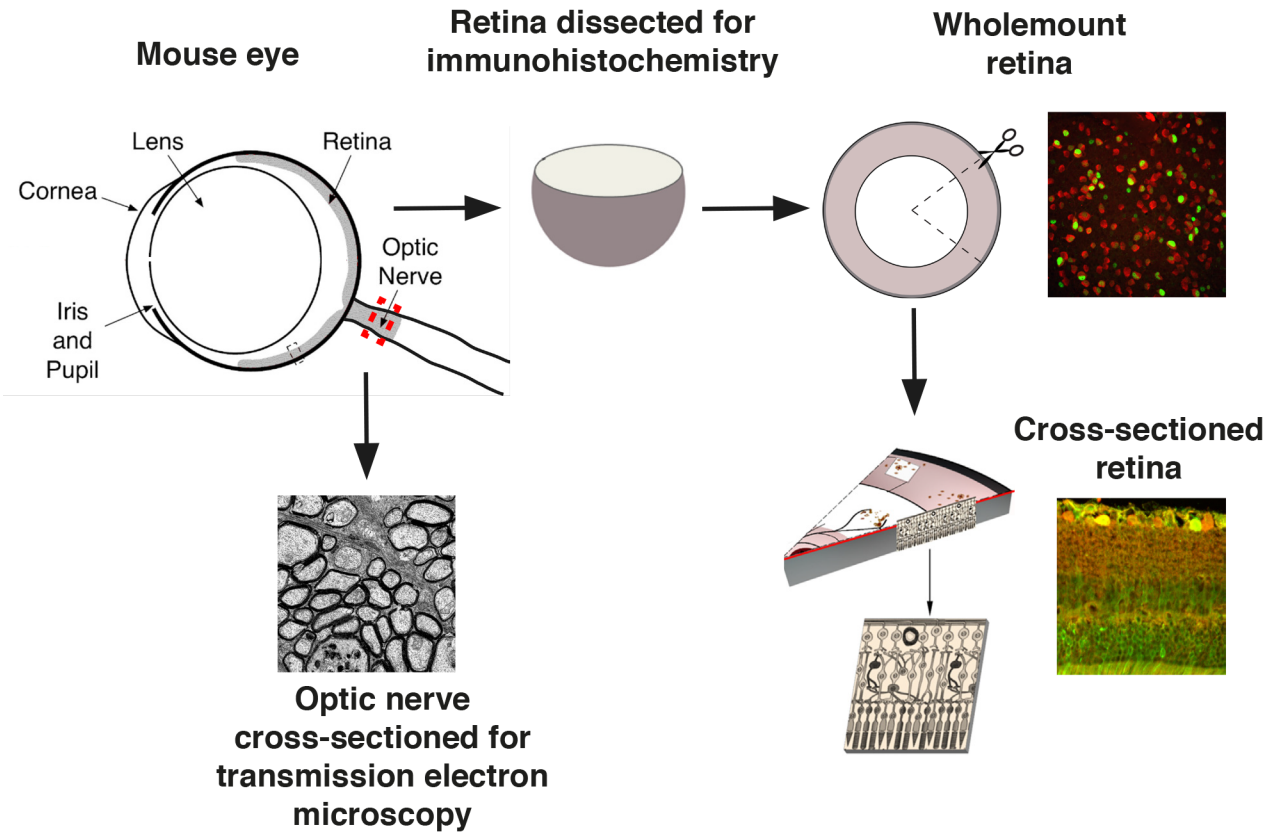
Mouse eye
Retina dissected for immunohistochemistry
Wholemount retina
Lens
Retina
Cornea
Optic Nerve
Iris and Pupil
Cross-sectioned retina
Optic nerve cross-sectioned for transmission electron microscopy

Figure 4.2 Retina and optic nerve dissection. Schematic of mouse eye indicating anatomical features. Retinas were dissected out and cut for immunohistochemistry on wholemount or cross-sectioned tissue. Optic nerves were removed and the proximal portion, indicated by dotted red line, was cross-sectioned for transmission electron microscopy. Figure adapted from Hart, Koronyo, Black, and Koronyo-Hamaoui (2016).

4.2.7 Analysis of cross sectioned retina:

4.2.7.1 Inflammatory response

Iba-1-immunolabelled retina cross sections were imaged and quantitated (n=4 animals/genotype, 4 images spanning across each retina). For analysis a 28mm^2 region of interest (ROI) was constructed over all layers of the retina for each image. Images were segmented using ImageSURF, a random forest classifier for ImageJ (O'Mara, King, Vickers, & Kirkcaldie, 2017), which was used instead of thresholding because it allows for non-biased and reproducible image segmentation based on a classifier, which is "trained" to recognise signal from background. The classifier was trained with sample Iba-1 labelled images, which were manually annotated for positive labelling or background. Based on these training images, the random forest classifier generated automated image segmentation rules. The Iba-1 classifier was then used to segment the provided ROI and ImageJ Particle Analysis tool was used to quantify the percentage area of labelling, which has previously been used as a proxy measure for numbers of microglia (Collins, King, Woodhouse, Kirkcaldie, & Vickers, 2015; Fernandez-Martos, King, Atkinson, Woodhouse, & Vickers, 2015). Qualitative analysis of Iba-1-positive microglia in retina layers was carried out by manual counting.

4.2.7.2 Retina layer thickness

ImageJ was used to measure the thickness of total retina and each retinal layer (ganglion cell layer (GCL), inner plexiform layer (IPL), inner nuclear layer (INL), outer plexiform layer (OPL), outer nuclear layer (ONL), photoreceptor layer (PL; Figure 4.1 C) using DAPI staining (n=4 animals/genotype, 4 images spanning across each retina). Due to potential differences in the sectioning plane between the retinas, thickness of each layer was divided by the total thickness of the retina (Dysli, Enzmann, Sznitman, & Zinkernagel, 2015).

4.2.7.3 Synapse quantitation

Synaptophysin immunolabelling within the IPL was imaged and number of puncta quantitated (n=4 animals/genotype, 4 images spanning across each retina). For analysis, a 300μm^2 ROI was constructed over the IPL layer of the retina in each image (demonstrated in Figure 4.9 A). Images were segmented using ImageSURF as described above, using sample synaptophysin labelled image to train the classifier. Following segmentation, individual puncta were identified using the segmentation and morphological segmentation features of the MorpholibJ plugin for ImageJ (Legland, 2016)) with watershed tolerance set to 10, and results displayed as catchment basins. Puncta between 0.15 and 2μm^2 were measured, as described previously (Mitew, Kirkcaldie, Dickson, & Vickers, 2013). The number of boutons counted per field (synaptophysin density) and the percentage area covered were analysed.

4.2.8 Transmission electron microscopy

4.2.8.1 Fixation

Following primary post-fixation in PFA and glutaraldehyde, the proximal half of the optic nerve (area indicated in Figure 4.2) was dissected for transmission electron microscopy (TEM) and stored in 0.1M phosphate buffer. Secondary fixation in 1% osmium tetroxide (Electron Microscopy Sciences) was carried out for 2 hours at room temperature followed by two washes at room temperature in 0.1M phosphate buffer, and a final wash in 4°C 0.1M phosphate buffer. Samples were then washed twice with deionised H_2O (dH_2O), and tertiary fixation was carried out with 1% uranyl acetate (Merck) for 30 minutes at room temperature. Samples were washed 3 times in dH_2O and dehydrated through graded acetone solutions (70% 1 × 8 minutes; 90% 1 × 8 minutes; 95% 1 × 8 minutes; 100% 4 × 5 minutes).

4.2.8.2 Embedding

Samples were incubated in propylene oxide (ProSciTech, 2 × 5 minutes) and embedded in resin. Embedding consisted of a 2 hour incubation in 1:1 mix of propylene oxide and resin (Procure 812,

ProSciTech); 10 minute incubation at 60°C in resin, followed by overnight incubation at room temperature in the dark in resin; and finally embedding in resin at 60°C for at least 24 hours.

4.2.8.3 Sectioning, staining and imaging

Semi-thin sections (350µm) were cut on a Reichert UltraS ultramicrotome and stained with Toluidine Blue (1% borax) for 30 seconds on a hotplate, and rinsed with cold dH_2O. Ultra-thin sections (70nm) were collected onto copper grids, and stored in a desiccator. Samples on grids were stained with uranyl acetate and lead citrate according to Reynolds (1963). Briefly, grids were incubated in saturated uranyl acetate solution (5% in 50% EtOH) in the dark for 30 minutes, washed in dH_2O and incubated in Reynolds' lead citrate (Sigma Aldrich) for 5 minutes at room temperature, in a CO_2 depleted environment. Samples were washed with dH_2O and stored in a desiccator until imaging on a Hitachi 7700 transmission electron microscope with a LaB6 filament, at 80kV in high contrast mode.

4.2.9 Optic nerve analysis

From each optic nerve (n= 3 animals per genotype), one good quality section was selected and four photomicrographs (2000× magnification) across the section were obtained. ImageJ software was used to select four 10µm^2 ROIs per photomicrograph (n=16 × 10µm^2 ROI across each optic nerve section). These ROIs were chosen at random, although glial nuclei were avoided as per DeMaman, Melo, Homem, Tavares, and Lachat (2010). Axon number and diameter were analysed using the MorphoLibJ plugin (Legland, 2016) and MRI g-ratio toolset ("MRI g-ratio Tools ImageJ macro," 2014). The number of degenerative profiles were manually counted while blinded to treatment group, and were defined as axon profiles with swellings, axonal debris or myelin abnormalities (as described in Joos, Li, and Sappington (2010).

4.2.10 Statistical analysis

Unless otherwise stated, statistical analysis was carried out using one-way ANOVAs with Tukey post hoc tests. Data are presented ± standard error of the mean (SEM), with $p<0.05$ considered

significant. For the optomotor data, linear mixed effects models were used for analysis. Graphical methods (Q-Q and residual plots) were used to determine normality of residuals and homogeneity of variance to satisfy the assumptions of a linear mixed effects model. Random intercepts and slopes were fitted for each animal to account for variance not attributable to the effect of treatment, enabling the assumption of independence to be relaxed for this repeated measures experiment. The R environment (R Foundation for Statistical Computing) and lme4 package (Bates et al. 2015) were used to fit the model using restricted maximum likelihood estimation. F-statistics and denominator degrees of freedom were approximated using the Kenward-Roger approximation implemented in the pbkrtest package (Halekoh & Hojsgaard, 2014). 95% confidence intervals were calculated and adjusted for multiple comparisons using the Tukey method. Detailed analyses are documented in Appendix 4.1.

4.3 RESULTS

4.3.1 Establishment of viral transduction of retina ganglion cells using intraocular injection

A pilot study was carried out to determine the optimal concentration of AAV2 virus to inject into mice. The mice in this cohort underwent serial dilutions of TDP-WT-GFP, and 1μL of virus at 3.375×10^{12} GC/ml was determined to be the optimal concentration to ensure transduction efficiency above 40% (Figure 4.3). A second pilot study was carried out with TDP-NLS^{-}-GFP AAV2 showing similar transduction efficiencies to TDP-WT-GFP AAV2. As these mice were perfused over a time course, GFP expression was detected at low levels at 7 days post injection, and robust expression by 14 days injection (data not shown).

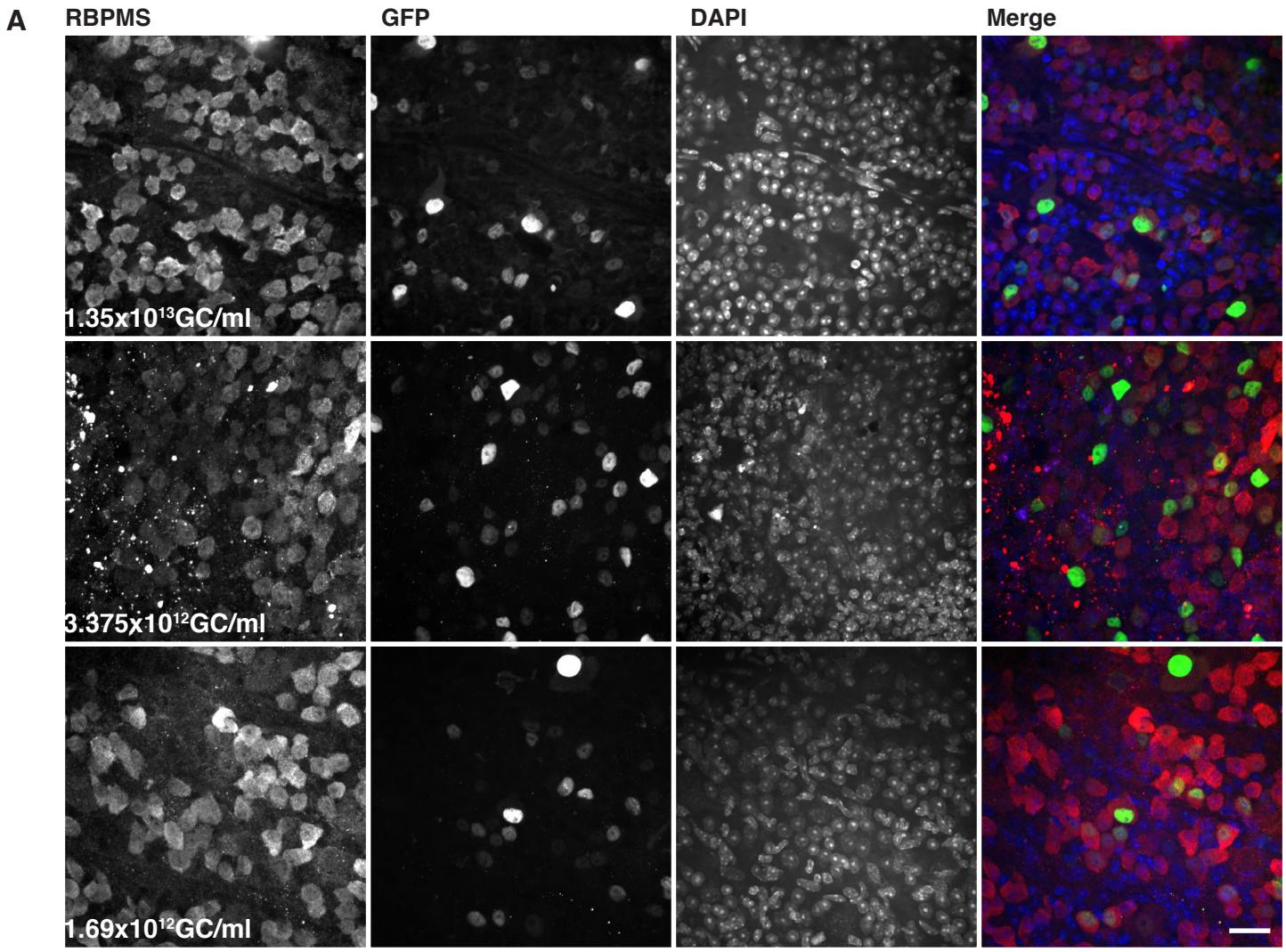
A
RBPMS
GFP
DAPI
Merge
1.35x10¹³GC/ml
3.375x10¹²GC/ml
1.69x10¹²GC/ml

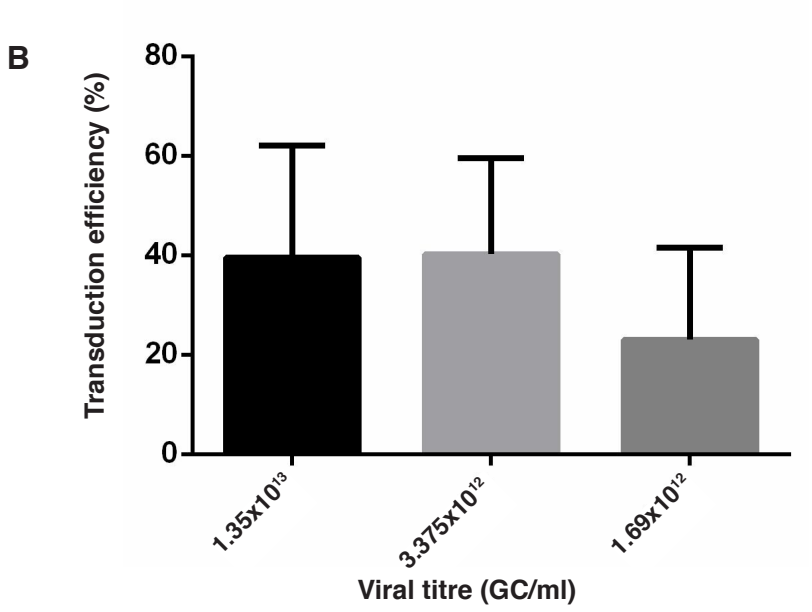
B
Transduction efficiency (%)
80
60
40
20
0
1.35x10¹³
3.375x10¹²
1.69x10¹²
Viral titre (GC/ml)

Figure 4.3 Optimisation of RGC transduction with TDP-WT-GFP. (A) Wholemount retina from mice injected with TDP-WT-GFP at different concentrations (n= 4 per treatment group) immunolabelled for RBPMS (red) GFP (green), and stained with DAPI (blue). (B) The percentage of co-localising GFP and RBPMS RGC bodies were quantified to provide an estimate of viral transduction efficiency for each concentration. Results are mean and deviation. Scale bar 20µm.

4.3.2 Transduction efficiency of AAV2 virus was high for TDP-43 inserts

To study the effect of overexpression of both WT and mislocalised TDP-43, AAV2 viruses were injected into the left eye of C57BL6 mice, and the effects analysed after 3 months. Viral transduction efficiency of RGCs in the retina was confirmed in wholemount retina. Tissue was labelled with antibodies against GFP and RNA-binding protein with multiple splicing (RBPMS), a selective marker of RGCs in the mammalian retina (Rodriguez, de Sevilla Muller & Brecha, 2014). GFP and RBPMS colocalisation (Figure 4.4 A) demonstrated that 67.6% ± 2.9% of RGCs were transduced in TDP-WT-GFP retinas, and 63.1% ± 6.9% of RGCs were transduced in TDP-NLS^{-}-GFP retinas (Figure 4.4 B).

4.3.3 Visual acuity was not altered by treatment

Functional changes to visual acuity following intravitreal injections were determined by the optomotor response (Figure 4.5 A), comparing whether treatment (TDP-WT, TDP-NLS^{-}-GFP or vehicle) altered the number of head turns over time (Figure 4.5 B I). There was no significant effect of treatment ($p>0.05$). The number of clockwise head turns (treated eye) decreased for all treatments, potentially indicating an effect of the injection itself. Differences between treatment groups with respect to direction of head movement were examined, and there was no significant difference in the number of head turns between treatment groups for either orientation (Figure 4.5 B II). Data pooled into pre-injection and 3 weeks post injection (Figure 4.5 C I), when our pilot study showed robust expression of GFP (data not shown), showed no effect of treatment on movement direction (Figure 4.5 C II).

4.3.4 TDP-NLS^{-}-GFP was localised to RGC cytoplasm and proximal neurites

GFP fluorescence was used to assess the localisation of TDP-WT-GFP and TDP-NLS^{-}-GFP within RGCs. Cross-sectioned retinas showed that GFP labelling was restricted to the RGC layer for both TDP-WT-GFP and TDP-NLS^{-}-GFP (Figure 4.6 A), with no GFP present in any other layers of the

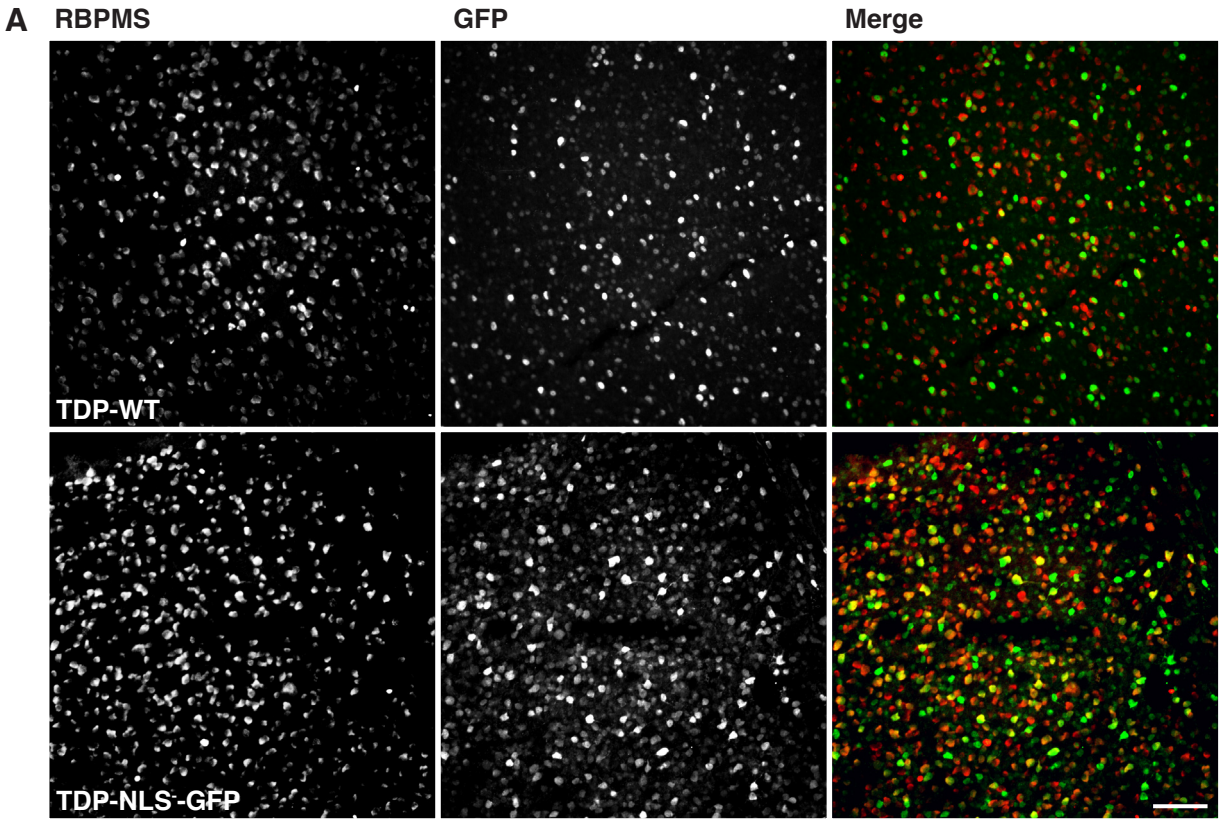
A
RBPMS
GFP
Merge
TDP-WT
TDP-NLS-GFP

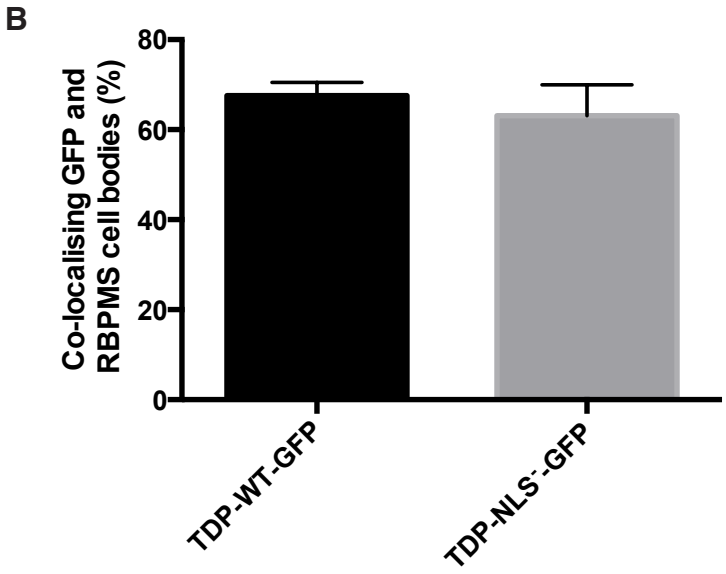
B
Co-localising GFP and RBPMS cell bodies (%)
80
60
40
20
0
TDP-WT-GFP
TDP-NLS-GFP

Figure 4.4 Viral transduction efficiency of TDP-WT-GFP and TDP-NLS-GFP. (A) Wholemount retina from mice injected with TDP-WT-GFP or TDP-NLS—GFP (n= 4 per treatment group) immunolabelled for RBPMS (red) and GFP (green). (B) The percentage of co-localising GFP and RBPMS RGC bodies were quantified to provide an estimate of viral transduction efficiency. Results are mean and standard error. Scale bar 100µm.

A

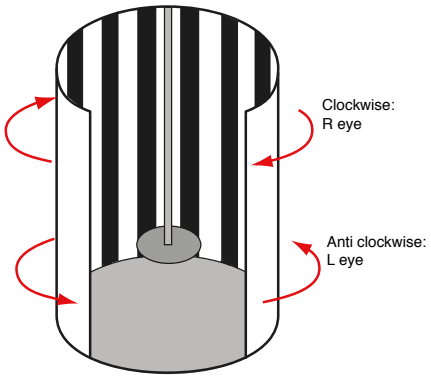

B

i

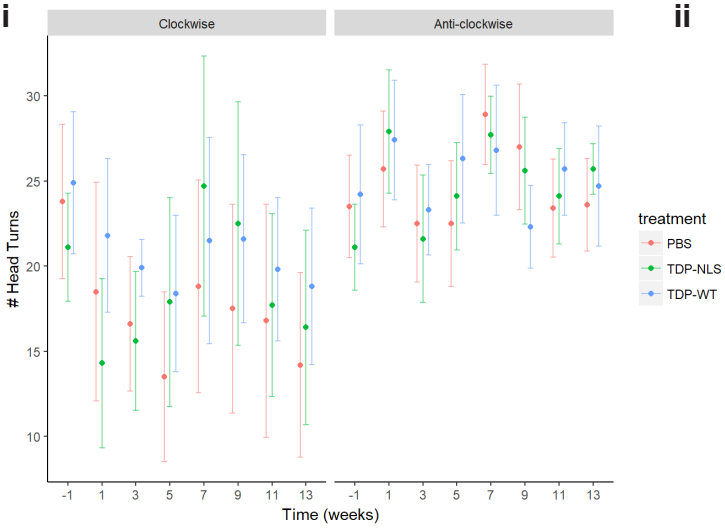

ii

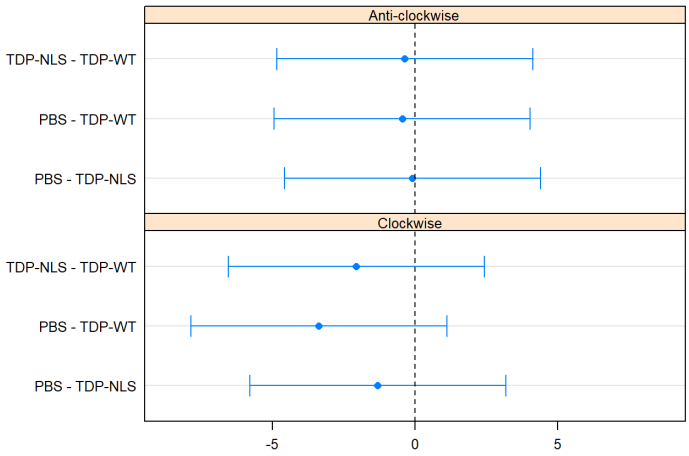

C Pre-injection: 3 week post injection

i

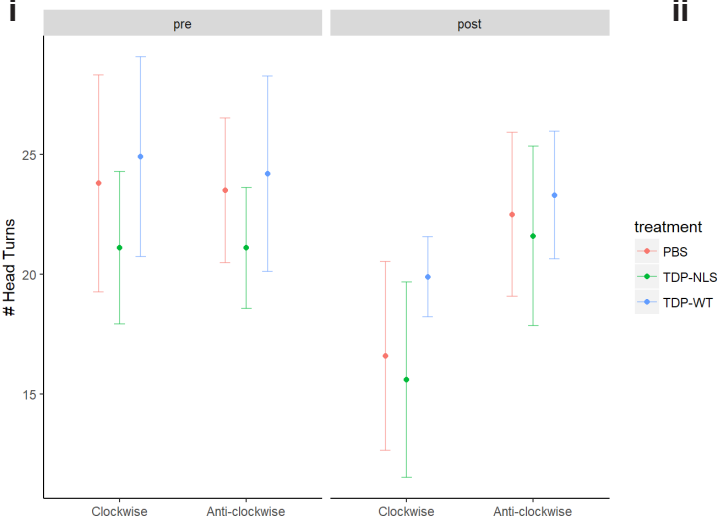

ii

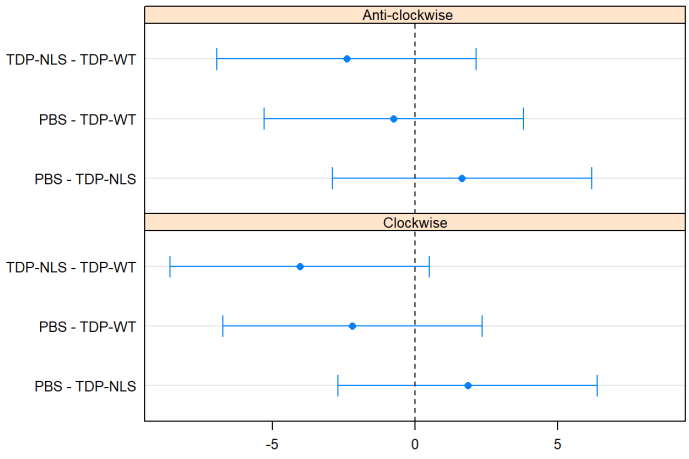

Figure 4.5 Optomotor response. (A) Schematic of the rig used to test optomotor response. (B) (I) Quantitation of number of head turns in clockwise (treated) and anticlockwise (untreated) for each treatment group eyes over time (weeks; n=7 per treatment group). (II) Pairwise comparisons showing mean difference in number of head turns between groups for both orientations, with 95% confidence intervals. (C) (I) Pooled data comparing the number of head turns pre-injection with 3 weeks post injection for clockwise and anticlockwise directions for each treatment group. (II) Pairwise comparisons showing mean difference in number of head turns between groups for both orientations, with 95% confidence intervals.

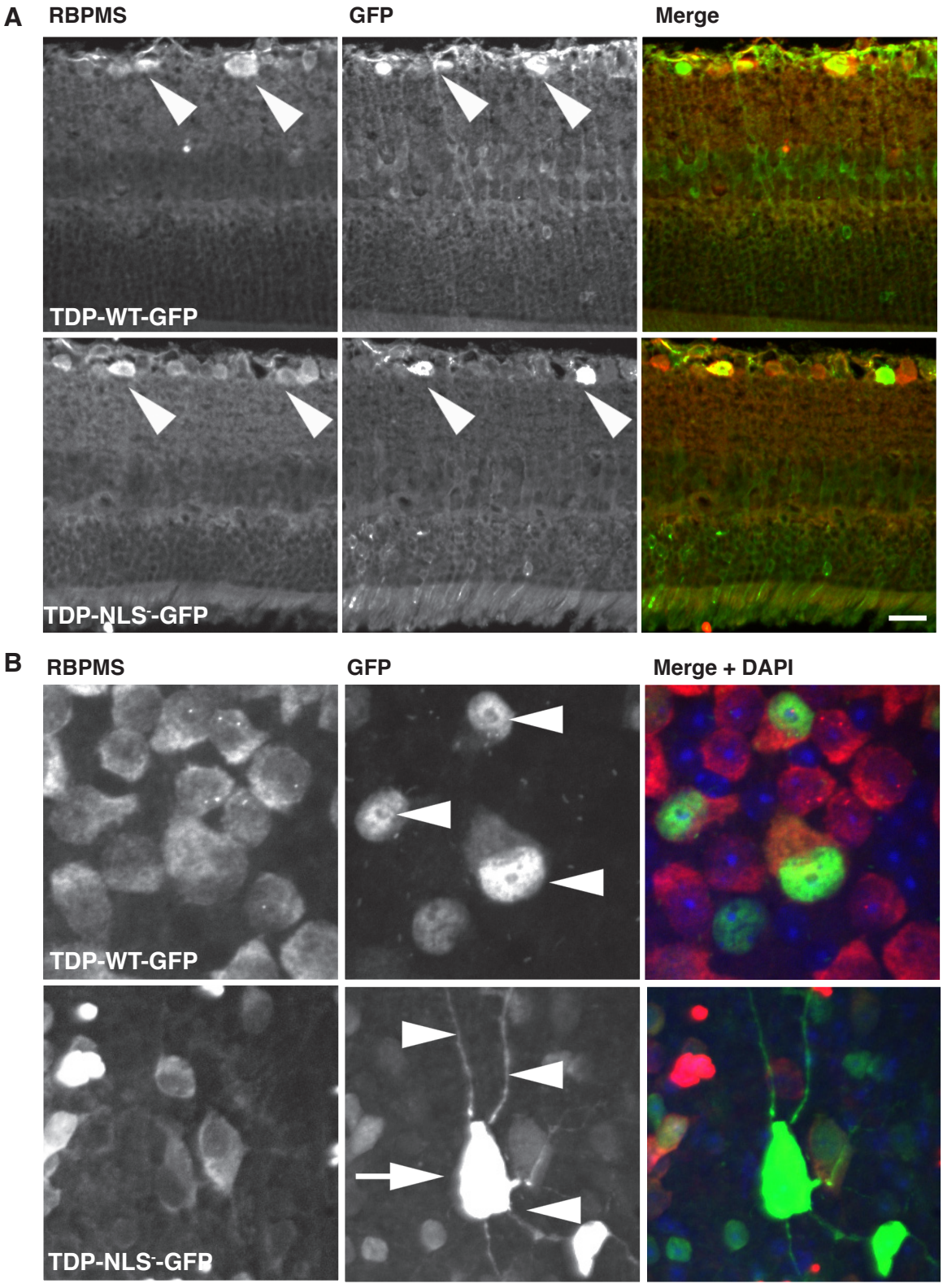
A
RBPMS
GFP
Merge
TDP-WT-GFP
TDP-NLS-GFP
B
RBPMS
GFP
Merge + DAPI
TDP-WT-GFP
TDP-NLS-GFP

Figure 4.6 Localisation of GFP in retinal ganglion cells. (A) Sectioned retinas from mice injected with TDP-WT-GFP or TDP-NLS^{-}-GFP (n= 4 per treatment group) immunolabelled for RBPMS (red) and GFP (green), showing GFP-positive RGC bodies in the upper ganglion cell layer (arrowheads). (B) Wholemount retina from mice injected with TDP-WT-GFP or TDP-NLS^{-}-GFP immunolabelled for RBPMS (red) and GFP (green). Upper panels show TDP-WT-GFP in nuclei (arrowheads). Lower panels show TDP-NLS^{-}-GFP in cell body (arrow) and in proximal neurites (arrowheads). Scale bar (A) 20µm, (B) 10µm.

retina. Flat-mount retina preparations showed GFP fluorescence within RGCs labelled with RBPMS (Figure 4.6 B). In TDP-WT-GFP retinas, fluorescence was localised to the nuclear portion of RGCs, with low expression in the cytoplasm. In TDP-NLS^{-}-GFP retinas, fluorescing cells had high expression throughout RGC somas. In approximately 12% of RGC expressing TDP-NLS^{-}-GFP, fluorescence was present in proximal neurites. These cells corresponded to those expressing GFP at a higher level. No fluorescent aggregates or inclusions (indicated by increased fluorescence in puncta) were observed in either TDP-NLS^{-}-GFP or TDP-WT-GFP.

4.3.5 Altered TDP-43 induced an inflammatory response

Neuroinflammation, indicated by the presence of activated microglia, is a pathological hallmark of many neurodegenerative diseases (Lopez-Valdes, 2016). To determine whether the intraocular injection itself, or expression of TDP-WT-GFP or TDP-NLS^{-}-GFP was associated with alterations in microglia, the expression of Iba-1 was examined in cross-sectioned retinas (Figure 4.7 A). Qualitatively, in vehicle tissue there were sparse numbers of ramified Iba-1 positive microglia across the retina, with the majority of cells located within the GCL, INL and ONL layers (Figure 4.7 A, arrowheads, B). In both TDP-WT-GFP and TDP-NLS^{-}-GFP transduced retinas, Iba-1 positive microglia were more highly ramified, indicative of a change in activation. These hyper-ramified microglia were found within the GCL, INL and ONL layers, as well as in the plexiform layers (Figure 4.7 A, arrowheads, B). As a proxy for the number of microglia in the sections (Collins et al., 2015; Fernandez-Martos et al., 2015), the area occupied by Iba-1 immunoreactivity across all layers of the retina was assessed. Significant differences were detected in the amount of Iba-1 labelling in TDP-NLS^{-}-GFP compared to vehicle retinas (Figure 4.7 C). Although morphology of microglia appeared changed in the TDP-WT-GFP retinas, there were no difference to area occupied by Iba-1

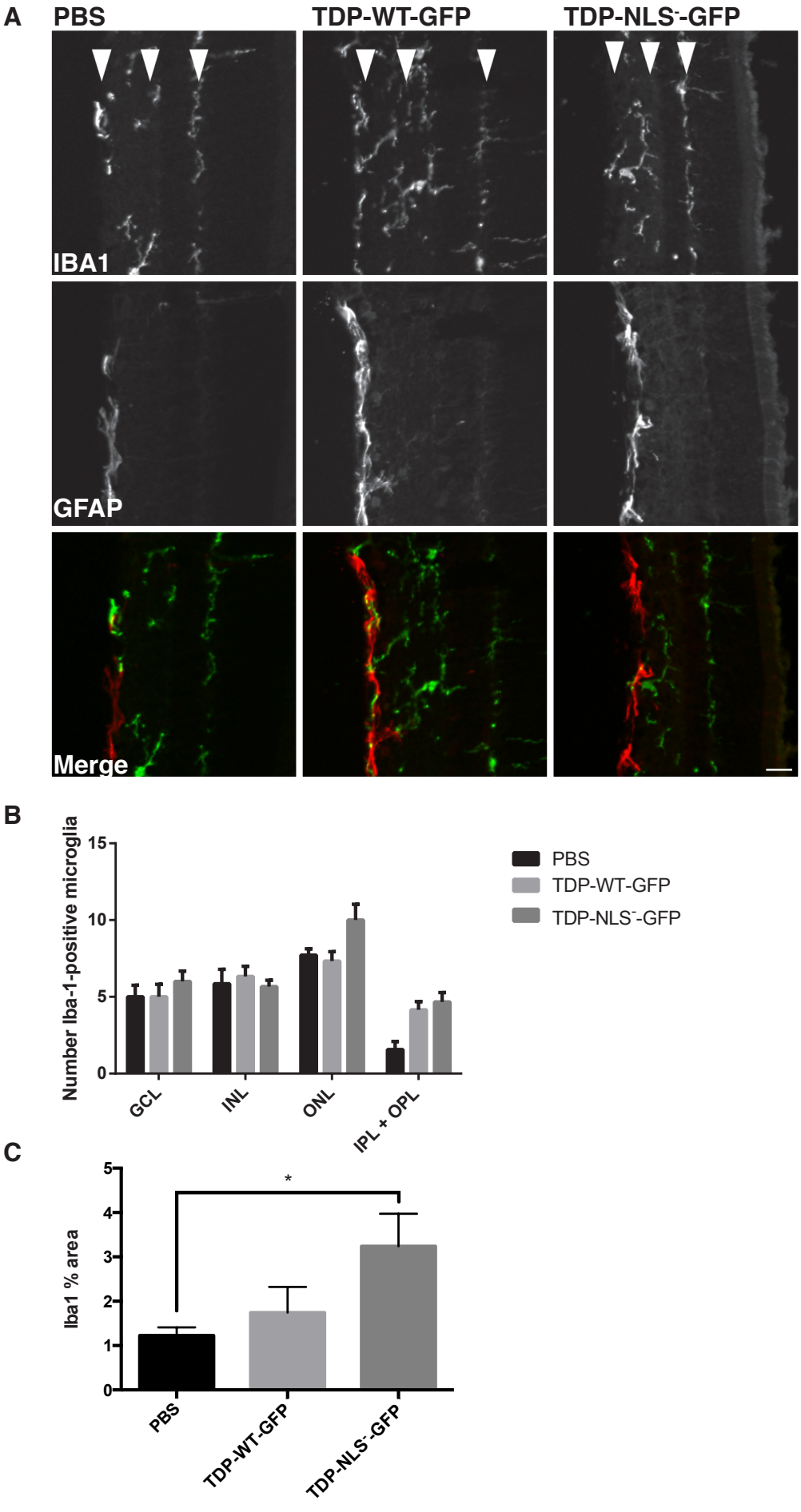
A
PBS
TDP-WT-GFP
TDP-NLS-GFP
IBA1
GFAP
Merge
B
Number Iba-1-positive microglia
15
10
5
0
GCL
INL
ONL
IPL + OPL
PBS
TDP-WT-GFP
TDP-NLS-GFP
C
Iba1 % area
5
4
3
2
1
0
*
PBS
TDP-WT-GFP
TDP-NLS-GFP

Figure 4.7 Microglial alterations associated with transduction with TDP-WT-GFP and TDP-NLS⁻-GFP. (A) Sectioned retinas from mice injected with vehicle (PBS), TDP-WT-GFP or TDP-NLS⁻-GFP (n= 4 per treatment group) immunolabelled with Iba1 (green) and GFAP (red). Arrow heads indicate the GCL, INL and ONL. (B) Counts of the number of Iba-1 positive microglia in each retina layer. (C) The percentage area occupied by Iba1-positive microglia was quantified. Values are mean and standard error. Statistical significance is defined as *p<0.05. Scale bar 25µm.

immunoreactivity. Qualitatively, GFAP-labelled astrocytes also appeared to have more intense labelling in the GCL in both TDP-WT-GFP and TDP-NLS^{-}-GFP retinas.

4.3.6 Laminar structure of the retina was not altered by treatment

Layers of the retina are known to undergo thinning in some neurodegenerative diseases affecting the eye, due to loss of cells, or loss of connectivity between layers of the retina (Abegg et al., 2014; Garcia-Martin, 2014; Syc et al., 2012). In order to determine whether TDP-43 expression in RGCs had downstream effects on the cells providing their inputs, the underlying layers of the retina were examined. The thickness of each of the retinal layers with respect to the total thickness were determined (Figure 4.8 A), and no differences were detected (Figure 4.8 B-H).

4.3.7 Synaptic density was increased in TDP-WT-GFP treated mice

To further determine the effect of TDP-43 expression on the connectivity of RGCs, alterations to presynaptic inputs were examined. Cross-sectioned retinas were immunolabelled with the presynaptic marker synaptophysin and puncta quantitated in the IPL (Figure 4.9). Images were processed using random forest segmentation (O'Mara et al., 2017) and synapses within a 300μm^2 ROI of the IPL were analysed. There was a significant increase (approximately 14%) in the number of synaptophysin immunoreactive puncta per 300μm^2 (synaptic density) in TDP-WT-GFP retinas compared to vehicle and TDP-NLS^{-}-GFP treatments ($p<0.001$) (Figure 4.9 C). There were no differences in synaptic bouton size or the percentage area covered by synaptophysin-positive synapses (Figure 4.9 D, E).

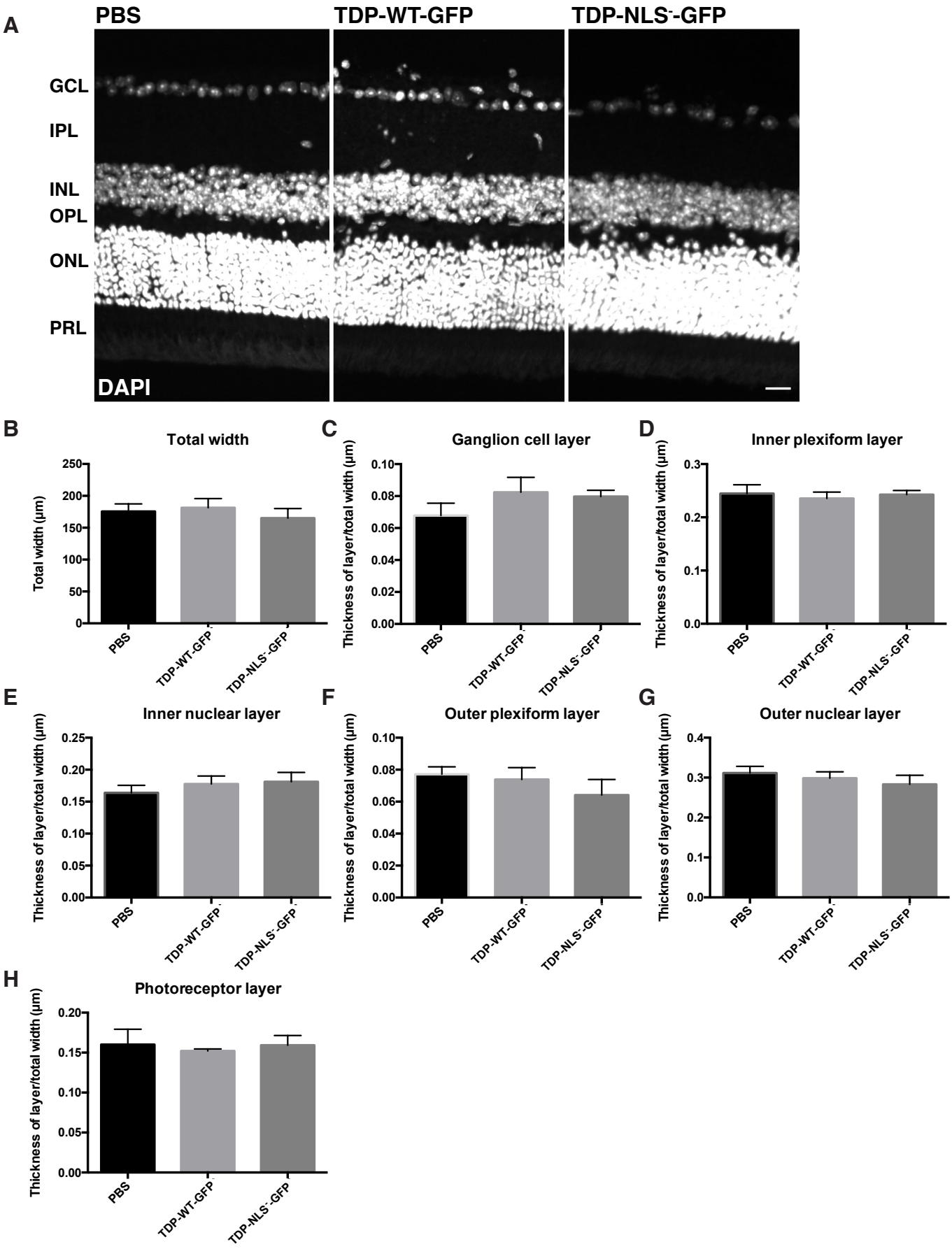
A
PBS
TDP-WT-GFP
TDP-NLS-GFP
GCL
IPL
INL
OPL
ONL
PRL
DAPI
B
Total width
Total width (µm)
C
Ganglion cell layer
Thickness of layer/total width (µm)
D
Inner plexiform layer
Thickness of layer/total width (µm)
E
Inner nuclear layer
Thickness of layer/total width (µm)
F
Outer plexiform layer
Thickness of layer/total width (µm)
G
Outer nuclear layer
Thickness of layer/total width (µm)
H
Photoreceptor layer
Thickness of layer/total width (µm)
PBS
TDP-WT-GFP
TDP-NLS-GFP

Figure 4.8 Thickness of retinal layers. (A) Representative images of sectioned retina from mice injected with vehicle (PBS), TDP-WT-GFP or TDP-NLS^{-}-GFP (n= 4 per treatment group) stained with DAPI showing retinal layers: ganglion cell layer (GCL), inner plexiform layer (IPL), inner nuclear layer (INL), outer plexiform layer (OPL), outer nuclear layer (ONL), and photoreceptor layer (PRL). (B-H) Thickness of each layer with respect to total thickness was quantified, yielding measures of each layer. Values are mean and standard error. Scale bar 20μm.

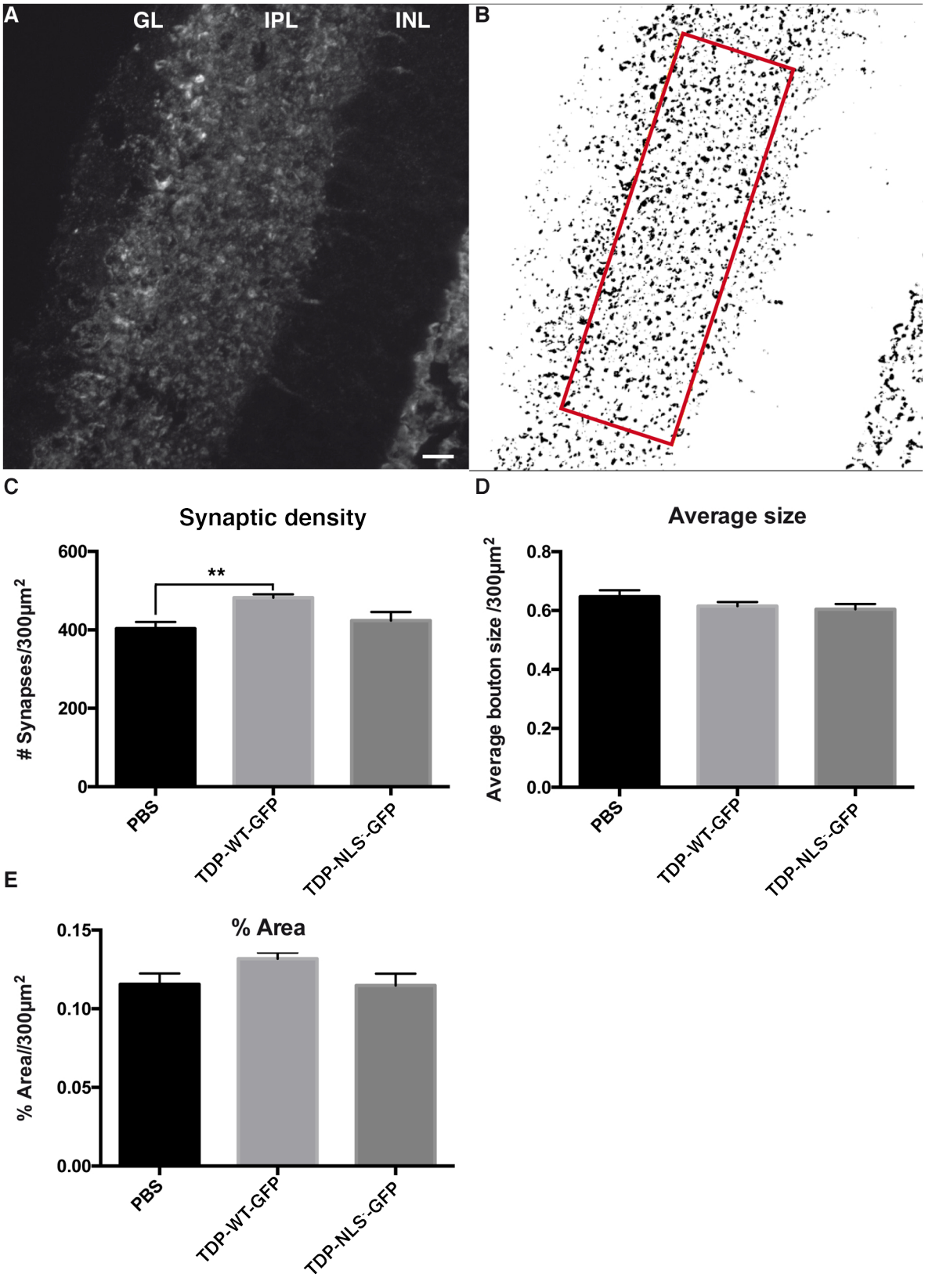
A
GL
IPL
INL
B
C
Synaptic density
Synapses/300µm²
600
400
200
0
**
PBS
TDP-WT-GFP
TDP-NLS-GFP
D
Average size
Average bouton size /300µm²
0.8
0.6
0.4
0.2
0.0
PBS
TDP-WT-GFP
TDP-NLS-GFP
E
% Area
% Area//300µm²
0.15
0.10
0.05
0.00
PBS
TDP-WT-GFP
TDP-NLS-GFP

Figure 4.9 Synaptic alterations in inner plexiform layer of retina. (A) Representative image of sectioned retina immunolabelled with synaptophysin indicating ganglion cell layer (GL), inner plexiform layer (IPL) and inner nuclear layer (INL). (B) Representative image showing segmentation of synaptophysin immunolabelling. Red box indicates 300μm^2 region of interest (ROI) constructed over IPL. (C-E) Quantitation of segmented puncta per 300μm^2 ROI yielded measurements of synaptic density, average size and percentage area occupied by synaptophysin-positive synaptic boutons (n= 4 per treatment group). Values are mean and standard error. Statistical significance is defined as $^{**}p<0.01$. Scale bar 25μm.

4.3.8 Neurofilament localisation was altered in TDP-NLS⁻-GFP retinas

Retinal ganglion cells extend a single axon along the surface of the retina to the optic disk, where it enters the optic nerve and becomes myelinated. The health of the RGC axons were qualitatively examined in the retina for morphological changes following overexpression of TDP-43. Wholemount retinas were labelled with a polyclonal antibody that detects both phosphorylated and non-phosphorylated NFH. This cytoskeletal protein is abundant in a subset of retinal axons, and alterations to NFH have been observed following injury (Mikucki, 1991; Moss, 1983). In axon bundles close to the optic disk, there was strong, continuous NFH immunolabelling along axonal structures, with no qualitative differences between treatment groups (Figure 4.10 A). In more peripheral portions of the retinas from all treatment groups, NFH labelling was also strongly expressed in axons. However, in TDP-NLS⁻-GFP expressing tissue, NFH labelling was also localised to cell bodies. This phenomenon was not observed in TDP-WT-GFP or vehicle treated tissue (Figure 4.10 B).

4.3.9 Ultrastructural alterations to RGC axons

In order to determine whether alterations to TDP-43 caused ultrastructural changes to the RGC axons, analysis of optic nerves was carried out using TEM (Figure 4.11 A). For this study, the optic nerve proximal to the optic nerve head was sectioned. Qualitative analysis of EM sections in vehicle treated mice demonstrated the presence of regularly spaced axons, each surrounded by a myelin sheath, and containing clearly visible cytoskeletal elements such as microtubules and neurofilaments. Occasional mitochondria were also observed. For more detailed analysis, sixteen 10μm^2 ROIs per optic nerve were used. There was a significant increase in the mean number of RGC axons per

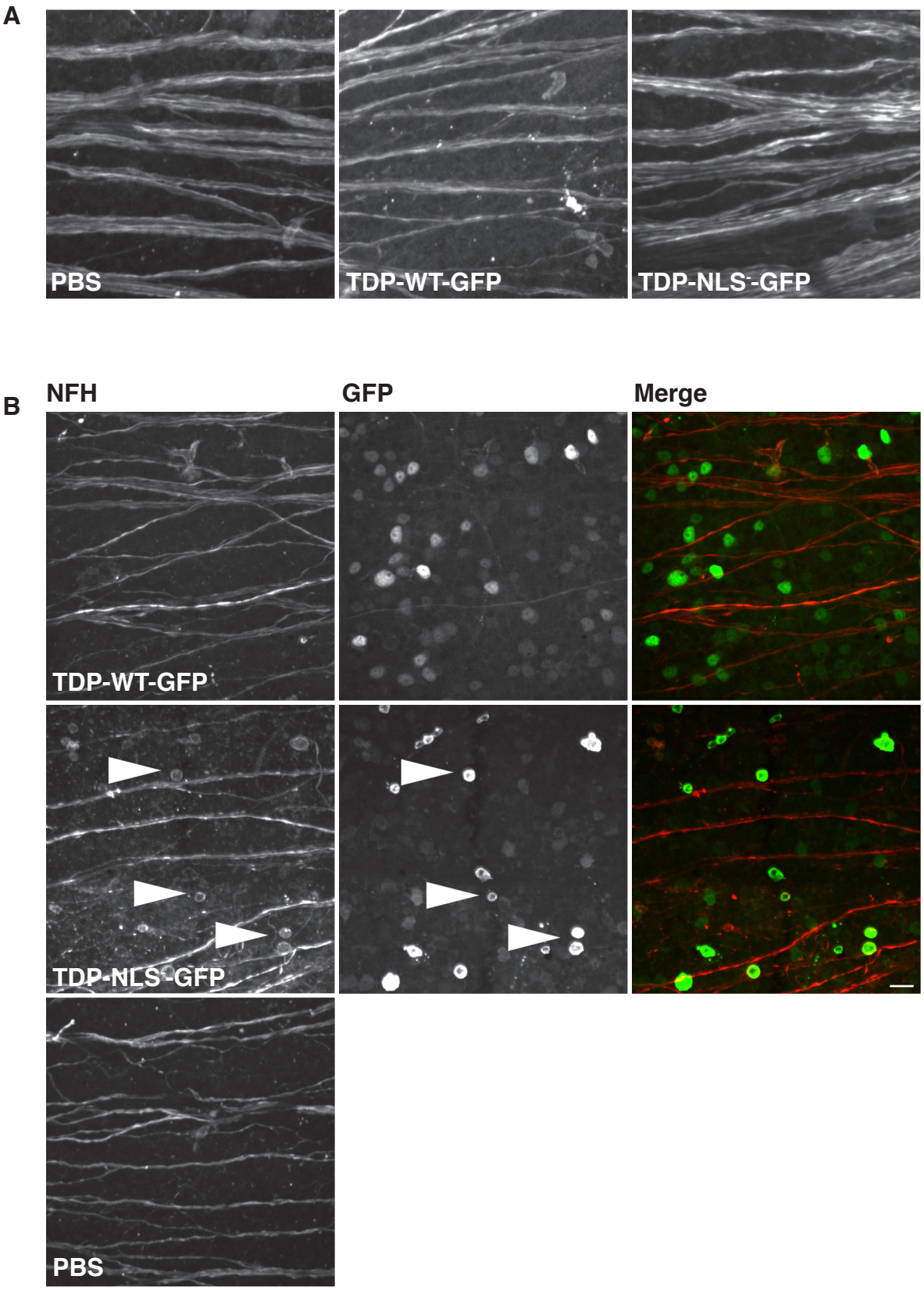
A
PBS
TDP-WT-GFP
TDP-NLS-GFP
B
NFH
GFP
Merge
TDP-WT-GFP
TDP-NLS-GFP
PBS

Figure 4.10 Neurofilament heavy immunolabelling of the retina. (A) Representative images taken close to the optic disk of wholemount retina from mice injected with vehicle, (PBS), TDP-WT-GFP or TDP-NLS^{-}-GFP (n= 4 per treatment group) immunolabelled for NFH. (B) Representative images taken in the peripheral portions of wholemount retina from mice treated as above immunolabelled for NFH (red) or GFP (green). Arrowheads show increased NFH labeling in cell bodies which also have high GFP labeling in TDP-NLS^{-}-GFP injected tissue. Scale bar 20μm.

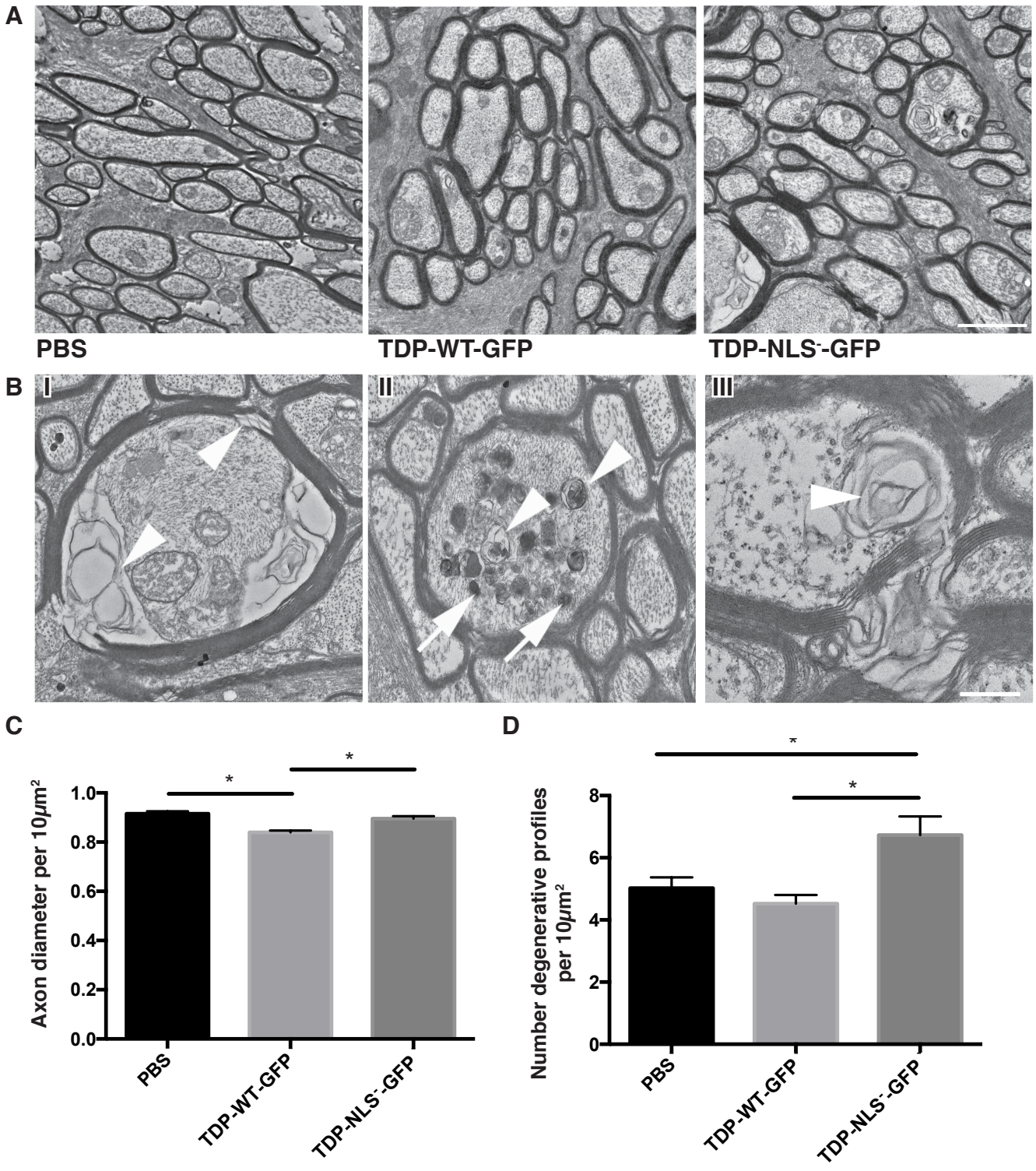
A
PBS
TDP-WT-GFP
TDP-NLS-GFP
B
I
II
III
C
Axon diameter per 10μm²
1.0
0.8
0.6
0.4
0.2
0.0
*
*
PBS
TDP-WT-GFP
TDP-NLS-GFP
D
Number degenerative profiles per 10μm²
8
6
4
2
0
*
*
PBS
TDP-WT-GFP
TDP-NLS-GFP

Figure 4.11 Ultrastructural changes in cross-sectioned optic nerve. (A) Representative electronmicrographs demonstrating 10μm^2 regions of interest of optic nerves from mice injected with vehicle, (PBS), TDP-WT-GFP or TDP-NLS$^-$-GFP (n= 3 per treatment group). (B) Representative electronmicrographs showing examples of degenerative profiles. (I) Arrowheads indicate myelin disruption. (II) Arrowheads indicate degenerating mitochondria, arrows indicate putative autophagosomes. (III) Arrowhead shows myelin disruption and membranous whorls. (C-D) Quantitation of axon profiles per 10μm^2 yielded measurements of axon diameter and number of degenerative profiles. Values are mean and standard error. Statistical significance is defined as *p<0.05. Scale bars: (A) 2μm, (BI-II) 1μm, (BIII) 300nm.

10μm^2 ROI from eyes treated with TDP-WT-GFP compared to both vehicle and TDP-NLS$^-$-GFP ($p<0.05$) (Figure 4.11 C), which corresponded with a significantly smaller diameter of axons in TDP-WT-GFP compared to both vehicle and TDP-NLS$^-$-GFP ($p<0.05$) (Figure 4.11 D). Qualitative analysis of the morphology of axons within the optic nerve suggested the presence of a number of degenerative profiles, identified by myelin breakage or disruption (Figure 4.11 B i, arrowheads), organelle accumulation (Figure 4.11 B ii), and/or membranous whorls (Figure 4.11 B iii). The number of degenerative profilesper 10μm^2 ROI were manually counted and demonstrated that while degenerative profiles were present in all genotypes, there was a significant increase in degenerative profiles in animals treated with TDP-NLS$^-$-GFP compared to vehicle or TDP-WT. It is possible that some degenerative profiles, such as myelin defects, were artefacts due to processing for EM, however the abnormal accumulation of organelles was specific to the TDP-NLS$^-$-GFP tissue. Accumulated organelles appeared to include degenerating mitochondria (similar to those observed by (Ferreirinha et al., 2004); Figure 4.11 B ii, white arrow heads) and autophagosomes (similar to those observed by (Komatsu et al., 2007); Figure 4.11 B ii, white arrows), however more detailed analysis would be required to definitively identify these structures.

4.4 DISCUSSION

Mislocalisation of TDP-43 from the nucleus to the cytoplasm is thought to be an important driver of cellular alterations in FTD and ALS. This study has established a new *in vivo* model for examining whether alterations to expression level and localisation of TDP-43 has downstream effects on cellular morphology, connectivity and cell health, and whether these alterations result in the development of pathological features similar to those found in neurodegenerative diseases with TDP-43 pathology. The visual system allows relatively less invasive access to the CNS and is a valuable model for examining axonal changes as it allows for axons to be traced into the optic nerve and the laminar

structure of the retina allows for examination of connectivity. High transduction efficiency rates for both of TDP-WT-GFP and TDP-NLS^{-}-GFP under the CAG promoter were demonstrated in this study, allowing downstream changes in the optic nerve to be more reliably attributed to overexpression of the transgene. The main findings were that TDP-WT-GFP expression caused an increase in pre-synaptic input into the RGC and was associated with a decrease in RGC axon diameter within the optic nerve. Mislocalisation of TDP-43 (TDP-NLS^{-}-GFP) induced increased density of microglia in the retina, caused mislocalisation of neurofilament proteins and led to axonal alterations in RGC axons.

RGCs transmit visual information from the outer retina layers to the visual areas of the brain. To assess visual function following RGC transduction, the well-established optomotor response test of visual acuity was used (Abdeljalil et al., 2005); RGC loss has been shown to reduce acuity (Ellouze et al., 2008). However, in the current study, there was no significant effect of treatment on this visual parameter despite alterations to RGCs observed in TDP-WT-GFP and TDP-NLS^{-}-GFP treated mice. There was a decrease in the number of head turns in the clockwise direction for all treatments, potentially indicating an effect of the injection itself. More sensitive tests of visual function such as an electroretinogram would be valuable in looking for more subtle changes to visual function caused by overexpression of TDP-43.

This study modeled both overexpression of wildtype TDP-43 and mislocalised TDP-43 due to their associations with disease processes in ALS/FTD. Eyes injected with TDP-WT-GFP demonstrated nuclear localisation within RGCs, with no mislocalisation to the cytoplasm, which was free of both diffuse or GFP-positive aggregates. Multiple studies suggest that mislocalisation of overexpressed WT TDP-43 depends on the rate of overexpression. In cell culture studies by Barmada et al. (2010), transfection with low levels of WT TDP-43 did not result in cytoplasmic localisation and there was no effect on cell survival, whereas higher concentrations of WT TDP-43 resulted in variable mislocalisation to the cytoplasm and a reduction in cell survival (Barmada et al., 2010). Similarly, overexpressing WT TDP-43 on the mouse prion promoter in mice at a rate 2.5x endogenous TDP-43

expression results in cytoplasmic mislocalisation accompanied by severe neurodegeneration (Xu et al., 2010). In contrast, overexpression at of TDP-43 at both 1.5x (Arnold et al., 2013) and 1.9x (Xu et al., 2010) the endogenous rate, results in phenotypically normal mice. In the current study, it is likely that the amount of TDP-43 that was overexpressed in the TDP-WT-GFP treated retinas was insufficient to cause degenerative features.

Expression of TDP-WT-GFP did however lead to an increase in the number of synapses in the IPL of the retina, which contains cell processes and synapses of RGC, amacrine cells and bipolar cells. This suggests that there may be an increase number of pre-synaptic inputs into the RGC. TDP-43 has previously been linked to synapse formation, and is expressed at synapses (Fallini et al., 2012), consistent with a role in regulation of synaptic plasticity by controlling transport of synaptic mRNAs (Wang, Wu, Chang, & Shen, 2008) which could occur *in situ* at the synapse (Liu-Yesucevitz et al., 2011). Both WT and mutant TDP-43 have been shown to reduce the number of synaptic vesicles at the neuromuscular junction (NMJ; Estes et al., 2011). Majumder et al. (2012) found that depletion of TDP-43 leads to an increase in hippocampal dendritic spines. This is consistent with a loss-of-function of TDP-43, suggested by a reduction of in cortical layer 5 pyramidal dendritic spines in an A315T TDP-43 transgenic mouse model (Handley et al., 2016). Together these two studies suggest that synaptic dysfunction may be related to the mislocalisation of TDP-43 to the cytoplasm, which is accompanied by ubiquitin aggregates. In contrast, findings of the current study were that overexpression of WT TDP-43 increased the number of synapses within the IPL of the retina. It is likely that these differences are due to upregulation of TDP-43 in the nucleus in the current study (normal localisation of the protein in healthy cells), possibly enhancing normal function, and the fact that RGCs are not spiny. TDP-43 is upregulated during periods of synaptogenesis in C56Bl/6 mice (Liu et al., 2015), which together with the results of the current study, may suggest that TDP-43 plays a role in the development of synapses. In light of increased branching following overexpression of

TDP-43 in Chapter 3, it would be interesting to examine dendritic abourisation in the retina in future studies.

In contrast to TDP-WT-GFP mice, transduction of RGC with TDP-NLS^{-}-GFP resulted in strong GFP fluorescence in the cytoplasm and the primary neurites in a subset of cells. This cytoplasmic expression may cause the axonal alterations observed within the optic nerve. Other studies, where cultured cells have been transfected with TDP-NLS^{-} constructs, have demonstrated high neuritic expression (Barmada et al., 2010) and axonal accumulation of exogenous TDP-43 (Winton et al., 2008), which has also been recapitulated *in vivo* (Tripathi et al., 2014).

ALS and FTD are characterised by severe white matter loss and axon degeneration, including axon swellings containing neurofilament proteins (Hirano, Donnenfeld, et al., 1984; Hirano, Nakano, et al., 1984). Previous studies using transgenic mice expressing TDP-43 with a mutated NLS recapitulate some features of axon degeneration (Igaz et al., 2011; Walker et al., 2015). Transduction of RGCs with TDP-NLS^{-}-GFP in the current study also led to increased numbers of degenerative profiles in the optic nerve, including accumulations of abnormal organelles, myelin disruption, vacuoles and membranous whorls. The organelles were similar to degenerating mitochondria and autophagosomes found in previous studies examining axon degeneration (Ferreirinha et al., 2004; Komatsu et al., 2007) and further studies will need to be carried out to positively identify the nature of these organelles. Organelle accumulation is an indicator of axon transport defects, which are an important feature of human ALS and mSOD1 models of ALS (reviewed in De Vos & Hafezparast, 2017).

In the peripheral portion of retinas, NFH was increased within cell bodies, which did not occur in TDP-WT-GFP or vehicle treated tissue. It is known that alterations to neurofilament proteins within the cell body are observed following injury. For example, following axotomy, neurons often demonstrate a decreased expression of neurofilament proteins within the cell body (Mikucki, 1991), and after nerve crush injury phosphorylated epitopes of neurofilaments, which are normally localised to axons, can be

observed in the cell body (Moss, 1983). There is tight topographical regulation of expression and phosphorylation of neurofilament proteins, but abnormal accumulation in the cell body may occur if filament assembly is abnormal (Liu et al., 2004). Phosphorylation of the N-terminus of neurofilaments governs their localisation to the soma or axon (Yates et al., 2009) suggesting a dysfunction of this process following transduction with TDP-NLS^{-}-GFP. Accumulation of neurofilament in the cell body could also be related to axon transport defects, characterised by axonal swellings of abnormal organelles, which were observed in the current study. Axonal accumulation of neurofilament is thought to be due to altered stoichiometry of the subunits (Strong et al., 2005; Strong et al. 2001), which may be affected by TDP-43 alterations, since it is known to stabilise NFL mRNA within the nucleus and may regulate its translation in the cytoplasm (Strong et al., 2007). In ALS, NFL mRNA is sequestered to stress granules and its expression is suppressed (Strong et al., 2007; Volkening et al., 2009), reducing the availability of this subunit. Alterations to the location of TDP-43 induced by TDP-NLS^{-}-GFP expression could cause changes to NFL expression and possibly promote the formation of stress granules, leading to altered stoichiometry of neurofilament polymers.

Axon calibre was significantly changed in TDP-WT-GFP optic nerves. This too could be related to alterations in neurofilament stoichiometry as NFM is a key regulator of establishing and maintaining axon calibre (Kirkcaldie & Dwyer, 2017). A major question raised by these results whether TDP-NLS^{-}-GFP leads to cell body changes, followed by axon pathology, or whether the axon pathology precedes cell body changes. Future studies will examine tissue from mice injected over a timecourse to determine if one change is observed before the other.

Inflammation is an important aspect of ALS and FTD, with alterations to microglia, the resident immune cells of the CNS, being a pathological hallmark of these diseases (Lopez-Valdes, 2016; Piguet, 2013). The current study shows increased microglia density within the retina of TDP-NLS^{-}-GFP treated tissue only, with no differences in TDP-WT-GFP or vehicle treated tissue, and qualitative changes to microglia distribution and morphology in TDP-43 transduced retinas. Microglial activation

and migration is observed following CNS injury (Kreutzberg, 1996), and also occurs in areas of protein inclusion pathology in ALS and FTD (Brettschneider et al., 2012). The latter study demonstrated microglial activation in brain regions with high TDP-43 pathology, and mouse models with an inducible form of TDP-NLS^{-}-GFP showed activated astrocytes and microglia in the cortex and hippocampus within one month of expressing the transgene (Igaz et al., 2011). Future studies further investigating the interaction between microglia in normal TDP-43 function, and in TDP-43-induced degeneration would be of interest.

This is the first study to characterize the effect of altered expression and localisation of TDP-43 within a retinal model. Although preliminary, it has provided important data to suggest that the visual system can be used to investigate the downstream effects of TDP-43 alterations on neuronal morphology and ultrastructural changes within axons. Future studies are needed to examine the downstream effects of TDP-43 expression on RGC presynaptic terminals in visual target areas, including the superior colliculus and lateral geniculate nucleus, as well as a more detailed examination of cytoskeletal alterations in the optic nerve and the characterisation of accumulated organelles in the optic nerve. Development of TDP-43 bicistronic constructs, which allow for both the localised expression of TDP-43 and GFP labelling throughout the cells, would be valuable for synaptic studies, and also for examining alterations in transduced axons in the optic nerve. The morphology and dendritic arbourisation of transduced RGS in the retina could also be examined using these constructs.

The current study has developed a new model allowing detailed examination of alterations caused by TDP-43 overexpression and mislocalisation of TDP-43. The eye presents as an ideal model for trialing therapeutic intervention due to the ease of access to the RGC and also the downstream analysis that can be carried out, exemplified in this chapter. While a virtue of the eye model, its simplicity means that results obtained would need to be tested further in models of degenerative disease that can more fully recapitulate disease complexities. Such models for ALS and FTD are currently lacking,

suggesting that more work in this area in required. The results from this chapter will contribute to the knowledge of TDP-43-mediated disease.

Chapter 5:

Results

5 C9ORF72 EXPRESSION AND CELLULAR LOCALISATION OVER MOUSE DEVELOPMENT

5.1 INTRODUCTION

Following on from studies of TDP-43 and how changes to this disease-related protein may cause changes to the neuronal cytoskeleton, the current study was also interested in characterising one of the most recently discovered proteins in FTD and ALS, C9ORF72. In 2011, two independent groups identified the repeat expansion of the hexanucleotide sequence GGGGCC in the *C9ORF72* gene as the largest genetic cause of ALS/FTLD (DeJesus-Hernandez et al., 2011; Renton et al., 2011). This expansion occurs in a non-coding region of chromosome 9. It is currently unknown how the repeat expansion contributes to FTLD and ALS, although several mechanisms have been proposed, including unconventional translation of the repeated sequence (repeat-associated non-ATG initiated translation) leading to intracellular accumulations of dipeptide repeat proteins (Ash et al., 2013; Mori et al., 2013), and the sequestration of RNA binding proteins into RNA foci, causing RNA dysfunction (DeJesus-Hernandez et al., 2011; Simón-Sánchez et al., 2012). An additional possibility is haploinsufficiency due to reduced expression of C9ORF72 transcripts (Ciura et al., 2013; DeJesus-Hernandez et al., 2011; Donnelly et al., 2013; Therrien, Rouleau, Dion, & Parker, 2013; Waite et al., 2014; Xiao et al., 2015).

While pathological features of *C9ORF72*-associated disease, such as TDP-43 aggregates, dipeptide repeat protein expression and RNA foci, are under intense investigation regarding their role in disease, to date, less attention has been paid to the normal expression and function of the encoded protein, C9ORF72. Elucidating the expression, localisation and function of this protein in neural cells may contribute further to knowledge regarding how the repeat expansion is associated with neurodegenerative changes.

In humans, alternative splicing of three RNA transcript variants from the *C9ORF72* gene produces two different isoforms of the C9ORF72 protein (Renton et al., 2011). Transcript variants 1 and 3

encode a 481 amino acid protein and variant 2 encodes a 222 amino acid protein (DeJesus-Hernandez et al., 2011) (Figure 5.1 A). In mice, there are 3 protein-coding regions reported of 481 (isoform 1), 420 (isoform 2) and 317 (isoform 3) amino acids, hence, likely encoding at least 3 different protein isoforms (Figure 5.1 B). However, the roles of the encoded proteins have not been well characterised. A role for C9ORF72 in trafficking has previously been demonstrated (Farg et al., 2014a), which was in line with earlier studies (Levine, Daniels, Gatta, Wong, & Hayes, 2013). Farg et al. (2014b) showed that C9ORF72 is involved in endosomal trafficking via Rab-dependent pathways. Rab proteins are part of the Rab-GDP/GTP exchange factor family (Rab-GEF) (as reviewed in Stenmark, 2009) that mediate all membrane trafficking events between organelles. Farg et al. (2014) provided the first experimental evidence that C9ORF72 regulates endocytosis and autophagy and recent studies have also added to this (Webster et al., 2016).

Other studies have examined the expression of the *C9orf72* gene using a transgenic mouse model harboring a targeted LacZ insertion (Suzuki et al., 2013). This study observed *C9orf72* in neuronal and non-neuronal cells within the central nervous system (CNS). Recently, the effect of ablating the 3 isoforms of C9ORF72 protein from neurons and glia has been examined, demonstrating a reduction in body weight but no motor neuron degeneration or motor deficits (Koppers et al., 2015). This suggests that complete lack of C9ORF72 throughout development and adulthood is not sufficient to cause a motor neuron disease phenotype in mice.

Several studies have examined the expression of C9ORF72 in human tissue (Cooper-Knock et al., 2012; DeJesus-Hernandez et al., 2011; Gijselinck et al., 2012; Hsiung et al., 2012; Snowden et al., 2012; Stewart et al., 2012) and cell lines (Gijselinck et al., 2012; Renton et al., 2011) using a variety of commercial antibodies. However, there has been a lack of consensus about the localisation of

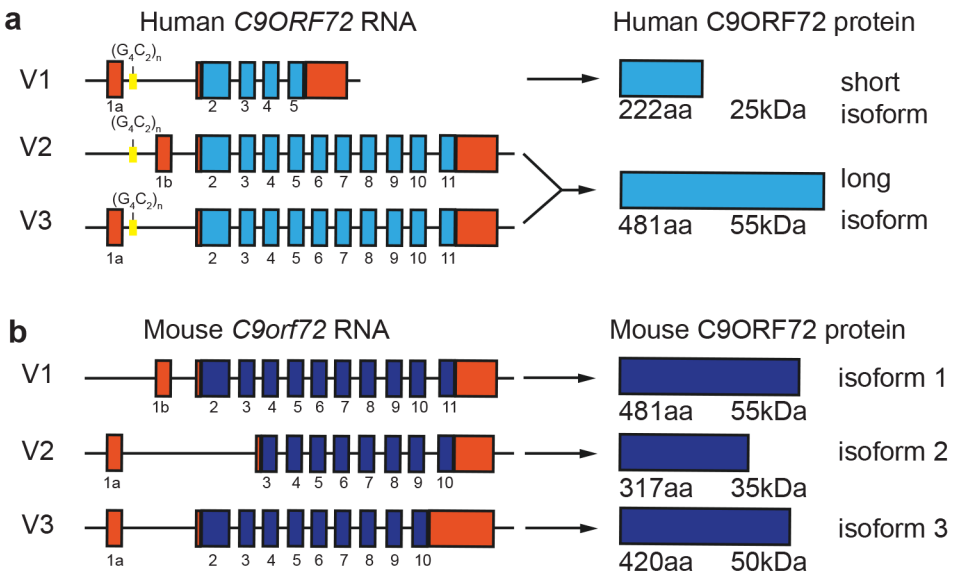
a
Human C9ORF72 RNA
Human C9ORF72 protein
V1
V2
V3
(G4C2)n
1a
1b
2 3 4 5
2 3 4 5 6 7 8 9 10 11
222aa 25kDa
short isoform
481aa 55kDa
long isoform
b
Mouse C9orf72 RNA
Mouse C9ORF72 protein
1b
2 3 4 5 6 7 8 9 10 11
481aa 55kDa
isoform 1
3 4 5 6 7 8 9 10
317aa 35kDa
isoform 2
420aa 50kDa
isoform 3

Figure 5.1 Schematic overview of human and mouse C9ORF72 transcripts and encoded proteins. Protein coding regions for transcript variants (V1 to 3) are indicated in light blue for human (A) and dark blue for mouse (B) as well as size of encoded proteins. Non-coding regions are indicated in red and location of the G4C2 repeat expansion in yellow.

C9ORF72 across these studies. Some investigations have described coarse punctate expression within the hippocampus, suggestive of synaptic terminals (Cooper-Knock et al., 2012; Hsiung et al., 2012; Satoh, Tabunoki, Ishida, Saito, & Arima, 2012; Snowden et al., 2012). Recently, Xiao et al. (2015) generated antibodies specific to the two human C9orf72 isoforms. They demonstrated diffuse cytoplasmic and 'speckled' localisation of the long isoform, as well as localisation of the short isoform to the nuclear membrane. This is in line with previous investigations which demonstrated a nuclear and punctate pattern of expression of C9ORF72 *in vitro* in both SH-SY5Y cells, typical of vesicles, as well as in primary cultured cortical neurons (Farg et al., 2014).

The current study examined the expression of C9ORF72 in the mouse CNS over development *in vivo* and *in vitro* in order to provide information about its expression and cellular localisation during neurite outgrowth, neuron maturation and synapse formation. This investigation demonstrated that C9ORF72 mRNA and protein have differential expression over a developmental time course, is expressed in both nuclear and cytoplasmic fractions in an isoform specific manner, and that the large isoform may be present in synaptic fractions.

5.2 METHODS

5.2.1 Animals

C57BL/6 mice were utilised in this study. All experiments involving animals were approved by the University of Tasmania Animal Ethics Committee (A12780) and were in accordance with the Australian Guidelines for the Care and Use of Animals for Scientific Purposes.

5.2.2 Tissue preparation

For molecular biology analysis, combined neocortical and hippocampal tissue were harvested from mice at embryonic day (E) 18, postnatal (P) 1, P7, P14, P28 and P56 (for Western blot) (n= 4 mice per

time-point) and P1, P7 and P56 (for real time qPCR) (n= 4 mice per time-point). Tissue was processed as previously per Chapter 2.6.

For immunohistochemical analysis, animals were terminally anaesthetised with sodium pentobarbitone (140 mg/kg) and transcardially perfused with 4% PFA. Brains were immediately dissected, post-fixed overnight in paraformaldehyde and then cryoprotected (Chapter 2.5). Serial 40µm coronal sections were cut on a cryostat (Leica CM 1850). For each mouse at each time point, four regularly spaced sections were examined from the rostral to caudal cortex corresponding to bregma 0.98 mm to -1.82 mm (in adult tissue) according to the stereotaxic mice atlas of Franklin and Paxinos (2008). Antigen retrieval was carried out prior to immunohistochemistry using citric acid, pH 6.0, in a pressure cooker for 14 mins (Chapter 2.5.2).

5.2.3 Protein extraction and Western blot analysis

Protein from combined cerebral cortex and hippocampus was extracted as described in Chapter 2.6.1. Denatured proteins samples (15 µg) from each time-point were used for western blotting (Chapter 2.6). A corresponding anti-rabbit or anti-mouse horseradish peroxidase (HRP)-conjugated secondary antibody (1:7000; Amersham) was used, as described previously (Liu et al., 2014). GAPDH (1:7000, Millipore) was used as a loading control and band intensity was measured as the integrated intensity using ImageJ software (v1.4; NIH), and normalised with respect to the loading controls.

5.2.4 Nuclear and cytoplasmic fractionation

Nuclear and cytoplasmic protein extractions were prepared from right hemispheres (excluding olfactory bulbs and cerebellum) of fresh E18, P1, P7, P56 brains using the NE-PER kit (Life Technologies; Chapter 2.6.2). Denatured protein samples were electrophoresed as described above. Fraction purity was confirmed by labelling with HDAC2 (1:700; Abcam) for nuclear fractions and GAPDH (as above) for cytoplasmic fractions. Membranes were also incubated with C9ORF72 (as above). Densitometry of bands was carried out using ImageJ. Results were normalised to total protein.

5.2.5 Synaptosome preparation

Synaptosomes were prepared as described previously (Dunkley, Jarvie, & Robinson, 2008; Mitew et al., 2013) with some modifications. Briefly, P56 mice (n= 4) were anaesthetised and perfused with sucrose buffer (0.32 M sucrose, 1 mM ethylenediaminetetraacetic acid, 5 mM dithiothreitol, pH 7.4). Whole brains were harvested and homogenised at 4 °C with a teflon-glass homogenizer using 12 strokes with 9:1 ratio of sucrose buffer supplemented with a protease cocktail inhibitor (Roche) to 1 g of tissue. Homogenate was centrifuged at 1000 g for 10 mins at 4 °C. The resulting pellet containing mostly nuclei was removed and the supernatant was layered onto a discontinuous gradient consisting of 3 %, 10 %, 15 % and 23 % (vol/vol) Percoll (GE Healthcare). Tubes were then centrifuged at 31,000 g for 8 mins at 4 °C in a Sorvall WX Ultra90 (70.I TI rotor).

The contents of the resulting fractions have been characterised previously (Dunkley et al., 2008; Stigliani et al., 2006). The resulting purified fractions were collected and protein was extracted in RIPA buffer for Western blotting. Denatured protein samples (15 μg) were electrophoresed as described above. Membranes were probed with C9ORF72 antibody, along with synaptic markers: synaptophysin (1:5000, Millipore), PSD-95 (1:1000, Abcam), GAD67 (1:2500, Millipore); and GFAP (1:1000, NeuroMAB) as a marker of glia.

5.2.6 RNA isolation and RT-PCR analysis

Total RNA from combined cerebral cortex and hippocampus tissue at the time-points P1, P7 and P56 (n = 4/group) was isolated using the RNeasy Mini Kit (Qiagen), according to the manufacturer's instructions and complementary DNA (cDNA) was synthesised from DNase-treated RNA (1μg) as described previously by Fernandez-Martos et al. (2009).

To semi-quantitatively analyse *C9orf72* gene expression, real time PCR analysis was conducted as previously described (Fernandez-Martos et al., 2011). Before relative quantification, *C9orf72* gene was subjected to a serial dilution assay to determine the optimum detection range of Ct values, with a

Ct threshold of 35 for undetectable mRNA levels of expression. Relative quantitation of *C9orf72* mRNA isoforms per time point was performed using 25 ng of reverse-transcribed total RNA, 20 pmol/ml of both sense and antisense primers and the SYBR Green PCR Master Mix (Applied Biosystems) in a final reaction volume of 10 µl. The reactions were run on an LightCycler® 480 System (Roche) according to the manufacturer's instructions. To standardize the amount of sample cDNA added to the reaction, amplification of endogenous control β-Actin (primer sequence obtained from Gonzalez-Fernandez et al., 2013) were included in a separate well as a real-time reporter. Primer efficiency was calculated (Figure 5.2 A) and at the end of each run, melting curve profiles were performed to confirm amplification of specific transcripts (Figure 5.2 B). Relative quantification for each gene was performed by the ΔΔCt method (Livak & Schmittgen, 2001).

All primers were designed using *NCBI/ Primer*-BLAST software (Table 1). Primers were designed to amplify the different isoforms of the C9ORF72 mouse ortholog (*3111004O21Rik*). As C9ORF72 isoforms 2 and 3 are contained within isoform 1, fold change in the mRNA expression of isoform 2 and 3 were calculated as the increment with respect to the expression levels of isoform 1.

Table 5.1 List of qPCR primers

Gene name	Forward Primer	Reverse Primer	Accession Number
***C9orf72* isoform 1**	5'-CCCACCATCTCCTGCTGTTG-3'	5'-GTAAGCAAAGGTAGCCGCCA-3'	NM_001081343.1
***C9orf72* isoform 2**	5'-CTTTCCTTGCACAGTTCCTCC-3'	5'-TCATCCTCGATGTACTTGATTAGTG-3'	XM_006538293.2
***C9orf72* isoform 3**	5'-TGGAAGATCAGGGTCAGAGT-3'	5'-GCAAGCAGCTCCATTACAGG-3'	XM_006538294.1

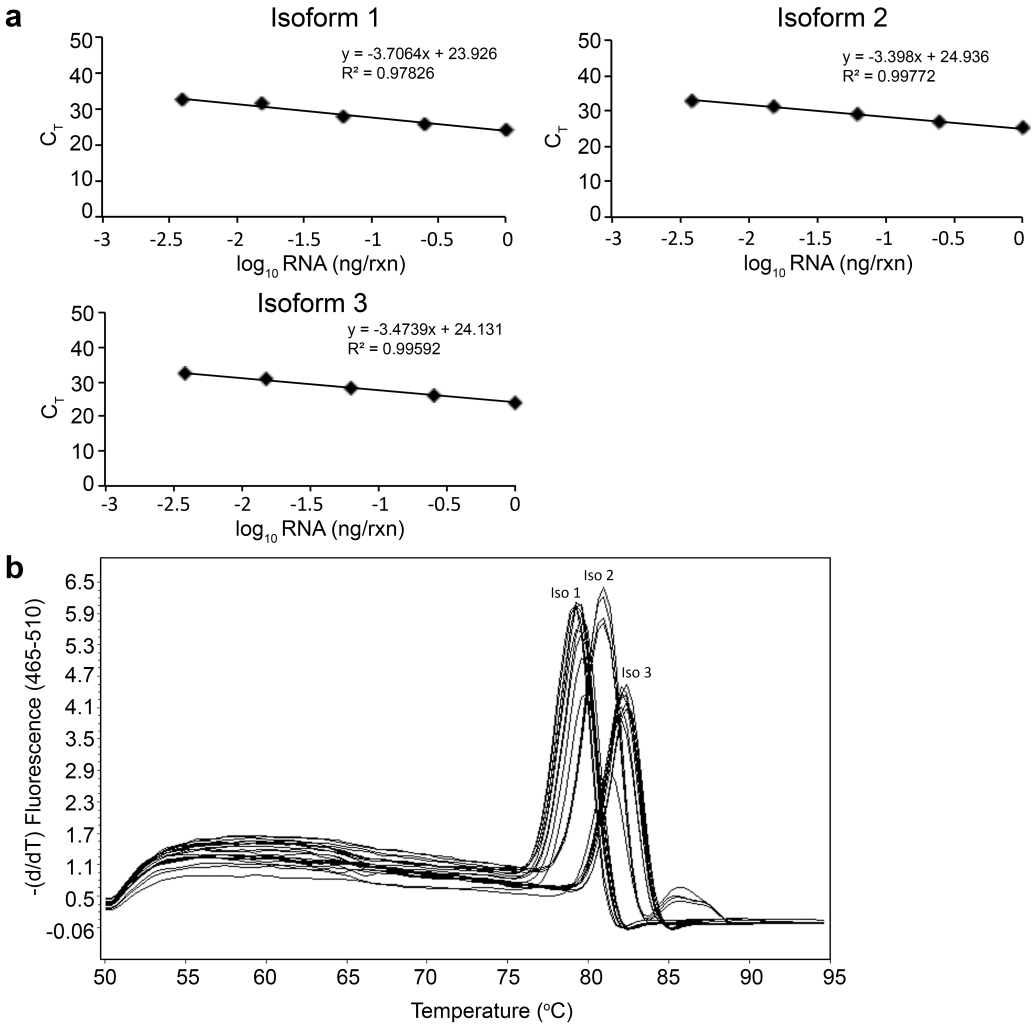
a
Isoform 1
y = -3.7064x + 23.926
R² = 0.97826
Isoform 2
y = -3.398x + 24.936
R² = 0.99772
Isoform 3
y = -3.4739x + 24.131
R² = 0.99592
C_T
log10 RNA (ng/rxn)
b
Iso 1
Iso 2
Iso 3
-(d/dT) Fluorescence (465-510)
Temperature (°C)

Figure 5.2 Primer efficiency and melting curve analysis. (A). The efficiency of the primer pairs for C9orf72 isoforms was assessed by plotting the cycle threshold value (Ct) at each concentration against the logarithm of the fold dilution of the sample. The slope of a linear-regression trendline is indicative of primer efficiency. Primer efficiencies were 1.86 for isoform 1 (a i), 1.94 for isoform 2 (a ii) and 1.97 for isoform 3 (a iii). (B) Representative melting curve analysis showing the specific amplification of the C9orf72 isoform products. Melting peaks (plotted as the negative derivative of fluorescence) revealed peaks at three different temperatures which indicate the identity of amplified C9orf72 isoforms. (TIFF 24326 kb)

Primers used for qPCR analysis of the 3 *C9orf72* isoforms including primer sequence (forward and reverse sequence respectively) and GenBank accession number.

5.2.7 Primary cell culture

Primary dissociated cortical cultures were prepared as described in Chapter 2.2 using standard culture techniques with slight modifications. Dissociated cells were plated onto 12mm coverslips in 24 well plates. Neurons were fixed with 4% PFA (Sigma Aldrich) at 1, 3, 7, 14 and 21 DIV ($n > 5$ cultures per time-point).

5.2.8 Immunofluorescence

Cultured cells and brain sections were incubated 3 x 10 mins in 0.01 M PBS followed by Dako serum-free protein block for 15 min at room temperature (RT). Immunofluorescence labeling was carried out for both cultured cells and brain tissue following standard procedures using C9ORF72 (1:1000 Santa Cruz), β-III Tubulin (1:5000, Promega) and MAP2 (1:1000, Millipore) diluted in 0.01 M PBS with 0.6% Triton-X-100 and incubated at room temperature (RT) overnight. Samples were incubated in secondary antibodies (AlexaFluor, Invitrogen Probes) for 2 hrs at RT, followed by incubation with the nuclear stain DAPI (5µg/ml; Molecular Probes®, Life Technologies), for 5 mins at RT. Immunoreactivity was visualised and captured using a Leica (Germany) DM BL2 upright fluorescence microscope. For the purpose of illustration, images were then adjusted for brightness and contrast using Adobe Photoshop CS6 (v 13).

Specificity of immunoreactivity was confirmed by two methods. Both brain sections and cultured cells were examined for non-specific labelling after processing without primary antibody. Additionally, tissue from P56 brain and 7 DIV cultures were incubated with C9ORF72 antibody combined with 7 times excess of C9ORF72 peptide (sc-138763 P; Santa Cruz).

5.2.9 Statistical analyses

Data from real time PCR studies were compared using a one-way ANOVA followed by a Tukey post-hoc and t-tests for a point-to-point comparison. Data from Western blots were compared using a two-way ANOVA followed by Tukey or Sidak post-hoc comparisons. All statistical analysis was performed using GraphPad Prism software (version 6.0) and p-values with $p<0.05$ (CI 95 %) considered significant. Values were reported as the mean ± standard error (SEM).

5.3 RESULTS

5.3.1 Cellular pattern of C9ORF72 protein changes over development of mouse cortex

This study utilised the commercially available anti-human C9ORF72 antibody (Santa Cruz) raised against amino acid residues 165 to 215 of C9ORF72 protein, which is contained within the sequence of all 3 mouse C9ORF72 isoforms. Previous data has shown a decrease in labeling in a Western blot with the antibody following treatment with C9ORF72 short interfering RNA (siRNA) (Farg et al., 2014). To further characterise the specificity of immunolabelling, the C9ORF72 antibody was preadsorped with recombinant peptide. Immunolabelling of tissue sections from P56 mice (8 5.3 A) and cultured cortical neurons at 7 DIV (Figure 5.3 B) with preadsorped C9ORF72 demonstrated that, relative to non-adsorbed antibody, there was a large reduction in immunolabelling.

Expression or localisation of C9ORF72 over a developmental time-course from E18 to P56 in mice was determined, which covers periods of neurite outgrowth and synapse development (Pfrieger, 2009; Workman et al., 2013). To determine potential alterations in the localisation of C9ORF72 over development, 40 μm coronal tissue sections from mice at ages E18, P1, P14, P28 and P56 were immunolabeled with C9ORF72 antibody along with the neuronal somatodendritic marker, MAP2. At both E18 (data not shown) and P1, there was strong labeling for C9ORF72 in discrete puncta throughout the neuropil (Figure 5.4 A) but little somal immunoreactivity was present. At P7, there

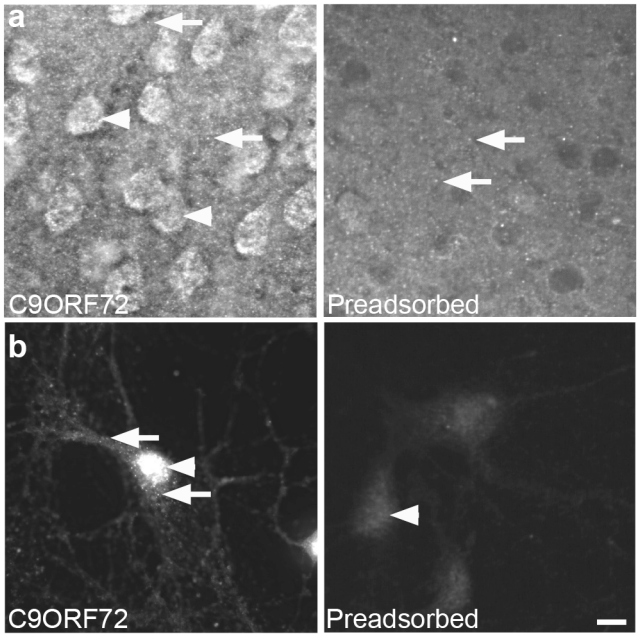
a
C9ORF72
Preadsorbed
b
C9ORF72
Preadsorbed

Figure 5.3 Preadsorbtion with C9ORF72 peptide. (a) P56 tissue from C57/Bl6 mice or (b) 7 DIV cortical neurons cultured from C57/Bl6 mice were labeled with C9ORF72 (sc-138763) antibody or C9ORF72 (sc-138763) antibody preadsorbed with the C9ORF72 peptide (sc-138763 P) (n= 4). Labeling was decreased in both preadsorbed samples. Labeling of puncta (arrows) and nuclei (arrowheads) with C9ORF72 antibody was present in brain tissue and cultured neurons (panel 1, a, b). In contrast, when labeled with preadsorbed C9ORF72 peptide, there was no nuclei labeling and non-specific puncta present in brain samples (arrows, panel 2, a), and in cultured samples there was faint non-specific nuclear labeling and an absence of puncta (arrowhead, panel 2, b). Scale bar: a, 12 μm; b, 10 μm.

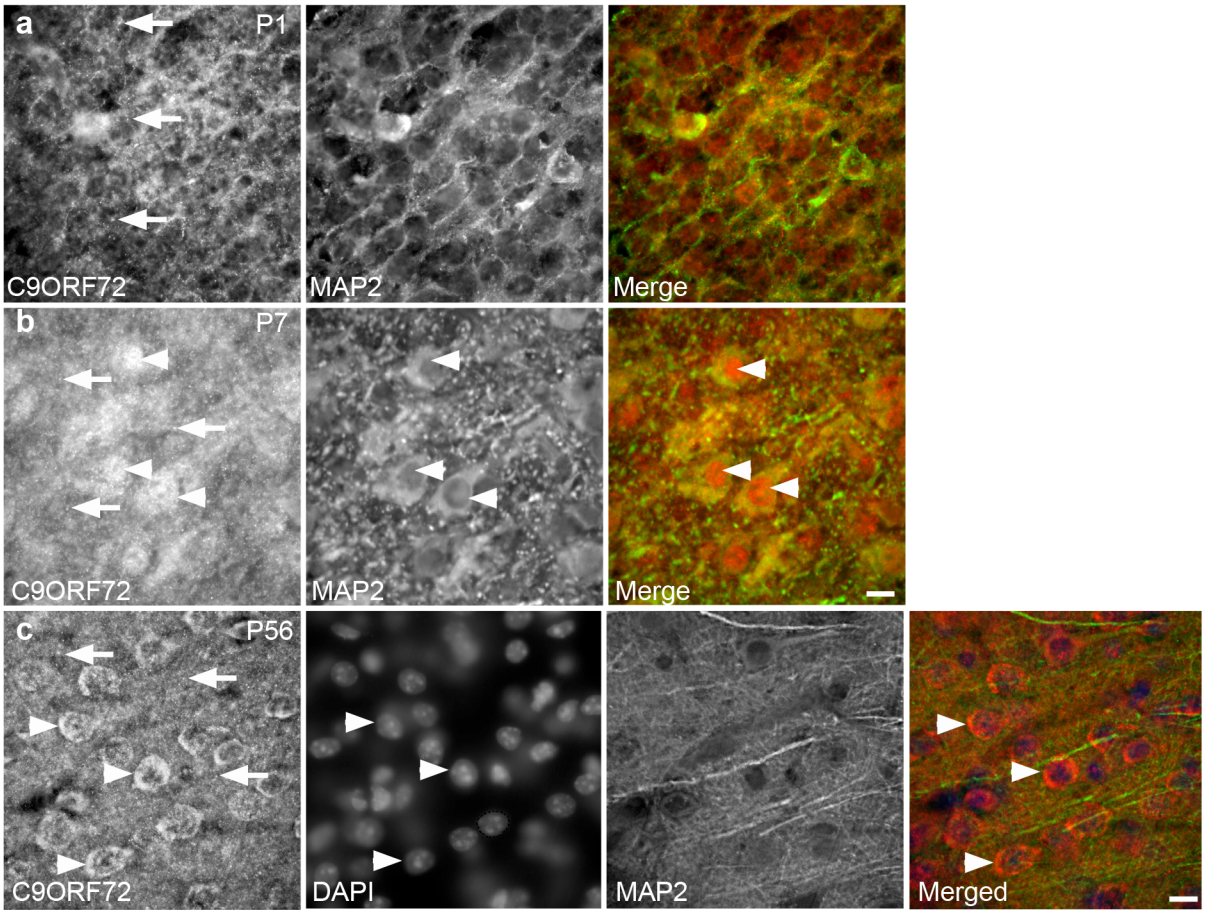
a
P1
C9ORF72
MAP2
Merge
b
P7
C9ORF72
MAP2
Merge
c
P56
C9ORF72
DAPI
MAP2
Merged

Figure 5.4 Localisation of C9ORF72 during development in vivo. (A) At P1, C9ORF72 (red) had punctate localization throughout the neuropil (arrows). (B) At P7, C9ORF72 labeling was present within nuclei (arrowheads) of neuronal cells (MAP2, green) and as strong puncta within cytoplasm and neuropil (arrows). (C) At P56, C9ORF72 labeling was present in the neuropil as puncta (arrows) and was localized to the cytoplasm surrounding nuclei (DAPI, arrowheads). N= 4 animals per timepoint. Scale bar: 10 μm

was distinct somal and nuclear expression, which was both diffuse and punctate in many MAP2-immunoreactive cells throughout the cortex and hippocampus (Figure 5.4 B) confirming the presence of C9ORF72 in neurons. At P14, P28 and P56, cytoplasmic labeling continued with apparent lower expression in nuclei (Figure 5.4 C) Punctate labeling was less distinct than at P1 and P7 (Figure 5.4 A, B).

5.3.2 Temporal expression of C9ORF72 isoforms over development

The temporal mRNA expression pattern of C9ORF72 isoforms (*C9orf72- 1, 2* and *3*) were then evaluated. As shown in Figure 5.5 A, the mRNA encoding for all *C9orf72* isoforms were detected in combined cerebral cortex and hippocampus tissue at all time-points P1, P7 and P56. Isoform 1 was significantly higher ($p<0.05$) at P1 compared to P7 and P56 (Figure 5.5 A) and, similarly, the expression of isoform 2 was significantly higher ($p<0.05$) at P56 relative to the other time points tested (Figure 5.5 A). There were no changes in the mRNA expression levels of isoform 2 over development (Figure 5.5 A). Next, by Western blot analysis, the temporal protein expression of C9ORF72 protein-coding regions (481, 420 and 317 amino acids) were evaluated, which correspond to predicted protein size isoforms of approximately 55, 50 and 35 kDa. Western blots of combined cerebral cortex and hippocampus tissue demonstrated that the Santa Cruz C9ORF72 antibody labelled the 3 predicted protein isoforms (Figure 5.5 B) C9ORF72 protein isoforms at 55, 50 and 35 kDa were detected in combined cerebral cortex and hippocampus tissue at all the time-points. Moreover, additional bands at 110 kDa were also detected. The identity of this band remains unknown.

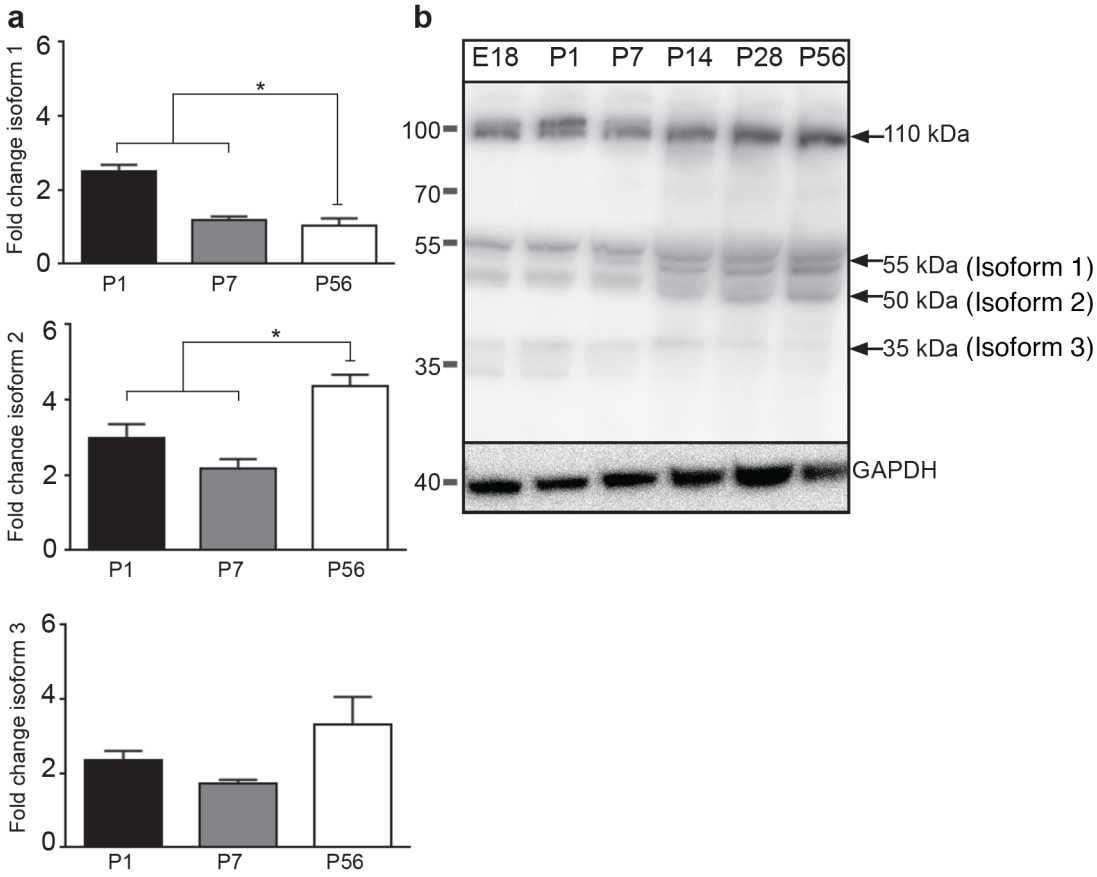
a
Fold change isoform 1
6
4
2
0
*
P1
P7
P56
Fold change isoform 2
6
4
2
0
*
P1
P7
P56
Fold change isoform 3
6
4
2
0
P1
P7
P56
b
E18
P1
P7
P14
P28
P56
100
70
55
35
40
110 kDa
55 kDa (Isoform 1)
50 kDa (Isoform 2)
35 kDa (Isoform 3)
GAPDH

Figure 5.5 Expression of C9ORF72 isoforms over development. (A) Relative expression of C9orf72 isoforms 1, 2 and 3 mRNA in combined cerebral cortex and hippocampus of C57Bl/6 mice (n= 4 per timepoint). Isoform 1 was significantly ($p < 0.05$) higher at P1 compared to P7 and P56 and isoform 2 was significantly ($p < 0.05$) higher at P56 compared to P1 and P7. (B) Western blot of C9ORF72 expression in mouse tissue over development. Bands corresponding to reported isoforms of C9ORF72 were present at 55, 50 and 35 kDa. Additional bands at 110 and 50 kDa were also present. GAPDH was used as a loading control. Values represent mean ± standard error. *$p < 0.05$ P1 and P7 vs. P56

5.3.3 Subcellular localisation of C9ORF72 over development

To further investigate the differential nuclear and cytoplasmic localisation of C9ORF72 over development *in vivo*, nuclear and cytoplasmic protein extractions were performed at E18, P1, P7 and P56. Purity of the nuclear and cytoplasmic extractions was confirmed with HDAC 2 and GAPDH proteins with HDAC2 being higher in the nuclear samples and GAPDH being higher in the cytoplasmic samples (Figure 5.6 A) As in non-fractionated samples, Western blot analysis of C9ORF72 showed protein bands at approximately 55, 50 and 35 kDa. The 55 kDa protein was significantly higher in the nuclear fractions compared to cytoplasmic fractions ($p<0.05$) (Figure 5.6 B). Post hoc tests showed that at E18 and P1 there was significantly ($p<0.05$) more of the 55 kDa protein in nuclear fractions compared to cytoplasmic. Post hoc tests also showed that within nuclear fractions, there was significantly more ($p<0.05$) of the 55 kDa protein at E18 compared to P56. There were no significant differences in cytoplasmic expression of the 55 kDa protein over the time course. There were also no significant differences in localisation of the 50 kDa protein over the time course (Figure 5.6 B). The 35 kDa protein was significantly higher in the cytoplasmic fractions compared to nuclear fractions ($p<0.05$) (Figure 5.6 B). Post hoc tests showed that, at E18 and P1, there was significantly ($p<0.05$) more of the 55 kDa protein in cytoplasmic fractions compared to nuclear. Post hoc tests also showed that within cytoplasmic fractions there was significantly more ($p<0.05$) of the 35 kDa protein at E18, P1 and P7 compared to P56. There were no significant differences in nuclear expression of the 35 kDa protein over the time course. These results suggest that C9ORF72 protein isoforms were differentially expressed in cellular compartments over development

5.3.4 C9ORF72 is present in synaptosome preparations

The results showed that C9ORF72 has punctate localisation in the neuropil, however, it is unclear if it is present in synapses. To address this, subcellular fractionation on P56 mouse brain tissue was

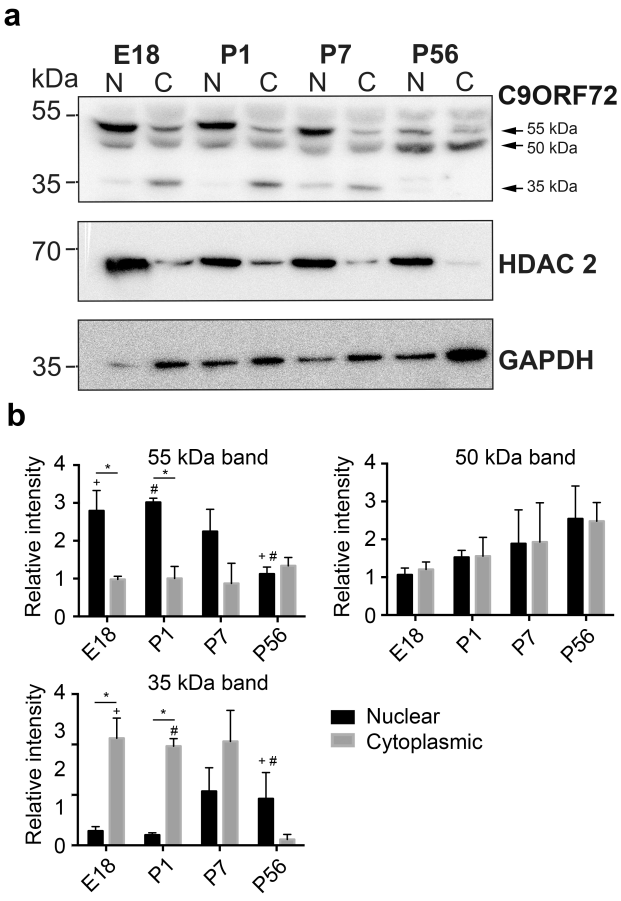
a
E18
P1
P7
P56
kDa
N C N C N C N C
C9ORF72
55
35
55 kDa
50 kDa
35 kDa
70
HDAC 2
35
GAPDH
b
55 kDa band
50 kDa band
35 kDa band
Relative intensity
0
1
2
3
4
E18
P1
P7
P56
Nuclear
Cytoplasmic

Figure 5.6 Expression of C9ORF72 in nuclear and cytoplasmic protein fractions over development. (A) Representative western blot of C9ORF72 in nuclear and cytoplasmic fractions from E18, P1, P7, and P56 mouse brain (n= 4 per timepoint). HDAC2 and GAPDH were used to demonstrate nuclear and cytoplasmic fractions respectively. C9ORF72 isoforms were present at differing levels and in specific fractions throughout the time course. (B) Relative quantitation of C9ORF72 isoform expression in nuclear and cytoplasmic fractions over the time course. Overall, the 55 kDa protein was significantly ($p < 0.05$) increased within nuclear fractions compared to cytoplasmic fractions and specifically at E18 and P1 compared to P56 ($p < 0.05$). Within nuclear fractions, the 55 kDa protein was significantly ($p < 0.05$) increased at P1 compared to P56. There were no significant differences in nuclear and cytoplasmic expression for the 50 kDa band. Overall, the 35 kDa band was significantly ($p < 0.05$) increased within cytoplasmic fractions compared to nuclear fractions and specifically at E18 compared to P56 ($p< 0.05$). Within cytoplasmic fractions, the 35 kDa protein was significantly increased ($p < 0.05$) at E18, P1 and P7 compared to P56. Values represent mean ± standard error. *$p < 0.05$ nuclear vs. cytoplasmic at E18 and P1. + $p < 0.05$ E18 vs. P56 (nuclear for 55 kDa bad, cytoplasmic for 35 kDa band). # $p < 0.05$ P1 vs. P56 (nuclear for 55 kDa band, cytoplasmic for 35 kDa band)

carried out to isolate synaptosome fractions according to the methods of Dunkley and colleagues (2008). The content of each resulting fraction have been characterised previously (Dunkley et al., 2008; Stigliani et al., 2006). F1 contains unidentified membranous material (Dunkley et al., 2008), F2 contains predominantly re-sealed plasma membranes from glial cells (Stigliani et al., 2006). F3 and F4 contain purified synaptosomes and these fractions were combined (Dunkley et al., 2008). To confirm the purity of the fractions, Western blotting was carried out with a range of antibodies. GFAP was used as a glia marker and was most abundant in F2 (Figure 5.7). As expected, synaptophysin, PSD95 and GAD67 were most abundant within the F3/F4 fraction (Figure 5.7). PSD-95 and synaptophysin were also present in F2, possibly binding to synaptic proteins within axonal transport vesicles. Only the 55 kDa protein band of C9ORF72 was observed within C9ORF72-positive fractions, and was most abundant within F3/F4 fractions where other synaptic proteins were found. It was also present at low levels in F2.

5.3.5 C9ORF72 is expressed in nuclei and neurites of cultured cortical neurons

For a more detailed examination of the localisation of C9ORF72 in neuronal soma and neurites, immunocytochemistry was performed in cultured cortical neurons fixed at 1, 3 and 7 DIV (during neurite outgrowth) and 14 and 21 DIV (during synaptogenesis and maturity). Cells were labeled with C9ORF72 along with neuronal cytoskeletal markers βIII-tubulin and MAP2 and the F-actin stain, phalloidin. At 1 and 3 DIV, C9ORF72 labeling was present in the cell soma, excluding the nucleus, and throughout the neurites as demonstrated by co-labeling with βIII-tubulin (Figure 5.8). C9ORF72 also extended into the actin cytoskeleton, including within growth cones and filopodia extending from the soma and down the length of neurites, as demonstrated by co-labeling with phalloidin (Figure 5.8).

From 7 DIV, immunolabelling for C9ORF72 increased in the soma and a large proportion of cells had high nuclear expression of the protein, accompanied by bright puncta in the soma (data not

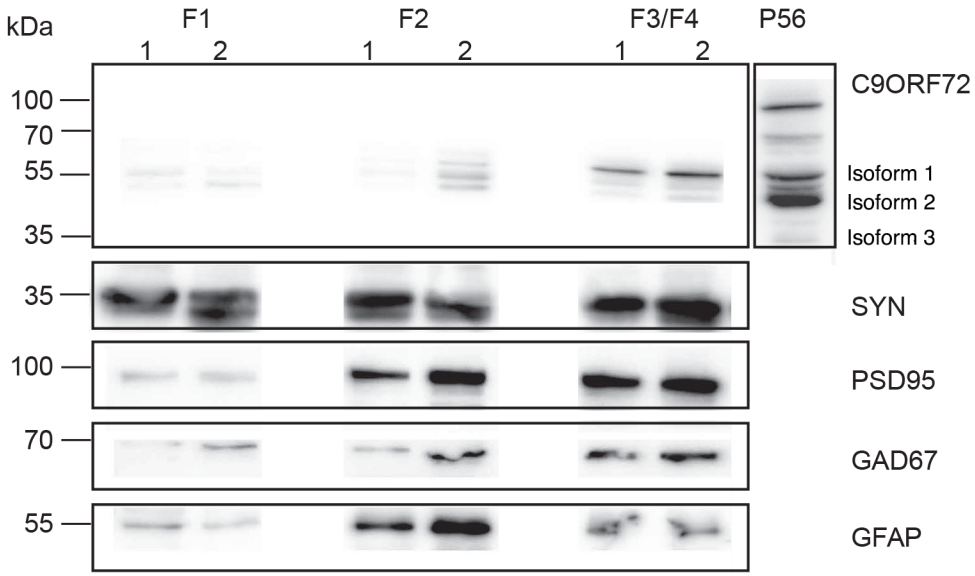
kDa
F1
F2
F3/F4
P56
1
2
1
2
1
2
100
70
55
35
C9ORF72
Isoform 1
Isoform 2
Isoform 3
35
SYN
100
PSD95
70
GAD67
55
GFAP

Figure 5.7 Expression of C9ORF72 in synaptosome preparations from mouse brains. Figure shows representative western blots with results from 2 animals for each marker (indicated by 1 and 2 on figure). The 55 kDa isoform of C9ORF72 was present in the combined F3/F4 fractions which contain synaptosomes. C9ORF72 expression was low in fraction F1, containing membranes, and F2 containing myelin, membranes and glia. Unfractionated brain at P56 was also included. Purity of fractions was determined by labeling with GFAP (F2) and synaptic markers, synaptophysin, PSD-95 and GAD67 (F3/F4).

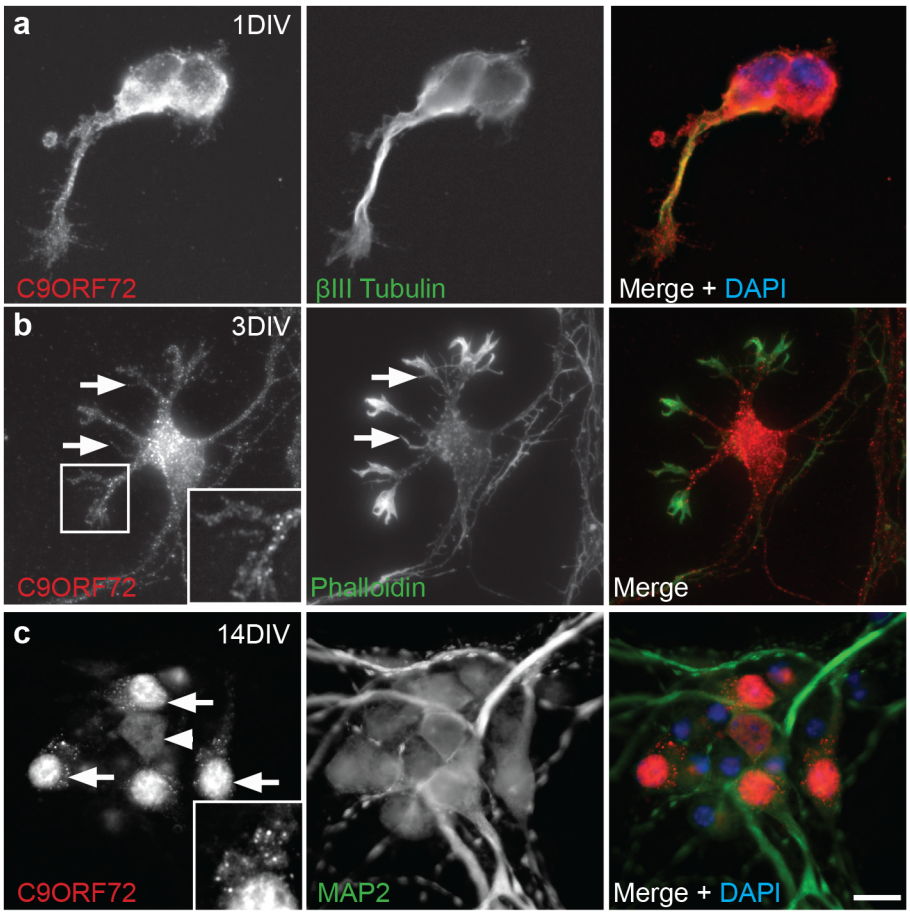
a
1DIV
C9ORF72
βIII Tubulin
Merge + DAPI
b
3DIV
C9ORF72
Phalloidin
Merge
c
14DIV
C9ORF72
MAP2
Merge + DAPI

Figure 5.8 Localization of C9ORF72 over development in vitro. Immunofluorescence was carried out on primary cultured cortical neurons (n= >5 cultures per timepoint). (A) At 1 DIV, C9ORF72 (red) labeling was present within cell bodies, excluding nuclei (DAPI, blue) and punctate localization was present in neurites and growth cones (β-III tubulin, green). (B) Co-staining with phalloidin (green) at 3 DIV confirmed localization of C9ORF72 (red) labeling to growth cones and to filopodia (arrows). (C) At 14 DIV, C9ORF72 (red) was localized to nuclei of a population of neurons (arrows) but was less intensely expressed in nuclei of other neurons (arrowhead). Neurons indicated by MAP2 (green). Neurons with nuclear immunolabeling for C9ORF72 frequently had punctate somal localization of this protein. Inset (c) shows C9ORF72 labeling in nuclei and in puncta in surrounding cytoplasm. Scale bar: A, 2.5 μm; B, C, 10 μm

shown). Similar cellular localisation was observed at 14 DIV with bright vesicular labeled puncta more prominent in, but not restricted to, neurons with nuclear expression of C9ORF72 (Figure 5.8). A smaller proportion of neurons had more diffuse immunolabelling which was present in less intensely stained puncta in the cytoplasm and neurites (axons and dendrites, demonstrated by MAP2 co-labeling) in cells with nuclear and non-nuclear labeling. Immunolabelling of C9ORF72 was similar at 21DIV. These results show that C9ORF72 was present throughout the microtubule cytoskeleton including throughout the axon, soma and dendritic arbor as well as within actin-rich structures such as growth cones and filopodia.

5.4 DISCUSSION

In this study, the expression of C9ORF72 was examined by multiple biochemical and molecular biological analyses conducted both *in vivo* and *in vitro*. Results from these investigations demonstrated that C9ORF72 undergoes alterations in cellular expression and localisation throughout the time-course analysed, which may reflect differential expression of isoforms that are present in specific locations. Furthermore C9ORF72 is found in synaptic-rich cellular fractions.

In order to gain some insight into the function of C9ORF72 protein, the expression level was examined over development. Neuronal development involves a number of different processes and therefore alterations in the expression or localisation of proteins during development may indicate a role in these processes. The results of the current study suggest that there are alterations in the cellular localisation of C9ORF72 protein as well as in the expression pattern of the isoforms over time. C9ORF72 was detected prenatally, consistent with previous studies looking at the protein in mouse tissue (Koppers et al., 2015). C9ORF72 was also observed in adult as well as in embryonic and larval stages in

zebrafish (Ciura et al., 2013; Koppers et al., 2015). A transcription expression study of the mouse ortholog of *C9orf72* found that it was only detectable from P1 in the CNS where it increased gradually until P60 (Suzuki et al., 2013). Koppers and colleagues (2015) suggested these differences could be explained by a failure of the heterozygous LacZ reporter mice used in this study to detect the low levels of gene expression present prenatally.

C9ORF72 isoforms were differentially expressed between the nucleus and cytoplasm. Western blot analysis of nuclear and cytoplasmic protein fractions showed that the 55 kDa band was predominantly nuclear, the 35 kDa band was predominantly cytoplasmic and the 50 kDa band was expressed similarly in both fractions. The expression of mRNA for isoform 1 was higher at P1 than in adult tissue corresponding with higher protein expression of isoform 1 at P1. The higher expression of isoform 1 during these developmental timepoints is consistent with the strong immunohistochemical labeling of C9ORF72 in mouse tissue in postnatal tissue and the localisation of C9ORF72 to nuclei at P7. At P56 there was an increase in isoform 3 mRNA compared to P1 and P7. However, this increase in mRNA content was not reflected at the protein level, where isoform 3 protein was significantly higher at early timepoints. These discrepancies may be explained by differences in mechanisms involved in the post-transcriptional regulation, or repression of translation of isoform 3 mRNA in adulthood. A recent study by Xiao et al. (2015) found differential localisation of human C9orf72 isoforms. The human short isoform (approximately 25 kDa) was localised to the nuclear membrane and the long isoform (approximately 55 kDa) was localised to cytoplasm with diffuse and punctate expression.

The identity of the 110 kDa labeled by C9ORF72 is unknown. These bands have been observed in previous studies (Renton et al., 2011) and also in Western blots from primary cell culture in the current study (data not shown). As the characteristic labeling of C9ORF72 was reduced following preadsorption, it is possible that it may be a dimer of the 55 kDa band resistant to the reducing agents used in the Western blot protocol. Further studies are required to further investigate these bands.

Throughout all time-points in the current study, C9ORF72 had a punctate pattern of immunolocalisation, which is consistent with other studies describing expression of this protein. In mice, synaptogenesis ranges from the first to third weeks of postnatal life (Pfrieger, 2009). It is therefore plausible that, in the current study, the presence of strongly labeled puncta during this time and reports of diffuse cytoplasmic and punctate labeling from other studies (Cooper-Knock et al., 2012; Hsiung et al., 2012; Satoh et al., 2012; Snowden et al., 2012; Xiao et al., 2015) suggest involvement of C9ORF72 at the synapse. Only the 55 kDa form of C9ORF72 was in synaptic-rich fractions in the synaptosome preparations, perhaps indicating a specific role of isoform 1 at synapses. This is also consistent with higher expression of isoform 1 at early postnatal timepoints.

It is unknown why specific populations of cells are vulnerable to degeneration in diseases such as FTLD and ALS. This study showed C9ORF72 expression in neurites and the neuropil. Previous studies have found C9ORF72 within dystrophic neurites within plaques of AD brains and within swollen neurites in the hippocampus of both AD and non-AD brains (Satoh et al., 2012), suggesting that it is present in neurites. Additionally, the protein is observed within swollen axons in the spinal cord ventral grey matter (Stewart et al., 2012). Motor deficits and abnormal motor neuron axons have been described following knockdown of C9orf72 in zebrafish (Ciura et al., 2013), although more recent studies in mice have found no effect of complete lack of C9ORF72 on motor function (Koppers et al., 2015). The results of the current study demonstrate the presence of C9ORF72 as puncta throughout the actin cytoskeleton, and the presence of the protein in synaptic-rich fractions. There are a number of vesicles known to be present in axons including those supplying the synapse, those involved in membrane trafficking and axon outgrowth, and vesicles containing RNA molecules and signaling vesicles (Millecamps & Julien, 2013). Membrane trafficking is critical for cell survival and defects in transport to the membrane are common hallmarks of neurodegenerative diseases, including FTLD (D. Wang, Chan, Cherry, & Hiesinger, 2013). In a similar line, it was recently demonstrated that C9ORF72 is involved in endosomal trafficking via Rab-dependent pathways (Farg et al., 2014). When C9ORF72

expression was knocked down, endocytosis and autophagy-related trafficking were inhibited. Human C9orf72 isoforms have also been shown to interact with nuclear pore complex components, suggesting a possible role in nucleocytoplasmic shuttling (Xiao et al., 2015). These studies, in combination with the results of the current study related to synaptosome preparations and differential nuclear and cytoplasmic localisation, may suggest that C9ORF72 plays a role in trafficking and raises the possibility that failure in such neuronal cellular transport during ageing may be linked to neurodegeneration.

Like many other genetic causes of neurodegenerative disorders, the repeat expansion found in the *C9ORF72* gene is present at birth but does not cause disease until later in life. If haploinsufficiency of the encoded protein, C9ORF72, does contribute to disease then this suggests that it is due to vulnerability caused by altered isoform expression in ageing.

This study has been the first to give a detailed description of the expression of C9ORF72 in mice, including expression over development, and lays a foundation for future studies examining the effects of altering C9ORF72 expression in rodent models, potentially providing insights into how abnormal repeat expansion may be associated with FTLD and ALS. The presence of C9ORF72 within vesicular puncta also warrants further study. Identification of these vesicles could be key to determining the role of this protein within cells.

Chapter 6:

Final Discussion

6 FINAL DISCUSSION

FTD and ALS are two neurodegenerative diseases, which often occur during mid- to latter-life. Currently, neither have effective therapeutics available. ALS has two approved drugs, neither of which offers substantial help: Edaravone has only recently been approved by the US Food and Drug Administration (The Writing Group on behalf of the Edaravone (MCI-186) ALS 19 Study Group, 2017) and its therapeutic benefits are yet to be described, and Riluzole only increases patient life-expectancy by 2 to 3 months (Bensimon, 1994; Miller, Mitchell, & Moore, 2012). For FTD, while there are drugs to alleviate some of the behavioural and psychiatric symptoms, there are no disease-modifying treatments available.

The most important step in developing effective therapeutics for these diseases is understanding their causes. ALS and FTD are likely on a continuum, due to their overlapping features. Both conditions often arise from mutations to the *C9orf72* gene, which can cause abnormal accumulation of TDP-43 in surviving cells of the brain and spinal cord. Accumulation and mislocalisation of TDP-43 also occur in other familial and sporadic forms of the FTD and ALS. In addition to gross brain and spinal cord atrophy, both diseases are characterised by significant neurite pathology including white matter loss, loss of dendrite arbours, synaptic dysfunction and axon swelling and degeneration. These abnormalities are likely to stem from cytoskeletal disruption, but the involvement of TDP-43 pathology in driving these abnormalities, and whether the C9ORF72 protein also plays a role in regulating the cytoskeleton, remain key questions. The main aim of this thesis was to characterise the roles of TDP-43 and C9ORF72 in the development of cytoskeletal pathology by examining their effect on neurites.

6.1 ALTERATIONS TO NEURON MORPHOLOGY

Neurons require tight regulation of processes like pathfinding, neurite outgrowth, branching, growth cone formation and synapse formation, which must be adequately maintained across the entire lifespan to preserve connectivity of the brain. In the intact CNS, connectivity via synapses depends upon arbourisation of both dendrites and axons, and thus remodeling of these structures may disrupt function. Dendrite arbourisation is damaged in both ALS and FTD, (Ferrer et al., 1991). The finding in chapter 3, that overexpression of WT TDP-43 alters cortical neurite branching, suggests a direct pathogenic role for TDP-43 when considered along with several studies linking TDP-43 to neurite branching (Herzog et al., 2017; Lu et al., 2009; Schwenk et al., 2016). Models of ALS, including the G93A SOD1 mouse model, exhibit reduced dendritic arbourisation associated with excitability changes (Fogarty, Noakes, & Bellingham, 2015; van Zundert, Izaurieta, Fritz, & Alvarez, 2012). In human ALS, hyper-excitability occurs in both upper and lower motor neurons (Kiernan, 2012; Vucic, 2006), and may leave them more susceptible to additional insults (Bae, Simon, Menon, Vucic, & Kiernan, 2013). Increased synapse numbers following overexpression of WT TDP-43 *in vivo* (Chapter 4) further imply a relationship between TDP-43 and neuronal connectivity. Although the origin of disease processes in both ALS and FTD remains unknown, alterations to TDP-43 may mediate changes in morphology and perhaps ultimately changes to connectivity.

When retinal ganglion cells (RGCs) were used as a model of TDP-43 axonal effects, overexpression of TDP-WT caused a decrease in axon caliber in optic nerves *in vivo*, further supporting a role for TDP-43 in regulating cytoskeletal composition in these axons. Specifically, neurofilament proteins, particularly NFM, are important for establishing and maintaining axon caliber (Barry et al., 2012), and changes to neurofilament composition may account for the decreased axon diameter. This range of evidence associating altered TDP-43 expression with changes to neurite morphology pinpoint this as a vulnerable pathway through which TDP-43 pathology may act.

6.2 ACTIN CYTOSKELETON

This thesis demonstrated a potentially significant relationship between TDP-43 and C9ORF72 and the actin cytoskeleton. Within neurons, actin plays several roles including support of membranes, regulating axonal transport, motility of the developing growth cone and pre- and post-synapse formation, and is the substrate for myosin motor proteins (e.g. myosin Va) which link cytoskeletal elements. Disruption to the actin cytoskeleton can perturb synapse formation and neuronal integrity (W. B. Zhang, D. L., 2001, reviewed in Eira et al., 2016), and it is closely regulated by a number of signalling pathways, particularly the Rho GTPase family, which act upstream of actin binding proteins (Nobes, 1995). In chapter 3, proteomic analysis identified actin binding proteins as one of the most upregulated groups in response to TDP-43 overexpression in culture, including Myh9 in agreement with previous work (Freibaum et al., 2010; Stalekar et al., 2015) but also including actin binding proteins not previously linked to TDP-43 changes. Consequent disruptions to the actin cytoskeletal network included changes to neurite branching and growth cone morphology, which could be attributed to interactions with Rac1 and Cdc42, key Rho GTPases which TDP-43 has previously been shown to modulate (Iguchi et al., 2009).

This thesis further identified novel potential links between C9ORF72 and the actin cytoskeleton. In chapter 5, C9ORF72 expression in cultured cortical neurons extended beyond the microtubule cytoskeleton and into actin-rich filopodia and growth cones. One subsequently published study found that C9ORF72 interacts with cofilin 1 (Sivadasan et al., 2016), an actin binding protein important for modulating organisation and dynamics of the actin cytoskeleton (Bravo-Cordero et al., 2013). It is currently not known how mutations in *C9orf72* lead to both ALS and FTD, but it is likely due to a combination of RNA toxicity, translation of the repeat expansion into harmful dipeptide repeat proteins, and a reduction in the amount of C9ORF72 protein. If C9ORF72 significantly interacts with the actin cytoskeleton and synapses, a reduction in the level of this protein is likely to have a detrimental effect. Mutations to C9ORF72 cause TDP-43 pathology, and it is currently unclear if

alterations to C9ORF72 at the transcriptional or translational level cause TDP-43 to become mislocalised and aggregate in the cytoplasm. The results indicate that actin associated processes need more investigation in ALS/FTD.

Actin is enriched in dendritic spines, and is important for synapse formation and maintenance (Jaworski et al., 2009). Altered synaptic terminals are observed in ALS/FTD (Zhou et al., 1998) and also feature in a range of other neurodegenerative diseases (reviewed in Vickers et al., 2009). In this thesis, C9ORF72 protein was enriched within synapses in adult mouse brains, further strengthening the association between this protein and the actin cytoskeleton. When RGCs were used to model synaptic alterations following transduction with altered TDP-43, transducing them with TDP-WT resulted in increased synapses in the IPL, which is pre-synaptic to the RGCs, and perhaps attributable to increased dendrite branching of RGCs and an increase in the number of dendritic spines available for IPL neurons to connect to. This phenomenon would need to be examined in a more disease-relevant model to determine whether it is significant for ALS/FTD, although previous work in primary hippocampal neurons (Majumder et al., 2012) and in the cortex of A315T TDP-43 transgenic mice (Handley et al., 2016) have also demonstrated that altered TDP-43 impacts dendritic spines.

6.3 AXON DEGENERATION

Axonal changes have been hypothesised to initiate pathological processes causing cell dysfunction and degeneration in a range of diseases (Vickers et al., 2009). In ALS and FTD, white matter tracts are lost, and axons swell and degenerate. Many clinical symptoms in ALS are thought to arise from axon degeneration, especially in peripheral motor pathways; axon degeneration is implied by the observed loss of motor neuron axons without corresponding cell body loss (Fischer et al., 2004; Gould et al., 2006; King et al., 2012). These diseases share axon-specific pathology, since neurofilament alterations are common in ALS and in the FTD variant NIFID. In *in vitro* studies in this thesis, neurofilament-

labelled axons were observed undergoing early alterations to their integrity, exhibiting 'beads on a string' labelling and neurofilament-labelled ring-like structures. Similarly, in an earlier study of an mSOD1 mouse model of ALS, axons expressing GFP showed axon blebbing in chains along white matter tracts (Anna E King et al., 2012). Neurofilament-labelled rings have also been observed in several pathological contexts, including around beta amyloid plaques in pre-clinical (Dickson et al., 1999) and end-stage AD cases (Dickson et al., 2005); and may represent microtubule dissolution and axonal collapse (Vickers et al., 2009). Slowing of axonal transport of neurofilaments is observed following glutamate excitotoxicity (Ackerley et al., 2000), and excitotoxic mechanisms are an important pathological feature of ALS (King et al., 2016). *In vivo,* NFH became abnormally localised to cell bodies of RGCs following transduction with TDP-NLS^{-}-GFP tissue, suggesting that TDP-43 may alter neurofilament stoichiometry and/or its transport into axons. TDP-43 has previously been shown to regulate NFL by stabilising its mRNA and thus its translation in the cytoplasm (Strong et al., 2007; Volkening et al., 2009), providing a plausible link between TDP-43 and neurofilament alterations.

Under ultrastructural examination of transduced RGC axons, TDP-NLS^{-}-GFP increased the number of degenerative profiles and the accumulation of abnormal organelles, resembling the disrupted axons observed in the ventral horn of human ALS spinal cords. Ultrastructural and neuropathological analyses show that these swellings contain accumulations of phosphorylated neurofilament proteins, mitochondria and lysosomes (Corbo & Hays, 1992; Hirano, Donnenfeld, et al., 1984; Hirano, Nakano, et al., 1984; Rouleau et al., 1996) and importantly, accumulations of kinesin, a key protein involved in transport of cargoes in the axon (Toyoshima et al., 1998). Determining the composition of the organelles accumulated in the RGC model will be an important future investigation.

6.4 LIMITATIONS AND FUTURE DIRECTIONS

Primary cell culture models were utilised in this thesis to allow for the examination of developmental processes, and detailed characterisations of individual cells and their connections. However, ALS and FTD are older adult-onset diseases. Although there are parallels between developmental and ageing processes, including plastic remodelling of synapses and branches, primary culture models present limitations in their ability to reproduce features of ageing-related diseases. However, these types of models are crucial in gaining mechanistic insights into diseases like ALS and FTD.

It has been particularly challenging to create models of TDP-43 pathology to recapitulate degenerative features observed in TDP-43-mediated disease. The TDP-43_{Prp} transgenic mouse model, overexpressing human TDP-43, was chosen for *in vitro* studies, but its two month postnatal onset of severe neurodegeneration does not resemble adult-onset ALS/FTD.

Future studies will further extend the *in vivo* eye model, introduced in chapter 4, to further investigate TDP-43 pathological and normal function. Transduction with bicistronic vectors allowing independent expression of TDP-43 and cell-wide fluorescent protein will enable tracing of transduced RGC through the optic nerve and into the brain, as well as analysis of neuron arborisation within the retina, to further extend *in vitro* findings.

To extend the key proteomic findings of Chapter 3, the effects of TDP-43 overexpression on different neuronal compartments could be investigated using microfluidic devices that allow separation of the somatodendritic and axonal compartments. Additionally, due to limitations with sample preparation, replication of whole cell proteomics at 3 DIV may allow stronger associations between neuron morphology changes and global protein alterations to be determined.

The interactions between both TDP-43 and C9ORF72 with the actin cytoskeleton represent the key findings of this thesis. Future studies to further elucidate the normal function of C9ORF72 will help determine its role in disease; specifically, knockdown studies will be of value to determine whether

reduction of C9ORF72 alters the functions suggested in this thesis, such as growth cone morphology/motility and synapse development.

6.5 THERAPEUTIC IMPLICATIONS

In both ALS and FTD, extensive pathology of neurites and synapses are present. Evidence from this thesis and other studies suggests that TDP-43 is a key regulator of cytoskeletal elements that are vital for maintaining healthy neurites. If the disruptive effects of altered TDP-43 on the neuronal cytoskeleton could be ameliorated, then it may be possible to protect vulnerable neurons from developing neurite and synaptic pathology and degenerating.

The neuronal cytoskeleton presents as an attractive target for therapeutic intervention. Currently, animal and human clinical trials of drugs targeting the neuronal cytoskeleton in other neurodegenerative diseases are underway, and show promising results (Eira et al., 2016). These include drugs that target microtubules and their stability, as well as regulators of cytoskeletal dynamics such as RhoA and GSK3b (Eira et al., 2016). There is accumulating model-based and clinical evidence that neurite abnormalities are an important consequence of altered TDP-43, and this thesis has provided further evidence that alterations to TDP-43 can alter neurite morphology, including induction of axon degeneration (Chapter 4), and changes in synapse numbers. Chapter 3 highlights actin-binding proteins as potential mediators of these changes, and chapter 5 adds to the growing body of evidence that C9ORF72 is also a regulator of the actin cytoskeleton. Further understanding how actin is involved in neuritic alterations, and what modulates these processes is an essential step to identify targets for therapeutic intervention. Currently, there are few trials targeting actin dynamics because actin is so widely expressed. However, a number of laboratories are working towards targeting drugs to specific cell types, and therefore a thorough understanding of the role of actin alterations in ALS/FTD could lead to directed future interventions.

6.6 CONCLUSIONS

An improved understanding of the pathological roles of genes and proteins implicated in ALS and FTD is an important step for developing therapeutic strategies. Based on the literature to date, it is reasonable to propose that neurite abnormalities observed in human post-mortem tissue may occur through altered TDP-43 modulation of the cytoskeleton, and that genetic mutations to C9ORF72 may also impact these pathological alterations. This thesis has added to a growing body of evidence that TDP-43 and possibly C9ORF72 play important roles in interacting with the neuronal cytoskeleton, particularly the actin and neurofilament cytoskeletons, and that alterations to TDP-43 levels may be a driver of axon degeneration. Future studies will help to unravel these interactions further. Modulation of the neuronal cytoskeleton is a compelling target for providing therapeutic protection to vulnerable cellular components, such as the axon, as well as potentially preventing neuritic changes that could lead to functional disruption and altered excitability. Studies such as those described in this thesis may provide insight for whether TDP-43- and C9ORF72-related FTD/ALS are candidates for these types of interventions.

7 REFERENCES

Abdeljalil, J., Hamid, M., Abdel-mouttalib, O., Stéphane, R., Raymond, R., Johan, A., . . . Serge, P. (2005). The optomotor response: A robust first-line visual screening method for mice. *Vision Research, 45*(11), 1439-1446.

Abegg, M., Dysli, M., Wolf, S., Kowal, J., Dufour, P., & Zinkernagel, M. (2014). Microcystic macular edema: retrograde maculopathy caused by optic neuropathy. *Ophthalmology, 121*(1), 142-149.

Ackerley, S., Grierson, A. J., Brownlees, J., Thornhill, P., Anderton, B. H., Leigh, P. N., . . . Miller, C. C. (2000). Glutamate slows axonal transport of neurofilaments in transfected neurons. *The Journal of Cell Biology, 150*(1), 165-176.

Agosta, F., Scola, E., Canu, E., Marcone, A., Magnani, G., Sarro, L., . . . Filippi, M. (2012). White matter damage in frontotemporal lobar degeneration spectrum. *Cerebral Cortex, 22*(12), 2705-2714.

Al-Chalabi, A., Andersen, P. M., Nilsson, P., Chioza, B., Andersson, J. L., Russ, C., . . . Leigh, P. N. (1999). Deletions of the heavy neurofilament subunit tail in amyotrophic lateral sclerosis. *Human Molecular Genetics, 8*(2), 157-164.

Alami, N. H., Smith, R. B., Carrasco, M. A., Williams, L. A., Winborn, C. S., Han, S. S. W., . . . Taylor, J. P. (2014). Axonal transport of TDP-43 mRNA granules is impaired by ALS-causing mutations. *Neuron, 81*(3), 536-543.

Amparan, D., Avram, D., Thomas, C. G., Lindahl, M. G., Yang, J., Bajaj, G., & Ishmael, J. E. (2005). Direct interaction of myosin regulatory light chain with the NMDA receptor. *Journal of Neurochemistry, 92* (2), 349-361.

Arai, T., Hasegawa, M., Akiyama, H., Ikeda, K., Nonaka, T., Mori, H., . . . Oda, T. (2006). TDP-43 is a component of ubiquitin-positive tau-negative inclusions in frontotemporal lobar degeneration and amyotrophic lateral sclerosis. *Biochemical and Biophysical Research Communications, 351*(3), 602-611.

Armijo-Weingart, L., & Gallo, G. (2017). It takes a village to raise a branch: Cellular mechanisms of the initiation of axon collateral branches. *Molecular and Cellular Neuroscience*, 1-12.

Armstrong, R. A. (2017). White matter pathology in sporadic frontotemporal lobar degeneration with TDP-43 pathology. *Clinical Neuropathology, 36*(2), 66-72.

Arnold, E. S., Ling, S.-C., Huelga, S. C., Lagier-Tourenne, C., Polymenidou, M., Ditsworth, D., . . . Cleveland, D. W. (2013). ALS-linked TDP-43 mutations produce aberrant RNA splicing and

adult-onset motor neuron disease without aggregation or loss of nuclear TDP-43. *Proceedings of the National Academy of Sciences of the United States of America, 110*(8), E736-E745.

Ash, P. E. A., Bieniek, K. F., Gendron, T. F., Caulfield, T., Lin, W.-L., DeJesus-Hernandez, M., . . . Petrucelli, L. (2013). Unconventional translation of C9ORF72 GGGGCC expansion generates insoluble polypeptides specific to c9FTD/ALS. *Neuron, 77*(4), 639-646.

Ayala, Y. M., De Conti, L., Avendaño-Vázquez, S. E., Dhir, A., Romano, M., D'Ambrogio, A., . . . Baralle, F. E. (2011). TDP-43 regulates its mRNA levels through a negative feedback loop. *The EMBO Journal, 30*(2), 277-288.

Bae, J. S., Simon, N. G., Menon, P., Vucic, S., & Kiernan, M. C. (2013). The puzzling case of hyperexcitability in amyotrophic lateral sclerosis. *Journal Clinical Neurology, 9*(2), 65-74.

Barmada, S. J., Skibinski, G., Korb, E., Rao, E. J., Wu, J. Y., & Finkbeiner, S. (2010). Cytoplasmic mislocalization of TDP-43 is toxic to neurons and enhanced by a mutation associated with familial amyotrophic lateral sclerosis. *Journal of Neuroscience, 30*(2), 639-649.

Barnat, M., Benassy, M.-N., Vincensini, L., Soares, S., Fassier, C., Propst, F., . . . Nothias, F. (2016). The GSK3b/MAP1B pathway controls neurite branching and microtubule dynamics. *Molecular and Cellular Neuroscience, 72* 9-21.

Barry, D. M., Stevenson, W., Bober, B. G., Wiese, P. J., Dale, J. M., Barry, G. S., . . . Garcia, M. L. (2012). Expansion of neurofilament medium C terminus increases axonal diameter independent of increases in conduction velocity or myelin thickness. *Journal of Neuroscience, 32*(18), 6209-6219.

Bates, D. M., M.; Bolker, B.; Walker, S. (2015). Fitting linear mixed-effects models using lme4. *Journal of Statistical Software, 67*(1), 1-48.

Belzil, V. V., Bauer, P. O., Prudencio, M., Gendron, T. F., Stetler, C. T., Yan, I. K., . . . Petrucelli, L. (2013). Reduced C9orf72 gene expression in c9FTD/ALS is caused by histone trimethylation, an epigenetic event detectable in blood. *Acta Neuropathologica, 126*(6), 895-905.

Bensimon, G. L., Lacomblez, L., Meininger, V., ALS/Riluzole Study Group,. (1994). A controlled trial of riluzole in amyotrophic lateral sclerosis. *New England Journal of Medicine, 330*(9), 585-591.

Braak, H., Ludolph, A., Thal, D. R., & Del Tredici, K. (2010). Amyotrophic lateral sclerosis: dash-like accumulation of phosphorylated TDP-43 in somatodendritic and axonal compartments of somatomotor neurons of the lower brainstem and spinal cord. *Acta Neuropathologica, 120*(1), 67-74.

Bravo-Cordero, J. J., Magalhaes, M. A. O., Eddy, R. J., Hodgson, L., & Condeelis, J. (2013). Functions of cofilin in cell locomotion and invasion. *Nature Reviews. Molecular Cell Biology, 14*(7), 405-415.

Brettschneider, J., Arai, K., Del Tredici, K., Toledo, J. B., Robinson, J. L., Lee, E. B., . . . Trojanowski, J. Q. (2014). TDP-43 pathology and neuronal loss in amyotrophic lateral sclerosis spinal cord. *Acta Neuropathologica, 128*(3), 423-437.

Brettschneider, J., Tredici, K. D., Toledo, J. B., Robinson, J. L., Irwin, D. J., Grossman, M., . . . Trojanowski, J. Q. (2013). Stages of pTDP-43 pathology in amyotrophic lateral sclerosis. *Annals of Neurology, 74*(1), 20-38.

Brettschneider, J., Van Deerlin, V. M., Robinson, J. L., Kwong, L., Lee, E. B., Ali, Y. O., . . . Trojanowski, J. Q. (2012). Pattern of ubiquilin pathology in ALS and FTLD indicates presence of C9ORF72 hexanucleotide expansion. *Acta Neuropathologica, 123*(6), 825-839.

Buratti, E. B., F. E. (2001). Characterization and functional implications of the RNA binding properties of nuclear factor TDP-43, a novel splicing regulator of CFTR exon 9. *The Journal of Biological Chemistry, 276*(39), 36337-36343.

Buratti, E. B., F. E. (2008). Multiple roles of TDP-43 in gene expression, splicing regulation, and human disease. *Frontiers in bioscience : a journal and virtual library, 13*, 867-878.

Burrell, J. R., Halliday, G. M., Kril, J. J., Ittner, L. M., Götz, J., Kiernan, M. C., & Hodges, J. R. (2016). The frontotemporal dementia-motor neuron disease continuum. *Lancet, 388*(10047), 919-931.

Cairns, N. J., Lee, V. M. Y., & Trojanowski, J. Q. (2004). The cytoskeleton in neurodegenerative diseases. *The Journal of Pathology, 204*(4), 438-449.

Cairns, N. J., Neumann, M., Bigio, E. H., Holm, I. E., Troost, D., Hatanpaa, K. J., . . . Mackenzie, I. R. A. (2007). TDP-43 in familial and sporadic frontotemporal lobar degeneration with ubiquitin inclusions. *The American Journal of Pathology, 171*(1), 227-240.

Cairns, N. J., Zhukareva, V., Uryu, K., Zhang, B., Bigio, E., Mackenzie, I. R. A., . . . Trojanowski, J. Q. (2010). Alpha-internexin is present in the pathological inclusions of neuronal intermediate filament inclusion disease. *The American Journal of Pathology, 164*(6), 2153-2161.

Chare, L., Hodges, J. R., Leyton, C. E., McGinley, C., Tan, R. H., Kril, J. J., & Halliday, G. M. (2014). New criteria for frontotemporal dementia syndromes: clinical and pathological diagnostic implications. *Journal of Neurology, Neurosurgery and Psychiatry, 85*(8), 865-870.

Chiang, P.-M., Ling, J., Jeong, Y. H., Price, D. L., Aja, S. M., & Wong, P. C. (2010). Deletion of TDP-43 down-regulates Tbc1d1, a gene linked to obesity, and alters body fat metabolism. *Proceedings of the National Academy of Sciences, 107*(37), 16320-16324.

Chitramuthu, B. P., Baranowski, D. C., Kay, D. G., Bateman, A., & Bennett, H. P. (2010). Progranulin modulates zebrafish motoneuron development in vivo and rescues truncation defects associated with knockdown of survival motor neuron 1. *Molecular Neurodegeneration, 5*, 41-49.

Ciura, S., Lattante, S., Le Ber, I., Latouche, M., Tostivint, H., Brice, A., & Kabashi, E. (2013). Loss of function of C9orf72 causes motor deficits in a zebrafish model of amyotrophic lateral sclerosis. *Annals of Neurology, 74*(2), 180-187.

Collins, J. M., King, A. E., Woodhouse, A., Kirkcaldie, M. T. K., & Vickers, J. C. (2015). The effect of focal brain injury on beta-amyloid plaque deposition, inflammation and synapses in the APP/PS1 mouse model of Alzheimer's disease. *Experimental Neurology, 267*, 219-229.

Colombrita, C., Zennaro, E., Fallini, C., Weber, M., Sommacal, A., Buratti, E., . . . Ratti, A. (2009). TDP-43 is recruited to stress granules in conditions of oxidative insult. *Journal of Neurochemistry, 111*(4), 1051-1061.

Cooper-Knock, J., Hewitt, C., Highley, J. R., Brockington, A., Milano, A., Man, S., . . . Shaw, P. J. (2012b). Clinico-pathological features in amyotrophic lateral sclerosis with expansions in C9ORF72. *Brain, 135*(3), 751-764.

Corbo, M., & Hays, A. P. (1992). Peripherin and neurofilament protein coexist in spinal spheroids of motor neuron disease. *Journal of Neuropathology and Experimental Neurology, 51*(5), 531-537.

Cox, J., Hein, M. Y., Luber, C. A., Paron, I., Nagaraj, N., & Mann, M. (2014). Accurate proteome-wide label-free quantification by delayed normalization and maximal peptide ratio extraction, termed MaxLFQ. *Molecular and Cellular Proteomics, 13*(9), 2513-2526.

Coyne, A. N., Siddegowda, B. B., Estes, P. S., Johannesmeyer, J., Kovalik, T., Daniel, S. G., . . . Zarnescu, D. C. (2014). Futsch/MAP1B mRNA is a translational target of TDP-43 and is neuroprotective in a drosophila model of amyotrophic lateral sclerosis. *Journal of Neuroscience, 34*(48), 15962-15974.

Dawson, H. N., Ferreira, A., Eyster, M. V., Ghoshal, N., Binder, L. I., & Vitek, M. P. (2001). Inhibition of neuronal maturation in primary hippocampal neurons from tau deficient mice. *Journal of Cell Science, 114*(6), 1179-1187.

De Conti, L., Borroni, B., & Baralle, M. (2017). New routes in frontotemporal dementia drug discovery. *Expert Opinion on Drug Discovery, 12*(7), 659-671.

De Felipe, J. M., P.; Fairen, A.; Jones, E. G. (1997). Inhibitory synaptogenesis in mouse somatosensory cortex. *Cerebral Cortex, 7*(7), 619-634.

De Vos, K. J., & Hafezparast, M. (2017). Neurobiology of axonal transport defects in motor neuron diseases: opportunities for translational research? *Neurobiology of Disease*, *105*, 283-299.

DeJesus-Hernandez, M., Mackenzie, I. R., Boeve, B. F., Boxer, A. L., Baker, M., Rutherford, N. J., . . . Rademakers, R. (2011). Expanded GGGGCC hexanucleotide repeat in noncoding region of C9ORF72 causes chromosome 9p-linked FTD and ALS. *Neuron, 72*(2), 245-256.

DeMaman, A. S., Melo, P., Homem, J. M., Tavares, M. A., & Lachat, J.-J. (2010). Effectiveness of iron repletion in the diet for the optic nerve development of anaemic rats. *Eye (London, England), 24*(5), 901-908.

Dewey, C. M., Cenik, B., Sephton, C. F., Dries, D. R., Mayer, P., Good, S. K., . . . Yu, G. (2011). TDP-43 is directed to stress granules by sorbitol, a novel physiological osmotic and oxidative stressor. *Molecular and Cellular Biology, 31*(5), 1098-1108.

Dickson, D. W., Yen, S. H., Suzuki, K. I., Davies, P., Garcia, J. H., & Hirano, A. (1986). Ballooned neurons in select neurodegenerative diseases contain phosphorylated neurofilament epitopes. *Acta Neuropathologica, 71*(3-4), 216-223.

Dickson, T. C., Chuckowree, J. A., Chuah, M. I., West, A. K., & Vickers, J. C. (2005). Alpha-internexin immunoreactivity reflects variable neuronal vulnerability in Alzheimer's disease and supports the role of the beta-amyloid plaques in inducing neuronal injury. *Neurobiology of Disease, 18*(2), 286-295.

Dickson, T. C. K., C. E.; McCormack, G. H.; Vickers, J. C. (1999). Neurochemical diversity of dystrophic neurites in the early and late stages of Alzheimer's disease. *Experimental Neurology, 1*, 100-110.

Dillon, C. G., Y. (2005). The actin cytoskeleton: integrating form and function at the synapse. *Annual Review of Neuroscience, 28*, 25-55.

Donnelly, C. J., Zhang, P.-W., Pham, J. T., Heusler, A. R., Mistry, N. A., Vidensky, S., . . . Rothstein, J. D. (2013). RNA Toxicity from the ALS/FTD C9ORF72 Expansion Is Mitigated by Antisense Intervention. *Neuron, 80*(2), 415-428.

Dos Remedios, C. G. C., D.; Kekic, M.; Dedova, L. V.; Tsubakihara, M.; Berry, D. A.; Nosworthy, N. J. (2003). Actin binding proteins: regulation of cytoskeletal microfilaments. *Physiological Reviews, 83*(433-473).

Dotti, C. G., Sullivan, C. A., & Banker, G. A. (1988). The establishment of polarity by hippocampal neurons in culture. *The Journal of Neuroscience, 8*(4), 1454-1468.

Dunkley, P. R., Jarvie, P. E., & Robinson, P. J. (2008). A rapid Percoll gradient procedure for preparation of synaptosomes. *Nature Protocols, 3*(11), 1718-1728.

Dysli, C., Enzmann, V., Sznitman, R., & Zinkernagel, M. S. (2015). Quantitative analysis of mouse retinal layers using automated segmentation of spectral domain optical coherence tomography images. *Translational Vision Science and Technology, 4*(4), 9.

Eira, J., Silva, C. S., Sousa, M. M., & Liz, M. A. (2016). The cytoskeleton as a novel therapeutic target for old neurodegenerative disorders. *Progress in Neurobiology, 141*, 61-82.

Ellouze, S., Augustin, S., Bouaita, A., Bonnet, C., Simonutti, M., Forster, V., . . . Corral-Debrinski, M. (2008). Optimized allotopic expression of the human mitochondrial ND4 prevents blindness in a rat model of mitochondrial dysfunction. *American Journal of Human Genetics, 83*(3), 373-387.

Estes, P. S., Boehringer, A., Zwick, R., Tang, J. E., Grigsby, B., & Zarnescu, D. C. (2011). Wild-type and A315T mutant TDP-43 exert differential neurotoxicity in a drosophila model of ALS. *Human Molecular Genetics, 20*(12), 2308-2321.

Fallini, C., Bassell, G. J., & Rossoll, W. (2010). High-efficiency transfection of cultured primary motor neurons to study protein localization, trafficking, and function. *Molecular Neurodegeneration, 5*, 17.

Fallini, C., Bassell, G. J., & Rossoll, W. (2012). The ALS disease protein TDP-43 is actively transported in motor neuron axons and regulates axon outgrowth. *Human Molecular Genetics, 21*(16), 3703-3718.

Farg, M. A., Sundaramoorthy, V., Sultana, J. M., Yang, S., Atkinson, R. A. K., Levina, V., . . . Atkin, J. D. (2014). C9ORF72, implicated in amytrophic lateral sclerosis and frontotemporal dementia, regulates endosomal trafficking. *Human Molecular Genetics, 23*(13), 3579-3595.

Feiguin, F., Godena, V. K., Romano, G., D'Ambrogio, A., Klima, R., & Baralle, F. E. (2009). Depletion of TDP-43 affects drosophila motoneurons terminal synapsis and locomotive behavior. *FEBS letters, 583*(10), 1586-1592.

Fernandez, C. M., Molto, E., Gallardo, N., del Arco, A., Martinez, C., Andres, A., . . . Arribas, C. (2009). The expression of rat resistin isoforms is differentially regulated in visceral adipose tissues: effects of aging and food restriction. *Metabolism, 58*(2), 204-211.

Fernandez-Martos, C. M., Gonzalez-Fernandez, C., Gonzalez, P., Maqueda, A., Arenas, E., & Rodriguez, F. J. (2011). Differential expression of Wnts after spinal cord contusion injury in adult rats. *PloS One, 6*(11), e27000.

Fernandez-Martos, C. M., King, A. E., Atkinson, R. A. K., Woodhouse, A., & Vickers, J. C. (2015). Neurofilament light gene deletion exacerbates amyloid, dystrophic neurite, and synaptic pathology in the APP/PS1 transgenic model of Alzheimer's disease. *Neurobiology of Aging, 36*(10), 2757-2767.

Ferreirinha, F., Quattrini, A., Pirozzi, M., Valsecchi, V., Dina, G., Broccoli, V., . . . Rugarli, E. I. (2004). Axonal degeneration in paraplegin-deficient mice is associated with abnormal

mitochondria and impairment of axonal transport. *Journal of Clinical Investigation, 113*(2), 231-242.

Ferrer, I., Roig, C., Espino, A., Peiro, G., & Matias Guiu, X. (1991). Dementia of frontal lobe type and motor neuron disease. A golgi study of the frontal cortex. *Journal of Neurology, Neurosurgery, and Psychiatry, 54*(10), 932-934.

Fiesel, F. C., Schurr, C., Weber, S. S., & Kahle, P. J. (2011). TDP-43 knockdown impairs neurite outgrowth dependent on its target histone deacetylase 6. *Molecular Neurodegeneration, 6*, 64.

Fiesel, F. C., Voigt, A., Weber, S. S., Van den Haute, C., Waldenmaier, A., Görner, K., . . . Kahle, P. J. (2010). Knockdown of transactive response DNA-binding protein (TDP-43) downregulates histone deacetylase 6. *The EMBO Journal, 29*(1), 209-221.

Fischer, L. R., Culver, D. G., Tennant, P., Davis, A. A., Wang, M., Castellano-Sanchez, A., . . . Glass, J. D. (2004). Amyotrophic lateral sclerosis is a distal axonopathy: evidence in mice and man. *Experimental neurology, 185*(2), 232-240.

Fogarty, M. J., Noakes, P. G., & Bellingham, M. C. (2015). Motor cortex layer V pyramidal neurons exhibit dendritic regression, spine loss, and increased synaptic excitation in the presymptomatic hSOD1(G93A) mouse model of amyotrophic lateral sclerosis. *Journal of Neuroscience, 35*(2), 643-647.

Franklin, K. B. J., & Paxinos, G. (2008). *The Mouse Brain in Stereotaxic Coordinates*. New York, NY: Academic Press.

Freibaum, B. D., Chitta, R. K., High, A. A., & Taylor, J. P. (2010). Global analysis of TDP-43 interacting proteins reveals strong association with RNA splicing and translation machinery. *Journal of Proteome Research, 9*(2), 1104-1120.

Gao, X., Joselin, A. P., Wang, L., Kar, A., Ray, P., Bateman, A., . . . Wu, J. Y. (2010). Progranulin promotes neurite outgrowth and neuronal differentiation by regulating GSK-3β. *Protein & Cell, 1*(6), 552-562.

Garcia-Martin, E. P., V.; Lorrosa, J. M.; Marques, M. L.; Herrero, R.; Martin, J.; Ara, J. R.; Fernandez, J.; Pablo, L. E. (2014). Retinal layer segmentation in patients with multiple Sclerosis Using Spectral Domain Optical Coherence Tomography. *Ophthalmology, 121*(2), 573-579.

Gass, J., Lee, W. C., Cook, C., Finch, N., Stetler, C., Jansen-West, K., . . . Petrucelli, L. (2012). Progranulin regulates neuronal outgrowth independent of sortilin. *Molecular Neurodegeneration, 7*, 33.

Ge, W.-W., Volkening, K., Leystra-Lantz, C., Jaffe, H., & Strong, M. J. (2007). 14-3-3 protein binds to the low molecular weight neurofilament (NFL) mRNA 3' UTR. *Molecular and Cellular Neurosciences, 34*(1), 80-87.

Geser, F. B., N. J.; Kwong, L. K.; Martinez-Lage, M.; Elman, L.; McCluskey, L.; Xie, S. X.; Lee, V. M.-Y.; Trojanowski, J. Q. (2008). Evidence of multisystem disorder in whole-brain map of pathological TDP-43 in amyotrophic lateral sclerosis. *Archives of Neurology., 65*(5), 636-641.

Gijselinck, I., van der Zee, J., Engelborghs, S., Goossens, D., Peeters, K., Mattheijssens, M., . . . Cruts, M. (2008). Progranulin locus deletion in frontotemporal dementia. *Human Mutation, 29*(1), 53-58.

Gijselinck, I., Van Langenhove, T., van der Zee, J., Sleegers, K., Philtjens, S., Kleinberger, G., . . . Van Broeckhoven, C. (2012). A C9orf72 promoter repeat expansion in a Flanders-Belgian cohort with disorders of the frontotemporal lobar degeneration-amyotrophic lateral sclerosis spectrum: a gene identification study. *Lancet Neurology, 11*(1), 54-65.

Godena, V. K., Romano, G., Romano, M., Appocher, C., Klima, R., Buratti, E., . . . Feiguin, F. (2011). TDP-43 regulates drosophila neuromuscular junctions growth by modulating Futsch/MAP1B levels and synaptic microtubules organization. *PloS One, 6*(3), e17808.

Gould, T. W., Buss, R. R., Vinsant, S., Prevette, D., Sun, W., Knudson, C. M., . . . Oppenheim, R. W. (2006). Complete dissociation of motor neuron death from motor dysfunction by Bax deletion in a mouse model of ALS. *Journal of Neuroscience, 26*(34), 8774-8786.

Grant, C. A., Ponnazhagan, S., Wang, X. S., Srivastava, A., & Li, T. (1997). Evaluation of recombinant adeno-associated virus as a gene transfer vector for the retina. *Current Eye Research, 16*(9), 949-956.

Groen, E. J. N., Fumoto, K., Blokhuis, A. M., Engelen-Lee, J., Zhou, Y., van den Heuvel, D. M. A., . . . Pasterkamp, R. J. (2013). ALS-associated mutations in FUS disrupt the axonal distribution and function of SMN. *Human Molecular Genetics*.

Halliday, G., Bigio, E. H., Cairns, N. J., Neumann, M., Mackenzie, I. R. A., & Mann, D. M. A. (2012). Mechanisms of disease in frontotemporal lobar degeneration: gain of function versus loss of function effects. *Acta Neuropathologica, 124*(3), 373-382.

Han, J.-H., Yu, T.-H., Ryu, H.-H., Jun, M.-H., Ban, B.-K., Jang, D.-J., & Lee, J.-A. (2013). ALS/FTLD-linked TDP-43 regulates neurite morphology and cell survival in differentiated neurons. *Experimental Cell Research, 319*(13), 1998-2005.

Handley, E. E., Pitman, K. A., Dawkins, E., Young, K. M., Clark, R. M., Jiang, T. C., . . . Blizzard, C. A. (2016). Synapse dysfunction of layer V pyramidal neurons precedes neurodegeneration in a mouse model of TDP-43 proteinopathies. *Cerebral Cortex*, *27* (7), 3630-3647.

Harada, A., Oguchi, K., Okabe, S., Kuno, J., Terada, S., Ohshima, T., . . . Hirokawa, N. (1994). Altered microtubule organization in small-calibre axons of mice lacking tau protein. *Nature, 369*(6480), 488-491.

Hart, N. J., Koronyo, Y., Black, K. L., & Koronyo-Hamaoui, M. (2016). Ocular indicators of Alzheimers: exploring disease in the retina. *Acta Neuropathologica, 132*(6), 767-787.

Hatanpaa, K. J., Bigio, E. H., Cairns, N. J., Womack, K. B., Weintraub, S., Morris, J. C., . . . White, C. L. (2008). TAR DNA-binding protein 43 immunohistochemistry reveals extensive neuritic pathology in FTLD-U: a midwest-southwest consortium for FTLD study. *Journal of Neuropathology and Experimental Neurology, 67*(4), 271-279.

Heitz, F. D., Erb, M., Anklin, C., Robay, D., Pernet, V., & Gueven, N. (2012). Idebenone protects against retinal damage and loss of vision in a mouse model of hereditary optic neuropathy. *PloS One, 7*(9), e45182.

Herzog, J. J., Deshpande, M., Shapiro, L., Rodal, A. A., & Paradis, S. (2017). TDP-43 misexpression causes defects in dendritic growth. *Science Reports, 7*(1), 15656.

Hirano, A., Donnenfeld, H., Sasaki, S., & Nakano, I. (1984). Fine structural observations of neurofilamentous changes in amyotrophic lateral sclerosis. *Journal of Neuropathology and Experimental Neurology, 43*(5), 461-470.

Hirano, A., Nakano, I., Kurland, L. T., Mulder, D. W., Holley, P. W., & Saccomanno, G. (1984). Fine structural study of neurofibrillary changes in a family with amyotrophic lateral sclerosis. *Journal of Neuropathology and Experimental Neurology, 43*(5), 471-480.

Hirokawa, N. (1994). Microtubule organization and dynamics dependent on microtubule-associated proteins. *Current Opinion in Cell Biology, 6*(1), 74-81.

Hsiung, G.-Y. R., DeJesus-Hernandez, M., Feldman, H. H., Sengdy, P., Bouchard-Kerr, P., Dwosh, E., . . . Mackenzie, I. R. A. (2012). Clinical and pathological features of familial frontotemporal dementia caused by C9ORF72 mutation on chromosome 9p. *Brain, 135*(3), 709-722.

Huang, D. W., Sherman, B. T., & Lempicki, R. A. (2009). Systematic and integrative analysis of large gene lists using DAVID bioinformatics resources. *Nature Protocols, 4*(1), 44-57.

Hubbert, C., Guardiola, A., Shao, R., Kawaguchi, Y., Ito, A., Nixon, A., . . . Yao, T.-P. (2002). HDAC6 is a microtubule-associated deacetylase. *Nature, 417*(6887), 455-458.

Hur, E.-M., Saijilafu, & Zhou, F.-Q. (2012). Growing the growth cone: remodeling the cytoskeleton to promote axon regeneration. *Trends in Neurosciences, 35*(3), 164-174.

Hutton, M., Lendon, C. L., Rizzu, P., Baker, M., Froelich, S., Houlden, H., . . . Heutink, P. (1998). Association of missense and 5'-splice-site mutations in tau with the inherited dementia FTDP-17. *Nature, 393*(6686), 702-705.

Igaz, L. M., Kwong, L. K., Chen-Plotkin, A., Winton, M. J., Unger, T. L., Xu, Y., . . . Lee, V. M. Y. (2009). Expression of TDP-43 C-terminal fragments in vitro recapitulates pathological features of TDP-43 proteinopathies. *The Journal of Biological Chemistry, 284*(13), 8516-8524.

Igaz, L. M., Kwong, L. K., Lee, E. B., Chen-Plotkin, A., Swanson, E., Unger, T., . . . Lee, V. M. Y. (2011). Dysregulation of the ALS-associated gene TDP-43 leads to neuronal death and degeneration in mice. *The Journal of Clinical Investigation, 121*(2), 726-738.

Iguchi, Y., Katsuno, M., Niwa, J.-i., Yamada, S.-i., Sone, J., Waza, M., . . . Sobue, G. (2009). TDP-43 depletion induces neuronal cell damage through dysregulation of Rho family GTPases. *The Journal of Biological Chemistry, 284*(33), 22059-22066.

Irwin, D. J., Cairns, N. J., Grossman, M., McMillan, C. T., Lee, E. B., Van Deerlin, V. M., . . . Trojanowski, J. Q. (2015). Frontotemporal lobar degeneration: defining phenotypic diversity through personalized medicine. *Acta Neuropathologica, 129*(4), 469-491.

Jaworski, J., Kapitein, L. C., Gouveia, S. M., Dortland, B. R., Wulf, P. S., Grigoriev, I., . . . Hoogenraad, C. C. (2009). Dynamic microtubules regulate dendritic spine morphology and synaptic plasticity. *Neuron, 61*(1), 85-100.

Jiang, H., Guo, W., Liang, X., & Rao, Y. (2005). Both the establishment and the maintenance of neuronal polarity require active mechanisms: critical roles of GSK-3beta and its upstream regulators. *Cell, 120*(1), 123-135.

Joos, K. M., Li, C., & Sappington, R. M. (2010). Morphometric changes in the rat optic nerve following short-term intermittent elevations in intraocular pressure. *Investigative Ophthalmology & Visual Science, 51*(12), 6431-6440.

Kabashi, E., Bercier, V., Lissouba, A., Liao, M., Brustein, E., Rouleau, G. A., & Drapeau, P. (2011). FUS and TARDBP but not SOD1 interact in genetic models of amyotrophic lateral sclerosis. *PLoS Genetics, 7*(8), e1002214.

Kabashi, E., Lin, L., Tradewell, M. L., Dion, P. A., Bercier, V., Bourgouin, P., . . . Drapeau, P. (2010). Gain and loss of function of ALS-related mutations of TARDBP (TDP-43) cause motor deficits in vivo. *Human Molecular Genetics, 19*(4), 671-683.

Khazaei, M. R., Girouard, M.-P., Alchini, R., Ong Tone, S., Shimada, T., Bechstedt, S., . . . Fournier, A. E. (2014). Collapsin Response Mediator Protein 4 regulates growth cone dynamics through the actin and microtubule cytoskeleton. *Journal of Biological Chemistry*, *289* (43), 30133-30143.

Kiernan, M. C. P., S. (2012). Hyperexcitability and amyotrophic lateral sclerosis. *Neurology, 78*, 1544-1545.

Kim, K. K., Kim, Y. C., Adelstein, R. S., & Kawamoto, S. (2011). Fox-3 and PSF interact to activate neural cell-specific alternative splicing. *Nucleic Acids Research, 39*(8), 3064-3078.

King, A., Maekawa, S., Bodi, I., Troakes, C., & Al-Sarraj, S. (2011). Ubiquitinated, p62 immunopositive cerebellar cortical neuronal inclusions are evident across the spectrum of TDP-43 proteinopathies but are only rarely additionally immunopositive for phosphorylation-dependent TDP-43. *Neuropathology : official journal of the Japanese Society of Neuropathology, 31*(3), 239-249.

King, A. E., Blizzard, C. A., Southam, K. A., Vickers, J. C., & Dickson, T. C. (2012). Degeneration of axons in spinal white matter in G93A mSOD1 mouse characterized by NFL and α-internexin immunoreactivity. *Brain Research, 1465*, 90-100.

King, A. E., Woodhouse, A., Kirkcaldie, M. T., & Vickers, J. C. (2016). Excitotoxicity in ALS: overstimulation, or overreaction? *Experimental Neurology, 275 Pt 1*, 162-171.

Kirkcaldie, M. T. K., & Dwyer, S. T. (2017). The third wave: intermediate filaments in the maturing nervous system. *Molecular and Cellular Neuroscience*, 1-9.

Knoferle, J., Koch, J. C., Ostendorf, T., Michel, U., Planchamp, V., Vutova, P., . . . Lingor, P. (2010). Mechanisms of acute axonal degeneration in the optic nerve in vivo. *Proceedings of the National Academy of Sciences of the United States of America, 107*(13), 6064-6069.

Komatsu, M., Wang, Q. J., Holstein, G. R., Friedrich, V. L., Jr., Iwata, J., Kominami, E., . . . Yue, Z. (2007). Essential role for autophagy protein Atg7 in the maintenance of axonal homeostasis and the prevention of axonal degeneration. *Proceedings of the National Academy of Sciences of the United States of America, 104*(36), 14489-14494.

Koppers, M., Blokhuis, A. M., Westeneng, H. J., Terpstra, M. L., Zundel, C. A., Vieira de Sa, R., . . . Pasterkamp, R. J. (2015). C9orf72 ablation in mice does not cause motor neuron degeneration or motor deficits. *Annals of Neurology*, *78* (3), 426-439.

Kraemer, B. C., Schuck, T., Wheeler, J. M., Robinson, L. C., Trojanowski, J. Q., Lee, V. M. Y., & Schellenberg, G. D. (2010). Loss of murine TDP-43 disrupts motor function and plays an essential role in embryogenesis. *Acta Neuropathologica, 119*(4), 409-419.

Kreutzberg, G. W. (1996). Microglia: a sensor for pathological events in the CNS. *Trends in Neurosciences, 19*, 312-318.

Lee, E. B., Lee, V. M. Y., & Trojanowski, J. Q. (2012). Gains or losses: molecular mechanisms of TDP43-mediated neurodegeneration. *Nature Reviews. Neuroscience, 13*(1), 38-50.

Legland, D. A.-C., I.; Andrey, P. (2016). MorphoLibJ: integrated library and plugins for mathematical morphology with ImageJ. *Bioinformatics (Oxford, England), 32*(22), 3532-3534.

Lei, P., Ayton, S., Finkelstein, D. I., Spoerri, L., Ciccotosto, G. D., Wright, D. K., . . . Bush, A. I. (2012). Tau deficiency induces parkinsonism with dementia by impairing APP-mediated iron export. *Nature Medicine, 18*(2), 293-297.

Lei, P., Ayton, S., Moon, S., Zhang, Q., Volitakis, I., Finkelstein, D. I., & Bush, A. I. (2014). Motor and cognitive deficits in aged tau knockout mice in two background strains. *Molecular Neurodegeneration, 9*(1), 29.

Levine, T. P., Daniels, R. D., Gatta, A. T., Wong, L. H., & Hayes, M. J. (2013). The product of C9orf72, a gene strongly implicated in neurodegeneration, is structurally related to DENN Rab-GEFs. *Bioinformatics (Oxford, England), 29*(4), 499-503.

Lipton, A. M., White, C. L., & Bigio, E. H. (2004). Frontotemporal lobar degeneration with motor neuron disease-type inclusions predominates in 76 cases of frontotemporal degeneration. *Acta Neuropathologica, 108*(5), 379-385.

Liu, S. J., Zhang, J. Y., Li, H. L., Fang, Z. Y., Wang, Q., Deng, H. M., . . . Wang, J. Z. (2004). Tau becomes a more favorable substrate for GSK-3 when it is prephosphorylated by PKA in rat brain. *The Journal of Biological Chemistry, 279*(48), 50078-50088.

Liu, Y. A., R. A. K.; Fernandez-Martos, C. M.; Kirkcaldie, M. T. K.; Cui, H.; Vickers, J. C.; King, A. E. (2015). Changes in TDP-43 expression in development, aging, and in the neurofilament light protein knockout mouse. *Neurobiology of Aging, 36*(2), 1151-1159.

Liu-Yesucevitz, L., Bassell, G. J., Gitler, A. D., Hart, A. C., Klann, E., Richter, J. D., . . . Wolozin, B. (2011). Local RNA translation at the synapse and in disease. *Journal of Neuroscience, 31*(45), 16086-16093.

Livak, K. J., & Schmittgen, T. D. (2001). Analysis of relative gene expression data using real-time quantitative PCR and the 2-Delta Delta CT Method. *Methods, 25*(4), 402-408.

Lomen-Hoerth, C., Anderson, T., & Miller, B. (2002). The overlap of amyotrophic lateral sclerosis and frontotemporal dementia. *Neurology, 59*(7), 1077-1079.

Lopez-Valdes, H. E. M.-C., H. (2016). The Role of Neuroinflammation in Age-Related Dementias. *Revista de Investigación Clinica; Organo del Hospital de Enfermedades de la Nutrición, 68*, 40-48.

Lu, Y., Ferris, J., & Gao, F.-B. (2009). Frontotemporal dementia and amyotrophic lateral sclerosis-associated disease protein TDP-43 promotes dendritic branching. *Molecular Brain, 2*, 30.

Mackenzie, I. R. A., & Neumann, M. (2016). Molecular neuropathology of frontotemporal dementia: insights into disease mechanisms from postmortem studies. *Journal of Neurochemistry, 138 Suppl 1*, 54-70.

Magrane, J., Cortez, C., Gan, W. B., & Manfredi, G. (2014). Abnormal mitochondrial transport and morphology are common pathological denominators in SOD1 and TDP43 ALS mouse models. *Human Molecular Genetics, 23*(6), 1413-1424.

Majumder, P., Chen, Y.-T., Bose, J. K., Wu, C.-C., Cheng, W.-C., Cheng, S.-J., . . . Shen, C.-K. J. (2012). TDP-43 regulates the mammalian spinogenesis through translational repression of Rac1. *Acta Neuropathologica, 124*(2), 231-245.

Marat, A. L., Dokainish, H., & McPherson, P. S. (2011). DENN domain proteins: regulators of Rab GTPases. *Journal of Biological Chemistry, 286*(16), 13791-13800.

Martin, K. R. G., Klein, R. L., & Quigley, H. A. (2002). Gene delivery to the eye using adeno-associated viral vectors. *Methods, 28*, 267-275.

Massoll, C., Mando, W., & Chintala, S. K. (2013). Excitotoxicity upregulates SARM1 protein expression and promotes Wallerian-like degeneration of retinal ganglion cells and their axons. *Investigative Ophthalmology & Visual Science, 54*(4), 2771-2780.

McDonald, K. K., Aulas, A., Destroismaisons, L., Pickles, S., Beleac, E., Camu, W., . . . Vande Velde, C. (2011). TAR DNA-binding protein 43 (TDP-43) regulates stress granule dynamics via differential regulation of G3BP and TIA-1. *Human Molecular Genetics, 20*(7), 1400-1410.

McMurray, C. T. (2000). Neurodegeneration: diseases of the cytoskeleton? *Cell death and Differentiation, 7*(10), 861-865.

Mihevc, S. P., Baralle, M., Buratti, E., & Rogelj, B. (2016). TDP-43 aggregation mirrors TDP-43 knockdown, affecting the expression levels of a common set of proteins. *Scientific Reports*, *6,* 1-9.

Mikucki, S. A. O., M. M. (1991). Corticospinal neurons exhibit a noven pattern of cytoskeletal gene expression after injury. *Journal of Neuroscience Research, 30*, 213-225.

Millecamps, S., & Julien, J. P. (2013). Axonal transport deficits and neurodegenerative diseases. *Nature Reviews: Neuroscience, 14*(3), 161-176.

Miller, R. G., Mitchell, J. D., & Moore, D. H. (2012). Riluzole for amyotrophic lateral sclerosis (ALS)/motor neuron disease (MND). The *Cochrane Database of Systematic Reviews,* (3), CD001447.

Mishra, M., Paunesku, T., Woloschak, G. E., Siddique, T., Zhu, L. J., Lin, S., . . . Bigio, E. H. (2007). Gene expression analysis of frontotemporal lobar degeneration of the motor neuron disease type with ubiquitinated inclusions. *Acta Neuropathologica, 114*(1), 81-94.

Mitew, S., Kirkcaldie, M. T. K., Dickson, T. C., & Vickers, J. C. (2013). Altered synapses and gliotransmission in Alzheimer's disease and AD model mice. *Neurobiology of Aging, 34*(10), 2341-2351.

Mori, K., Weng, S.-M., Arzberger, T., May, S., Rentzsch, K., Kremmer, E., . . . Edbauer, D. (2013). The C9orf72 GGGGCC repeat is translated into aggregating dipeptide-repeat proteins in FTLD/ALS. *Science, 339*(6125), 1335-1338.

Moss, T. H. L., S. J. (1983). The axon reaction in motor and sensory neurones of mice studied by a monoclonal antibody marker of neurofilament protein. *Journal of the Neurological Sciences, 60*(267-280).

MRI g-ratio Tools ImageJ macro. (2014). Retrieved from http://dev.mri.cnrs.fr/projects/imagej-macros/wiki/MRI_g-ratio_Tools.

Münch, C., Rosenbohm, A., Sperfeld, A.-D., Uttner, I., Reske, S., Krause, B. J., . . . Ludolph, A. C. (2005). Heterozygous R1101K mutation of the DCTN1 gene in a family with ALS and FTD. *Annals of Neurology, 58*(5), 777-780.

National Health and Medical Research Council. (2013). *Australian code for the care and use of animals for scientific purposes, 8th edition*.

Neumann, M., Kwong, L. K., Lee, E. B., Kremmer, E., Flatley, A., Xu, Y., . . . Lee, V. M. Y. (2009). Phosphorylation of S409/410 of TDP-43 is a consistent feature in all sporadic and familial forms of TDP-43 proteinopathies. *Acta Neuropathologica, 117*(2), 137-149.

Neumann, M., Kwong, L. K., Truax, A. C., Vanmassenhove, B., Kretzschmar, H. A., Van Deerlin, V. M., . . . Lee, V. M. Y. (2007). TDP-43-positive white matter pathology in frontotemporal lobar degeneration with ubiquitin-positive inclusions. *Journal of Neuropathology and Experimental Neurology, 66*(3), 177-183.

Neumann, M., Sampathu, D. M., Kwong, L. K., Truax, A. C., Micsenyi, M. C., Chou, T. T., . . . Lee, V. M. Y. (2006). Ubiquitinated TDP-43 in frontotemporal lobar degeneration and amyotrophic lateral sclerosis. *Science (New York, N.Y.), 314*(5796), 130-133.

Nobes, C. D. H., A. (1995). Rho, Rac, and Cdc42 GTPases regulate the assembly of multimolecular focal complexes associated with actin stress fibers, lamellipodia, and filopodia. *Cell, 81*, 53-62.

O'Rourke, J. G., Bogdanik, L., Muhammad, A. K. M. G., Gendron, T. F., Kim, K. J., Austin, A., . . . Baloh, R. H. (2015). C9orf72 BAC transgenic mice display typical pathologic features of ALS/FTD. *Neuron, 88*(5), 892-901.

O'Mara, A., King, A. E., Vickers, J. C., & Kirkcaldie, M. T. K. (2017). ImageSURF: an ImageJ plugin for batch pixel-based image segmentation using random forests. *Journal of Open Research Software, 5*. doi:10.5334/jors.172

Omotade, O. F., Pollitt, S. L., & Zheng, J. Q. (2017). Actin-based growth cone motility and guidance. *Molecular and Cellular Neuroscience*, *84,* 1-7.

Onyike, C. U., & Diehl-Schmid, J. (2013). The epidemiology of frontotemporal dementia. *International Review of Psychiatry, 25*(2), 130-137.

Perrone, F., Nguyen, H. P., Van Mossevelde, S., Moisse, M., Sieben, A., Santens, P., . . . Belgian Neurology, c. (2017). Investigating the role of ALS genes CHCHD10 and TUBA4A in Belgian FTD-ALS spectrum patients. *Neurobiology of Aging, 51*, 177 e179-177 e116.

Petkau, T. L., Neal, S. J., Milnerwood, A., Mew, A., Hill, A. M., Orban, P., . . . Leavitt, B. R. (2012). Synaptic dysfunction in progranulin-deficient mice. *Neurobiology of Disease, 45*(2), 711-722.

Pfrieger, F. W. (2009). Roles of glial cells in synapse development. *Cellular and Molecular Life Sciences, 66*(13), 2037-2047.

Phukan, J., Pender, N. P., & Hardiman, O. (2007). Cognitive impairment in amyotrophic lateral sclerosis. *The Lancet Neurology, 6*(11), 994-1003.

Piguet, O. (2013). Neurodegenerative disease: frontotemporal dementia--time to target inflammation? *Nature Reviews. Neurology, 9*(6), 304-305.

Poorkaj, P., Bird, T. D., Wijsman, E., Nemens, E., Garruto, R. M., Anderson, L., . . . Schellenberg, G. D. (1998). Tau is a candidate gene for chromosome 17 frontotemporal dementia. *Annals of Neurology, 43*(6), 815-825.

Puls, I., Jonnakuty, C., LaMonte, B. H., Holzbaur, E. L. F., Tokito, M., Mann, E., . . . Fischbeck, K. H. (2003). Mutant dynactin in motor neuron disease. *Nature Genetics, 33*(4), 455-456.

R Core Team. (2016). R: A language and environment for statistical computing. *R Foundation for Statistical Computing, Viena, Austria*.

Rademakers, R., Neumann, M., & Mackenzie, I. R. (2012). Advances in understanding the molecular basis of frontotemporal dementia. *Nature Reviews. Neurology, 8*(8), 423-434.

Rademakers, R. C., M.; van Broeckhoven, C. (2004). The role of tau (MAPT) in frontotemporal dementia and related tauopathies. *Human Mutation, 24*(4), 277-295.

Renton, A. E., Majounie, E., Waite, A., Simón-Sánchez, J., Rollinson, S., Gibbs, J. R., . . . Traynor, B. J. (2011). A hexanucleotide repeat expansion in C9ORF72 is the cause of chromosome 9p21-linked ALS-FTD. *Neuron, 72*(2), 257-268.

Reynolds, E. S. (1963). The use of lead citrate at high pH as an electron opaque stain in electronic microscope. *Journal of Cell Biology, 17*, 208-212.

Roberson, E. D. (2012). Mouse models of frontotemporal dementia. *Annals of Neurology, 72*(6), 837-849.

Rodriguez, A. R., de Sevilla Müller, L. P., & Brecha, N. C. (2014). The RNA binding protein RBPMS is a selective marker of ganglion cells in the mammalian retina. *The Journal of comparative neurology, 522*(6), 1411-1443.

Romano, M., Buratti, E., Romano, G., Klima, R., Del Bel Belluz, L., Stuani, C., . . . Feiguin, F. (2014). Evolutionarily conserved heterogeneous nuclear ribonucleoprotein (hnRNP) A/B proteins functionally interact with human and Drosophila TAR DNA-binding protein 43 (TDP-43). *Journal of Biological Chemistry, 289*(10), 7121-7130.

Rouleau, G. A., Clark, A. W., Rooke, K., Pramatarova, A., Krizus, A., Suchowersky, O., . . . Figlewicz, D. (1996). SOD1 mutation is associated with accumulation of neurofilaments in amyotrophic lateral sclerosis. *Annals of Neurology, 39*(1), 128-131.

Sasaki, S., & Iwata, M. (1996). Ultrastructural study of synapses in the anterior horn neurons of patients with amyotrophic lateral sclerosis. *Neuroscience Letters, 204*(1-2), 53-56.

Sasaki, S. I., M. (2007). Mitochondrial Alterations in the Spinal Cord of Patients With Sporadic Amyotrophic Lateral Sclerosis. *Journal of Neuropathology and Experimental Neurology, 66*(1).

Satoh, J.-i., Tabunoki, H., Ishida, T., Saito, Y., & Arima, K. (2012). Dystrophic neurites express C9orf72 in Alzheimer's disease brains. *Alzheimer's Research & Therapy, 4*(4), 33.

Schofield, E. K., C.; Sheperd, C. E.; Kril, J. J.; Halliday, G. M. (2003). Severity of gliosis in Pick's disease and frontotemporal lobar degeneration: tau-positive glia differentiate these disorders. *Brain, 126*(4), 827-840.

Schwenk, B. M., Hartmann, H., Serdaroglu, A., Schludi, M. H., Hornburg, D., Meissner, F., . . . Edbauer, D. (2016). TDP-43 loss of function inhibits endosomal trafficking and alters trophic signaling in neurons. *The EMBO Journal, 35*(21), 2350-2370.

Scotter, E. L., Vance, C., Nishimura, A. L., Lee, Y. B., Chen, H. J., Urwin, H., . . . Shaw, C. E. (2014). Differential roles of the ubiquitin proteasome system and autophagy in the clearance of soluble and aggregated TDP-43 species. *Journal of Cell Science, 127*(6), 1263-1278.

Sephton, C. F., Cenik, B., Cenik, B. K., Herz, J., & Yu, G. (2012). TDP-43 in central nervous system development and function: clues to TDP-43-associated neurodegeneration. *Biological Chemistry, 393*(7), 589-594.

Sephton, C. F., Good, S. K., Atkin, S., Dewey, C. M., Mayer, P., Herz, J., & Yu, G. (2010). TDP-43 is a developmentally regulated protein essential for early embryonic development. *The Journal of Biological Chemistry, 285*(9), 6826-6834.

Sephton, C. F., & Yu, G. (2015). The function of RNA-binding proteins at the synapse: implications for neurodegeneration. *Cellular and Molecular Life Sciences*

Sieben, A., Van Langenhove, T., Engelborghs, S., Martin, J.-J., Boon, P., Cras, P., . . . Cruts, M. (2012). The genetics and neuropathology of frontotemporal lobar degeneration. *Acta Neuropathologica, 124*(3), 353-372.

Simón-Sánchez, J., Dopper, E. G. P., Cohn-Hokke, P. E., Hukema, R. K., Nicolaou, N., Seelaar, H., . . . van Swieten, J. C. (2012). The clinical and pathological phenotype of C9ORF72 hexanucleotide repeat expansions. *Brain, 135*(Pt 3), 723-735.

Sivadasan, R., Hornburg, D., Drepper, C., Frank, N., Jablonka, S., Hansel, A., . . . Sendtner, M. (2016). C9ORF72 interaction with cofilin modulates actin dynamics in motor neurons. *Nature Neuroscience*, *19,* 1-12.

Smith, B. N., Ticozzi, N., Fallini, C., Gkazi, A. S., Topp, S., Kenna, K. P., . . . Landers, J. E. (2014). Exome-wide rare variant analysis identifies TUBA4A mutations associated with familial ALS. *Neuron, 84*(2), 324-331.

Snowden, J. S., Rollinson, S., Thompson, J. C., Harris, J. M., Stopford, C. L., Richardson, A. M. T., . . . Pickering-Brown, S. M. (2012). Distinct clinical and pathological characteristics of frontotemporal dementia associated with C9ORF72 mutations. *Brain, 135*(3), 693-708.

Spillantini, M. G., Murrell, J. R., Goedert, M., Farlow, M. R., Klug, A., & Ghetti, B. (1998). Mutation in the tau gene in familial multiple system tauopathy with presenile dementia. *Proceedings of the National Academy of Sciences of the United States of America, 95*(13), 7737-7741.

Sreedharan, J., Blair, I. P., Tripathi, V. B., Hu, X., Vance, C., Rogelj, B., . . . Shaw, C. E. (2008). TDP-43 mutations in familial and sporadic amyotrophic lateral sclerosis. *Science (New York, N.Y.), 319*(5870), 1668-1672.

Sreedharan, J., Neukomm, L. J., Brown, R. H., & Freeman, M. R. (2015). Age-dependent TDP-43-mediated motor neuron degeneration requires GSK3, hat-trick, and xmas-2. *Current Biology*, *16,* 2130-2136.

Stalekar, M., Yin, X., Rebolj, K., Darovic, S., Troakes, C., Mayr, M., . . . Rogelj, B. (2015). Proteomic analyses reveal that loss of TDP-43 affects RNA processing and intracellular transport. *Neuroscience, 293*, 157-170.

Stenmark, H. (2009). Rab GTPases as coordinators of vesicle traffic. *Nature, 10*(8), 513-525.

Stewart, H., Rutherford, N. J., Briemberg, H., Krieger, C., Cashman, N., Fabros, M., . . . Mackenzie, I. R. A. (2012). Clinical and pathological features of amyotrophic lateral sclerosis caused by mutation in the C9ORF72 gene on chromosome 9p. *Acta Neuropathologica, 123*(3), 409-417.

Stigliani, S., Zappettini, S., Raiteri, L., Passalacqua, M., Melloni, E., Venturi, C., . . . Bonanno, G. (2006). Glia re-sealed particles freshly prepared from adult rat brain are competent for exocytotic release of glutamate. *Journal of Neurochemistry, 96*(3), 656-668.

Stoica, R., De Vos, K. J., Paillusson, S., Mueller, S., Sancho, R. M., Lau, K.-F., . . . Miller, C. C. J. (2014). ER-mitochondria associations are regulated by the VAPB-PTPIP51 interaction and are disrupted by ALS/FTD-associated TDP-43. *Nature Communications, 5*, 3996.

Strong, M. J., Kesavapany, S., & Pant, H. C. (2005). The pathobiology of amyotrophic lateral sclerosis: a proteinopathy? *Journal of Neuropathology and Experimental Neurology, 64*(8), 649-664.

Strong, M. J., Volkening, K., Hammond, R., Yang, W., Strong, W., Leystra-Lantz, C., & Shoesmith, C. (2007). TDP43 is a human low molecular weight neurofilament (hNFL) mRNA-binding protein. *Molecular and Cellular Neurosciences, 35*(2), 320-327.

Sullivan, P. M., Zhou, X., Robins, A. M., Paushter, D. H., Kim, D., Smolka, M. B., & Hu, F. (2016). The ALS/FTLD associated protein C9orf72 associates with SMCR8 and WDR41 to regulate the autophagy-lysosome pathway. *Acta Neuropathologica Communications, 4*(1), 51.

Suzuki, N., Maroof, A. M., Merkle, F. T., Koszka, K., Intoh, A., Armstrong, I., . . . Eggan, K. (2013). The mouse C9ORF72 ortholog is enriched in neurons known to degenerate in ALS and FTD. *Nature Neuroscience, 16*(12), 1725-1727.

Swaroop, A., ; Douglas, K.; Forrest, D. (2010). Transcriptional regulation of photoreceptor development and homeostasis in the mammalian retina. *Nature Reviews Neuroscience, 11*, 563-576.

Swarup, V., Phaneuf, D., Bareil, C., Robertson, J., Rouleau, G. A., Kriz, J., & Julien, J.-P. (2011). Pathological hallmarks of amyotrophic lateral sclerosis/frontotemporal lobar degeneration in transgenic mice produced with TDP-43 genomic fragments. *Brain, 134*(9), 2610-2626.

Syc, S. B., Saidha, S., Newsome, S. D., Ratchford, J. N., Levy, M., Ford, E., . . . Calabresi, P. A. (2012). Optical coherence tomography segmentation reveals ganglion cell layer pathology after optic neuritis. *Brain, 135*(2), 521-533.

Takei, Y., Teng, J., Harada, A., & Hirokawa, N. (2000). Defects in axonal elongation and neuronal migration in mice with disrupted tau and map1b genes. *The Journal of Cell Biology, 150*(5), 989-1000.

The Writing Group on behalf of the Edaravone (MCI-186) ALS 19 Study Group. (2017). Safety and efficacy of edaravone in well defined patients with amyotrophic lateral sclerosis: a randomised, double-blind, placebo controlled trial. *Lancet Neurology, 16*(7), 505-512.

Therrien, M., Rouleau, G. A., Dion, P. A., & Parker, J. A. (2013). Deletion of C9ORF72 results in motor neuron degeneration and stress sensitivity in C. elegans. *PloS One, 8*(12), e83450.

Tiloca, C., Ticozzi, N., Pensato, V., Corrado, L., Del Bo, R., Bertolin, C., . . . Consortium, S. (2013). Screening of the PFN1 gene in sporadic amyotrophic lateral sclerosis and in frontotemporal dementia. *Neurobiology of Aging, 34*(5), 1517.e1519-1510.

Toyoshima, I., Sugawara, M., Kato, K., Wada, C., Hirota, K., Hasegawa, K., . . . Masamune, O. (1998). Kinesin and cytoplasmic dynein in spinal spheroids with motor neuron disease. *Journal of the Neurological Sciences, 159*(1), 38-44.

Tripathi, V. B., Baskaran, P., Shaw, C. E., & Guthrie, S. (2014). Tar DNA-binding protein-43 (TDP-43) regulates axon growth in vitro and in vivo. *Neurobiology of Disease, 65*, 25-34.

Valenzuela-Fernández, A., Cabrero, J. R., Serrador, J. M., & Sánchez-Madrid, F. (2008). HDAC6: a key regulator of cytoskeleton, cell migration and cell-cell interactions. *Trends in Cell Biology, 18*(6), 291-297.

van Blitterswijk, M., Baker, M. C., Bieniek, K. F., Knopman, D. S., Josephs, K. A., Boeve, B., . . . Rademakers, R. (2013). Profilin-1 mutations are rare in patients with amyotrophic lateral sclerosis and frontotemporal dementia. *Amyotrophic Lateral Sclerosis & Frontotemporal Degeneration, 14*(5-6), 463-469.

Van Damme, P., Van Hoecke, A., Lambrechts, D., Vanacker, P., Bogaert, E., van Swieten, J., . . . Robberecht, W. (2008). Progranulin functions as a neurotrophic factor to regulate neurite outgrowth and enhance neuronal survival. *The Journal of Cell Biology, 181*(1), 37-41.

van Eersel, J., Stevens, C. H., Przybyla, M., Gladbach, A., Stefanoska, K., Chan, C. K.-X., . . . Ittner, L. M. (2015). Early-onset axonal pathology in a novel P301S-Tau transgenic mouse model of frontotemporal lobar degeneration. *Neuropathology and Applied Neurobiology, 41*(7), 906-925.

Van Vactor, D. (1998). Adhesion and signaling in axonal fasciculation. *Current Opinion in Neurobiology, 1998*(8), 80-85.

van Zundert, B., Izaurieta, P., Fritz, E., & Alvarez, F. J. (2012). Early pathogenesis in the adult-onset neurodegenerative disease amyotrophic lateral sclerosis. *Journal of Cellular Biochemistry, 113*(11), 3301-3312.

Vickers, J. C., King, A. E., Woodhouse, A., Kirkcaldie, M. T., Staal, J. A., McCormack, G. H., . . . Dickson, T. C. (2009). Axonopathy and cytoskeletal disruption in degenerative diseases of the central nervous system. *Brain Research Bulletin, 80*(4-5), 217-223.

Volkening, K., Leystra-Lantz, C., Yang, W., Jaffee, H., & Strong, M. J. (2009). Tar DNA binding protein of 43 kDa (TDP-43), 14-3-3 proteins and copper/zinc superoxide dismutase (SOD1) interact to modulate NFL mRNA stability. Implications for altered RNA processing in amyotrophic lateral sclerosis (ALS). *Brain Research, 1305*, 168-182.

Vucic, S. K., M. C. (2006). Axonal excitability properties in amyotrophic lateral sclerosis. *Clinical Neurophysiology, 117*(7), 1458-1466.

Waite, A. J., Bäumer, D., East, S., Neal, J., Morris, H. R., Ansorge, O., & Blake, D. J. (2014). Reduced C9orf72 protein levels in frontal cortex of amyotrophic lateral sclerosis and frontotemporal degeneration brain with the C9ORF72 hexanucleotide repeat expansion. *Neurobiology of Aging, 35*(7), 1779.e1775-1779.e1713.

Walker, A. K., Spiller, K. J., Ge, G., Zheng, A., Xu, Y., Zhou, M., . . . Lee, V. M. Y. (2015). Functional recovery in new mouse models of ALS/FTLD after clearance of pathological cytoplasmic TDP-43. *Acta Neuropathologica, 130*(5), 643-660.

Wang, D., Chan, C.-C., Cherry, S., & Hiesinger, P. R. (2013). Membrane trafficking in neuronal maintenance and degeneration. *Cellular and Molecular Life Sciences, 70*(16), 2919-2934.

Wang, G., Yang, H., Yan, S., Wang, C.-E., Liu, X., Zhao, B., . . . Lai, L. (2015). Cytoplasmic mislocalization of RNA splicing factors and aberrant neuronal gene splicing in TDP-43 transgenic pig brain. *Molecular Neurodegeneration, 10*(1), 42.

Wang, I.-F., Wu, L. S., Chang, H.-Y., & Shen, C. K. (2008). TDP-43, the signature protein of FTLD-U, is a neuronal activity-responsive factor. *Journal of Neurochemistry, 105*(3), 797-806.

Wang, W., Li, L., Lin, W.-L., Dickson, D. W., Petrucelli, L., Zhang, T., & Wang, X. (2013). The ALS disease-associated mutant TDP-43 impairs mitochondrial dynamics and function in motor neurons. *Human Molecular Genetics, 22*(23), 4706-4719.

Wang, Y., & Mandelkow, E. (2016). Tau in physiology and pathology. *Nature Reviews Neuroscience, 17*(1), 5-21.

Watts, G. D. J., Wymer, J., Kovach, M. J., Mehta, S. G., Mumm, S., Darvish, D., . . . Kimonis, V. E. (2004). Inclusion body myopathy associated with Paget disease of bone and frontotemporal dementia is caused by mutant valosin-containing protein. *Nature Genetics, 36*(4), 377-381.

Webster, C. P., Smith, E. F., Bauer, C. S., Moller, A., Hautbergue, G. M., Ferraiuolo, L., . . . De Vos, K. J. (2016). The C9orf72 protein interacts with Rab1a and the ULK1 complex to regulate initiation of autophagy. *The EMBO Journal*, e201694401.

Wilson, R., Diseberg, A. F., Gordon, L., Zivkovic, S., Tatarczuch, L., Mackie, E. J., . . . Bateman, J. F. (2010). Comprehensive profiling of cartilage extracellular matrix formation and maturation using sequential extraction and label-free quantitative proteomics. *Molecular & Cellular Proteomics, 9*(6), 1296-1313.

Wilson, R., Golub, S. B., Rowley, L., Angelucci, C., Karpievitch, Y. V., Bateman, J. F., & Fosang, A. J. (2016). Novel elements of the chondrocyte stress response identified using an in vitro model of mouse cartilage degradation. *Journal of Proteome Research, 15*(3), 1033-1050.

Winton, M. J., Igaz, L. M., Wong, M. M., Kwong, L. K., Trojanowski, J. Q., & Lee, V. M. Y. (2008). Disturbance of nuclear and cytoplasmic TAR DNA-binding protein (TDP-43) induces disease-like redistribution, sequestration, and aggregate formation. *The Journal of Biological Chemistry, 283*(19), 13302-13309.

Wong, N. K. H., B.P.; Strong, M.J. (2000). Characterization of neuronal intermediate filament protein expression in cervical spinal motor neurons in sporadic amyotrophic lateral sclerosis (ALS). *Journal of Neuropathology and Experimental Neurology, 59*(11), 972-982.

Woo, S., & Gomez, T. M. (2006). Rac1 and RhoA promote neurite outgrowth through formation and stabilization of growth cone point contacts. *Journal of Neuroscience, 26*(5), 1418-1428.

Workman, A. D., Charvet, C. J., Clancy, B., Darlington, R. B., & Finlay, B. L. (2013). Modeling transformations of neurodevelopmental sequences across mammalian species. *Journal of Neuroscience, 33*(17), 7368-7383.

Workman, A. D., Charvet, C. J., Clancy, B., Darlington, R. B., & Finlay, B. L. (2013). Modeling transformations of neurodevelopmental sequences across mammalian species. *Journal of Neuroscience, 33*(17), 7368-7383.

Wu, C.-H., Fallini, C., Ticozzi, N., Keagle, P. J., Sapp, P. C., Piotrowska, K., . . . Landers, J. E. (2012). Mutations in the profilin 1 gene cause familial amyotrophic lateral sclerosis. *Nature, 488*(7412), 499-503.

Wu, L.-S., Cheng, W.-C., & Shen, C. K. J. (2012). Targeted depletion of TDP-43 expression in the spinal cord motor neurons leads to the development of amyotrophic lateral sclerosis-like phenotypes in mice. *Journal of Biological Chemistry, 287*(33), 27335-27344.

Wylie, S. R. W., P.-J.; Patel, H.; Chantler, P. D. (1998). A conventional myosin motor drives neurite outgrowth. *Proceedings of the National Academy of Sciences of the United States of America, 95*, 12967-12972.

Xi, Z., Zinman, L., Moreno, D., Schymick, J., Liang, Y., Sato, C., . . . Rogaeva, E. (2013). Hypermethylation of the CpG island near the G4C2 repeat in ALS with a C9orf72 expansion. *American Journal of Human Genetics*.

Xiao, S., MacNair, L., McGoldrick, P., McKeever, P. M., McLean, J. R., Zhang, M., . . . Robertson, J. (2015). Isoform specific antibodies reveal distinct subcellular localizations of C9orf72 in amyotrophic lateral sclerosis. *Annals of Neurology, 78* (4), 568-583.

Xu, Y.-f., Gendron, T. F., Zhang, Y.-J., Lin, W.-L., D'Alton, S., Sheng, H., . . . Petrucelli, L. (2010). Wild-type human TDP-43 expression causes TDP-43 phosphorylation, mitochondrial aggregation, motor deficits, and early mortality in transgenic mice. *Journal of Neuroscience, 30*(32), 10851-10859.

Yates, D. M. M., C.; de Vos, K. J.; Shaw, C. E.; McLoughlin, D. M.; Miller, C. C. J. (2009). Neurofilament subunit (NFL) head domain phosphorylation regulates axonal transport of neurofilaments. *European Journal of Cell Biology, 88*, 193-202.

Zhang, H.-X., Tanji, K., Mori, F., & Wakabayashi, K. (2008). Epitope mapping of 2E2-D3, a monoclonal antibody directed against human TDP-43. *Neuroscience Letters, 434*(2), 170-174.

Zhang, W. B., D. L. (2001). Stages of Synapse Development Defined by Dependence on F-Actin. *Journal of Neuroscience, 21*(14), 5169-5181.

Zhou, L., Miller, B. L., McDaniel, C. H., Kelly, L., Kim, O. J., & Miller, C. A. (1998). Frontotemporal dementia: neuropil spheroids and presynaptic terminal degeneration. *Annals of Neurology, 44*(1), 99-109.

Zhukareva, V. V.-R., V.; Van Deerlin, V.; Bruce, J.; Shuck, T.; Grossman, M.; MD, Clark, C. M.; Arnold, S. E.; Masliah, E.; Galasko, D.; Trojanowski, J. Q.; Lee, V. M.-Y. (2001). Loss of brain tau defines novel sporadic and familial tauopathies with frontotemporal dementia. *Annals of Neurology, 49*, 165-175.

8 APPENDICES

8.1 COMMON LABORATORY REAGENTS

0.01M Phosphate Buffered Saline (PBS) – 1.0L

850mL MilliQ® water
100mL 90.0g/L Sodium chloride (NaCl; BDH, USA)
40mL 28.0g/L Di-sodium hydrogen orthophosphate (Na_2HPO; BDH, USA)
10mL 31.2g/L Sodium di-hydrogen orthophosphate ($NaH_2PO_4.2H_2O$; Ajax, Australia)

4% Paraformaldehyde – 1.0L

40g granulated paraformaldehyde (PFA)
500mL MilliQ® water
400mL 28.0g/L Na_2HPO
100mL 31.2g/L $NaH_2PO_4.2H_2O$
1.0M NaOH & 1.0M HCl to pH

Heat MilliQ® to 80^oC, add granulated PFA and 5 drops of NaOH. Stir until PFA dissolved, add $NaH_2PO_4.H_2O$ and Na_2HPO. Filter and pH to 7.4.

0.4M phosphate buffer – 1.0L

45.42 g NaH_2PO_4

12.48g Na_2HPO_4

Dissolve in 900ml of distilled water

pH to 7.4 with NaOH or HCl

Make up to 1L with distilled water

2% PFA/ 2.5% glutaraldehyde – 0.1L

250ml 0.4M phosphate buffer

20g PFA powder

700ml distilled water (pre-heated in microwave to reduce dissolving time)

Dissolve PFA on heat stirrer

Filter with whatman paper

Add 50ml 50% glutaraldehyde (defrost at room temp for 1hr prior to adding)

Tissue Storage Solution – 500mL

500mL 0.01M PBS
0.5g sodium azide

Cryoprotectant Solution (30% sucrose) – 500mL

500mL 0.01M PBS
150g sucrose
0.02% sodium azide

8.2 CHAPTER 3 APPENDIX

Appendix 3.1 Proteomic MS peptide and protein group counts and intensities

This data is available in Microsoft Excel 2011 format as a supplementary electronic file to this thesis.

Appendix 3.2 Proteomic data set after filtering, imputation of missing values, calculation of differential expression and calculation of FDR, and Complete DAVID functional annotation clustering analysis of proteins up and down regulated greater than 1.3-fold by wildtype TDP-43

This data is available in Microsoft Excel 2011 format as a supplementary electronic file to this thesis.

Appendix 3.3 Statistical appendix for growth cone morphology and Neurolucida analysis

8.2.1 Growth-cone morphology

Data were loaded from Excel files and collated into tables. Boxplots suggest tg-het genotypes had a different distribution of growth cone morphologies than tg-hom and wt mice, with fewer lamelopodial cones and more filopodial cones observed.

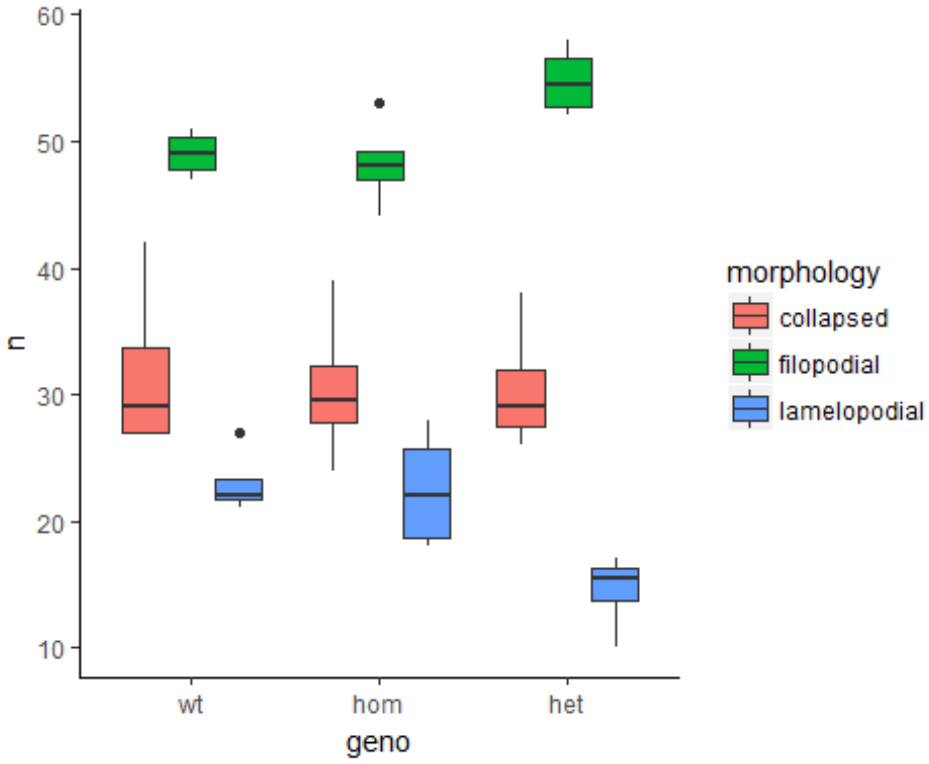

Data were collapsed into a 3 x 3 contingency table and a Pearson's Chi-squared test of homogeneity was calculated.

```
##     collapsed filopodial lamelopodial
## wt        127        196           92
## hom       122        193           90
## het       122        219           58

##
##  Pearson's Chi-squared test
##
## data:  df1
## X-squared = 11.009, df = 4, p-value = 0.02647
```

The chi-squared test shows that one genotype has a different distribution of growth cone morphologies to the other two. We can safely assume from the plot that this is the tg-het genotype.

8.2.1.1 Filopodia length

```
## Data: df
## Models:
## fit3a_null: log(length.filo) ~ 1 + (1 | embryo)
## fit3a: log(length.filo) ~ geno + (1 | embryo)
##            Df    AIC    BIC  logLik deviance  Chisq Chi Df Pr(>Chisq)
## fit3a_null  3 1174.5 1188.7 -584.26   1168.5
## fit3a       5 1178.5 1202.0 -584.23   1168.5 0.0563      2     0.9722
```

8.2.1.2 Actin : β-tubulin ratio

```
## Data: na.omit(df)
## Models:
## fit3a_log_null: log(actin.tubulin.ratio) ~ 1 + (1 | embryo)
## fit3a_log: log(actin.tubulin.ratio) ~ geno + (1 | embryo)
##                Df     AIC     BIC logLik deviance  Chisq Chi Df Pr(>Chisq)
## fit3a_log_null  3 -47.275 -40.019 26.638  -53.275
## fit3a_log       5 -45.360 -33.266 27.680  -55.360 2.0845      2     0.3527

## Analysis of Variance Table
##      Df  Sum Sq Mean Sq F value
## geno  2 0.34742 0.17371  0.6634

## Analysis of Variance Table
##      Df  Sum Sq Mean Sq F value
## geno  2 0.26581  0.1329  0.6751
```

8.2.2 Neuorolucida analysis of neuron morphology

Number of branch points

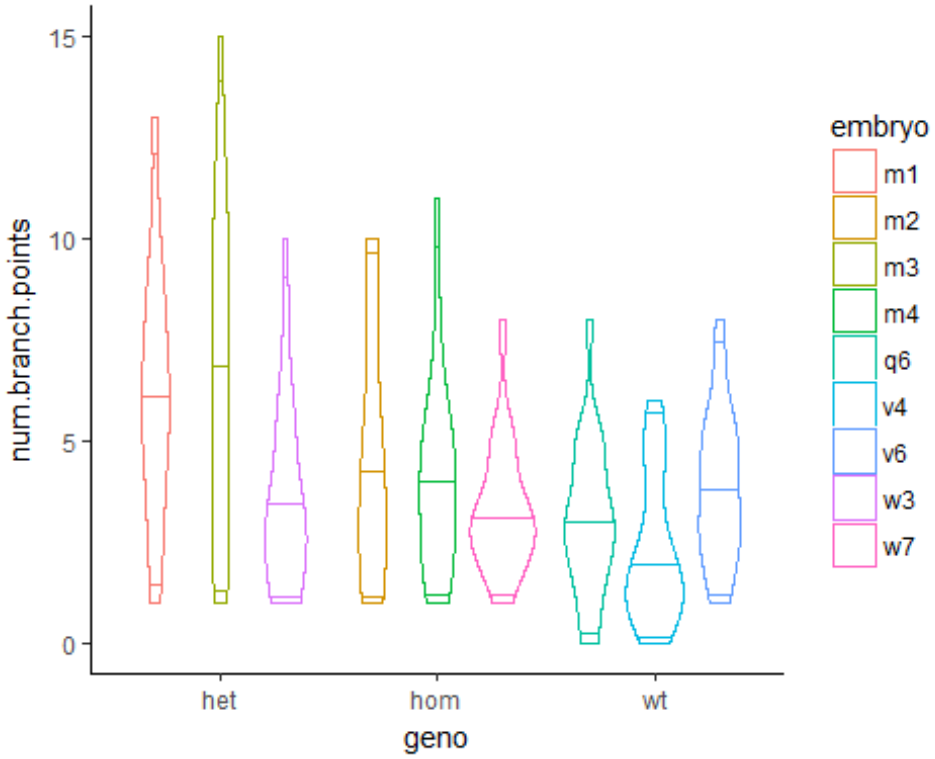


```
## Generalized linear mixed model fit by maximum likelihood (Laplace
##   Approximation) [glmerMod]
##  Family: poisson  ( log )
## Formula: num.branch.points ~ geno + (1 | embryo)
##    Data: bp
##
##      AIC      BIC   logLik deviance df.resid
##    831.7    844.4   -411.8    823.7      173
##
```

```
## Scaled residuals:
##     Min      1Q  Median      3Q     Max
## -2.1064 -0.9799 -0.2971  0.7409  3.4814
##
## Random effects:
##  Groups Name        Variance Std.Dev.
##  embryo (Intercept) 0.03354  0.1832
## Number of obs: 177, groups:  embryo, 9
##
## Fixed effects:
##             Estimate Std. Error z value Pr(>|z|)
## (Intercept)   1.6690     0.1193  13.985  < 2e-16 ***
## genohom      -0.2806     0.1733  -1.620  0.10532
## genowt       -0.5603     0.1758  -3.188  0.00143 **
## ---
## Signif. codes:  0 '***' 0.001 '**' 0.01 '*' 0.05 '.' 0.1 ' ' 1
##
## Correlation of Fixed Effects:
##         (Intr) genohm
## genohom -0.688
## genowt  -0.677  0.467
```

```
## Single term deletions
##
## Model:
## num.branch.points ~ geno + (1 | embryo)
##        Df    AIC    LRT Pr(Chi)
## <none>    831.67
## geno    2 834.46 6.7952 0.03345 *
## ---
## Signif. codes:  0 '***' 0.001 '**' 0.01 '*' 0.05 '.' 0.1 ' ' 1
```

```
## # A tibble: 3 x 3
##    geno     MEAN        SE
##   <chr>    <dbl>     <dbl>
## 1   het 5.396825 0.4326295
## 2   hom 4.055556 0.3491196
## 3    wt 3.083333 0.2507522
```

8.3 CHAPTER 4 APPENDIX

Appendix 4.1 Statistical appendix for optomotor data

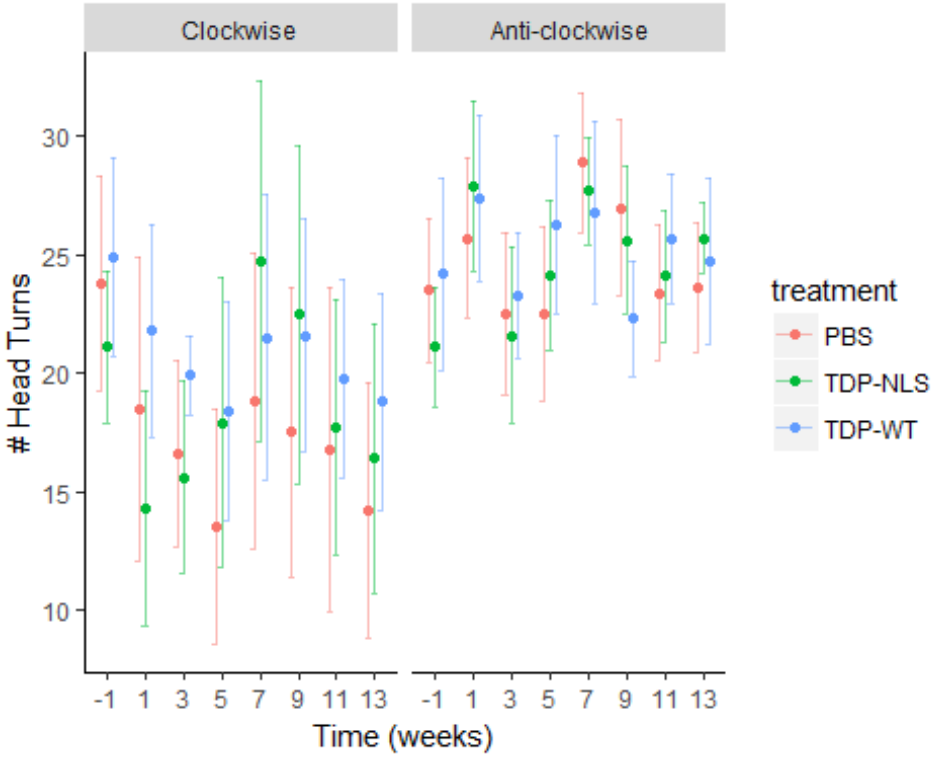

A main effect of direction (t >= 1) or direction x time (for all t) would convincingly show an effect of injection. Differences in treatment groups can be detected by direction x treatment (t >= 1).

We note that the response variable is count data, and thus $Y \sim Pois(\lambda)$, but inspection of the density plots (below) suggests the variable may be better modelled assuming $Y \sim N(\mu, \sigma^2)$. We will fit models both ways to determine the best using AIC (where the model with the smaller AIC is considered a better fit).

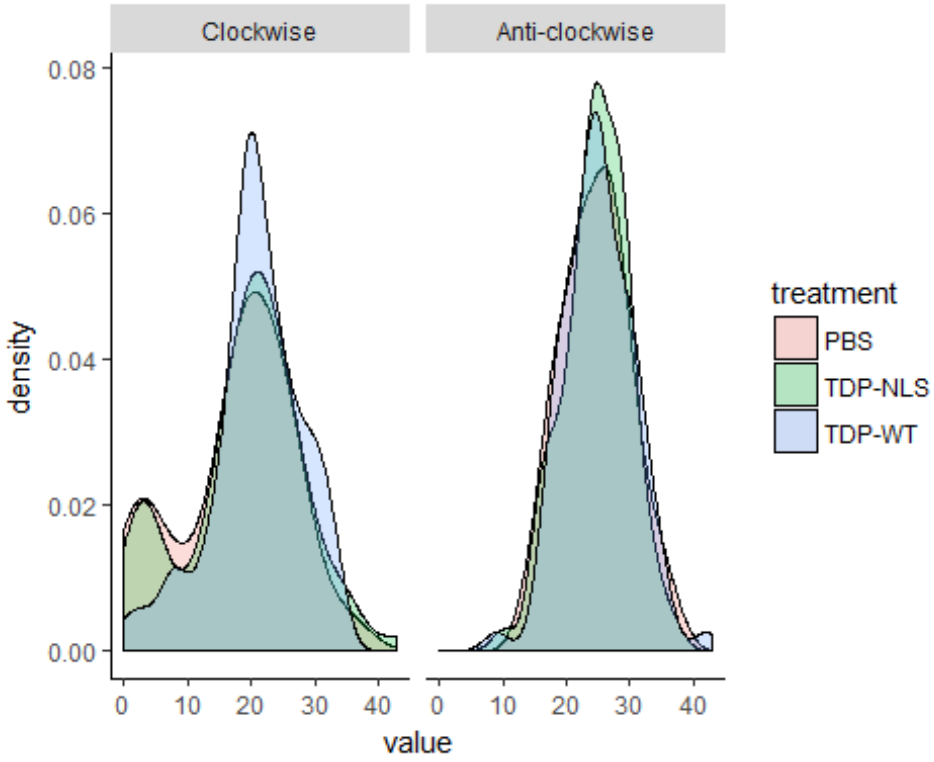


```
m1 <- glmer(value ~ movdir*time + movdir*treatment*time + (time|id), family = "p
oisson", df)
m2 <- lmer(value ~ movdir*time + movdir*treatment*time + (time|id),  df)
anova(m1, m2)
```

```
## Data: df
## Models:
## m1: value ~ movdir * time + movdir * treatment * time + (time | id)
## m2: value ~ movdir * time + movdir * treatment * time + (time | id)
##    Df    AIC    BIC  logLik deviance  Chisq Chi Df Pr(>Chisq)
## m1 15 3607.0 3669.6 -1788.5   3577.0
## m2 16 3201.8 3268.5 -1584.9   3169.8 407.26      1  < 2.2e-16 ***
## ---
## Signif. codes:  0 '***' 0.001 '**' 0.01 '*' 0.05 '.' 0.1 ' ' 1
```

A general linear model provides the best fit. Now we test whether the 3-way interaction is significant using a likelihood ratio test (LRT).

```
m3 <- lmer(value ~ time + movdir + treatment + time:movdir + time:treatment + mo
vdir:treatment + (time|id),  df)
anova(m2, m3)
```

```
## Data: df
## Models:
## ..1: value ~ time + movdir + treatment + time:movdir + time:treatment +
## ..1:     movdir:treatment + (time | id)
## object: value ~ movdir * time + movdir * treatment * time + (time | id)
##        Df    AIC    BIC  logLik deviance  Chisq Chi Df Pr(>Chisq)
## ..1    14 3199.2 3257.6 -1585.6   3171.2
## object 16 3201.8 3268.5 -1584.9   3169.8 1.4385      2     0.4871
```

The model with 2-way interactions is equivalent to the model with 3-way interactions, so unless the 3-way interaction is significant, there is no convincing argument to include it.

```
## Analysis of Variance Table of type III  with  Satterthwaite
## approximation for degrees of freedom
##                       Sum Sq Mean Sq NumDF DenDF F.value    Pr(>F)
## movdir                791.86  791.86     1   414 20.5074 7.778e-06 ***
## time                   28.83   28.83     1    27  0.7466   0.39516
## treatment             108.78   54.39     2    27  1.4086   0.26188
## movdir:time           170.25  170.25     1   414  4.4091   0.03635 *
## movdir:treatment       43.58   21.79     2   414  0.5643   0.56919
## time:treatment        107.54   53.77     2    27  1.3925   0.26573
## movdir:time:treatment  54.84   27.42     2   414  0.7102   0.49216
## ---
## Signif. codes:  0 '***' 0.001 '**' 0.01 '*' 0.05 '.' 0.1 ' ' 1
```

We can exclude the 3-way interaction (p = .49)

ANOVA table for two-way interaction model,

```
anova(m3, ddf = "Kenward-Roger")
```

```
## Analysis of Variance Table of type III  with  Kenward-Roger
## approximation for degrees of freedom
##                   Sum Sq Mean Sq NumDF  DenDF F.value    Pr(>F)
## time               28.79   28.79     1  32.91  0.7466   0.39381
## movdir            791.86  791.86     1 416.00 20.5360 7.659e-06 ***
## treatment         108.63   54.32     2  38.15  1.4086   0.25690
## time:movdir       170.25  170.25     1 416.00  4.4152   0.03622 *
## time:treatment    107.39   53.69     2  32.91  1.3925   0.26271
## movdir:treatment 172.62   86.31     2 416.00  2.2383   0.10792
## ---
## Signif. codes:  0 '***' 0.001 '**' 0.01 '*' 0.05 '.' 0.1 ' ' 1
```

Use standard graphical methods to test the assumption of normality (qq-plot) of residuals and homogeneity of variance (plot of residuals)

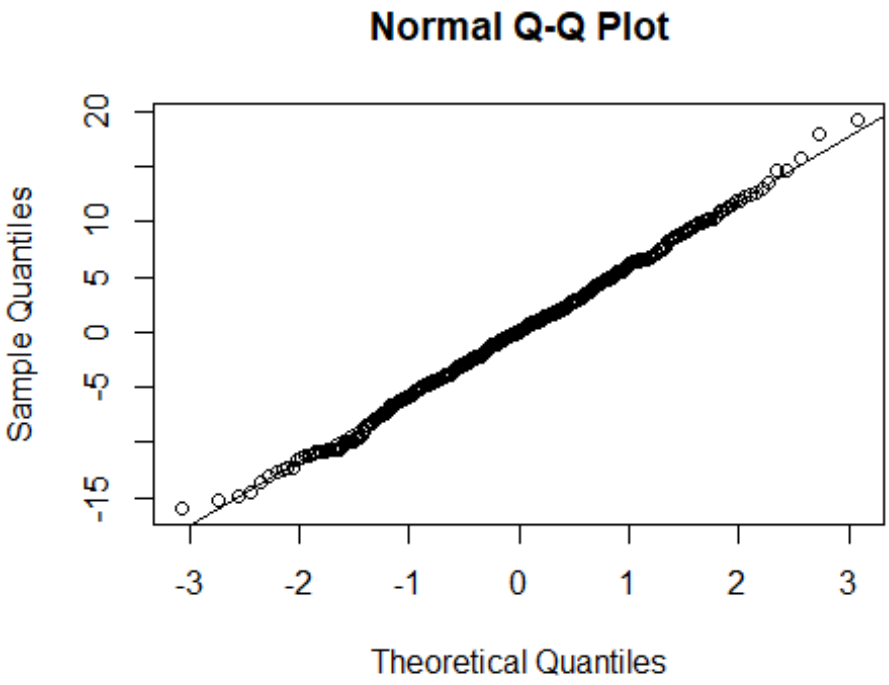

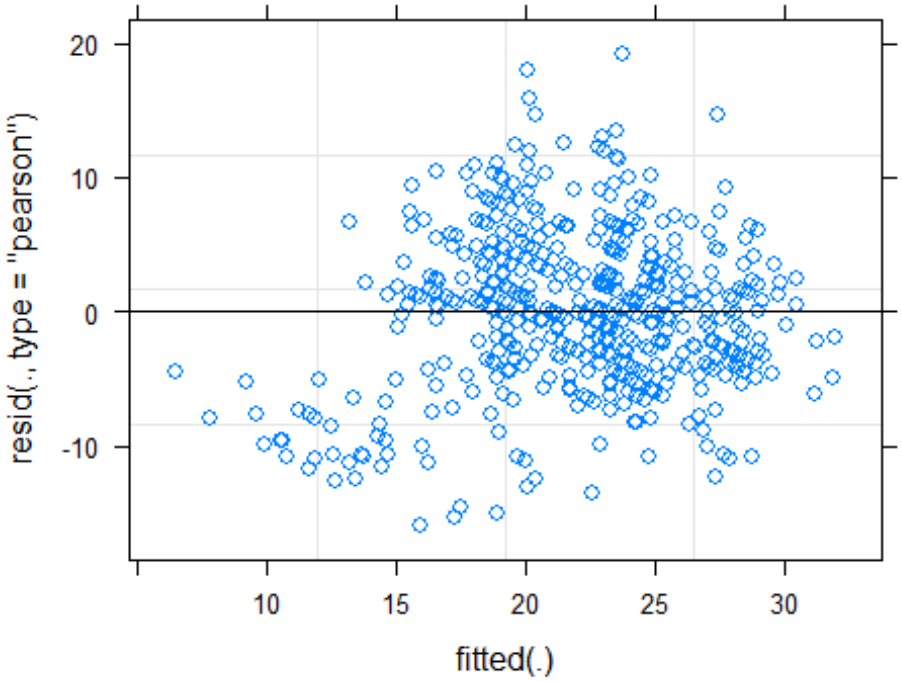

The 2-way interaction time x treatment is not significant, but it may still be important to *report this result* if it evidences a hypothesis that was formed *a-priori* (i.e "there were no significant differences between treatment groups over time"). Similarly, there is no differences between treatment groups with respect to movement direction (movdir x treatment interaction).

Tukey contrasts and 95% CIs:

```
## $lsmeans
## movdir = Clockwise:
##  treatment  lsmean       SE    df lower.CL upper.CL
##  PBS       17.4625 1.301929 36.63 14.82363 20.10137
##  TDP-NLS   18.7750 1.301929 36.63 16.13613 21.41387
##  TDP-WT    20.8375 1.301929 36.63 18.19863 23.47637
##
## movdir = Anti-clockwise:
##  treatment  lsmean       SE    df lower.CL upper.CL
##  PBS       24.6375 1.301929 36.63 21.99863 27.27637
##  TDP-NLS   24.7250 1.301929 36.63 22.08613 27.36387
##  TDP-WT    25.0875 1.301929 36.63 22.44863 27.72637
##
## Degrees-of-freedom method: satterthwaite
## Confidence level used: 0.95
##
## $contrasts
## movdir = Clockwise:
##  contrast         estimate       SE    df t.ratio p.value
##  PBS - TDP-NLS     -1.3125 1.841205 36.63  -0.713  0.7575
##  PBS - TDP-WT      -3.3750 1.841205 36.63  -1.833  0.1731
##  TDP-NLS - TDP-WT  -2.0625 1.841205 36.63  -1.120  0.5080
##
## movdir = Anti-clockwise:
##  contrast         estimate       SE    df t.ratio p.value
##  PBS - TDP-NLS     -0.0875 1.841205 36.63  -0.048  0.9988
##  PBS - TDP-WT      -0.4500 1.841205 36.63  -0.244  0.9676
##  TDP-NLS - TDP-WT  -0.3625 1.841205 36.63  -0.197  0.9789
##
## P value adjustment: tukey method for comparing a family of 3 estimates
```

Difference in number of head turns with 95% CI

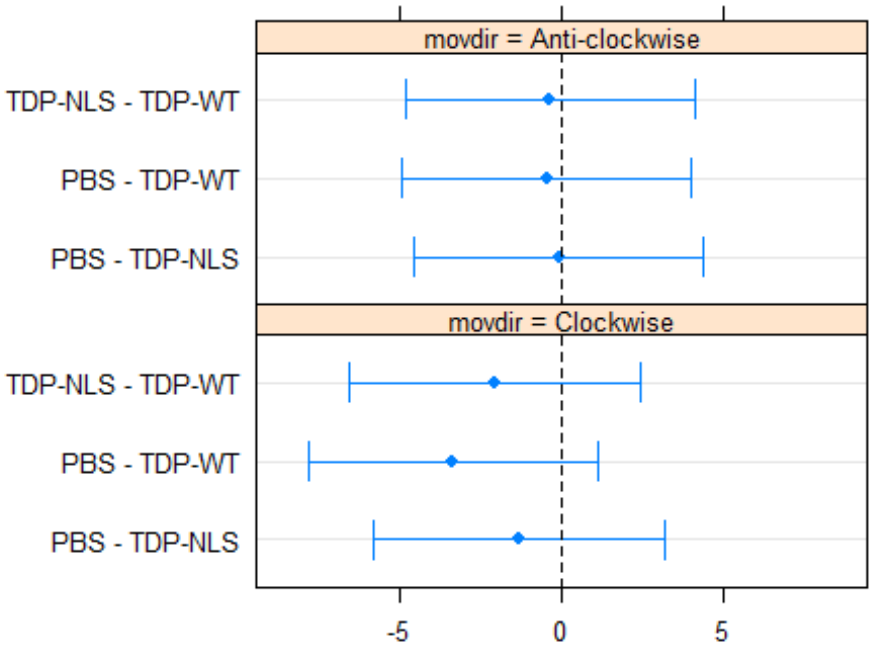

Reducing `time` to two levels, pre-test and the first observation post-treatment (14 days post treatment)

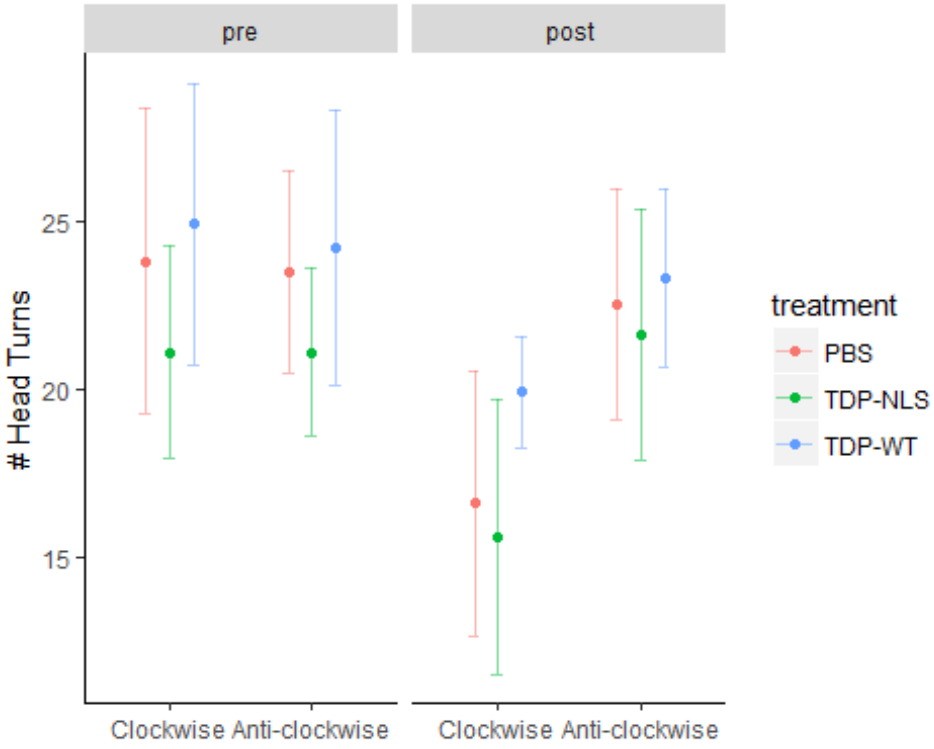


```
## Analysis of Variance Table of type III  with  Kenward-Roger
## approximation for degrees of freedom
##                  Sum Sq Mean Sq NumDF  DenDF F.value   Pr(>F)
## time_f          298.629 298.629     1 27.304 11.0600 0.002525 **
## movdir          170.408 170.408     1 56.000  6.3112 0.014906 *
```

```
## treatment        125.256  62.628     2 27.113  2.3195 0.117522
## time_f:movdir    221.408 221.408     1 56.000  8.2001 0.005885 **
## time_f:treatment  13.376   6.688     2 27.304  0.2477 0.782336
## movdir:treatment  16.217   8.108     2 56.000  0.3003 0.741781
## ---
## Signif. codes:  0 '***' 0.001 '**' 0.01 '*' 0.05 '.' 0.1 ' ' 1

## $lsmeans
## movdir = Clockwise:
##  treatment lsmean       SE    df lower.CL upper.CL
##  PBS        20.20 1.341172 62.15 17.51916 22.88084
##  TDP-NLS    18.35 1.341172 62.15 15.66916 21.03084
##  TDP-WT     22.40 1.341172 62.15 19.71916 25.08084
##
## movdir = Anti-clockwise:
##  treatment lsmean       SE    df lower.CL upper.CL
##  PBS        23.00 1.341172 62.15 20.31916 25.68084
##  TDP-NLS    21.35 1.341172 62.15 18.66916 24.03084
##  TDP-WT     23.75 1.341172 62.15 21.06916 26.43084
##
## Results are averaged over the levels of: time_f
## Degrees-of-freedom method: satterthwaite
## Confidence level used: 0.95
##
## $contrasts
## movdir = Clockwise:
##  contrast         estimate       SE    df t.ratio p.value
##  PBS - TDP-NLS        1.85 1.896704 62.15   0.975  0.5951
##  PBS - TDP-WT        -2.20 1.896704 62.15  -1.160  0.4814
##  TDP-NLS - TDP-WT    -4.05 1.896704 62.15  -2.135  0.0910
##
## movdir = Anti-clockwise:
##  contrast         estimate       SE    df t.ratio p.value
##  PBS - TDP-NLS        1.65 1.896704 62.15   0.870  0.6611
##  PBS - TDP-WT        -0.75 1.896704 62.15  -0.395  0.9175
##  TDP-NLS - TDP-WT    -2.40 1.896704 62.15  -1.265  0.4200
##
## Results are averaged over the levels of: time_f
## P value adjustment: tukey method for comparing a family of 3 estimates
```

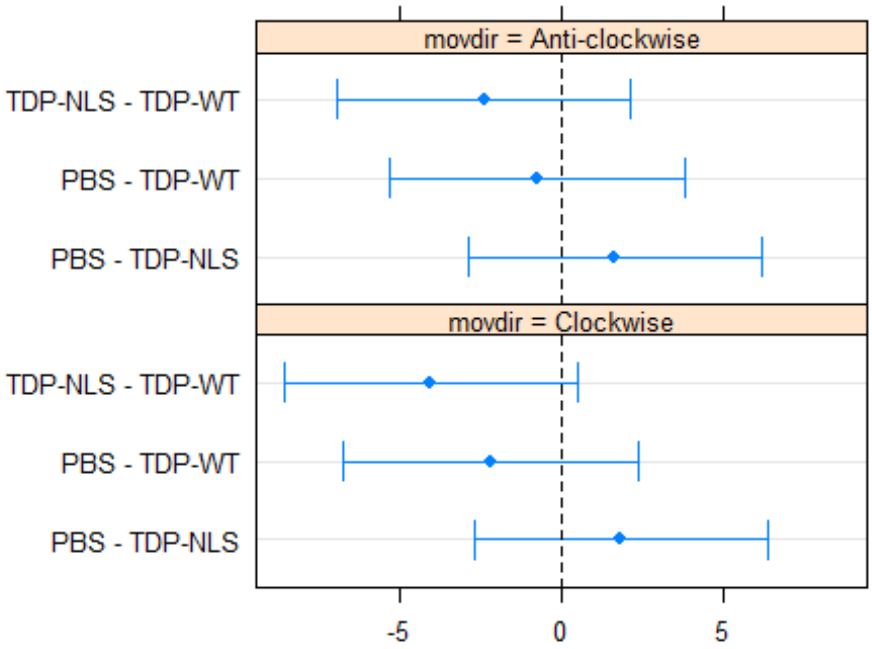

Reducing `time` to two levels, pre-test and post-treatment (all observations post-treatment)

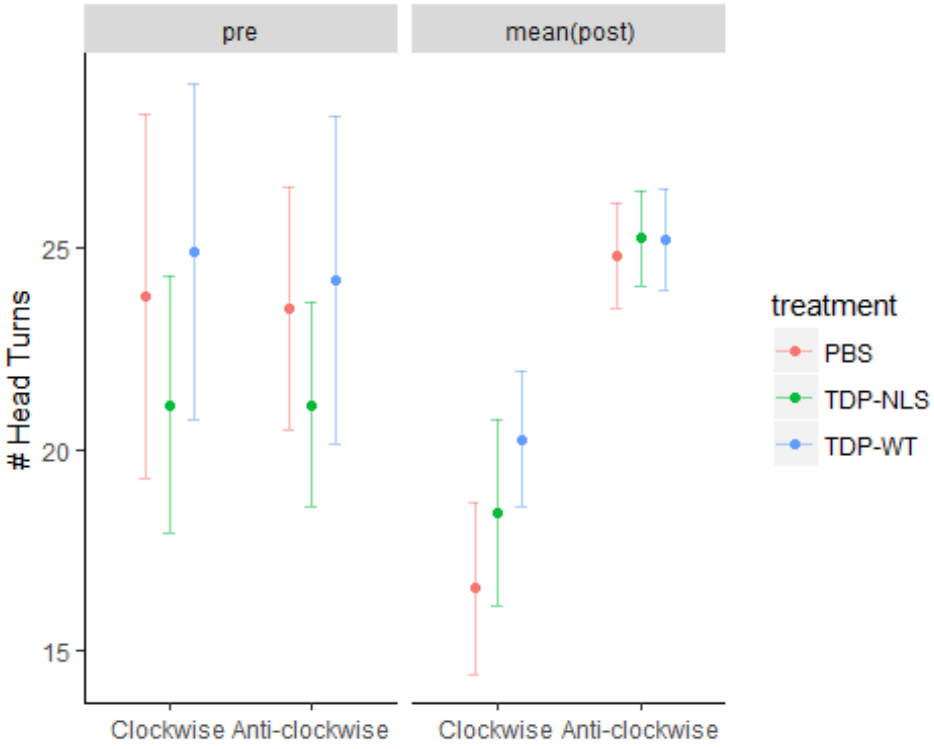


```
## Analysis of Variance Table of type III  with  Kenward-Roger
## approximation for degrees of freedom
##                     Sum Sq Mean Sq NumDF  DenDF F.value    Pr(>F)
## t2                   79.64   79.64     1  34.77  2.0526    0.1609
## movdir                1.67    1.67     1 414.00  0.0430    0.8359
```

```
## treatment           112.27   56.13     2  32.84  1.4467    0.2500
## t2:movdir           643.13  643.13     1 414.00 16.5745 5.605e-05 ***
## t2:treatment        105.61   52.81     2  34.77  1.3609    0.2698
## movdir:treatment      1.23    0.62     2 414.00  0.0159    0.9842
## t2:movdir:treatment  18.48    9.24     2 414.00  0.2381    0.7882
## ---
## Signif. codes:  0 '***' 0.001 '**' 0.01 '*' 0.05 '.' 0.1 ' ' 1

## Analysis of Variance Table of type III  with  Kenward-Roger
## approximation for degrees of freedom
##                   Sum Sq Mean Sq NumDF  DenDF F.value    Pr(>F)
## t2                 78.88   78.88     1  37.15  2.0373    0.1618
## movdir              1.67    1.67     1 416.00  0.0430    0.8357
## treatment          62.20   31.10     2  35.33  0.8033    0.4559
## t2:movdir         643.13  643.13     1 416.00 16.6107 5.498e-05 ***
## movdir:treatment 172.62   86.31     2 416.00  2.2292    0.1089
## ---
## Signif. codes:  0 '***' 0.001 '**' 0.01 '*' 0.05 '.' 0.1 ' ' 1

## $lsmeans
## movdir = Clockwise:
##  treatment   lsmean       SE   df lower.CL upper.CL
##  PBS       17.91814 1.250189 41.2 15.39370 20.44257
##  TDP-NLS   18.18842 1.250189 41.2 15.66398 20.71285
##  TDP-WT    20.96845 1.250189 41.2 18.44401 23.49288
##
## movdir = Anti-clockwise:
##  treatment   lsmean       SE   df lower.CL upper.CL
##  PBS       25.09314 1.250189 41.2 22.56870 27.61757
##  TDP-NLS   24.13842 1.250189 41.2 21.61398 26.66285
##  TDP-WT    25.21845 1.250189 41.2 22.69401 27.74288
##
## Degrees-of-freedom method: satterthwaite
## Confidence level used: 0.95
##
## $contrasts
## movdir = Clockwise:
##  contrast           estimate       SE    df t.ratio p.value
##  PBS - TDP-NLS    -0.2702804 1.727882 40.27  -0.156  0.9866
##  PBS - TDP-WT     -3.0503085 1.727882 40.27  -1.765  0.1942
##  TDP-NLS - TDP-WT -2.7800281 1.727882 40.27  -1.609  0.2536
##
## movdir = Anti-clockwise:
##  contrast           estimate       SE    df t.ratio p.value
##  PBS - TDP-NLS     0.9547196 1.727882 40.27   0.553  0.8458
##  PBS - TDP-WT     -0.1253085 1.727882 40.27  -0.073  0.9971
##  TDP-NLS - TDP-WT -1.0800281 1.727882 40.27  -0.625  0.8073
##
## P value adjustment: tukey method for comparing a family of 3 estimates
```

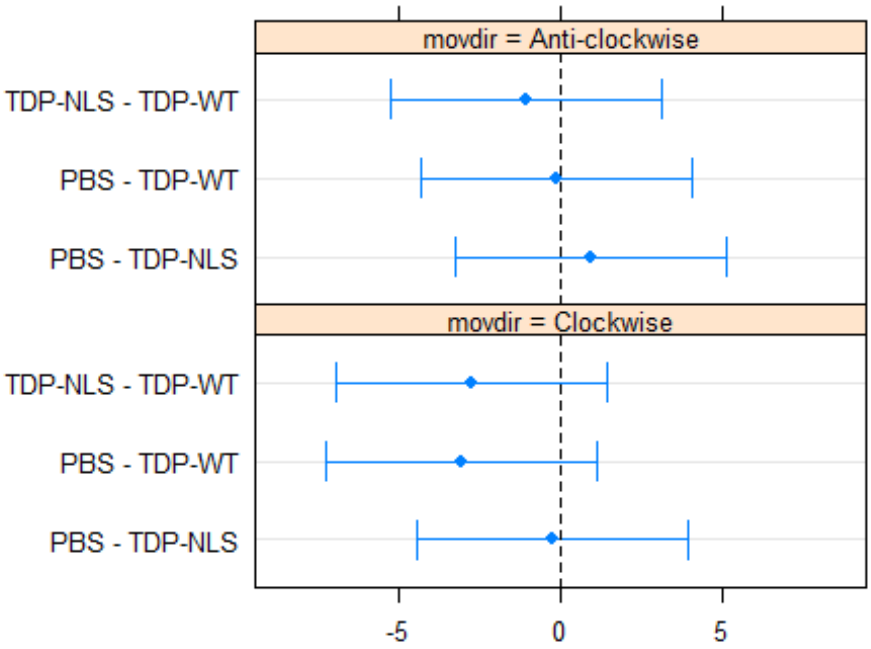

8.4 Chapter 5 PDF version of C9ORF72 Expression and Localisation over mouse development

Atkinson et al. Acta Neuropathologica Communications (2015) 3:59
DOI 10.1186/s40478-015-0238-7

ACTA NEUROPATHOLOGICA COMMUNICATIONS

RESEARCH Open Access

C9ORF72 expression and cellular localization over mouse development

Rachel A K Atkinson[1], Carmen M. Fernandez-Martos[1], Julie D. Atkin[2], James C. Vickers[1] and Anna E. King[1*]

Abstract

Introduction: A majority of familial frontotemporal lobar dementia and amyotrophic lateral sclerosis cases are associated with a large repeat expansion in a non-coding region of the *C9ORF72* gene. Currently, little is known about the normal function and the expression pattern of the C9ORF72 protein. The aims of this study were to characterize the expression pattern and cellular localization of the three reported mouse isoforms of *C9orf72*, over a developmental time-course in primary cultured cortical neurons and brain tissue from C57BL/6 mice.

Results: We demonstrated that the different isoforms of C9ORF72 at the mRNA and protein level undergo alterations in expression during development and into adulthood. Cellular fractionation and immunofluorescence demonstrated that levels of nuclear and cytoplasmic expression of isoforms changed significantly over the time course. Additionally, immunofluorescence studies showed C9ORF72 labeling as puncta throughout neurons, extending beyond the microtubule cytoskeleton into actin-rich structures such as filopodia and growth cones. Finally, synaptosome preparations demonstrated the presence of C9ORF72 isoform 1 in synaptic-rich fractions from adult mouse brain.

Conclusion: In summary, the presence of C9ORF72 as puncta and within synaptic-rich fractions may indicate involvement at the synapse and differential expression of isoforms in nuclei and cytoplasm may suggest distinct roles for the isoforms. Determining the physiological role of C9ORF72 protein may help to determine the role it plays in disease.

Keywords: C9ORF72, FTLD, ALS

Introduction

Frontotemporal lobar dementia (FTLD) and amyotrophic lateral sclerosis (ALS) are progressive neurodegenerative disorders, which due to their overlapping features, are now thought to represent two ends of a disease spectrum [17]. In 2011, two independent groups identified the largest genetic cause of FTLD and ALS as a repeat expansion of the hexanucleotide sequence GGGGCC in the *C9ORF72* gene [4, 25]. This expansion occurs in a non-coding region of chromosome 9. It is currently unknown how the repeat expansion contributes to FTLD and ALS, although several mechanisms have been proposed, including potential unconventional translation of the repeated sequence (repeat-associated non-ATG initiated translation) leading to intracellular accumulations of dipeptide repeat proteins [1, 23], and the sequestration of RNA binding proteins into RNA foci, causing RNA dysfunction [4, 27]. Alternatively, the hexanucleotide expansion may result in haploinsufficiency due to reduced expression of C9ORF72 transcripts [2, 4, 5, 33, 34, 37].

While pathological features of *C9ORF72*-associated disease, such as TDP-43 aggregates, dipeptide repeat protein expression and RNA foci, are under intense investigation regarding their role in disease, to date, less attention has been paid to the normal expression and function of the encoded protein, C9ORF72. Elucidating the expression, localization and function of this protein in neural cells may contribute further to knowledge regarding how the repeat expansion is associated with neurodegenerative changes.

In humans, alternative splicing of three RNA transcript variants from the *C9ORF72* gene produces two different isoforms of the C9ORF72 protein (Fig. 1a) [25]. Transcript variants 1 and 3 encode a 481 amino acid protein and variant 2 encodes a 222 amino acid protein [4]. In mice, there are 3 protein-coding regions reported of 481 (isoform 1), 420 (isoform 2) and 317 (isoform 3) amino acids, likely encoding at least 3 different protein

* Correspondence: A.E.King@utas.edu.au
[1]Wicking Dementia Research and Education Centre, Faculty of Health, University of Tasmania, Hobart, Tasmania, Australia
Full list of author information is available at the end of the article

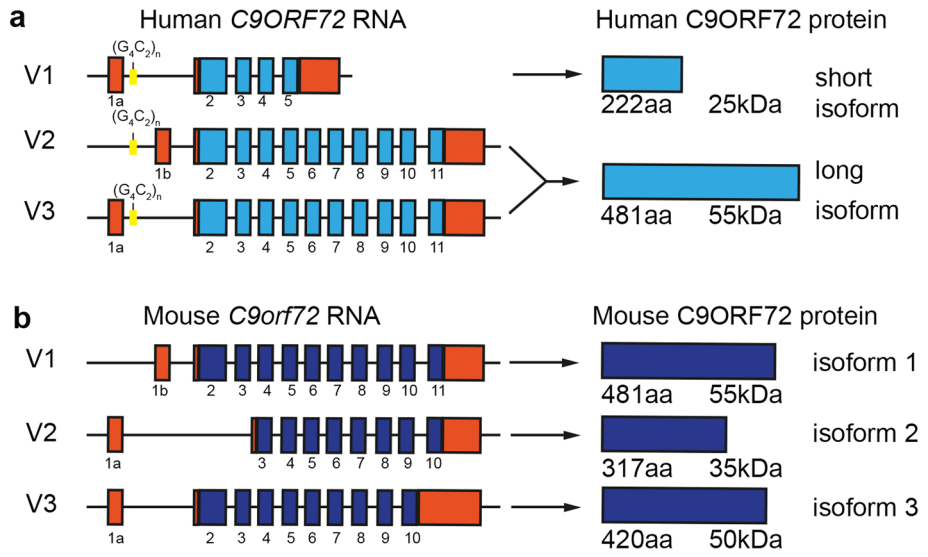

Fig. 1 Schematic overview of human and mouse *C9ORF72* transcripts and encoded proteins. Protein coding regions for transcript variants (V1 to 3) are indicated in *light blue* for human (**a**) and *dark blue* for mouse (**b**) as well as size of encoded proteins. Non-coding regions are indicated in *red* and location of the G_4C_2 repeat expansion in *yellow*.

isoforms (Fig. 1b). However, the roles of the encoded proteins have not been well characterized. We have previously demonstrated a role for C9ORF72 in trafficking [7] which was in line with previous studies [16]. C9ORF72 is involved in endosomal trafficking via Rab-dependent pathways. Rab proteins are part of the Rab-GDP/GTP exchange factor family (Rab-GEF) (as reviewed in [29]) that mediate all membrane trafficking events between organelles. We provided the first experimental evidence for this, when we established that C9ORF72 regulates endocytosis and autophagy [7].

Other studies have examined the expression of the *C9orf72* gene using a transgenic mouse model harboring a targeted LacZ insertion [32]. This study observed *C9orf72* in neuronal and non-neuronal cells within the central nervous system (CNS). Recently, the effect of ablating the 3 isoforms of C9ORF72 protein from neurons and glia has been examined, demonstrating a reduction in body weight but no motor neuron degeneration or motor deficits [15]. This suggests that complete lack of C9ORF72 throughout development and adulthood is not sufficient to cause a motor neuron disease phenotype in mice.

Several studies have examined the expression of C9ORF72 in human tissue [3, 4, 11, 13, 28, 30] and cell lines [11, 25] using a variety of commercial antibodies. However, there has been a lack of consensus about the localization of C9ORF72 across these studies. Some investigations have described coarse punctate expression within the hippocampus, suggestive of synaptic terminals [3, 13, 26, 28]. Recently, Xiao and colleagues [37] generated antibodies specific to the two human C9ORF72 isoforms. They demonstrated diffuse cytoplasmic and 'speckled' localization of the long isoform, as well as localization of the short isoform to the nuclear membrane. This is in line with our previous investigation which demonstrated a nuclear and punctate pattern of expression (typical of vesicles) of C9ORF72 *in vitro* in both SH-SY5Y cells and in primary cultured cortical neurons [7].

The current study examined the expression of C9ORF72 in the mouse CNS over development *in vivo* and *in vitro* in order to provide information about its expression and cellular localization during neurite outgrowth, neuron maturation and synapse formation. This investigation demonstrated that expression of C9ORF72 mRNA and protein differ over a developmental time course, are expressed in both nuclear and cytoplasmic fractions in an isoform specific manner, and that the large isoform may be present in synaptic fractions.

Materials and methods

Animals

C57BL/6 mice were utilized in this study. All experiments involving animals were approved by the University of Tasmania Animal Ethics Committee (A12780) and were in accordance with the Australian Guidelines for the Care and Use of Animals for Scientific Purposes.

Tissue preparation

For molecular biology analysis, combined neocortical and hippocampal tissue was harvested from mice at embryonic day (E) 18, postnatal day (P) 1, P7, P14, P28 and P56 (for western blot) ($n = 4$ mice per time-point) and P1, P7 and P56 (for real time qPCR) ($n = 4$ mice per time-point). Tissue was processed as previously described [18].

For immunohistochemical analysis, animals were terminally anaesthetized with sodium pentobarbitone (140 mg/kg) and transcardially perfused with 4 % paraformaldehyde. Brains were immediately dissected, post-fixed overnight in paraformaldehyde and then cryoprotected as previously described [19]. Serial 40 μm coronal sections were cut on a cryostat (Leica CM 1850). For each mouse at each time point, four regularly spaced sections were examined from the rostral to caudal cortex corresponding to bregma 0.98 mm to −1.82 mm (in adult tissue) according to the stereotaxic mice atlas [10]. Antigen retrieval was carried out prior to immunohistochemistry using citric acid, pH 6.0, in a pressure cooker for 14 min.

Protein extraction and western blot analysis

Protein from combined cerebral cortex and hippocampus was extracted with RIPA Buffer (Sigma Aldrich) containing a cocktail of protease inhibitors (Roche). Protein extract was then placed at 4 °C for 30 min, centrifuged at 13,000 rpm for 20 min and supernatant stored at −80 °C.

Denatured proteins samples (15 μg) from each time-point were electrophoresed into 10 % SDS-PAGE gels (BioRad), transferred to PVDF membranes (BioRad) and incubated in primary antibodies overnight (Table 1). A corresponding anti-rabbit or anti-mouse horseradish peroxidase (HRP)-conjugated secondary antibody (1:7000; Amersham) was used, as described previously [18]. GAPDH (1:7000, Millipore) was used as a loading control and band intensity was measured as the integrated intensity using ImageJ software (v1.4; NIH), and normalized with respect to the loading controls. Three experimental repeats were carried out.

Nuclear and cytoplasmic fractionation

Nuclear and cytoplasmic protein extractions were prepared from right hemispheres (excluding olfactory bulbs and cerebellum) of fresh P1, P7, P56 brains using the NE-PER kit (Thermo Fisher Scientific) according to manufacturer instructions. Denatured protein samples were electrophoresed as described above. Fraction purity was confirmed by labeling with HDAC2 (1:700; Abcam) for nuclear fractions and GAPDH (as above) for cytoplasmic fractions. Membranes were also incubated with C9ORF72 antibody (as above). Densitometry analysis of bands was carried out using ImageJ. Results were normalized to total protein. Three experimental repeats were carried out.

Synaptosome preparation

Synaptosomes were prepared as described previously [6, 22] with some modifications. Briefly, P56 mice ($n = 4$) were anaesthetized and perfused with sucrose buffer (0.32 M sucrose, 1 mM ethylenediaminetetraacetic acid, 5 mM dithiothreitol, pH 7.4). Whole brains were harvested and homogenized at 4 °C with a teflon-glass homogenizer using 12 strokes with 9:1 ratio of sucrose buffer supplemented with a protease cocktail inhibitor (Roche) to 1 g of tissue. Homogenate was centrifuged at 1000xg for 10 min at 4 °C. The resulting pellet containing mostly nuclei was removed and the supernatant was layered onto a discontinuous gradient consisting of 3, 10, 15 and 23 % (vol/vol) Percoll (GE Healthcare). Tubes were then centrifuged at 31,000xg for 8 min at 4 °C in a Sorvall WX Ultra90 (70.I TI rotor).

The contents of the resulting fractions have been characterized previously [6, 31]. The resulting purified fractions were collected and protein was extracted in RIPA buffer for western blotting. Denatured protein samples (15 μg) were electrophoresed as described above. Membranes were probed with C9ORF72 antibody, along with synaptic markers: synaptophysin (1:5000, Millipore), PSD-95 (1:1000, Abcam), GAD67 (1:2500, Millipore); and GFAP (1:1000, NeuroMAB) as a marker of glia.

RNA isolation and RT-PCR analysis

Total RNA from combined cerebral cortex and hippocampus tissue at the time-points P1, P7 and P56 ($n = 4$ mice per time point) was isolated using the RNeasy Mini Kit (Qiagen), according to the manufacturer's instructions and complementary DNA (cDNA) was synthesized from DNase-treated RNA (1 μg) as described previously [8].

To semi-quantitatively analyse *C9orf72* gene expression, quantitative PCR (qPCR) analysis was conducted as previously described [9]. Before relative quantification, *C9orf72* gene was subjected to a serial dilution assay to determine the optimum detection range of Ct values, with a Ct threshold of 35 for undetectable mRNA levels of expression. Relative quantitation of *C9orf72* mRNA isoforms per time point was performed using 25 ng of reverse-transcribed total RNA, 20 pmol/ml of both sense and antisense primers and the SYBR Green PCR master mix (Applied Biosystems) in a final reaction volume of 10 μl. The reactions were run on an LightCycler® 480 System (Roche) according to the manufacturer's instructions.

Table 1 List of qPCR primers

Gene name	Forward primer	Reverse primer	Accession number
C9orf72 isoform 1	5′- CCCACCATCTCCTGCTGTTG-3′	5′-GTAAGCAAAGGTAGCCGCCA-3′	NM_001081343.1
C9orf72 isoform 2	5′- TGGAAGATCAGGGTCAGAGT-3′	5′- GCAAGCAGCTCCATTACAGG-3′	XM_006538294.1
C9orf72 isoform 3	5′-CTTTCCTTGCACAGTTCCTCC-3′	5′- TCATCCTCGATGTACTTGATTAGTG-3′	XM_006538292.2

Primers used for qPCR analysis of the 3 *C9orf72* isoforms including primer sequence (forward and reverse sequence respectively) and GenBank accession number

To standardize the amount of sample cDNA added to the reaction, amplification of endogenous control β-Actin (primer sequence obtained from Gonzalez-Fernandez and colleagues [12]) were included in a separate well as a real-time reporter. Primer efficiency was calculated (Additional file 1: Figure S1a), and at the end of each run, melting curve profiles were performed to confirm amplification of specific transcripts (Additional file 1: Figure S1b). Relative quantification for each gene was performed by the ΔΔCt method [20].

All primers were designed using NCBI/Primer-BLAST software (Table 1). Primers were designed to amplify the different isoforms of the *C9orf72* mouse ortholog (*3111004O21Rik*). As *C9orf72* isoforms 2 and 3 are contained within isoform 1, fold change in the mRNA expression of isoform 2 and 3 were calculated as the increment with respect to the expression levels of isoform 1.

Cell culture

Primary dissociated cortical cultures were prepared as previously described [14] using standard culture techniques with slight modifications. Briefly, neocortical tissue was harvested from E15.5 C57BL/6 mice and enzymatically dissociated in 0.0125 % trypsin for 4 min, prior to plating. Cells were plated onto poly L-lysine (Sigma Aldrich) coated 12 mm coverslips in 24 well plates at a density of 30,000 viable cells per coverslip. Cells were grown in an initial plating media consisting of Neurobasal™ medium (Gibco), 2 % B27 supplement, 10 % fetal calf serum (Gibco), 0.5 mM glutamine, 25 mM glutamate and 1 % antibiotic/antimycotic (Gibco). Medium was replaced on the following day with subsequent growth media consisting of initial media without the fetal calf serum and glutamate, and half the media was replenished weekly with fresh subsequent growth medium. Cultures were grown at 37 °C and 5 % CO_2. Neurons were fixed with 4 % paraformaldehyde (Sigma Aldrich) at 1, 3, 7, 14 and 21 days *in vitro* (DIV) ($n > 5$ cultures per time-point).

Immunofluorescence

Cultured cells and brain sections were washed 3x10 minutes in 0.01 M PBS followed by serum-free protein block (Dako) for 15 min at room temperature (RT). Immunofluorescence labeling was carried out for both cultured cells and brain tissue following standard procedures using antibodies against C9ORF72 (as above), β-III Tubulin (1:5000, Promega) and MAP2 (1:1000, Millipore) diluted in PBS with 0.6 % Triton-X-100 and incubated at RT overnight. Samples were incubated in secondary antibodies (AlexaFluor, Invitrogen Probes) for 2 h at RT, followed by incubation with the nuclear stain DAPI (5 μg/ml; Molecular Probes®, Life Technologies), for 5 min at RT. Immunoreactivity was visualized and captured using a Leica (Germany) DM BL2 upright fluorescence microscope. For the purpose of illustration, images were then adjusted for brightness and contrast using Adobe Photoshop CS6 (v 13).

Specificity of immunoreactivity was confirmed by two methods. Both brain sections and cultured cells were examined for non-specific labeling after processing without primary antibody. Additionally, tissue from P56 brain and seven DIV cultures were incubated with C9ORF72 antibody combined with seven times excess of C9ORF72 peptide (sc-138763 P; Santa Cruz).

Statistical analyses

All statistical analysis was performed using GraphPad Prism software (version 6.0) and p-values with $p < 0.05$ (CI 95 %) considered significant. Values were reported as the mean ± standard error (SEM). Data from real time PCR studies were compared using a one-way ANOVA followed by a Tukey post-hoc and t-tests for a point-to-point comparison. Data from western blots were compared using a two-way ANOVA followed by Tukey or Sidak post-hoc comparisons.

Results

Cellular pattern of C9ORF72 protein changes over development of mouse cortex

This study utilized the commercially available anti-human C9ORF72 antibody raised against amino acid residues 165 to 215 of C9ORF72 protein, which is contained within the sequence of all three mouse C9ORF72 isoforms. We have previously shown a decrease in labeling in a western blot with the antibody following treatment with C9ORF72 short interfering RNA (siRNA) [7]. To further characterize the specificity of immunolabeling, the C9ORF72 antibody was preadsorbed with recombinant peptide. Immunolabeling of tissue sections from P56 mice (Additional file 2: Figure S2a) and cultured cortical neurons at 7 DIV (Additional file 2: Figure S2b) with preadsorbed C9ORF72 demonstrated that, relative to non-adsorbed antibody, there was a large reduction in immunolabeling (Additional file 2: Figure S2).

We next determined the expression or localization of C9ORF72 over a developmental time course from E18 to P56 in mice, which covers periods of neurite outgrowth and synapse development [24, 36]. To determine how C9ORF72 localization changes over development, 40 μm coronal tissue sections from mice at ages E18, P1, P14, P28 and P56 were immunolabeled with C9ORF72 antibody along with the neuronal somatodendritic marker, MAP2. At both E18 (data not shown) and P1, there was strong labeling for C9ORF72 in discrete puncta throughout the neuropil (Fig. 2a) but little somal immunoreactivity was present. At P7, there was distinct

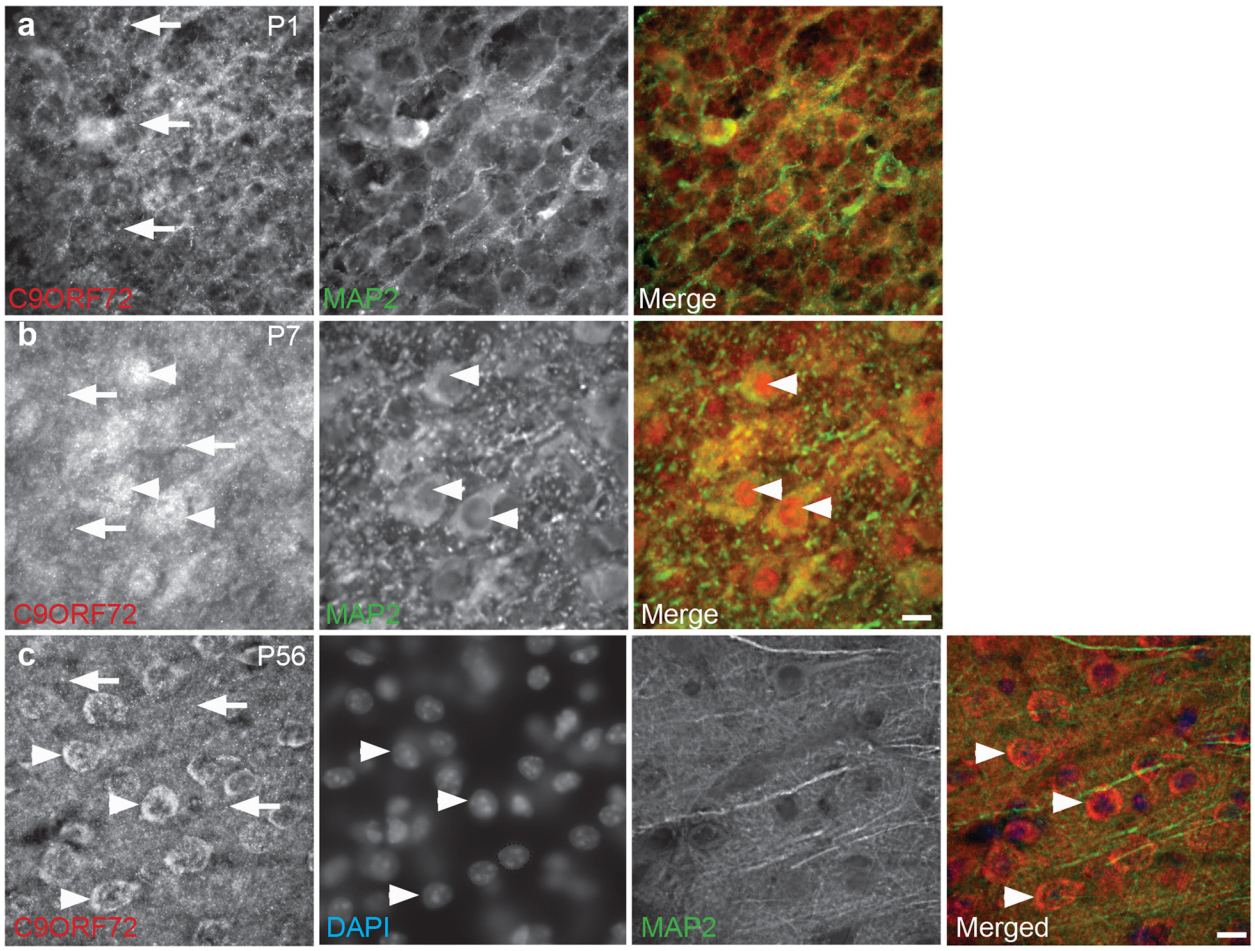

Fig. 2 Localization of C9ORF72 during development *in vivo*. **a** At P1, C9ORF72 (red) had punctate localization throughout the neuropil (*arrows*). **b** At P7, C9ORF72 labeling was present within nuclei (*arrowheads)* of neuronal cells (MAP2, green) and as strong puncta within cytoplasm and neuropil (*arrows*). **c** At P56, C9ORF72 labeling was present in the neuropil as puncta (*arrows*) and was localized to the cytoplasm surrounding nuclei (DAPI, arrowheads) Scale bar: 10 μm

somal and nuclear expression, which was both diffuse and punctate in many MAP2-immunoreactive cells throughout the cortex and hippocampus (Fig. 2b), confirming the presence of C9ORF72 in neurons. At P14, P28 and P56, cytoplasmic labeling continued with apparent lower expression in nuclei (Fig. 2c). Punctate labeling was less distinct than at P1 and P7 (Fig. 2a and b).

Temporal expression of C9ORF72 isoforms over development

We evaluated the temporal mRNA expression pattern of *C9orf72* isoforms (*C9orf72- 1, 2* and *3*; Fig. 1). As shown in Fig. 3a, the mRNA encoding for all *C9orf72* isoforms were detected in combined cerebral cortex and hippocampus tissue at all time-points P1, P7 and P56. Isoform 1 was significantly ($p < 0.05$) higher at P1 compared to P7 and P56 (Fig. 3a) and, similarly, the expression of isoform 2 was significantly ($p < 0.05$) higher at P56 relative to the other time points tested (Fig. 3a). There were no changes in the mRNA expression levels of isoform 3 over development (Fig. 3a). Next, by western blot analysis, we evaluated the temporal protein expression of C9ORF72 protein-coding regions (481, 420 and 317 amino acids), which correspond to predicted protein size isoforms of approximately 55, 50 and 35 kDa. Western blots of combined cerebral cortex and hippocampus tissue demonstrated that the Santa Cruz C9ORF72 antibody labeled the three predicted protein isoforms at 55, 50 and 35 kDa at all the time points (Fig. 3b). Moreover, we also detected additional bands at 110 kDa. The identity of this band remains unknown.

Subcellular localization of C9ORF72 over development

To further investigate the differential nuclear and cytoplasmic localization of C9ORF72 over development *in vivo*, nuclear and cytoplasmic protein extractions were performed at E18, P1, P7 and P56. Purity of the nuclear

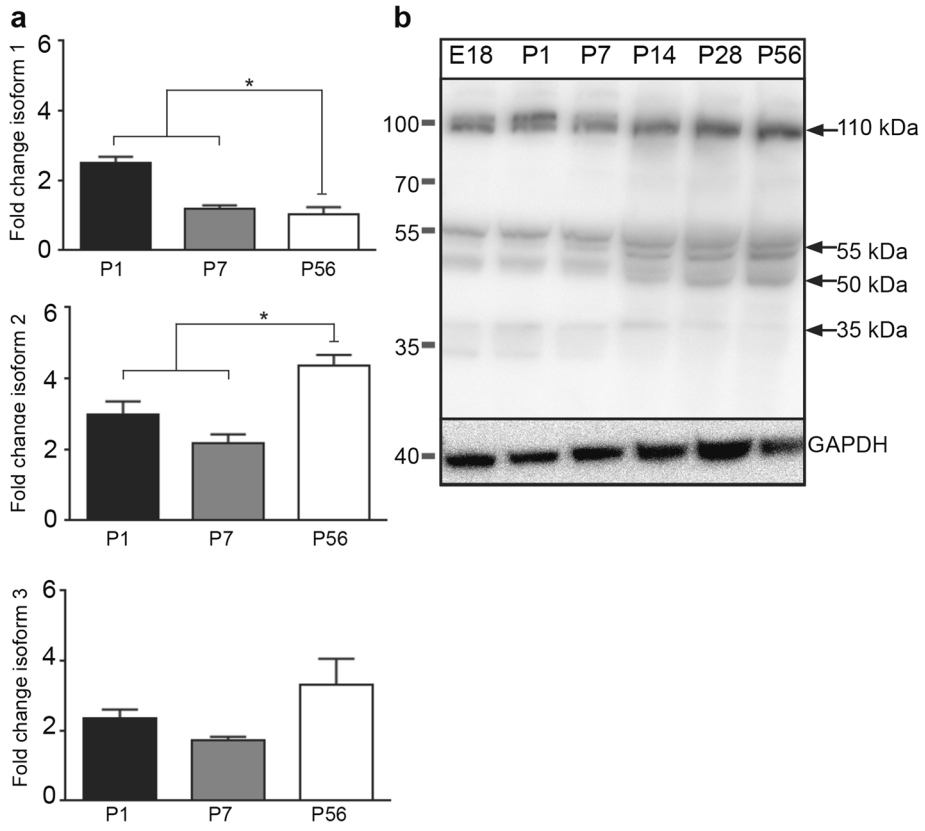

Fig. 3 Expression of C9ORF72 isoforms over development. **a** Relative expression of *C9orf72* isoforms 1, 2 and 3 mRNA in combined cerebral cortex and hippocampus of C57Bl/6 mice. Isoform 1 was significantly ($p < 0.05$) higher at P1 compared to P7 and P56 and isoform 2 was significantly ($p < 0.05$) higher at P56 compared to P1 and P7. **b** Western blot of C9ORF72 expression in mouse tissue over development. Bands corresponding to reported isoforms of C9ORF72 were present at 55, 50 and 35 kDa (b). Additional bands at 110 and 50 kDa were also present. GAPDH was used as a loading control. Values represent mean ± standard error. *$p < 0.05$ P1 and P7 vs. P56

and cytoplasmic extractions was confirmed with HDAC 2 and GAPDH antibodies with HDAC2 being higher in the nuclear samples and GAPDH being higher in the cytoplasmic samples (Fig. 4a). As in non-fractionated samples, western blot analysis of C9ORF72 showed protein bands at approximately 55, 50 and 35 kDa. The 55 kDa protein was significantly ($p < 0.05$) higher in the nuclear fractions compared to cytoplasmic fractions (Fig. 4b). Post hoc tests showed that at E18 and P1 there was significantly ($p < 0.05$) more of the 55 kDa protein in nuclear fractions compared to cytoplasmic fractions. Post hoc tests also showed that within nuclear fractions, there was significantly ($p< 0.05$) more 5 kDa protein at E18 compared to P56. There were no significant differences in cytoplasmic expression of the 55 kDa protein over the time course. There were also no differences in localization of the 50 kDa protein over the time course (Fig. 4b). The 35 kDa protein was significantly higher in the cytoplasmic fractions compared to nuclear fractions ($p < 0.05$) (Fig. 4b). Post hoc tests showed that, at E18 and P1, there was significantly ($p < 0.05$) more of the 55 kDa protein in cytoplasmic fractions compared to nuclear. Post hoc tests also showed that within cytoplasmic fractions there was significantly ($p < 0.05$) more 35 kDa protein at E18, P1 and P7 compared to P56. There were no significant differences in nuclear expression of the 35 kDa protein over the time course. These results suggest that C9ORF72 protein isoforms were differentially expressed in cellular compartments over development.

C9ORF72 is present in synaptosome preparations

Our results showed that C9ORF72 has punctate localization in the neuropil, however, it is unclear if it is present in synapses. To address this, we performed subcellular fractionation on P56 mouse brain tissue to isolate synaptosome fractions according to the methods of Dunkley, Jarvie and Robinson [6]. The content of each resulting fraction have been characterized previously [6, 31]. F1 contains unidentified membranous material [6], F2 contains predominantly re-sealed plasma membranes from glial cells [31]. F3 and F4 contain purified synaptosomes and these fractions were combined [6]. To confirm the purity of the fractions, western blotting

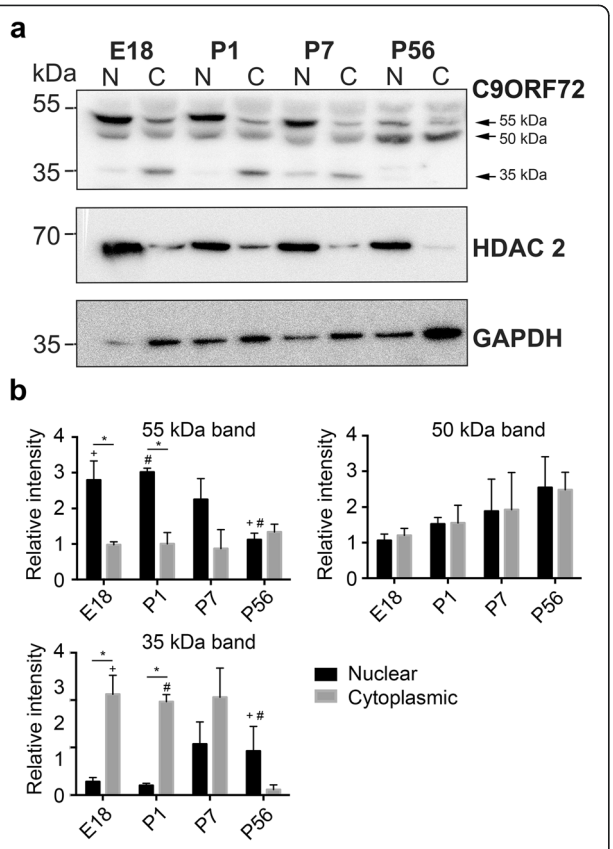

Fig. 4 Expression of C9ORF72 in nuclear and cytoplasmic protein fractions over development. **a** Representative western blot of C9ORF72 in nuclear and cytoplasmic fractions from E18, P1, P7, and P56 mouse brain. HDAC2 and GAPDH were used to demonstrate nuclear and cytoplasmic fractions respectively. C9ORF72 isoforms were present at differing levels and in specific fractions throughout the time course. **b** Relative quantitation of C9ORF72 isoform expression in nuclear and cytoplasmic fractions over the time course. Overall, the 55 kDa protein was significantly ($p < 0.05$) increased within nuclear fractions compared to cytoplasmic fractions and specifically at E18 and P1 compared to P56 ($p < 0.05$). Within nuclear fractions, the 55 kDa protein was significantly ($p < 0.05$) increased at P1 compared to P56. There were no significant differences in nuclear and cytoplasmic expression for the 50 kDa band. Overall, the 35 kDa band was significantly ($p < 0.05$) increased within cytoplasmic fractions compared to nuclear fractions and specifically at E18 compared to P56 ($p< 0.05$). Within cytoplasmic fractions, the 35 kDa protein was significantly increased ($p < 0.05$) at E18, P1 and P7 compared to P56. Values represent mean ± standard error. *$p < 0.05$ nuclear vs. cytoplasmic at E18 and P1. + $p < 0.05$ E18 vs. P56 (nuclear for 55 kDa bad, cytoplasmic for 35 kDa band). # $p < 0.05$ P1 vs. P56 (nuclear for 55 kDa band, cytoplasmic for 35 kDa band)

was carried out with a range of antibodies. GFAP was used as a glia marker and was most abundant in F2 (Fig. 5). As expected, synaptophysin, PSD95 and GAD67 were most abundant within the F3/F4 fraction (Fig. 5). Only the 55 kDa protein band of C9ORF72 was observed within C9ORF72-positive fractions, and was most abundant within F3/F4 fractions where other synaptic proteins were found. It was also present at low levels in F2.

C9ORF72 is expressed in nuclei and neurites of cultured cortical neurons

For a more detailed examination of the localization of C9ORF72 in neuronal soma and neurites, immunocytochemistry was performed in cultured cortical neurons fixed at 1, 3 and 7 DIV (during neurite outgrowth) and 14 and 21 DIV (during synaptogenesis and maturity). Neurons were labeled with C9ORF72 along with neuronal cytoskeletal markers βIII-tubulin and MAP2 and the F-actin stain, phalloidin. At 1 and 3 DIV, C9ORF72 labeling was present in the cell soma, excluding the nucleus, and throughout the neurites as demonstrated by co-labeling with βIII-tubulin (Fig. 6a). C9ORF72 also extended into the actin cytoskeleton, including within growth cones and filopodia extending from the soma and down the length of neurites, as demonstrated by co-labeling with phalloidin (Fig. 6b).

From 7 DIV, immunolabeling for C9ORF72 increased in the soma and a large proportion of cells had high nuclear expression of the protein, accompanied by bright puncta in the soma (data not shown). Similar cellular localization was observed at 14 DIV with bright vesicular labeled puncta more prominent in, but not restricted to, neurons with nuclear expression of C9ORF72 (Fig. 6c). A smaller proportion of neurons had more diffuse immunolabeling which was present in less intensely stained puncta in the cytoplasm and neurites (axons and dendrites, demonstrated by MAP2 co-labeling) in cells with nuclear and non-nuclear labeling. Immunolabeling of C9ORF72 was similar at 21 DIV. These results show that C9ORF72 was present throughout the microtubule cytoskeleton including throughout the axon, soma and dendritic arbor as well as within actin-rich structures such as growth cones and filopodia.

Discussion and conclusions

In this study, we have examined the expression of C9ORF72 by multiple biochemical and molecular biological analyses conducted both *in vivo* and *in vitro*. Results from these investigations demonstrated that C9ORF72 undergoes alterations in cellular expression and localization throughout the time course analyzed, which may reflect differential expression of isoforms that are present in specific locations. Furthermore C9ORF72 is found in synaptic-rich cellular fractions.

In order to gain some insight into the function of C9ORF72 protein, we examined whether the expression level was altered throughout development. Neuronal development involves a number of different processes and therefore alterations in the expression or localization of proteins during development may indicate a role in these processes. Our results suggest that there are alterations in the cellular localization of C9ORF72 protein as well as in the expression pattern of the isoforms over

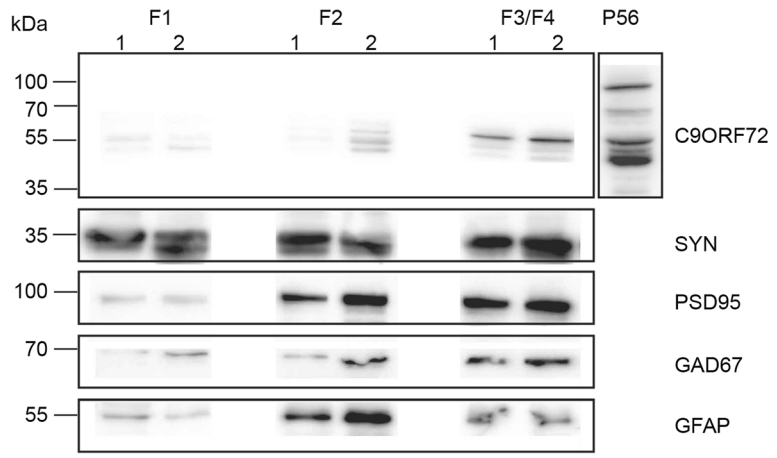

Fig. 5 Expression of C9ORF72 in synaptosome preparations from mouse brains. Figure shows representative western blots with results from 2 animals for each marker (indicated by 1 and 2 on figure). The 55 kDa isoform of C9ORF72 was present in the combined F3/F4 fractions which contain synaptosomes. C9ORF72 expression was low in fraction F1, containing membranes, and F2 containing myelin, membranes and glia. Unfractionated brain at P56 was also included. Purity of fractions was determined by labeling with GFAP (F2) and synaptic markers, synaptophysin, PSD-95 and GAD67 (F3/F4)

time. C9ORF72 was detected prenatally, consistent with previous studies looking at the protein in mouse tissue [15]. C9ORF72 was also observed in adult as well as in embryonic and larval stages in zebrafish [2, 15]. A transcription expression study of the mouse ortholog of *C9orf72* found that it was only detectable from P1 in the CNS where it increased gradually until P60 [32]. Koppers [15] suggested these differences could be explained by a failure of the heterozygous LacZ reporter mice used in this study to detect the low levels of gene expression present prenatally.

C9ORF72 isoforms were differentially expressed between the nucleus and cytoplasm. Western blot analysis of nuclear and cytoplasmic protein fractions showed that the 55 kDa band was predominantly nuclear, the 35 kDa band was predominantly cytoplasmic and the 50 kDa band was expressed similarly in both fractions. The expression of mRNA for isoform 1 was higher at P1 than in adult tissue corresponding with higher protein expression of isoform 1 at P1. The higher expression of isoform 1 during these developmental timepoints is consistent with the strong immunohistochemical labeling of C9ORF72 in mouse tissue in postnatal tissue and the localization of C9ORF72 to nuclei at P7. At P56 there was an increase in isoform 2 mRNA compared to P1 and P7. However, this increase in mRNA content was not reflected at the protein level, where isoform 2 protein was significantly higher at early timepoints. These discrepancies may be explained by differences in mechanisms involved in the post-transcriptional regulation, or repression of translation of isoform 2 mRNA in adulthood. A recent study by Xiao and colleagues [37] found differential localization of human C9ORF72 isoforms. The human short isoform (approximately 25 kDa) was localized to the nuclear membrane and the long isoform (approximately 55 kDa) was localized to cytoplasm with diffuse and punctate expression.

The identity of the 110 kDa band labeled by C9ORF72 is unknown. These bands have been observed in previous studies [25] and also in our western blots from primary cell culture (data not shown). As the characteristic labeling of C9ORF72 was reduced following preadsorbtion, we speculate that there is a possibility that it could be a dimer of the 55 kDa band resistant to the reducing agents used in the western blot protocol. Further studies are required to investigate these bands.

Throughout all time points in the current study, C9ORF72 had a punctate pattern of immunolabeling, which is consistent with other studies describing expression of this protein. In mice, synaptogenesis ranges from the first to third weeks of postnatal life [24]. It is therefore plausible that, in the current study, the presence of strongly labeled puncta during this time and reports of diffuse cytoplasmic and punctate labeling from other studies [3, 13, 26, 28, 37] suggest involvement of C9ORF72 at the synapse. Only the 55 kDa form of C9ORF72 was in synaptic-rich fractions in the synaptosome preparations, perhaps indicating a specific role of isoform 1 at synapses. This is also consistent with higher expression of isoform 1 at early postnatal timepoints.

It is unknown why specific populations of cells are vulnerable to degeneration in diseases such as FTLD and ALS. In this study, we showed C9ORF72 expression in neurites and the neuropil. Previous studies have found C9ORF72 within dystrophic neurites within plaques of AD brains and within swollen neurites in the hippocampus of both AD and non-AD brains [26], suggesting that

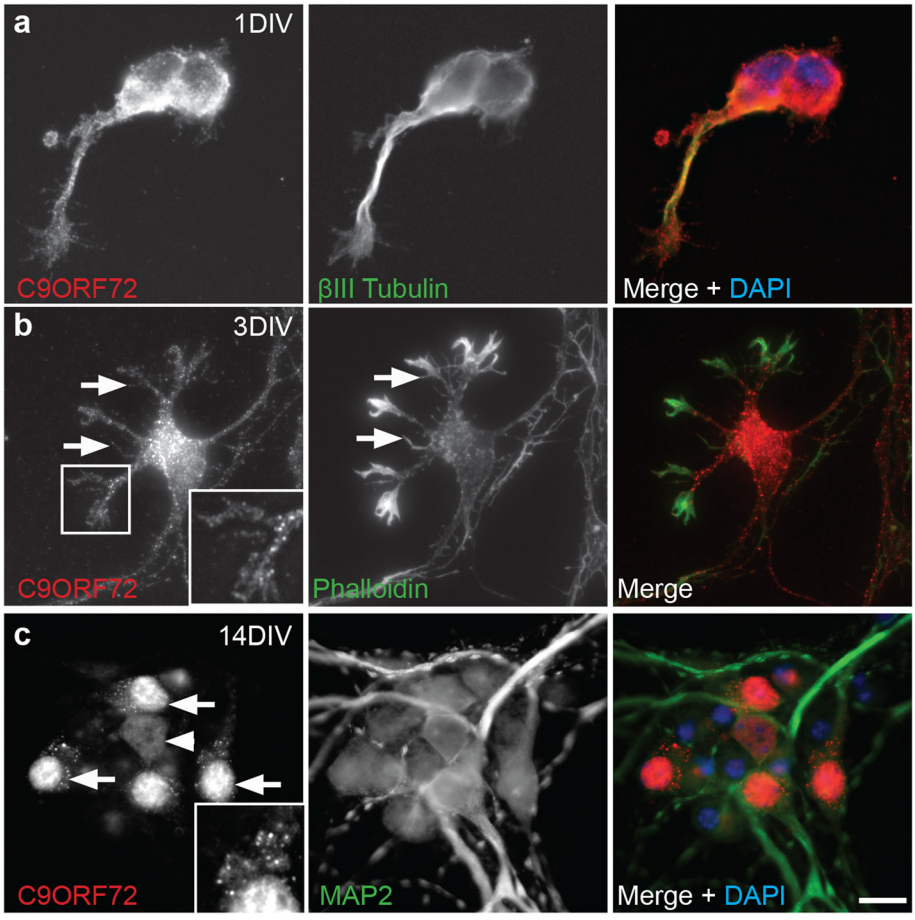

Fig. 6 Localization of C9ORF72 over development *in vitro*. Immunofluorescence was carried out on primary cultured cortical neurons. **a** At 1 DIV, C9ORF72 (*red*) labeling was present within cell bodies, excluding nuclei (DAPI, *blue*) and punctate localization was present in neurites and growth cones (β-III tubulin, *green*). **b** Co-staining with phalloidin (*green*) at 3 DIV confirmed localization of C9ORF72 (*red*) labeling to growth cones and to filopodia (*arrows*). **c** At 14 DIV, C9ORF72 (*red*) was localized to nuclei of a population of neurons (*arrows*) but was less intensely expressed in nuclei of other neurons (*arrowhead*). Neurons indicated by MAP2 (*green*). Neurons with nuclear immunolabeling for C9ORF72 frequently had punctate somal localization of this protein. Inset (**c**) shows C9ORF72 labeling in nuclei and in puncta in surrounding cytoplasm. Scale bar: A, 2.5 μm; B, C, 10 μm

it is present in neurites. Additionally, the protein is observed within swollen axons in the spinal cord ventral gray matter [30]. Motor deficits and abnormal motor neuron axons have been described following knockdown of C9orf72 in zebra-fish [2], although more recent studies in mice have found no effect of complete lack of C9ORF72 on motor function [15]. Our results demonstrate the presence of C9ORF72 as puncta throughout the actin cytoskeleton, and the presence of the protein in synaptic-rich fractions. There are a number of vesicles known to be present in axons including those supplying the synapse, those involved in membrane trafficking and axon outgrowth, and vesicles containing RNA and signaling vesicles [21]. Membrane trafficking is critical for cell survival and defects in transport to the membrane are common hallmarks of neurodegenerative diseases, including FTLD [35]. In a similar line, we recently showed that C9ORF72 is involved in endosomal trafficking via Rab-dependent pathways [7]. When C9ORF72 expression was knocked down, endocytosis and autophagy-related trafficking were inhibited. Human C9ORF72 isoforms have also been shown to interact with nuclear pore complex components, suggesting a possible role in nucleocytoplasmic shuttling [37]. These studies, in combination with our current results related to synaptosome preparations and differential nuclear and cytoplasmic localization, may suggest that C9ORF72 plays a role in trafficking and raises the possibility that failure in such neuronal cellular transport during ageing may be linked to neurodegeneration.

Like many other genetic causes of neurodegenerative disorders, the repeat expansion found in the *C9ORF72* gene is present at birth but does not cause disease until later in life. If haploinsufficiency of the encoded protein, C9ORF72, does contribute to disease then this suggests

that it is due to vulnerability caused by altered isoform expression in ageing.

This study has been the first to give a detailed description of the expression of C9ORF72 in mice, including expression over development, and lays a foundation for future studies examining the effects of altering C9ORF72 expression in rodent models, potentially providing insights into how abnormal repeat expansion may be associated with FTLD and ALS. The presence of C9ORF72 within vesicular puncta also warrants further study. Identification of these vesicles could be key to determining the role of this protein within cells.

Compliance with ethical standards

All applicable international, national, and/or institutional guidelines for the care and use of animals were followed. All procedures performed in studies involving animals were in accordance with the ethical standards of the University of Tasmania.

Additional files

Additional file 1: Figure S1. Primer efficiency and melting curve analysis. (a). The efficiency of the primer pairs for *C9orf72* isoforms was assessed by plotting the cycle threshold value (Ct) at each concentration against the logarithm of the fold dilution of the sample. The slope of a linear-regression trendline is indicative of primer efficiency. Primer efficiencies were 1.86 for isoform 1 (a i), 1.94 for isoform 2 (a ii) and 1.97 for isoform 3 (a iii). (b) Representative melting curve analysis showing the specific amplification of the *C9orf72* isoform products. Melting peaks (plotted as the negative derivative of fluorescence) revealed peaks at three different temperatures which indicate the identity of amplified *C9orf72* isoforms. (TIFF 24326 kb)

Additional file 2: Figure S2. Preadsorbtion with C9ORF72 peptide. (a) P56 tissue from C57/Bl6 mice or (b) 7 DIV cortical neurons cultured from C57/Bl6 mice were labeled with C9ORF72 (sc-138763) antibody or C9ORF72 (sc-138763) antibody preadsorbed with the C9ORF72 peptide (sc-138763 P). Labeling was decreased in both preadsorbed samples. Labeling of puncta (*arrows*) and nuclei (*arrowheads*) with C9ORF72 antibody was present in brain tissue and cultured neurons (panel 1, a, b). In contrast, when labeled with preadsorbed C9ORF72 peptide, there was no nuclei labeling and non-specific puncta present in brain samples (*arrows*, panel 2, a), and in cultured samples there was faint non-specific nuclear labeling and an absence of puncta (*arrowhead*, panel 2, b). Scale bar: a, 12 μm; b, 10 μm. (TIFF 999 kb)

Competing interests

The authors declare that they have no competing interests.

Authors' contributions

AK, CFM, JV, JA, and RA contributed to the conception and design of the study; RA, CFM, AKcontributed to data collection and analysis; RA, CFM, AK, wrote the manuscript.

Acknowledgements

The authors would like to gratefully acknowledge Justin Dittmann for technical support. This work was supported by a PhD scholarship to RA from Alzheimer's Australia Dementia Research Foundation as well as funding from the Motor Neuron Disease Research Institute of Australia and the JO and JR Wicking Trust (Equity Trustees).

Author details

[1]Wicking Dementia Research and Education Centre, Faculty of Health, University of Tasmania, Hobart, Tasmania, Australia. [2]Australian School of Advanced Medicine, Macquarie University, North Ryde, New South Wales, Australia.

Received: 25 August 2015 Accepted: 15 September 2015
Published online: 25 September 2015

References

1. Ash PEA, Bieniek KF, Gendron TF, Caulfield T, Lin W-L, DeJesus-Hernandez M et al. (2013) Unconventional translation of C9ORF72 GGGGCC expansion generates insoluble polypeptides specific to c9FTD/ALS. Neuron 77:639–646. doi:10.1016/j.neuron.2013.02.004
2. Ciura S, Lattante S, Le Ber I, Latouche M, Tostivint H, Brice A et al. (2013) Loss of function of C9orf72 causes motor deficits in a zebrafish model of Amyotrophic Lateral Sclerosis. Ann Neurol 74:180–187. doi:10.1002/ana.23946
3. Cooper-Knock J, Hewitt C, Highley JR, Brockington A, Milano A, Man S et al. (2012) Clinico-pathological features in amyotrophic lateral sclerosis with expansions in C9ORF72. Brain 135:751–764. doi:10.1093/brain/awr365
4. DeJesus-Hernandez M, Mackenzie IR, Boeve BF, Boxer AL, Baker M, Rutherford NJ et al. (2011) Expanded GGGGCC hexanucleotide repeat in noncoding region of C9ORF72 causes chromosome 9p-linked FTD and ALS. Neuron 72:245–256. doi:10.1016/j.neuron.2011.09.011
5. Donnelly CJ, Zhang P-W, Pham JT, Heusler AR, Mistry NA, Vidensky S et al. (2013) RNA Toxicity from the ALS/FTD C9ORF72 Expansion Is Mitigated by Antisense Intervention. Neuron 80:415–428. doi:10.1016/j.neuron.2013.10.015
6. Dunkley PR, Jarvie PE, Robinson PJ. (2008) A rapid Percoll gradient procedure for preparation of synaptosomes. Nat Protoc 3:1718–1728. doi:10.1038/nprot.2008.171
7. Farg MA, Sundaramoorthy V, Sultana JM, Yang S, Atkinson RAK, Levina V et al. (2014) C9ORF72, implicated in amytrophic lateral sclerosis and frontotemporal dementia, regulates endosomal trafficking. Hum Mol Genet 23:3579–3595. doi:10.1093/hmg/ddu068
8. Fernandez CM, Molto E, Gallardo N, del Arco A, Martinez C, Andres A et al. (2009) The expression of rat resistin isoforms is differentially regulated in visceral adipose tissues: effects of aging and food restriction. Metabolism 58:204–211
9. Fernandez-Martos CM, Gonzalez-Fernandez C, Gonzalez P, Maqueda A, Arenas E, Rodriguez FJ. (2011) Differential expression of Wnts after spinal cord contusion injury in adult rats. PLoS ONE 6:e27000. doi:10.1371/journal.pone.0027000
10. Franklin KBJ, Paxinos G. (2008) The Mouse Brain in Stereotaxic Coordinates. Academic, City
11. Gijselinck I, Van Langenhove T, van der Zee J, Sleegers K, Philtjens S, Kleinberger G et al. (2012) A C9orf72 promoter repeat expansion in a Flanders-Belgian cohort with disorders of the frontotemporal lobar degeneration-amyotrophic lateral sclerosis spectrum: a gene identification study. Lancet Neurol 11:54–65. doi:10.1016/S1474-4422(11)70261-7
12. Gonzalez-Fernandez C, Fernandez-Martos CM, Shields SD, Arenas E, Javier Rodriguez F. (2014) Wnts are expressed in the spinal cord of adult mice and are differentially induced after injury. J Neurotrauma 31:565–581. doi:10.1089/neu.2013.3067
13. Hsiung G-YR, DeJesus-Hernandez M, Feldman HH, Sengdy P, Bouchard-Kerr P, Dwosh E et al. (2012) Clinical and pathological features of familial frontotemporal dementia caused by C9ORF72 mutation on chromosome 9p. Brain 135:709–722. doi:10.1093/brain/awr354
14. King AE, Chung RS, Vickers JC, Dickson TC. (2006) Localization of glutamate receptors in developing cortical neurons in culture and relationship to susceptibility to excitotoxicity. J Comp Neurol 498:277–294. doi:10.1002/cne.21053
15. Koppers M, Blokhuis AM, Westeneng HJ, Terpstra ML, Zundel CA, Vieira de Sa R et al. (2015) C9orf72 ablation in mice does not cause motor neuron degeneration or motor deficits. Ann Neurol. doi:10.1002/ana.24453
16. Levine TP, Daniels RD, Gatta AT, Wong LH, Hayes MJ. (2013) The product of C9orf72, a gene strongly implicated in neurodegeneration, is structurally related to DENN Rab-GEFs. Bioinformatics 29:499–503. doi:10.1093/bioinformatics/bts725
17. Ling S-C, Polymenidou M, Cleveland DW. (2013) Converging Mechanisms in ALS and FTD: Disrupted RNA and Protein Homeostasis. Neuron 79:416–438. doi:10.1016/j.neuron.2013.07.033

18. Liu Y, Atkinson RA, Fernandez-Martos CM, Kirkcaldie MT, Cui H, Vickers JC et a.l (2014) Changes in TDP-43 expression in development, aging, and in the neurofilament light protein knockout mouse. Neurobiol Aging 36:1151–1159. doi:10.1016/j.neurobiolaging.2014.10.001
19. Liu Y, Staal JA, Canty AJ, Kirkcaldie MT, King AE, Bibari O et al. (2013) Cytoskeletal changes during development and aging in the cortex of neurofilament light protein knockout mice. J Comp Neurol 521:1817–1827. doi:10.1002/cne.23261
20. Livak KJ, Schmittgen TD (2001) Analysis of relative gene expression data using real-time quantitative PCR and the 2-Delta Delta CT Method. Methods 25:402–408. doi:10.1006/meth.2001.1262
21. Millecamps S, Julien JP (2013) Axonal transport deficits and neurodegenerative diseases. Nat Rev Neurosci 14:161–176. doi:10.1038/nrn3380
22. Mitew S, Kirkcaldie MTK, Dickson TC, Vickers JC (2013) Altered synapses and gliotransmission in Alzheimer's disease and AD model mice. Neurobiol Aging 34:2341–2351. doi:10.1016/j.neurobiolaging.2013.04.010
23. Mori K, Weng S-M, Arzberger T, May S, Rentzsch K, Kremmer E et al. (2013) The C9orf72 GGGGCC repeat is translated into aggregating dipeptide-repeat proteins in FTLD/ALS. Science 339:1335–1338. doi:10.1126/science.1232927
24. Pfrieger FW (2009) Roles of glial cells in synapse development. Cell Mol Life Sci 66:2037–2047. doi:10.1007/s00018-009-0005-7
25. Renton AE, Majounie E, Waite A, Simón-Sánchez J, Rollinson S, Gibbs JR et al. (2011) A hexanucleotide repeat expansion in C9ORF72 is the cause of chromosome 9p21-linked ALS-FTD. Neuron 72:257–268. doi:10.1016/j.neuron.2011.09.010
26. J-i S, Tabunoki H, Ishida T, Saito Y, Arima K (2012) Dystrophic neurites express C9orf72 in Alzheimer's disease brains. Alzheimers Res Ther 4:33. doi:10.1186/alzrt136
27. Simón-Sánchez J, Dopper EGP, Cohn-Hokke PE, Hukema RK, Nicolaou N, Seelaar H et al (2012) The clinical and pathological phenotype of C9ORF72 hexanucleotide repeat expansions. Brain 135:723–735. doi:10.1093/brain/awr353
28. Snowden JS, Rollinson S, Thompson JC, Harris JM, Stopford CL, Richardson AMT et al (2012) Distinct clinical and pathological characteristics of frontotemporal dementia associated with C9ORF72 mutations. Brain 135:693–708. doi:10.1093/brain/awr355
29. Stenmark H (2009) Rab GTPases as coordinators of vesicle traffic. Nature 10:513–525. doi:10.1038/nrm2728
30. Stewart H, Rutherford NJ, Briemberg H, Krieger C, Cashman N, Fabros M et al. (2012) Clinical and pathological features of amyotrophic lateral sclerosis caused by mutation in the C9ORF72 gene on chromosome 9p. Acta Neuropathol 123:409–417. doi:10.1007/s00401-011-0937-5
31. Stigliani S, Zappettini S, Raiteri L, Passalacqua M, Melloni E, Venturi C et al. (2006) Glia re-sealed particles freshly prepared from adult rat brain are competent for exocytotic release of glutamate. J Neurochem 96:656–668. doi:10.1111/j.1471-4159.2005.03631.x
32. Suzuki N, Maroof AM, Merkle FT, Koszka K, Intoh A, Armstrong I et al. (2013) The mouse C9ORF72 ortholog is enriched in neurons known to degenerate in ALS and FTD. Nat Neurosci 16:1725–1727. doi:10.1038/nn.3566
33. Therrien M, Rouleau GA, Dion PA, Parker JA (2013) Deletion of C9ORF72 results in motor neuron degeneration and stress sensitivity in C. elegans. PLoS ONE 8:e83450. doi:10.1371/journal.pone.0083450
34. Waite AJ, Bäumer D, East S, Neal J, Morris HR, Ansorge O et al. (2014) Reduced C9orf72 protein levels in frontal cortex of amyotrophic lateral sclerosis and frontotemporal degeneration brain with the C9ORF72 hexanucleotide repeat expansion. Neurobiol Aging 35:1779.e1775-1779.e1713. doi:10.1016/j.neurobiolaging.2014.01.016
35. Wang D, Chan C-C, Cherry S, Hiesinger PR (2013) Membrane trafficking in neuronal maintenance and degeneration. Cell Mol Life Sci 70:2919–2934. doi:10.1007/s00018-012-1201-4
36. Workman AD, Charvet CJ, Clancy B, Darlington RB, Finlay BL (2013) Modeling transformations of neurodevelopmental sequences across mammalian species. J Neurosci 33:7368–7383. doi:10.1523/JNEUROSCI.5746-12.2013
37. Xiao S, MacNair L, McGoldrick P, McKeever PM, McLean JR, Zhang M et al. Isoform Specific Antibodies Reveal Distinct Subcellular Localizations of C9orf72 in Amyotrophic Lateral Sclerosis. Ann Neurol. 2015 Accepted Article. doi: 10.1002/ana.24469